An analysis of the reaction $(^{+})N$ßPXat4GeV/c

Michael Dale

TO MY

PARENTS

AN ANALYSIS OF THE REACTION $\pi^+ N \rightarrow P X^0$ AT 4 GeV/c

A THESIS PRESENTED

BY

MICHAEL DALE

FOR THE

DEGREE OF DOCTOR OF PHILOSOPHY

AT THE

UNIVERSITY OF DURHAM

APRIL 1975

ABSTRACT

This thesis presents an account of the analysis of the reactions

$$\pi^+ D \rightarrow P_S P \omega^0$$

and $$\pi^+ D \rightarrow P_S P \eta^0$$

at 4.0 GeV/c incident momentum, carried out by the author whilst at the University of Durham.

The experiment, undertaken in collaboration with the University of Birmingham and the Rutherford Laboratory, is described in detail, particular emphasis being applied to the limitations of the experimental setup, the accuracy of the resulting data and the problems associated with the use of a deuterium target.

Following a description of the selection of the channel

$$\pi^+ D \rightarrow P_S P \pi^+ \pi^- \pi^0$$

the production and decay processes of the ω^0 - mesons are analysed in detail. The results are compared with those from previous analyses and with the predictions of various Regge Pole models. To describe the various features of the data it is found necessary to infer the presence of significant contributions from unnatural parity exchanges such as the B - meson, in disagreement with the earlier theoretical interpretations which assumed the complete domination of the natural parity component, namely ρ - exchange.

As part of this analysis the nature of the associated background is determined, and the results indicate the possible breakthrough of events from the 4c channel,

$$\pi^+ D \rightarrow P_S P \pi^+ \pi^-$$

The characteristics of these events in the 1.0 GeV/c^2 region of the tripion mass spectrum is investigated, and it is concluded that they may well affect the interpretation of the observed enhancements attributed to the controversial H^o and A_1 resonances.

Finally the production mechanism of the η - meson is analysed.

CONTENTS PAGE

PAGE

LIST OF FIGURES.

CHAPTER 4

CHAPTER 7

LIST OF TABLES

TABLES FOLLOWING PAGE

CHAPTER 6

CHAPTER 7

CHAPTER ONE

INTRODUCTION

The production of the ω^0 - meson via π - N collisions has in recent years created a certain amount of controversy. This arose from the inability of the early ρ - Regge Pole models to describe the experimental data. Although the model could describe very well other channels dominated by ρ - exchange, such as

$$\pi^- \; P \rightarrow \; \pi^0 \; n$$

none could explain the ω^0 - production data. The main difficulty was the absence of any structure in the differential cross section at $t \sim 0.6$ $(GeV/c^2)^2$, corresponding to the nonsense wrong signature zero of the ρ - trajectory. Attempts were made to explain this by the introduction of strong cuts or absorption, but none was satisfactory. Moreover, whereas ρ - exchange predicts the spin density matrix element ρ_{00} to be zero, the experimental values were observed to be very large. Adding further to these difficulties were the observed inconsistencies in the results from different experiments, whereas some reported a minimum in the differential cross section at low t, or structure in the spin density matrix elements, others did not. The main cause of the latter problem has essentially been the lack of statistics, and it is the intention of this analysis to utilize the high statistics available from the 4 GeV/c π^+ D experiment to examine in detail both the differential cross section and spin density matrix elements for those ω^0 - mesons produced in the channel

$$\pi^+ D \longrightarrow P_S P \pi^+ \pi^- \pi^0$$

where possible extracting the effects due to background.

In chapters 2 and 3, the experimental setup is described, from the beam line and the bubble chamber, to the formation of the final data summary tape, the inherent inaccuracies and limitations being described at all stages. In addition the problems and characteristics associated with the use of a deuterium target are discussed. The concept of seen and unseen spectator proton events is introduced and in particular preliminary results are presented indicating the possible effects due to the Pauli exclusion principle. Whereas in previous analyses the production mechanisms associated with the latter two classes of events have been considered identical at all values of t, the examination of the effects due to the Pauli principle indicate that this may not be correct.

In chapters 4 and 6, the production and decay of the ω^0 - mesons are analysed in detail, and the results compared with the predictions of various Regge Pole models. The nature of the associated background is discussed in chapter 5, the results indicating the possible breakthrough of events from the 4c channel

$$\pi^+ D \rightarrow P_S P \pi^+ \pi^-$$

which may have important consequences for the interpretation of the H^0 and A_1 regions of the tripion mass spectrum.

In chapter 7, the production mechanism of the η - mesons produced in the channel

$$\pi^+ D \rightarrow P_S P \pi^+ \pi^- \pi^0$$

are analysed, the total and differential cross sections

being determined.

Finally a conclusion to the thesis is given summarising the results.

CHAPTER TWO

GENERAL EXPERIMENTAL CONSIDERATIONS

INTRODUCTION

The 4 GeV/c π^+D experiment was designed as a high statistics experiment for the specific study of neutral meson resonances, and in particular for those containing neutral decay products such as the ω^o, $A_1{}^o$ and $A_2{}^o$ mesons. In all, some 850K pictures were taken. In this chapter the experimental setup is described, particular emphasis being applied to the inherent limitations imposed on the accuracy and quality of the data.

2.1 THE BEAM LINE

A proton beam, which was extracted from the CERN proton synchroton, impinged on a copper target in the U5 beam line. From the numerous particles produced, the required 4 GeV/c π^+ - mesons were seperated in the beam line and directed into the bubble chamber.

The beam line is illustrated schematically in FIG. 2.1, the corresponding key to the components being shown in table 2.1. The optics of the system can essentially be divided into 3 sections:-

(a) The formation and momentum analysis stage

(b) The separation

and (c) The final cleaning and preparation for the bubble chamber.

To achieve the required separation of the 4 GeV/c pions it was

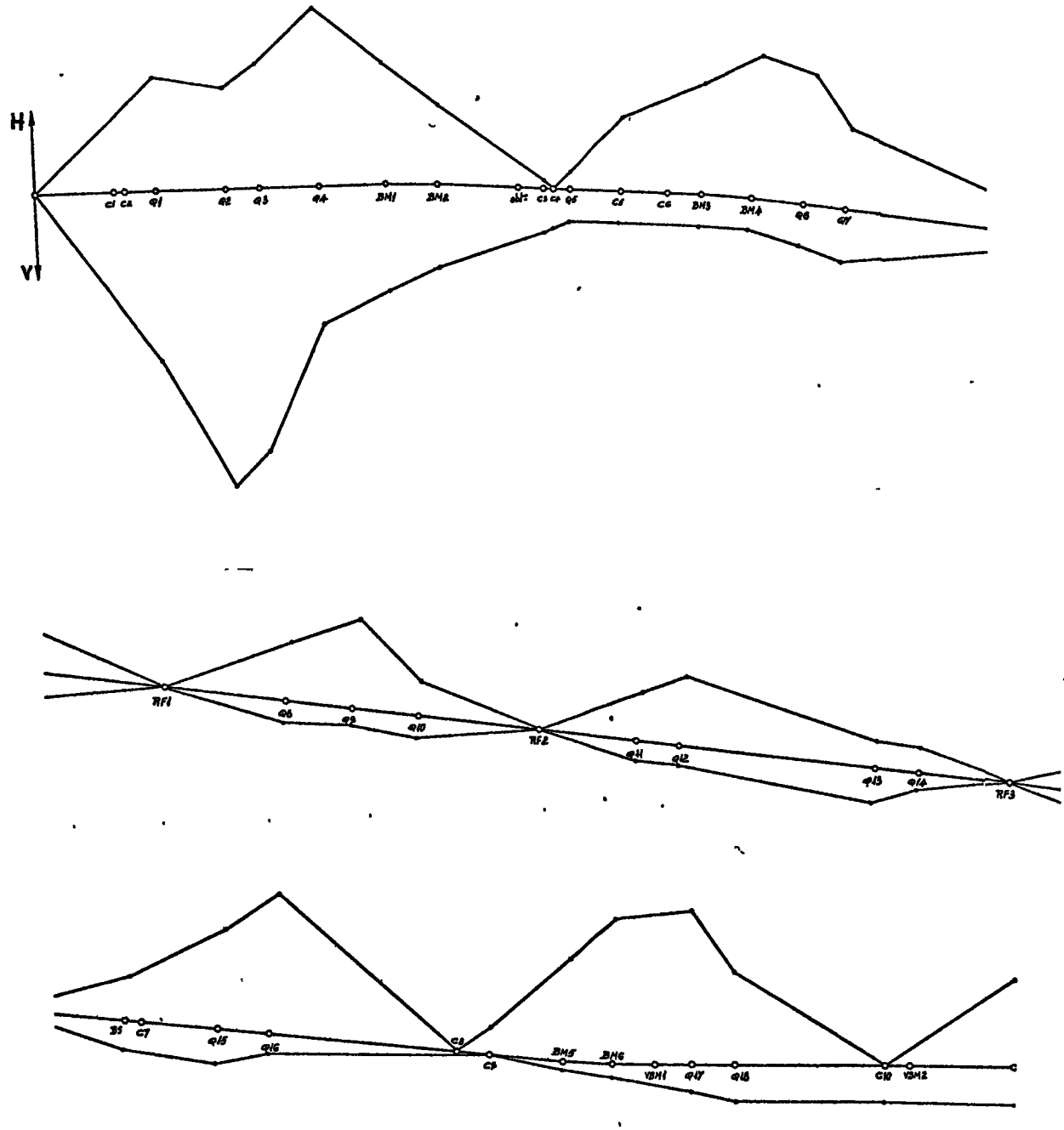

FIG. 2.1 THE BEAM LINE

TABLE 2.1

LIST OF U5 BEAM LINE ELEMENTS

No.	Element Description	Symbol in Fig.2.1	Distance From Preceding Element (M)	
1	Target - Copper	T	0	
2	Horizontal Collinator	C1	4.5	
3	Vertical Collinator	C2	0.65	
4	2M Quadrupole	Q1	1.85	
5	2M Quadrupole	Q2	4.00	FORMATION
6	1M Quadrupole	Q3	2.50	AND
7	2M Quadrupole	Q4	3.50	MOMENTUM
8	Bending Magnet	BM1	3.87	ANALYSIS
9	Bending Magnet	BM2	3.00	STAGE
10	Vertical Collinator	C3	5.92	
11	Horizontal Collinator	C4	0.58	62 m
12	0.75 M Quadrupole	Q5	1.00	
13	Horizontal Collinator	C5	2.25	
14	Vertical Collinator	C6	2.35	
15	Bending Magnet	BM3	2.00	
16	Bending Magnet	BM4	3.00	
17	2M Quadrupole	Q6	3.05	
18	2M Quadrupole	Q7	2.50	
19	Separator	RF1	15.50	
20	2M Quadrupole	Q8	7.09	
21	2M Quadrupole	Q9	3.91	SEPARATION
22	2M Quadrupole	Q10	3.91	STAGE
23	Separator	RF2	7.09	50 m
24	2M Quadrupole	Q11	5.75	
25	2M Quadrupole	Q12	2.50	
26	2M Quadrupole	Q13	11.50	
27	2M Quadrupole	Q14	2.50	
28	Separator	RF3	5.75	
29	Beam Stopper	BS	7.55	
30	Vertical Collinator	C7	1.50	
31	2M Quadrupole	Q15	3.30	
32	2M Quadrupole	Q16	3.00	PREPERATION
33	Horizontal Collinator	C8	11.00	FOR BUBBLE
34	Vertical Collinator	C9	1.90	CHAMBER
35	Bending Magnet	BM5	4.26	STAGE
36	Bending Magnet	BM6	3.00	
37	Vertical Bending Magnet	VBM1	2.18	53 m
38	2M Quadrupole	Q17	2.22	
39	2M Quadrupole	Q18	2.50	
40	Horizontal Collinator	C10	9.00	
41	Vertical Bending Magnet	M8	2.00	
42	Bubble Chamber	BC	5.00	

considered sufficient to use only 2 of the 3 available R.F. cavities. In essence the operation of this system is such that the relative phasing between RF1 and RF2 is so arranged to provide a maximum deflection to the particles away from the original beam axis, the unwanted particles being returned to this axis and subsequently absorbed in the beam stopper. Stabilisation of the momentum and focussing of the resulting beam was then maintained by careful monitoring of the current levels within the bending magnets and quadrupole magnets. In addition the various collimators were regulated to maintain a reasonable flux of particles into the chamber.

The exposure was undertaken in two parts. In the first exposure of August 71, with an operating beam momentum of 4.02 ± 0.01 GeV/c, a flux level of some 12 pions per pulse was maintained. In the second exposure of 1973 however, it was considered advisable to increase this level to 15 per pulse in order to increase the effective rate of data collection. As illustrated in FIG. 2.2, the beam momentum of the second exposure was slightly lower and centred at 3.94 ± 0.01 GeV/c.

2.2 THE CONTAMINATION OF THE π^+ BEAM

At beam momenta of 4 GeV/c, the separation produced by the R.F. cavities is sufficient to reduce the possible contamination to the following 3 charged components, namely P, μ^+ and K^+.

(a) THE μ^+ CONTAMINATION

The most probable source of μ^+ contamination arises from the decay of the pions via the process $\pi \rightarrow \mu + \nu$. Those muons produced within the beam line are momentum analysed and

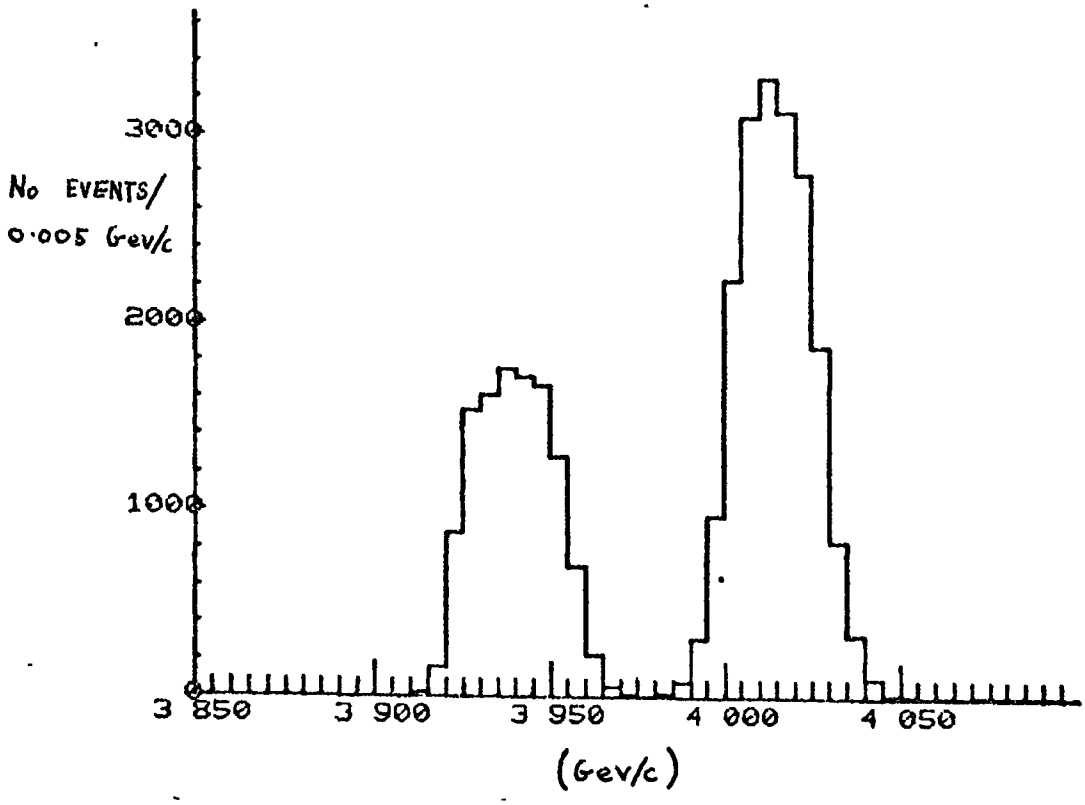

FIG. 2.2 THE BEAM MOMENTUM

subsequently removed. Hence the only effective contamination arose from the pions decaying between the last collimator, C9, and the bubble chamber. Using a pion lifetime of 2.6×10^{-8} secs., and a lorentz factor of 29.1, the percentage of pions decaying over this distance of some 7 metres is in the region of 3%. The vast majority of these however, will appear "off beam" in the chamber, and the estimate of the final contamination is of the order of $0.4 \pm 0.1\%$.

(b) THE K^+ CONTAMINATION

This was estimated from the number of Tau decays of the K- mesons which could be fitted to a sample of some 3000 3 - prong events. An upper limit of 1 event was found as a Tau candidate. Hence, allowing for the branching ratio of the K - decay, and the observed length of beam track, an upper limit to the degree of K^+ contamination was found to be $0.5 \pm 0.1\%$.

(c) THE PROTON CONTAMINATION

This has been estimated by using a method described by Gordon, (Ref. 2.1). He has shown that in the two reactions

$$\pi^+ D \rightarrow P P \pi^+ \pi^- \qquad (1)$$

and

$$P D \rightarrow P P P \pi^- \qquad (2)$$

$$\sigma(1) \Big/ \sigma(\pi D)\ \text{TOTAL} = \sigma(2) \Big/ \sigma(PD)\ \text{TOTAL}$$

and

$$\frac{\text{Probability } (\pi \text{ - fit to a real P beam})}{\text{Probability } (\text{P - fit to a real } \pi \text{ beam})} = \frac{1}{2}$$

From these, an estimate of the contamination can be made. The

probability of producing a pion fit to a real proton beam can be determined by producing reaction (2) from the pure proton beam direct from the proton synchrotron. This enables a comparison to be made of the expected and experimental probability for producing a proton fit to the pion beam. Following this procedure provided an estimated proton contamination of $4 \pm 3\%$.

2.3 THE BUBBLE CHAMBER

For both exposures the chamber used was the CERN 2 metre deuterium filled bubble chamber, (CERN 2m DBC). Its general construction is described briefly below. As in any detection system, the bubble chamber has certain intrinsic errors and limitations, and in the subsequent sections the more important cases are discussed.

(a) THE GENERAL CONSTRUCTION OF THE CHAMBER

The chamber consists of a single aluminium casting, with an internal clear section of dimensions 200 x 51 x 60 cms. This is filled with the order of 1000 litres of liquid deuterium at a temperature of 27° K under a pressure of approximately 6 atmospheres. As illustrated in FIG. 2.3, the inner section is enclosed by a cold tank, and a stainless steel vacuum tank in order to reduce heat losses. The chamber was operated in its double pulsed mode, with the order of $^{1}/10$ of a second between pictures, and some 2 seconds between each double pulse. The sequence of operation is illustrated in FIG. 2.4. Surrounding the vacuum tank is a large electromagnet producing a near uniform field over the entire liquid chamber volume, the current

2 METRE C.E.R.N BUBBLE CHAMBER (HORIZONTAL SECTION)

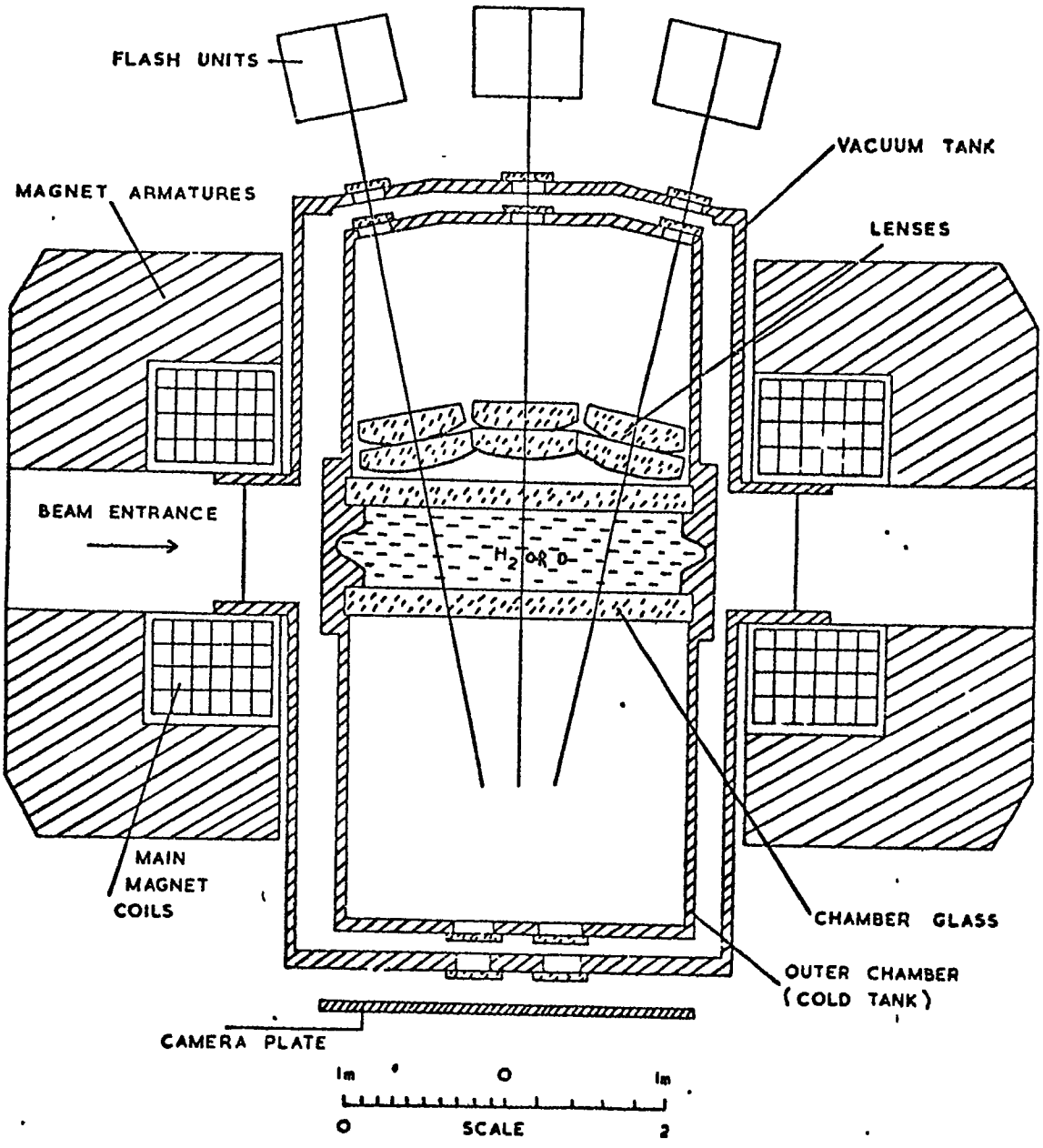

FIG. 2.3

in the magnetic windings being of the order of 1000 amperes. A "through illumination" system was provided by 3 monochromatic electron flash tubes via the back glass of the chamber. The illuminated volume was then observed from the front by a triangular array of cameras. In addition, etched onto both the front and back glass, were the measuring fiducial marks required for the geometrical reconstruction of the events.

(b) THE RESOLUTION OF THE SYSTEM

The accuracy attained depends initially upon the photography. In order to achieve the required depth of focus it is necessary to stop down the camera lenses. This however, results in diffraction effects, such that instead of seeing the bubbles, their corresponding Airy discs are observed. Ultimately, the optimum value is decided by the photographic plate, since this sets a lower limit to the resolution. Assuming a typical film resolution of 700 lines per cm., then the Airy disc has to be as large as 14 μ (= $^{1}/_{700}$ cm), to be resolved. If the required depth of focus is then 50 cm. it can be shown that the Airy disc image will correspond to an effective bubble size in the chamber of some 200μ.

(c) OPTICAL DISTORTIONS

Although the quality of both the camera lenses and glass windows is very high, distortions are nevertheless introduced, and in order to achieve reliable reconstruction of the events it is necessary to make the appropriate corrections. The main sources of distortion are the non alignment of the optic axes, the film tilt, and the distortions within the lens system

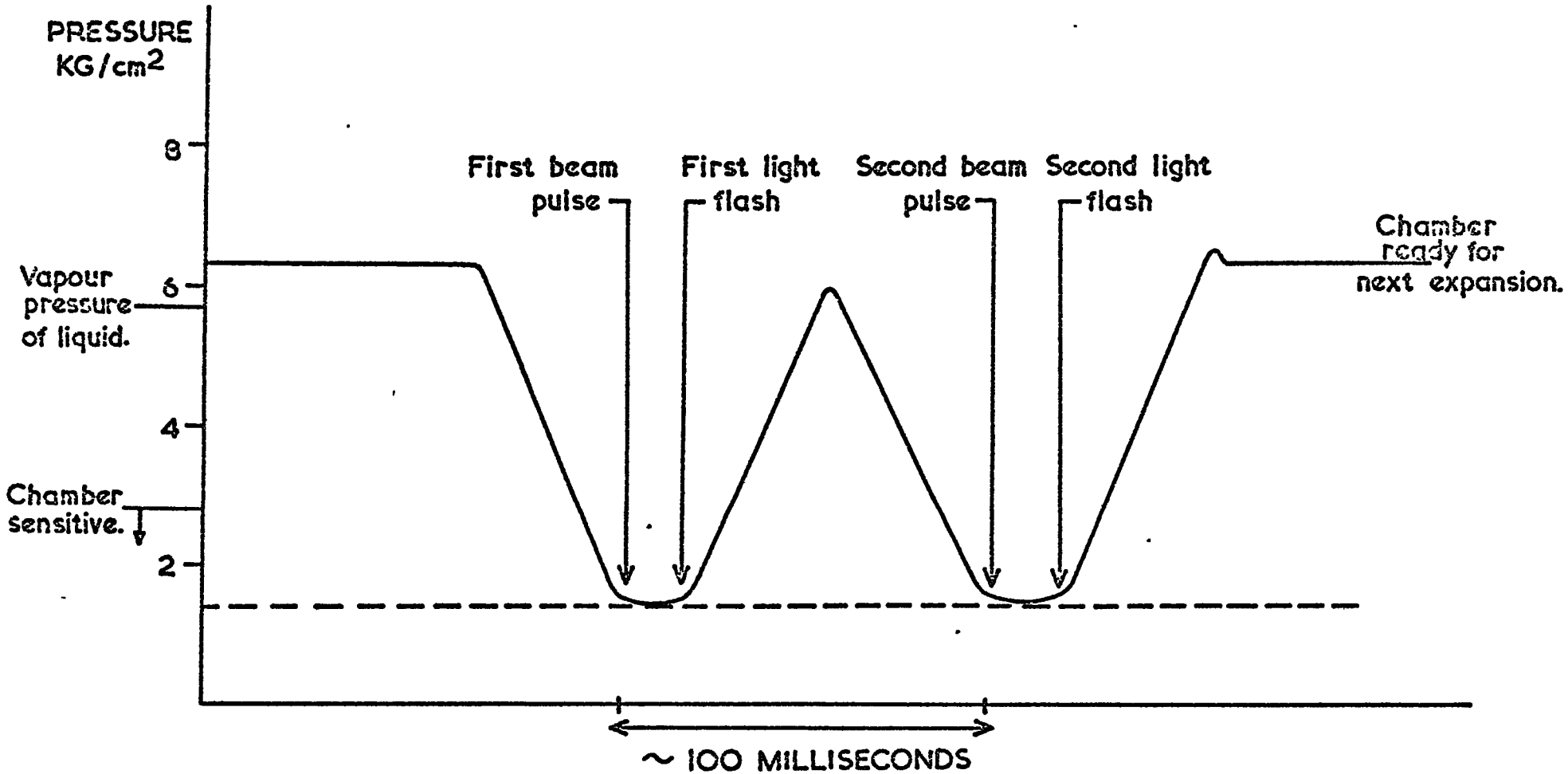

FIG. 2.4 THE SEQUENCE OF OPERATION OF THE CHAMBER

and glass windows. A study of these effects by Kellner in 1965, (Ref.2.2), showed that the distortions could be represented by a simple power series. If x and y represent the distortion free coordinates on the "ideal film plane", then the relation between these and the experimental film plane coordinates is given by:-

$$\begin{pmatrix} x' \\ y' \end{pmatrix} = \begin{pmatrix} x \\ y \end{pmatrix} \left[1 + \frac{\alpha_1 x}{f} + \frac{\alpha_2 y}{f} + \frac{\alpha_3 xy}{f^2} + \frac{\alpha_4 x^2}{f^2} + \frac{\alpha_5 y^2}{f^2} + \frac{\alpha_6 (x^2+y^2)^2}{f^4} \right]$$

where f is the focal length. The distortion coefficients α_1 and α_2 are the coefficients related to the tilt angle and film stretch, α_3, α_4 and α_5 take into account the elliptical distortions created by the non-alignment of the optic and mechanical axis of the lens, and any additional higher order distortions are included in α_6.

(d) THERMAL CONVECTION AND TURBULENCE

The chamber contains some 1000 litres of liquid deuterium, which is double pulsed the order of every 2 seconds. Understandably, this and the subsequent creation of temperature differences produces thermal convection and turbulence within the liquid. The bubble velocities resulting from convection are of ~3 cms/sec., which for a bubble growth time of 1 ms. before photography, corresponds to a movement of some 30μ. In addition, the temperature differences result in the so called "twinkling effect", arising from the subsequent variations in the refractive index of the liquid. Estimates made by Thomas, (Ref.2.3), indicate that this effect results in an apparent movement of the bubble by some 30 μ. From the previous

section however, it is evident that both of these effects are negligible compared to the apparent size of the bubbles.

(e) VARIATIONS IN THE MAGNETIC FIELD

The magnetic field in the chamber is usually denoted by its central value, and in the CERN 2m chamber this is 17.5 K gauss. Any variations in the field are mapped with an accuracy of about 1% of the central value, so that the corresponding corrections to the particle paths can be made in the kinematics reconstruction programme. The maximum variation occurs at the edges of the chamber, and amount to some 3%. Since the field is at the saturation value for the electromagnet, current variations have little or no effect.

(f) THE EFFECTS OF MULTIPLE SCATTERING

Coulomb scattering within the chamber liquid results in a spurious track curvature even under the influence of a zero magnetic field. Such an effect creates errors in the momentum measurements calculated from the curvature of the tracks resulting from the applied magnetic field. From scattering theory it can be shown that the effective sagitta introduced by this effect can be expressed as

$$Sc = \frac{2.14}{P\beta c} \ell \left[\ell/\lambda\right]^{0.5}$$

where P is the momentum of the particle in MeV/c, βc its velocity, λ the radiation length in cms, ℓ the track length in cm, and 2.14 is the scattering constant. The magnitude of Sc is sufficient in nuclear emulsions, where the scattering constant is larger, to enable direct $P\beta$ measure-

ments to be made. In bubble chambers however, it is an undesirable secondary effect compared to the applied magnetic field, and represents a noise level ranging from 1% in hydrogen to about 30% in propane. From the above expression for Sc it is evident that the effect of multiple scattering is of particular importance for short tracks and low values of $P\beta$ In addition, as explained in the following chapter, the measurement errors are sufficiently small, ~0.4%, that the limit on the experimental accuracy is due to these multiple scattering errors rather than the measurement errors.

2.4 DEUTERIUM TARGETS

In the previous section the bubble chamber has been described and discussed from the point of view of its construction and limitations. In this section the motivation for using a deuterium target will be discussed, and in particular, the concept of "spectators" introduced.

(a) THE CHOICE OF TARGET

As mentioned in the introduction to this chapter, the experiment was specifically designed to study neutral meson resonances, and in particular to study those containing single neutral decay products such as the ω^0, $A_1{}^0$ and $A_2{}^0$ mesons. Such resonances are observed in the 3 pion combination $\pi^+\pi^-\pi^0$ and this particular configuration can be formed in several types of interactions, the most obvious choices being:-

(1)	$\pi^+ P \rightarrow P$	$\pi^+\pi^-\pi^0$	π^+
(2)	$\pi^- P \rightarrow N$	$\pi^+\pi^-\pi^0$	
(3)	$\pi^+ N \rightarrow P$	$\pi^+\pi^-\pi^0$	
and (4)	$\pi^- N \rightarrow N$	$\pi^+\pi^-\pi^0$	π^-

The no - fit channels (2) and (4) however, where 2 neutral particles are present, contain insufficient information to make a thorough analysis. Hence the obvious candidates are reactions (1) and (3). Of the two, reaction (3) is simpler, since it does not contain the inherent ambiguity of the two π^+ mesons, one of which in reaction (1) may be associated with a Δ^{++}.

The least complex and hence most easily analysed neutron target is the deuteron. For this and the above mentioned reasons a deuterium target was chosen, and the use of such a target introduces the following additional features.

(b) THE NATURE OF THE INTERACTIONS

Essentially two different initial interactions can occur, firstly the so called coherent interactions in which the deuteron remains intact, and secondly, interactions in which the deuteron binding energy is overcome, and subsequent breakup occurs. At incident energies of 4 GeV, coherence occurs in only some 2 or 3% of the cases, and throughout the remainder of this analysis the channels considered are necessarily associated with deuteron breakup. Such reactions introduce the so called spectator neutron or proton which essentially corresponds to the non-interacting nucleon. In this analysis, where the neutron interactions are required, we are concerned with the spectator protons.

(c) IDENTIFICATION OF THE SPECTATOR

The deuteron binding energy is sufficiently small ~ 2.2 MeV that by invoking the impulse approximation, (Ref. 2.4), the

assumption can be made that the interaction is effectively with free particles. This assumption implies a zero momentum transfer between the target nucleons, and consequently the momentum of the non-interacting particle, allowing for secondary scatters, should be typified by the Hulthen distribution. Experimentally however, the non-interacting so called spectator nucleon cannot always be distinguished unambiguously. In the particular case of π^+ N charge exchange, the final state involves two candidate spectator protons, both of which can lie within the Hulthen distribution. Fortunately however, at incident pion momenta of 4 GeV/c this ambiguity only occurs at low 4 - momentum transfers to the target nucleon, and hence only affects a relatively small percentage of the total events. Throughout the analysis the ambiguity is resolved by arbitrarily assigning the slower proton to be the spectator. Fake calculations indicate such an assignment to be wrong in some 3% of the cases.

(d) SEEN AND UNSEEN SPECTATOR PROTON EVENTS

In deuterium, the minimum momentum required to produce a visible proton track is ~85 MeV/c. Hence proton momenta below this limit will remain undetected. From the form of the Hulthen distribution, illustrated in FIG.2.5, it is implied that $\sim 2/3$ of the spectator protons will be unseen. In the fitting of these events the unseen spectator protons are essentially treated as badly measured tracks. A zero momentum is assigned to the tracks with errors consistent with the maximum observable momentum. The subsequent fitting procedure then iterates to the optimum value for its momentum and direction. The laboratory momenta and angular distributions for the

FIG. 2.5 THE LABORATORY MOMENTA AND ANGULAR DISTRIBUTIONS FOR THE SPECTATOR PROTONS ASSOCIATED WITH THE 4C AND 1C EVENTS.

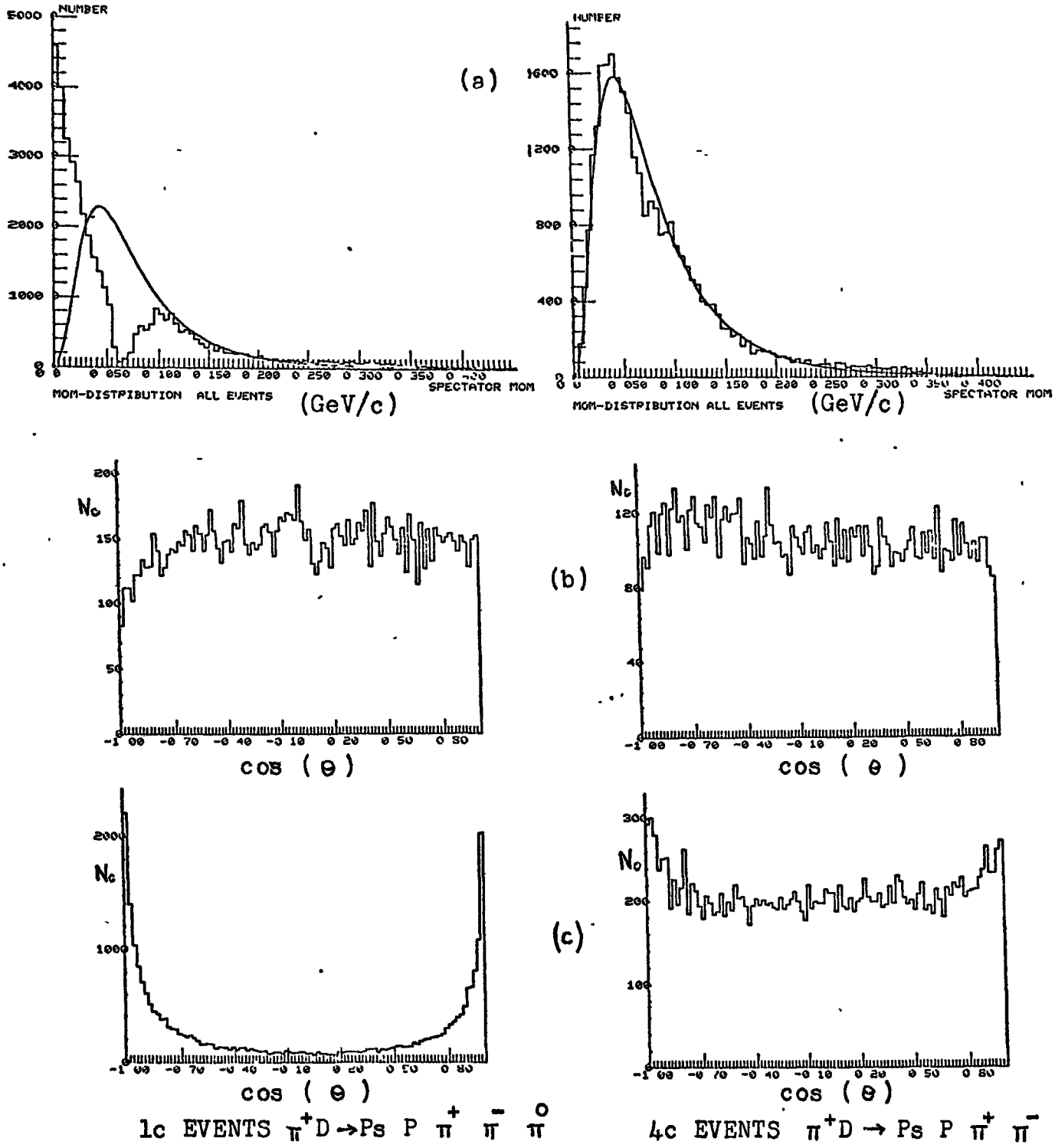

(a) THE SPECTATOR PROTON MOMENTUM DISTRIBUTIONS.

(b) THE ANGULAR DISTRIBUTIONS FOR THE SEEN SPECTATOR PROTONS.

(c) THE ANGULAR DISTRIBUTIONS FOR THE UNSEEN SPECTATOR PROTONS.

spectator protons identified in the manner specified above, are illustrated in FIG. 2.5. For both the 4c events

$$\pi^+ D \rightarrow Ps\ P\pi^+\pi^-$$

and the 1c events

$$\pi^+ D \rightarrow Ps\ P\pi^+\pi^-\pi^o$$

in which the spectator proton is seen, the spectator protons are found to follow closely the Hulthen distribution and exhibit the expected angular isotropy in the laboratory, thereby confirming that the initial interactions are well described by the impulse approximation. The observed discrepancies for the unseen spectator proton 1c events are due to the fact that both the π^o and the spectator proton are missing. As a result, the unseen spectator protons tend to be fitted along or opposite to the π^o momentum, and hence lead to the forward backward peaking of the angular distribution. In addition, the inaccurate fitting of the spectator momentum results in a discontinuity in the expected Hulthen distribution in the region of 65 MeV/c. This arises because the sharing of the missing momentum for the unseen spectator proton events is weighted in favour of the π^o and hence the fitted unseen spectator proton momentum tends to be underestimated. Although the fitting of these events is incorrect, the momentum vector of the spectator is sufficiently small not to adversely affect the fitting of the rest of the tracks.

The minor discrepancies that exist for the well fitted 4c and seen spectator 1c events can be explained qualitatively by the additional modifications discussed below.

(e) THE VARIATION IN THE CENTRE OF MASS ENERGY

For interactions with stationary laboratory targets the variation in the centre of mass energy is entirely the result of the experimental spread in the beam momentum. For deuterium however, the constituent target nucleons follow the Hulthen distribution in momentum and hence add an additional spread of some 10% to the overall centre of mass energy in the π-N system. To calculate the π-N centre of mass energy, either the initial or final state particles can be used. However, in using the initial state particles it must be remembered that the target nucleon is off the mass shell. It is therefore insufficient to put the target momentum equal and opposite to the spectator, the effective mass of the two nucleons must also be constrained to the deuteron mass. The experimental distribution for the centre of mass energy determined from the secondaries is illustrated in FIG. 2.6.

(f) THE EFFECT OF THE FLUX FACTOR

A further consequence of the non zero momentum of the target nucleon is the flux variation depending on whether the target nucleon is moving towards or away from the primary. Both the flux and the centre of mass energy will be increased for the case where the interacting particles are moving towards one another. Hence if the cross section is independent of the centre of mass energy, a slight asymmetry will result in the spectator angular distribution, exhibiting a preference for forward going spectators in the laboratory. For resonance production however, the cross section has a strong dependence on the centre of mass energy, as described by the relation

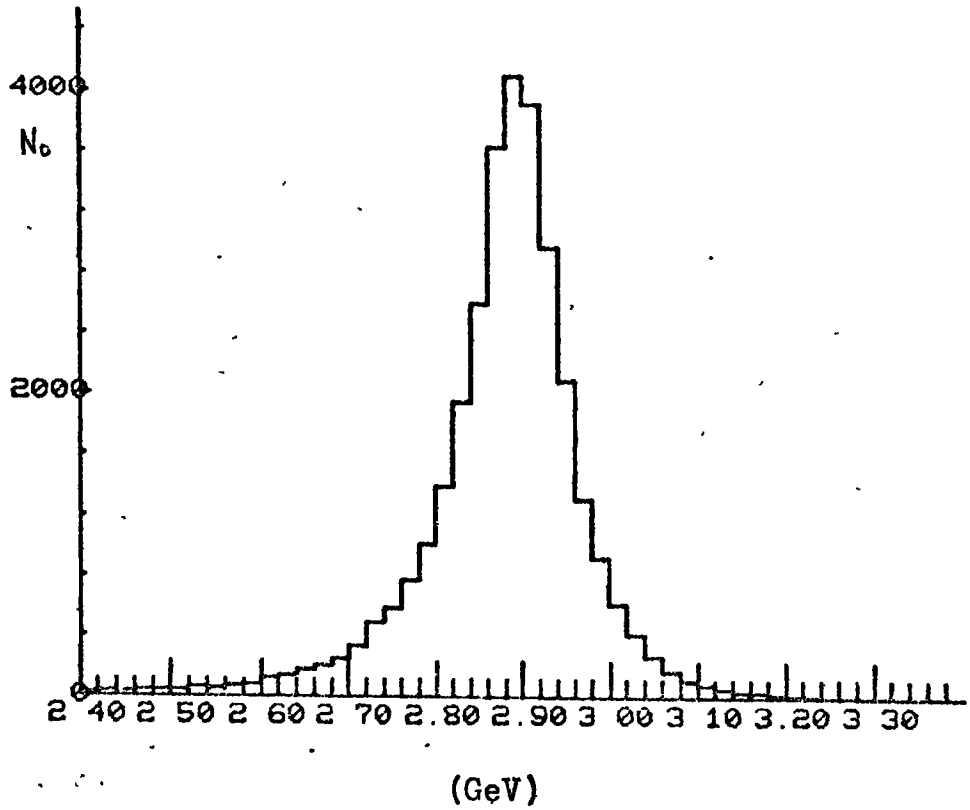

FIG. 2.6

THE CENTRE OF MASS ENERGY

$$\sigma \propto p^{-n}$$

where P is the primary momentum, and n is typically the order of 2. Hence in channels such as

$$\pi^+ D \rightarrow Ps\ P\pi^+\pi^-$$

which are dominated by resonance production, the variation of the resonance cross section with centre of mass energy is sufficient to reverse the above mentioned asymmetry in preference of backward going spectators. Experimentally such an asymmetry is observed for this channel in the ratio of 1 : 1.01. For the channel

$$\pi^+ D \rightarrow Ps\ P\pi^+\pi^-\pi^o$$

however, where the resonance production is less significant, the effects of the flux variation are found to dominate, and an asymmetry of 1 : 0.97 in preference of forward going spectators is observed. A plot of the experimental variation in the flux for the 4c channel

$$\pi^+ D \rightarrow Ps\ P\pi^+\pi^-$$

calculated from the relation

$$\text{FLUX} = \left| \frac{\vec{P\pi}^+}{E\pi^+} - \frac{\vec{P}N}{EN} \right|$$

where P and E refer to the momentum and energy of the particles indicated, is illustrated in FIG. 2.7.

(g) SECONDARY SCATTERING

The expression for the π - D scattering amplitude involves not only the one step amplitudes of the impulse approximation, but also the subsequent multiple scattering terms. In addition,

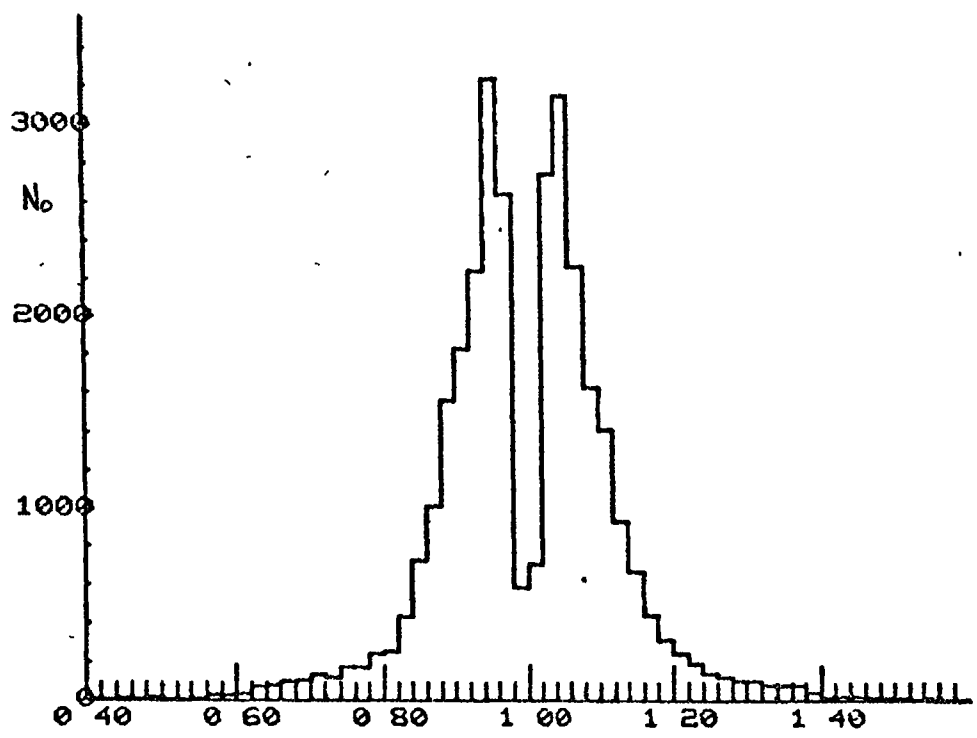

FIG. 2.7

THE FLUX VARIATION

a small but finite probability exists for the final state scattering between the spectator and any one of the other secondary particles. Either of these effects will result in a distortion of the expected Hulthen - like momentum distribution for the spectators. A further contribution to this effect may arise from the possible Δ-Δ states of the deuteron. The uncertainty principle enables the normal N - P components to transform momentarily into a $\Delta^{++}\ \Delta^{-}$ or $\Delta^{+}\ \Delta^{o}$ state. The existence of such states has never been confirmed, and recent results produced by members of the collaboration from the University of Birmingham, (Ref. 2.5), set an upper limit of 1% to this process. The resulting "spectator protons" from such a process are typified by momenta in excess of 0.8 GeV/c, and will therefore to a small and perhaps negligible extent add to the distortion of the expected Hulthen - like momentum distribution. The cumulative effect of these processes can account for the observed excess of spectator momenta greater than 300 MeV/c, illustrated in FIG. 2.5.

(h) SHADOWING EFFECTS

The mutual shadowing of the constituent nucleons implies that the total deuterium cross section is less than the sum of the individual nucleon cross sections. Hence the microbarn equivalent for a π-N event from a deuteron target is greater than its counterpart produced from a free neutron target. The relation between the cross sections is given by

$$\sigma(\pi D) = \sigma(\pi N) + \sigma(\pi P) - \frac{\sigma(\pi N).\sigma(\pi P)}{4\pi\langle r^2\rangle}$$

where $\langle r^2 \rangle$ is the average separation of the nucleons. Although this expression is not charge independent, the necessary correction terms are negligible, (Ref.2.6). Therefore, using the values for the π - P cross sections

$$\sigma(\pi^+ P) = 27.5 \text{ mb}$$

$$\sigma(\pi^- P) = 34.1 \text{mb} = \sigma(\pi^+ N)$$

and the experimentally determined $\pi^+ D$ cross section of 56 mb, the magnitude of the R.M.S. separation of the nucleons is evaluated as 3.7 ± 0.2 f which compares favourably with the value determined from electron scattering data, (Ref. 2.7).

(I) THE PAULI EXCLUSION PRINCIPLE.

The Pauli exclusion principle postulates that a symmetric wave function of two identical fermions is not allowed. This has important consequences in deuterium interactions since the occurence of two final state identical fermions leads to a depletion of events in the low 4 - momentum transfer region to the target nucleon.

The overall deuteron wave function factorises into the spin component and the orbital angular momentum component. The spin terms which are all symmetric can be written as

$$\chi(1,1) = \chi_{N1}(\tfrac{1}{2},\tfrac{1}{2}) \cdot \chi_{N2}(\tfrac{1}{2},\tfrac{1}{2}) \quad \ldots\ldots\ldots (1)$$

$$\chi(1,0) = \frac{1}{\sqrt{2}} \left[\chi_{N1}(\tfrac{1}{2},\tfrac{1}{2}) \cdot \chi_{N2}(\tfrac{1}{2},-\tfrac{1}{2}) + \chi_{N1}(\tfrac{1}{2},-\tfrac{1}{2}) \cdot \chi_{N2}(\tfrac{1}{2},\tfrac{1}{2})\right] \ldots\ldots (2)$$

$$\chi(1,-1) = \chi_{N1}(\tfrac{1}{2},-\tfrac{1}{2}) \cdot \chi_{N2}(\tfrac{1}{2},-\tfrac{1}{2}) \quad \ldots\ldots\ldots (3)$$

where the subscripts indicate the two nucleons and the indices the values of (S, Sz). If spin non-flip occurs then the above functions still describe the final spin states, and only the orbital components alter. However, since the Pauli principle forbids overall symmetric wave functions, the orbital components must be antisymmetric and contain only odd ℓ values. Alternatively, in the case of spin flip, events described by (1) and (3) flip into (2), or the anti-symmetric state (4).

$$\chi(0,0) = \frac{1}{\sqrt{2}} \left[\chi_{N1}(\tfrac{1}{2},\tfrac{1}{2}) \cdot \chi_{N2}(\tfrac{1}{2},-\tfrac{1}{2}) - \chi_{N1}(\tfrac{1}{2},-\tfrac{1}{2}) \cdot \chi_{N2}(\tfrac{1}{2},\tfrac{1}{2}) \right] \quad \ldots\ldots(4)$$

This situation only allows events with odd ℓ for the spin states (1) to (3), and even ℓ for the spin state (4). From this discussion it is evident that the correction for the number of events lost via spin flip is smaller than that for spin non-flip, since in the latter case all even ℓ - states are forbidden.

To estimate the loss of events in the differential cross section, $d\sigma/dt$ is expressed in terms of the partial flip and non-flip cross sections, (see Ref. 2.8 and Appendix one).

$$\left(\frac{d\sigma}{dt}\right) = \left[1 - \tfrac{1}{3} H(q)\right] \left(\frac{d\sigma}{dt}\right)_{\text{FLIP}} + \left[1 - H(q)\right] \left(\frac{d\sigma}{dt}\right)_{\text{NON FLIP}} \quad \ldots(5)$$

where H(q) is the deuteron form factor, and q the 3-momentum transfer ($\sim t^{\frac{1}{2}}$). H(q) however, can be written as

$$H(q) = 4\pi \int \phi(r)^2 \quad \frac{\sin q\, r}{q\, r} \quad r^2 \, dr$$

where $\phi(r)$ is the spacial wave function,

and evaluated as a function of t by using the value of r calculated in the previous section. The upper and lower limits to the event loss can then be determined as a function of t, by assuming the domination of either spin flip or spin non-flip. The resulting correction factors are illustrated in FIG. 2.8, the division of the experimental results by these figures giving the corrected values. The results indicate that the effect is only of importance for t - values less than 0.05 $(GeV/c^2)^2$.

In the above calculation however, the use of equation (5) does not allow the effects of the Pauli principle to be determined for the seen and the unseen spectator proton events separately. Its use effectively implies an integration over all final state proton momenta and hence does not differentiate between the above two classes of events.

The work of the Durham collaboration however, summarised in Appendix one, illustrates how this situation can be avoided. Essentially a visibility limit is specified for the protons and the integration is performed separately over the seen and unseen spectator proton events. The correction factors resulting from such a calculation are shown in FIG. 2.9, and as can be seen the results for the spin flip and spin non-flip cases are in excellent agreement with the above calculations. This approach however, also enables a calculation to be made of how the spin flip and spin non-flip processes will affect the seen and unseen spectator proton events. The results of such a calculation are shown in FIG. 2.10, which illustrates the expected ratio of these two classes of events plotted as a function of the square of the momentum transfer t ,

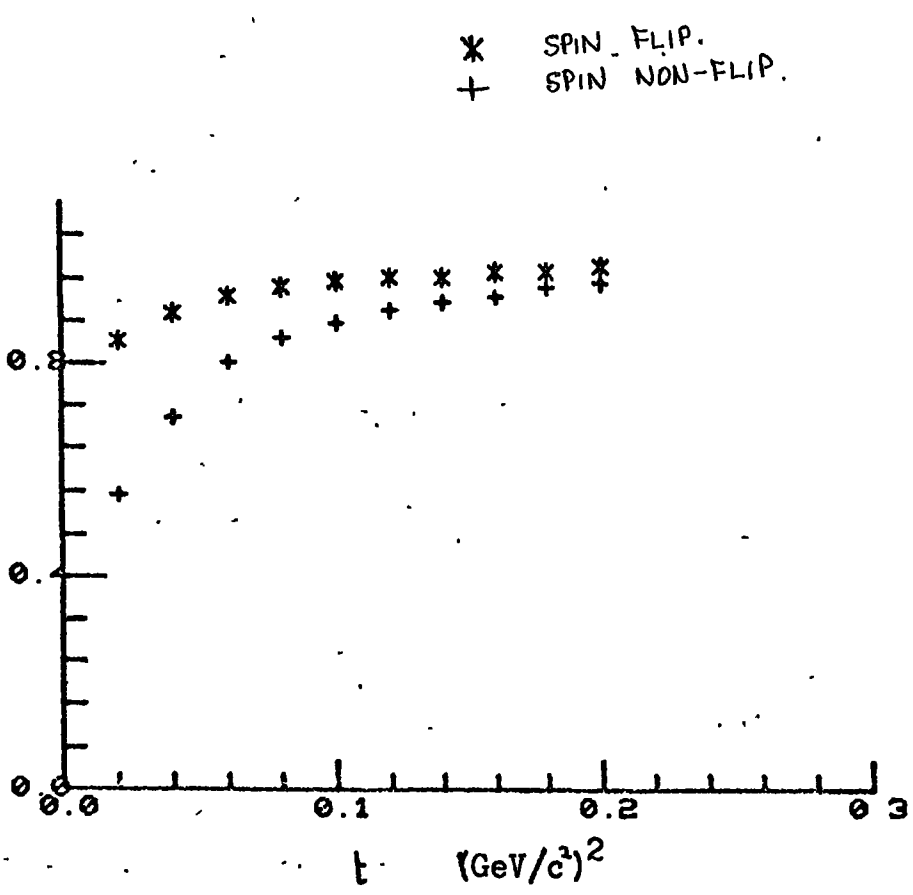

FIG. 2.8 THE PAULI CORRECTIONS

(ENERGY AND MOMENTUM NOT CONSERVED)

SEE APPENDIX ONE

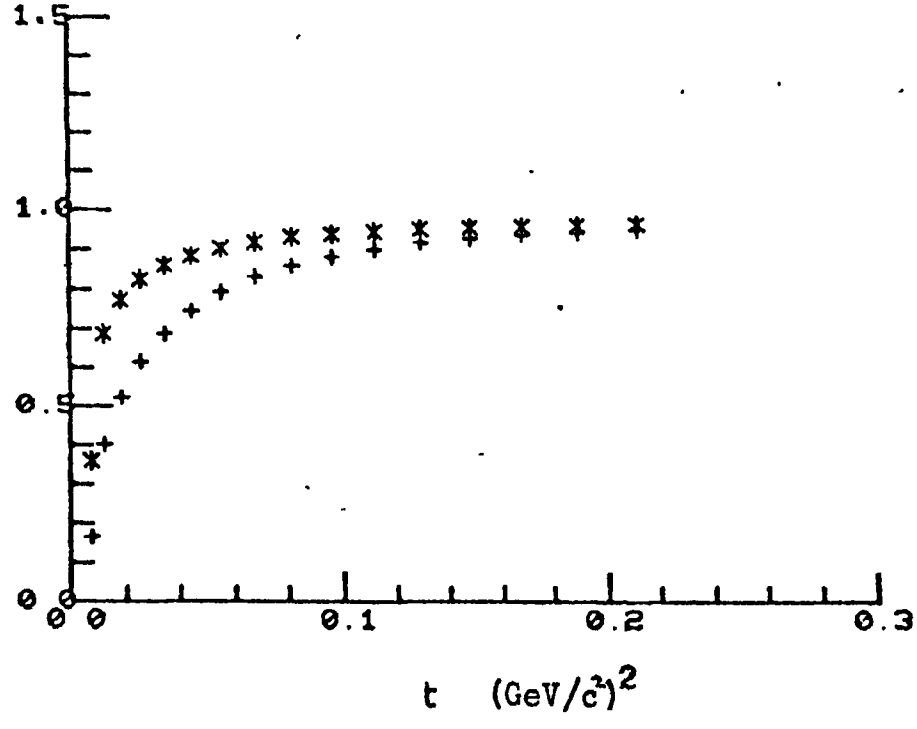

FIG. 2.9 THE PAULI CORRECTIONS

(ENERGY AND MOMENTUM CONSERVED)

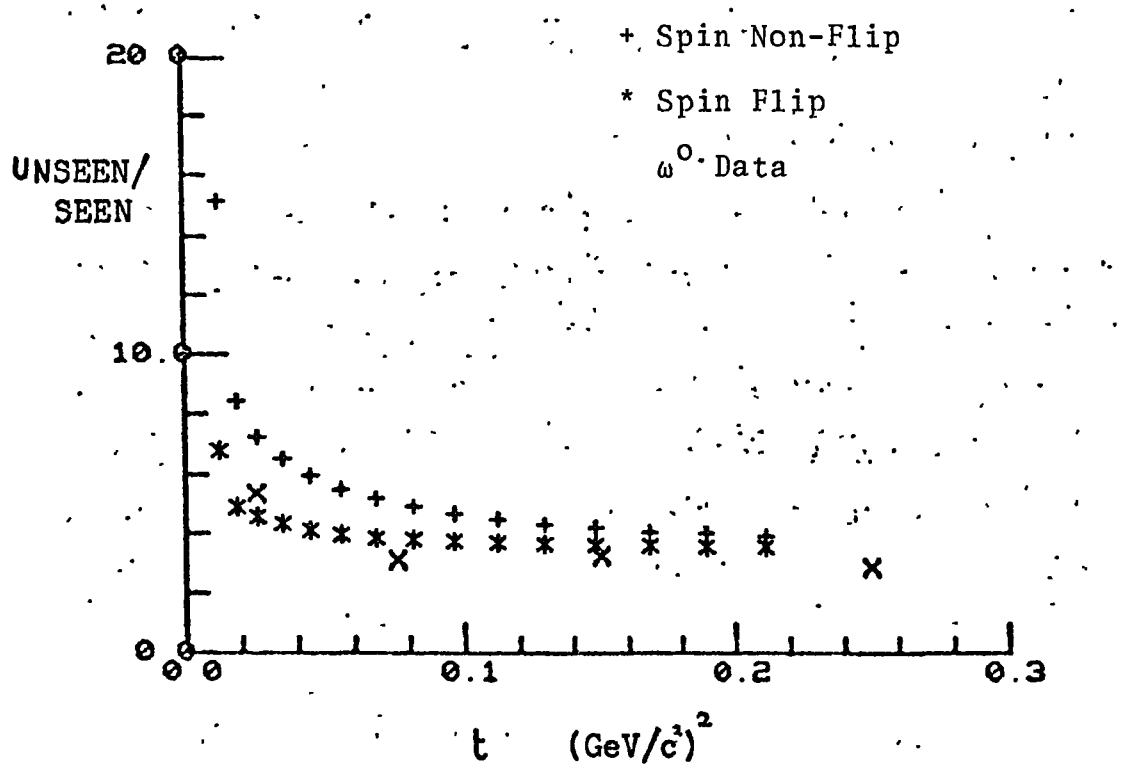

FIG. 2.10 THE RATIO OF SEEN AND UNSEEN † SPECTATOR PROTONS AS A FUNCTION OF THE MOMENTUM TRANSFER.

† The visibility limit was set to 110 MeV/c

measured from the target deuteron to the di-proton system. The results are preliminary results only, and have yet to be confirmed. In their present form however, they have some very important implications. Namely that the Pauli exclusion principle does not have the same effect on the seen and unseen spectator proton events, and in particular implies that the production processes resulting in the spin non-flip of the recoiling proton will dominate the unseen spectator proton events at low t. Consequently consistency between these two classes of events should not be expected in the low t - region.

CHAPTER THREE

THE PROCESSING OF THE EVENTS

INTRODUCTION

In this chapter, the stages from the scanning of the events to the production of the final sample for analysis are discussed, particular emphasis being applied to the errors introduced and to the quality of the data finally achieved.

3.1 THE SCANNING OF THE FILM

Throughout the exposure test strips of the film were taken consisting of some 30 frames from the end of each roll. By this procedure, the general quality of the film was monitored. Checks were made on the uniformity of the illumination and for signs of consistent scratching or stretching of the film. In addition, the track density, bubble size and track count were observed in order to ensure correct operation of the chamber and beam line. An example of the quality of the film is illustrated in FIG. 3.1, which shows a sample frame of the film taken during the first exposure. In all some 850K frames were taken, with an average yield of about 2 events per frame. Initially all events were scanned for in order to estimate the total $\pi^+ D$ cross section, but throughout the majority of the analysis scanning rules were used to select the required events for measurement.

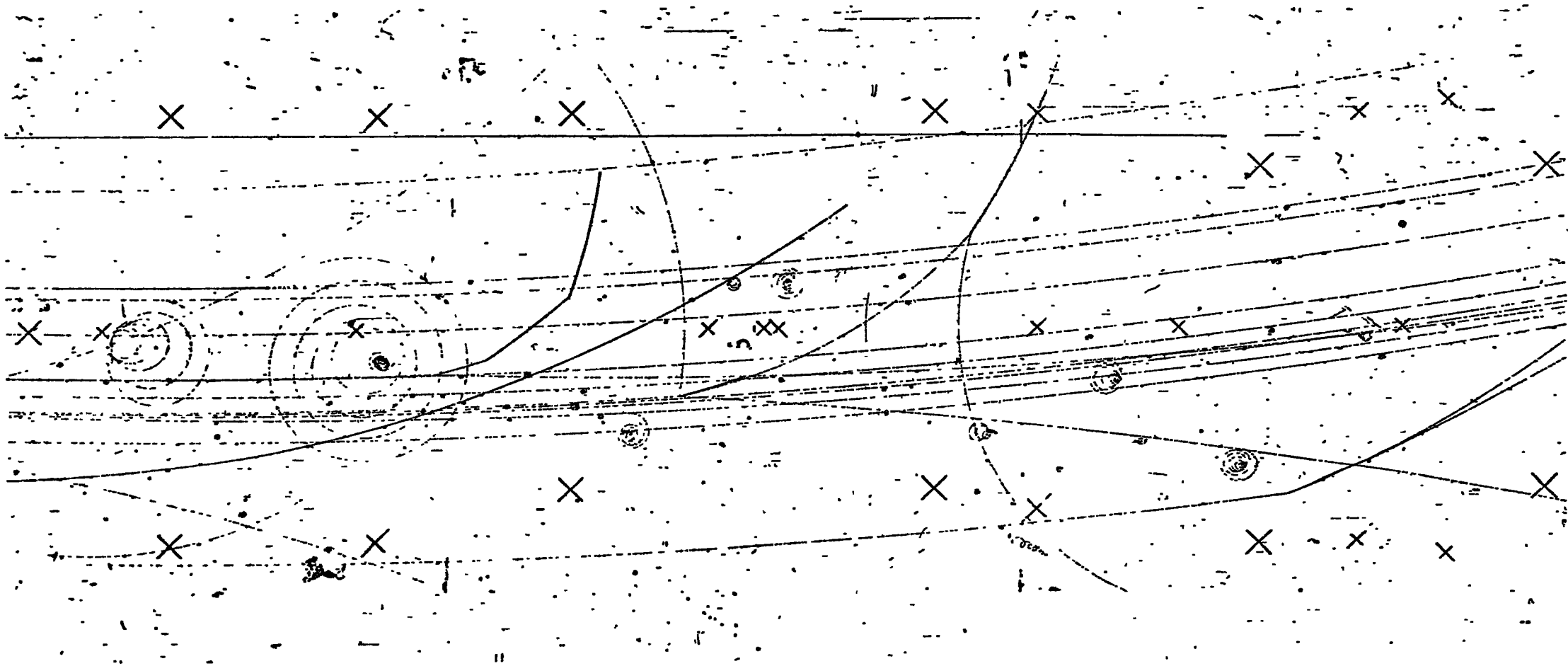

FIG. 3.1

A SAMPLE FRAME FROM THE 1st EXPOSURE

(a) THE SCANNING RULES

The events to be sought were all π^+N events apart from 1 - prong scatterings, and all events produced in association with V^o's. As mentioned in the previous chapter the characteristic of π^+N events is the occurrence of the proton spectators. Events in which the spectator proton is not visible will have an odd number of outgoing tracks and are therefore unambiguously identified as neutron target events. For even prong events however, where the spectator proton must be seen, the form of the Hulthen distribution shown in FIG. 2.5, implies that the majority of the spectator protons will have momenta less than 300 MeV/c and should stop within the chamber, with a maximum track length of some 25 cms. Therefore the even prong π^+N events are characterised by at least one stopping proton. The above rule is modified for the particular case of two - prong events. Here, two identifiable protons are required, and in addition, at least one must be observed to stop. The final category, corresponding to the strange particle productions are identified by the associated V^o and hence all V^o events are recorded. In all cases, the off-beam events were excluded and the accepted events restricted to the fiducial volume illustrated in FIG. 3.2.

To summarise therefore, the scanning rules were as follows:-

(a) All events with a V^o

(b) All odd pronged events

(c) All even prongs (>2) with at least one associated stopping proton.

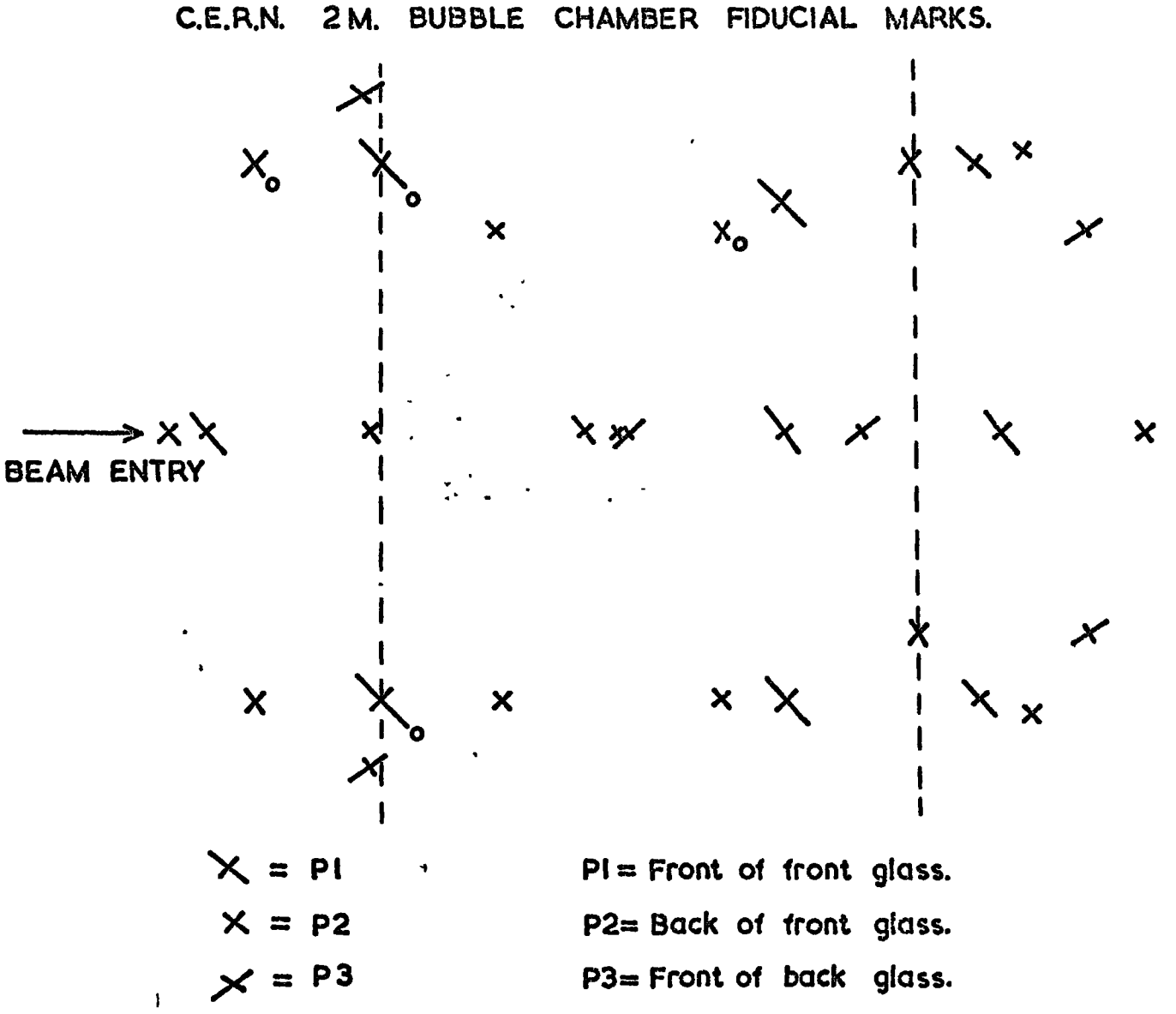

FIG. 3.2

THE FIDUCIAL VOLUME

and (d) Two prong events with two identifiable protons, one of which must be observed to stop.

In addition, kinks, secondary scatters and Dalitz pairs were recorded, and at intervals of every 50 frames a beam count was made for both the first and second pulses. The number of events selected by the procedure corresponded to approximately 1 event every 2 frames.

(b). SCANNING LOSES

A small number of frames were considered unmeasurable either as a result of fogging or from excessive scratching on the film. In addition there are losses of events through imperfect scanning efficiencies, or from events undetected by the chamber. By re-scanning several of the rolls, the scanning efficiency was found to be of the order of 95% with an even spread over all topologies. The most common omissions were the small spectator proton stubs, effectively hidden by other secondaries, or produced at steep angles in the chamber. This loss however, is not thought critical since these events will be reduced to odd prongs and consequently treated as missing spectator events. As a result the majority of the lost information is regained. An additional loss to the missing spectator events arises from events in which the 4 - momentum transfer to the target nucleon is so small that both the interaction and spectator protons will be unobservable. This loss however, as discussed in the previous chapter is effectively included in the correction for the Pauli exclusion principle, since the vast majority of these events will lie in the t - interval dominated by this effect. In conclusion therefore, the scanning losses are considered negligible.

3.2 THE CROSS SECTION EVALUATION

As mentioned in the previous section, initially all events were scanned for, and from a sample of some 38,750 frames the number of events found was 85,067. A breakdown of the events into prong sizes is shown in table 3.1, along with the corresponding cross sections.

The total cross section is calculated from the expression

$$\sigma = (n\lambda)^{-1}$$

where n is the number of interaction centres /c.c. , and λ the mean free path between interactions. When expanded in terms of the total length of beam track, L, for all interactions it becomes,

$$\sigma = \frac{N A}{L N_o d}$$

where N is the total number of interactions, A, the atomic weight for deuterium, No avogadros number, and d the density of liquid deuterium. Since the distribution of interaction points is effectively linear throughout the fiducial volume, the total length of beam track L, is given by

$$L = 10.3\left(L f\right) N' - \left(Lf\right) n/2$$

where Lf is the length of the fiducial volume scanned (= 107 cm), N' the total number of frames, n the number of events, and 10.3 the average number of beam tracks per frame. Allowing therefore for a 5% beam contamination, the above sample of scanned events yields a total $\pi^+ D$ cross section of 50.4 $\pm$ 4 mb, which is in good agreement with the value of 56 $\pm$ 1 mb obtained from counter experiments, (Ref. 3.1). The microbarn equivalent for the total experiment was calculated by assuming the

TABLE 3.1

THE TOPOLOGICAL CROSS SECTIONS

PRONG SIZE	THE NUMBERS OF EVENTS	CROSS SECTION mb
1	8776	5.21
2	30834	18.32
3	14574	8.66
4	24197	14.37
5	3109	1.85
6	3143	1.87
7	118	0.07
8	93	0.06
9	2	0.001
ALL	84846	50.4

counter experiment value of 56 $\pm$ 1mb. This yielded a value of 0.066 $\pm$ 0.007 μb/event.

3.3 THE MEASUREMENT OF THE EVENTS

The measurement of the film was undertaken in two stages. Firstly each event was pre-digitised to a point accuracy of some 25 μ on the table. At Durham, 4 image plane digitisers were used, and the sequence of measurements for each event were:-

(a) The primary vertex
(b) The beam track
(c) Two fiducial crosses
(d) Any secondary vertex
(e) The tracks associated with the secondary vertex
(f) The tracks associated with the primary vertex
(g) Two more fiducial crosses

and (h) The primary vertex again..

This was repeated for each view, and in all cases two points per track were taken. This information was then passed on to the measuring device.

(a) THE R.H.E.L. HPD1 AUTOMATIC MEASURING MACHINE

This machine uses the flying spot technique, whereby a light spot of some 10μ diameter scans across and along the film in the region specified by the pre-digitising, and by simultaneously focussing on a digitising grating records the x and y coordinates of the tracks. The spacing of the scan lines on the film is of the order of 90 μ and the typical R.M.S. error for a track so measured is in the region of 2 to 3 μ on

the film. The main advantage of this device is its speed of measurement, whereby it can handle some 100 events per hour compared to only some 3 per hour on a conventional machine. In addition the machine measures the relative bubble density of all the tracks in an event. Utilization of this information reduces the necessity for human intervention, whereby certain events have to be returned to the scanning table to estimate track ionisation and thereby resolve certain ambiguities in the final fits. After the HPD has digitised the tracks the results are converted into master points, and on average one master point is produced every 2.5 cms. of track in real space. A typical error on such a point is 30μ in the x - y plane and 300μ in the z direction.

(b) THE MEASUREMENT ERRORS

At incident pion moments of 4 GeV/c, the typical momentum for a secondary is in the region of 1 GeV/c, with a track length of some 50 cms. in the chamber. From the previous section this implies that some 20 master points will be produced for most of the tracks. In addition, since the tracks are mainly produced in the x - y plane a typical error on the location of these points will be of the order of 50μ. If we consider just 3 of these points as illustrated in FIG. 3.3, the relative error on the track momentum is given by,

$$\left(\frac{\Delta P}{P}\right)_{MEAS.} = \frac{(1.5)^{\frac{1}{2}}\,\sigma P}{3.75 \times 10^{-5}\, L^2 H}$$

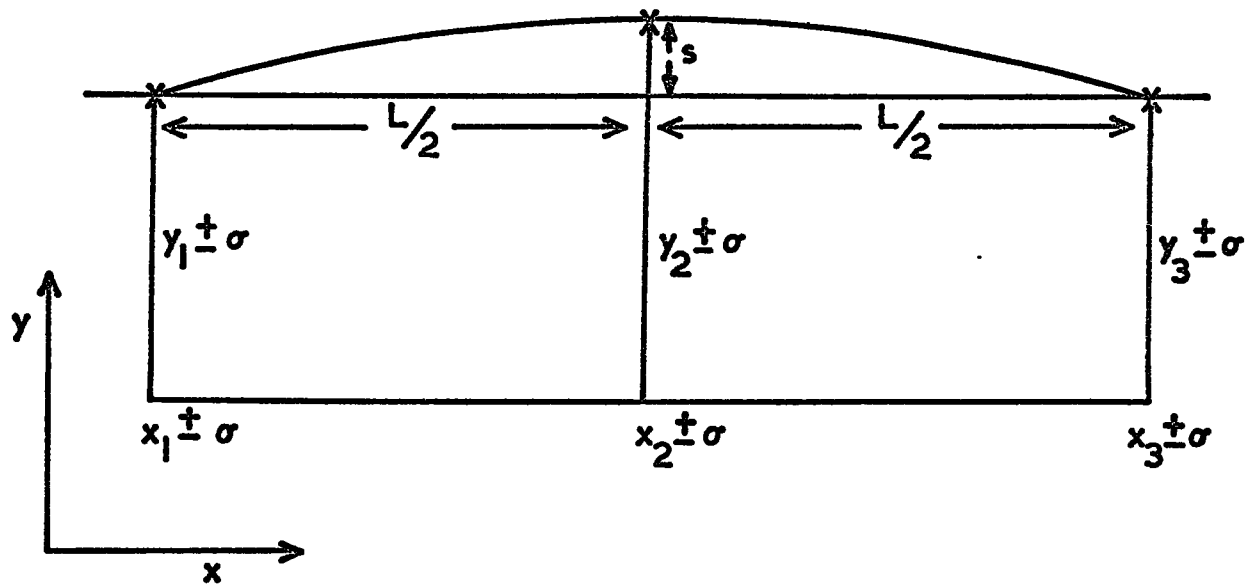

FIG. 3·3

ERRORS ON CURVATURE MEASUREMENTS.

By substituting in this expression with values of $\sigma = 50\mu$ P = 1.0 GeV/c, L = 50 cms. and H = 17.5 K gauss, the resulting error is 0.4%. This obviously represents an upper limit since the accuracy will be improved considerably by using all 20 points as opposed to just 3. Comparing this error with the 1% multiple scattering error mentioned in the previous chapter it is evident that the precision is restricted mainly by the coulomb errors rather than the measurement errors.

3.4 THE RECONSTRUCTION OF THE EVENTS

This is achieved by using the Rutherford Laboratory 3 - dimensional reconstruction programme GEOMETRY, (Ref.3.2). After allowing for optical distortions and film stretch, the master point film coordinates are used to reconstruct the event, and thereby calculate the vertex positions and centre of track momenta. In addition, the corresponding azimuthal angles, dip angles and associated errors are calculated. The magnitude of the errors in terms of a percentage are illustrated in FIG. 3.4 and represent the total error estimates after including all the above mentioned effects. The results shown correspond to a π^- secondary and the seen spectator protons from the reaction

$$\pi^+ D \rightarrow Ps\ P\ \pi^+\pi^-\pi^0$$

Apart from the spectator proton, the results for the π^- are typical for all the measured secondaries from both the 4c and 1c channels i.e.

$$\left(\frac{\Delta P}{P}\right) \sim 1.5\% \ , \quad \left(\frac{\Delta\lambda}{\lambda}\right) \sim 0.5\% \quad \text{and} \quad \left(\frac{\Delta\phi}{\phi}\right) \sim 0.1\%$$

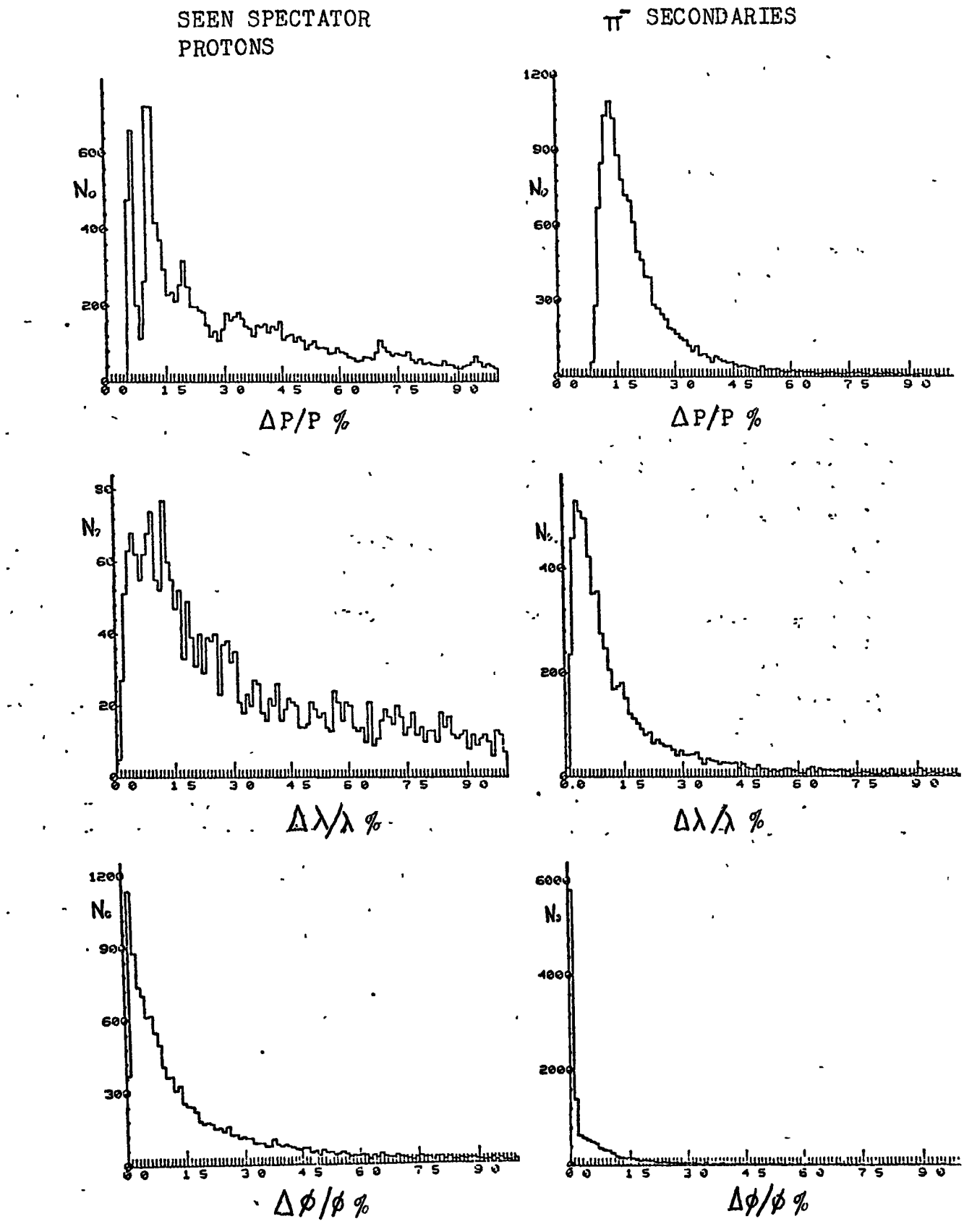

FIG. 3.4 THE MEASUREMENT ERRORS FOR THE SEEN SPECTATOR PROTONS AND π^- SECONDARIES EXPRESSED AS A PERCENTAGE.

The relative errors for the dip angles (λ) are larger than for the azimuthal angles (ϕ) since the measurement errors in the z - direction are larger than in the x - y plane. The results for the spectator protons are different because of the shorter track lengths available for measurement. As illustrated in FIG. 3.4 the angular errors are greater, and in addition, the relative error on the centre of track momentum exhibits a double structure. The two peaks result from the fact that a large number of the spectators are observed to stop in the chamber. Hence for this particular class of events the track momenta can be estimated from the range, which for short tracks results in smaller errors than the curvature measurements.

3.5 THE KINEMATIC FITTING OF THE EVENTS

After reconstruction, the events are fitted to a series of hypotheses. This was achieved by using the Rutherford Laboratory KINEMATICS programme, (Ref. 3.3). Each hypothesis is tested by demanding conservation of energy and momentum as described by the following equations, and in each case a χ^2 probability for the fit is calculated.

$$\Sigma\, Px = \sum_i (P_i \cos\lambda_i \cos\phi_i) - P\cos\lambda\cos\phi \;\rightarrow\; 0$$

$$\Sigma\, Py = \sum_i (P_i \cos\lambda_i \sin\phi_i) - P\cos\lambda\sin\phi \;\rightarrow\; 0$$

$$\Sigma\, Pz = \sum_i (P_i \sin\lambda_i) - P\sin\lambda \;\rightarrow\; 0$$

$$\Sigma\, E = \sum_i (P_i^2 + m_i^2)^{\frac{1}{2}} - ((P^2+m^2)^{\frac{1}{2}} + M_D) \;\rightarrow\; 0$$

where the summation is over the outgoing particles

If there are no neutral particles in the final state, all four constraint equations can be used and hence the fits are termed 4 - constraint, (4c), fits. With a neutral particle of known mass missing however, the 3 momentum equations have to be used to solve for P, λ and ϕ for the missing particle, leaving the energy equation as the only constraint. This results in the so called 1c fits. The fits to the channel

$$\pi^+_D \rightarrow p_s p\pi^+\pi^-\pi^0$$

are 1c fits, and the relative error on the momentum, dip, and azimuthal angles for the fitted π^0 and unseen spectator protons are illustrated in FIG. 3.5. As expected, these are considerably larger than the corresponding errors on the seen tracks which have relative errors of a similar magnitude to those shown at the reconstruction stage in FIG. 3.4. If all the measured variables were known exactly, the above constraints would be sufficient to restrict only one acceptable hypothesis to each event. In practice however, the limited experimental accuracy enables several hypotheses to fit each event, and therefore a process for deciding which fit is most likely to be correct has to be devised.

3.6 IONISATION TESTS

The number of hypotheses fitting each event can be reduced by making ionisation tests on the secondary tracks. If the calculated ionisation for a track of a given hypothesis differs by more than a pre - determined amount from that measured, the hypothesis is rejected. The majority of these tests are handled internally by the programme JUDGE, (Ref.3.4),

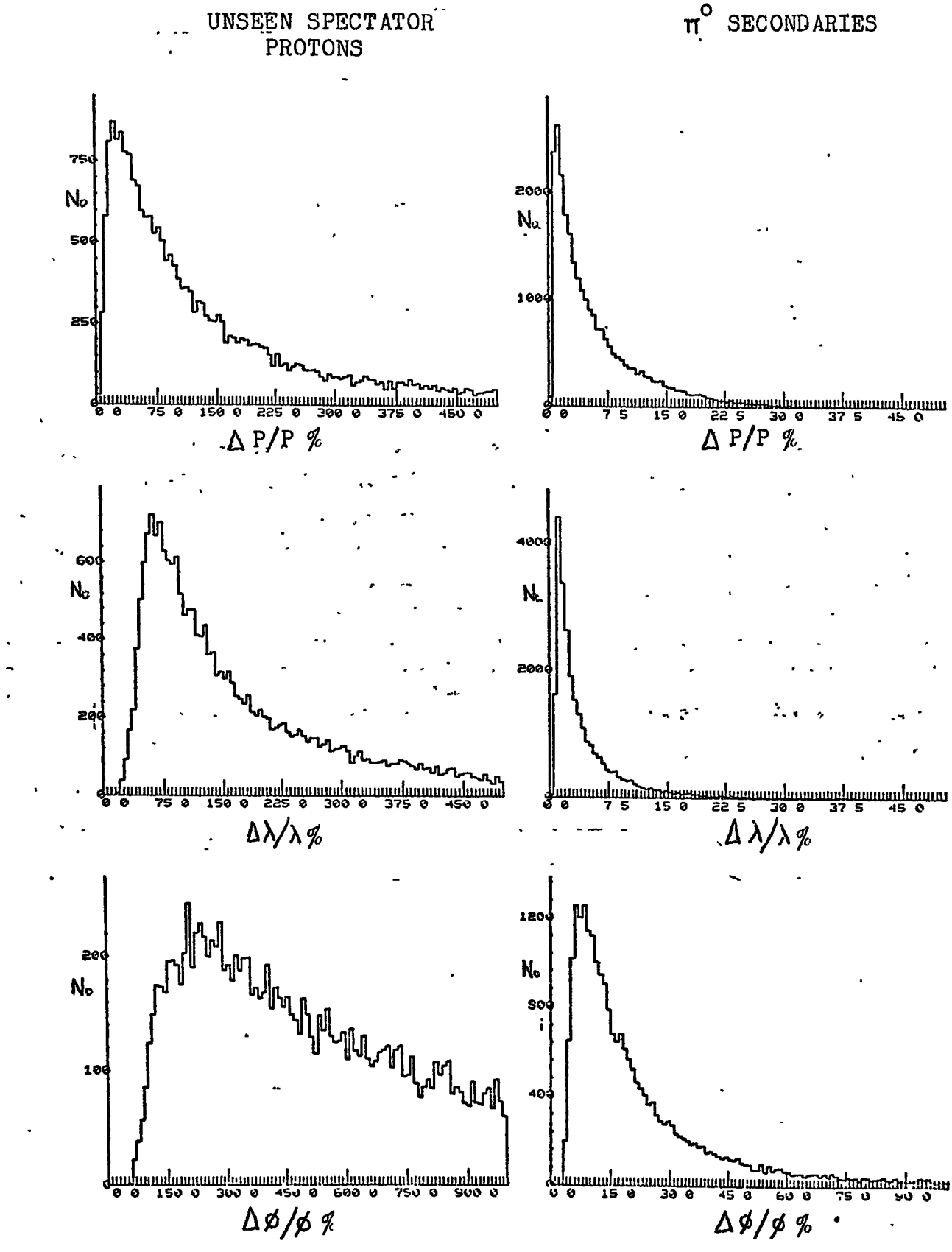

FIG. 3.5 THE FITTING ERRORS FOR THE UNSEEN SPECTATOR PROTONS AND π^0 SECONDARIES EXPRESSED AS A PERCENTAGE.

and only some 5% require human intervention by returning them to the scanning table and estimating the ionisation by eye.

3.7 THE AMBIGUITIES

After the above processing a data summary tape of the accepted events was made. The number of events which gave a fit to the 4c channel

$$\pi^+ D \rightarrow P_s p \pi^+ \pi^-$$

was 32,417, and the number fitting the 1c channel

$$\pi^+ D \rightarrow P_s P \pi^+ \pi^- \pi^0$$

was 58,891. However, as mentioned above, many of these fits are ambiguous, since the same events also provide fits to other channels. An indication of the types of ambiguities for these channels is given in table 3.2. The results illustrate that the events with unseen spectator protons and π^0's provide more ambiguities. This effect arises from the fact that the extra missing information makes the constraints to the fit less rigorous, thereby allowing more hypotheses to be fitted.

From the ambiguity table it can be seen that there is a large number of proton beam fits. For the well constrained 4c fits to the channel

$$\pi^+ D \rightarrow P_s P \pi^+ \pi^- \quad \ldots\ldots\ldots (1)$$

some 48% are ambiguous with the 4c proton beam hypothesis

$$P D \rightarrow P P P \pi^- \quad \ldots\ldots\ldots (2)$$

Since however, as calculated in section 2.2, the estimated proton beam contamination was found to be only $4 \pm 3\%$ it was decided to disregard the proton beam fits. Additional

TABLE 3.2

THE AMBIGUITIES

MAIN HYPOTHESIS →	$\pi^+ D \rightarrow P_S P \pi^+ \pi^-$		$\pi^+ D \rightarrow P_S P \pi^+ \pi^- \pi^0$	
AMBIGUITIES	SEEN SPECTATOR PROTON EVENTS	UNSEEN SPECTATOR PROTON EVENTS	SEEN SPECTATOR PROTON EVENTS	UNSEEN SPECTATOR PROTON EVENTS
$\pi^+ D \rightarrow P_S P \pi^+ \pi^-$	542	2,312	593	3,136
$\pi^+ D \rightarrow P_S P \pi^+ \pi^- \pi^0$	1,537	4,516	2,744	6,187
$\pi^+ D \rightarrow P_S N \pi^+ \pi^+ \pi^-$	620	547	5,222	8,000
$\pi^+ D \rightarrow D \pi^+ \pi^+ \pi^-$	71	78	129	27
$\pi^+ D \rightarrow D \pi^+ \pi^+ \pi^- \pi^0$	1,511	2,447	1,623	1,805
$\pi^+ D \rightarrow P P K^+ K^-$	1,235	4,545	694	2,720
$P D \rightarrow P P P \pi^-$	3,849	11,885	1,054	5,334
UNAMBIGUOUS EVENTS	5,307	5,551	11,617	23,157
THE TOTAL NUMBER OF EVENTS	11,048	21,369	18,844	40,047

Note, any one event may be ambiguous with more than one hypothesis.

confirmation that the proton beam fits are erroneous is the observed strong ρ^0 and f^0 signals seen in the $\pi^+\pi^-$ effective mass combination for reaction (1), confirming that this hypothesis represents the true fit. The $\pi^+\pi^-$ mass spectrum for the proton beam ambiguous events with χ^2 probability > 0.5 is illustrated in FIG. 3.6, and from this it is evident that the proton beam contamination is consistent with the $4 \pm 3\%$ level previously estimated.

The remaining ambiguities were resolved by the following procedure. Fake calculations indicate that a fit to a 4c hypothesis should always be taken in preference to a 1c hypothesis. The basis of this selection arises from the fact that the generated 1c events rarely provide acceptable 4c fits unless the errors on the measured tracks are made unduly large. Since this experiment has relatively small measurement errors, the above selection procedure was adopted.

It should be noted however, that the reverse case of a true 4c event rarely providing a fit to a 1c channel is not correct. As mentioned in more detail in chapter 5 it has been found that from a sample of 10,000 generated 4c events of the type

$$\pi^+ D \rightarrow P_S\ P\ \pi^+\pi^-$$

6% provide unambiguous fits to the 1c channel

$$\pi^+ D \rightarrow P_S\ P\ \pi^+\pi^-\pi^0$$

This has important consequences, since not only will events be lost from reaction (1), but they will also contribute towards reaction (2) in the form of good unambiguous events.

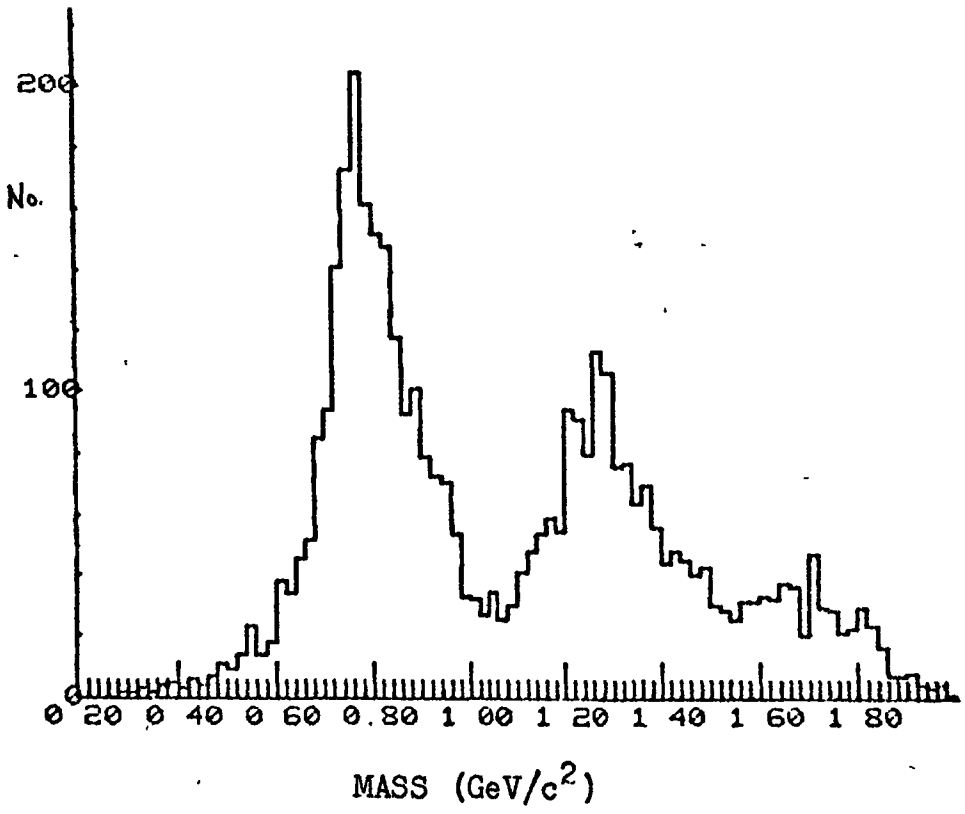

FIG. 3.6 THE $\pi^+ \pi^-$ EFFECTIVE MASS SPECTRUM FOR PROTON BEAM FITS WITH $P(\chi^2)>0.5$

(a) THE SELECTION OF THE CHANNEL $\pi^+ D \rightarrow Ps\ P\pi^+\pi^-\pi^o$

The ambiguities for this channel are shown in table 3.2. Since this hypothesis corresponds to a 1c fit, the 4c ambiguities were always taken in preference. Hence the only relevant ambiguities are the other 1c hypotheses fitting the event. These ambiguities were resolved by always accepting the fits with the greatest χ^2 probabilities. The danger here is that the true fits to the events may be rejected in favour of a spuriously better fitting hypothesis. That this is not important can be seen in FIG. 3.7, where the $\pi^+\pi^-\pi^o$ effective mass distribution is shown for the accepted and rejected events. Since the dominant feature of the ω^o production seen in the accepted events is not observed in the rejected events there is evidently no serious loss of genuine events.

An indication of the purity of the final sample is given by the χ^2 probability and missing mass squared distributions. For a pure sample the χ^2 probability should be evenly distributed between zero and 1.0, and the missing mass squared distribution symmetric about the π^o mass squared. In practice however, an excess of events was found at low χ^2 probabilities and large missing mass squared values. The most probable source of these events is NOFITS, i.e.events with more than one missing neutral. Hence the following χ^2 probability cuts were made, the accepted events corresponding to

χ^2 probability > 0.06 for unseen spectator proton events

and χ^2 probability > 0.02 for seen spectator proton events.

These correspond to approximately a two standard deviation

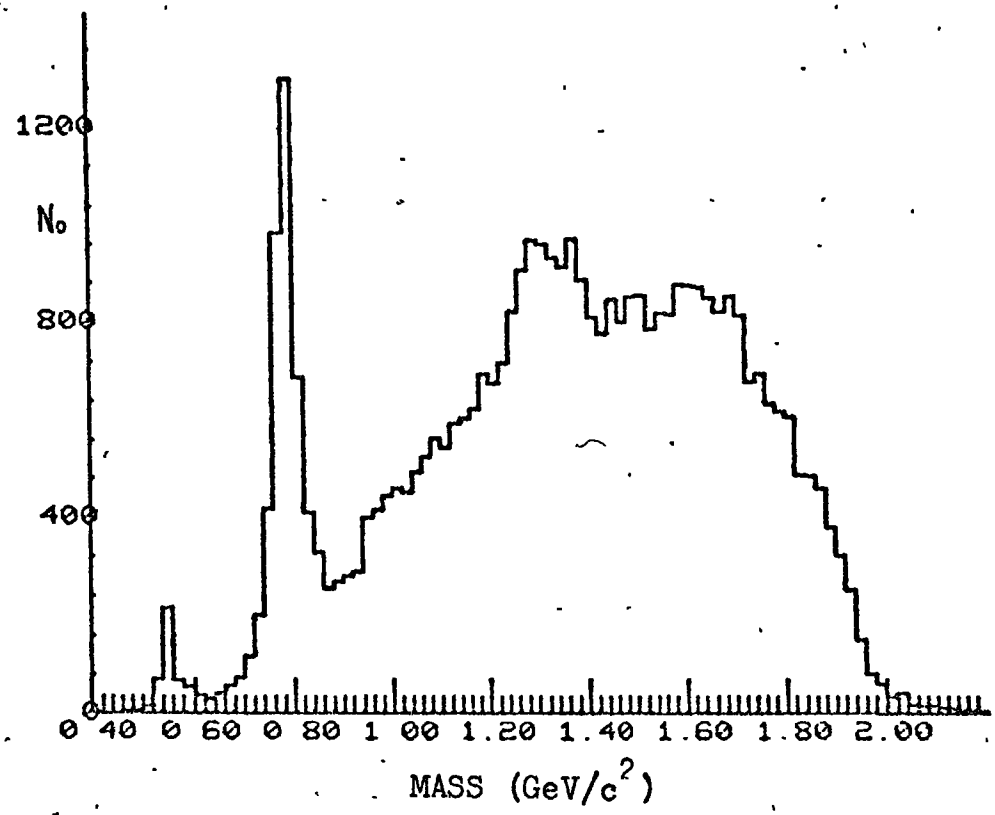

FIG. 3.7(a) THE ($\pi^+ \pi^- \pi^0$) EFFECTIVE MASS SPECTRUM FOR THE ACCEPTED EVENTS

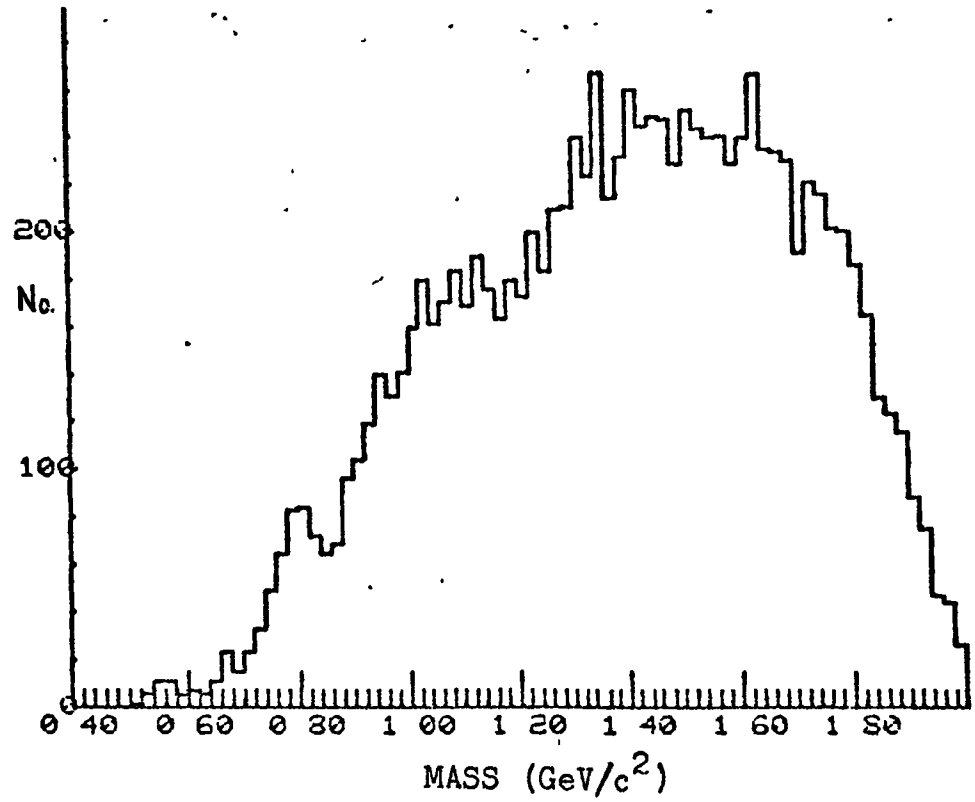

FIG. 3.7(b) THE ($\pi^+ \pi^- \pi^0$) EFFECTIVE MASS SPECTRUM FOR THE REJECTED EVENTS

cut on the missing mass squared distribution, i.e.

$$MM^2 - 2\,\Delta MM^2 < m\pi^{o2} \qquad \text{for } MM^2 > m\pi^{o2}$$

and $$MM^2 + 2\,\Delta MM^2 > m\pi^{o2} \qquad \text{for } MM^2 < m\pi^{o2}$$

thereby effectively removing the excess of events at large MM^2 values. After the above selection, the final sample for analysis was 41,341 events. The corresponding MM^2, missing energy, missing momentum and χ^2 probability distributions for the seen and unseen spectator proton events are shown in FIG. 3.8.

In the selection of the above channel it must be remembered that the selection criteria are not absolutely efficient and although any breakthrough of wrongly assigned events is obviously greatly reduced, a certain number will nevertheless remain in the final sample.

3.8 THE RESOLUTION IN MASS AND THE SQUARE OF THE 4 - MOMENTUM TRANSFER

When analysing structure in mass spectra or 4 - momentum transfer squared distributions it is essential to know the experimental resolution.

(a) THE MASS RESOLUTION

A knowledge of the mass resolution is of particular importance when parameterising narrow resonance signals such as the ω^o and η resonances. As discussed in chapters 4 and 7, the observed experimental widths and shapes of these resonances are highly dependent on the shape of the resolution function. This is particularly true for the η resonance since its narrow width of some 3 KeV implies that the resolution

FIG. 3.8(a) THE MISSING MASS SQUARED (MM^2), MISSING ENERGY (ME), MISSING MOMENTUM (MP), AND χ^2 PROBABILITY (P) DISTRIBUTIONS FOR SEEN SPECTATOR PROTON EVENTS OF THE CHANNEL $\pi^+ D \rightarrow Ps\ P\ \pi^+ \pi^- \pi^0$

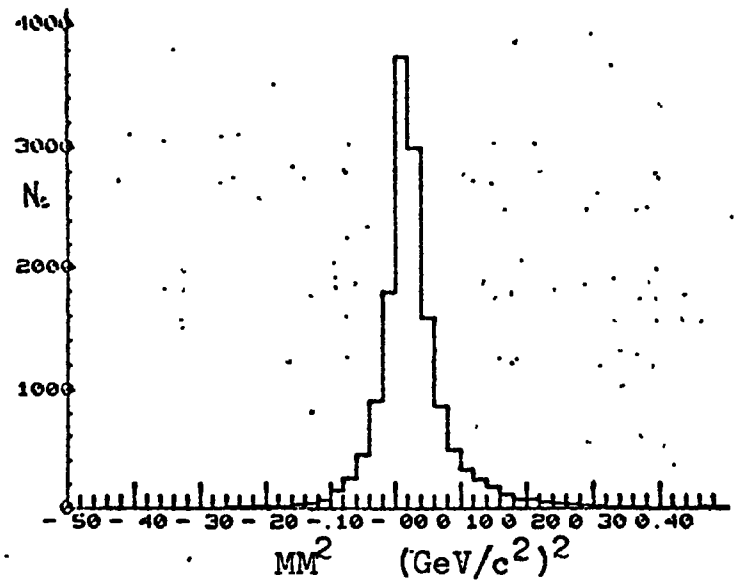

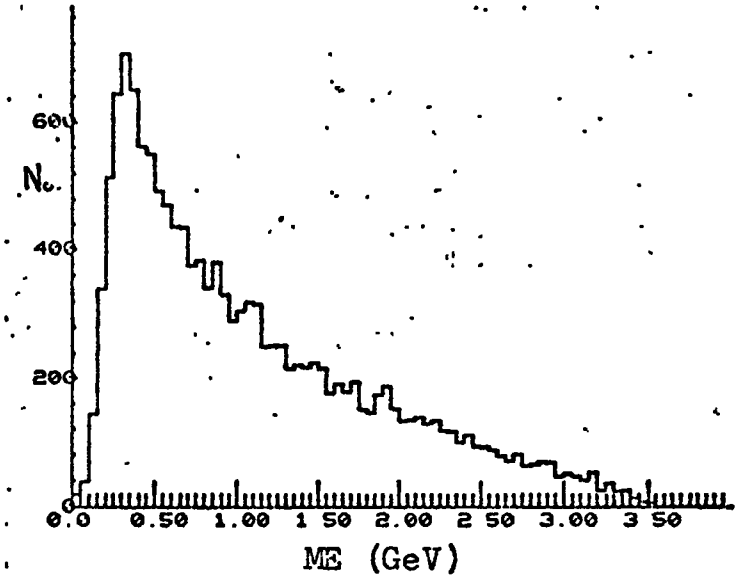

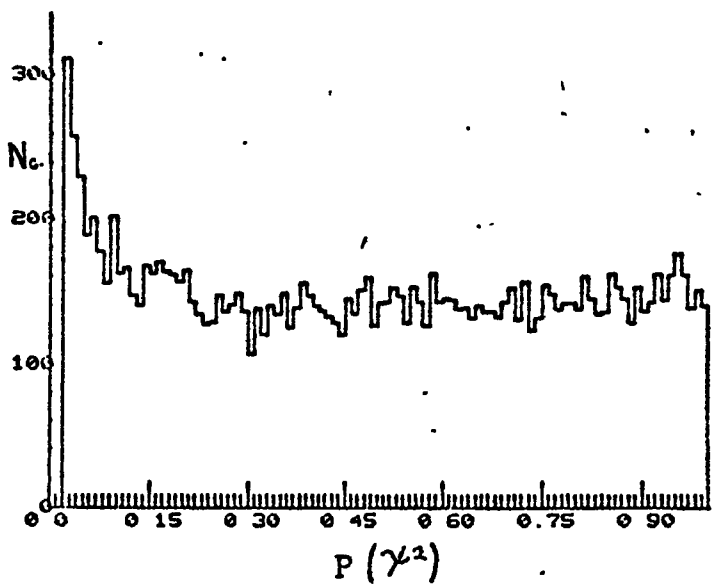

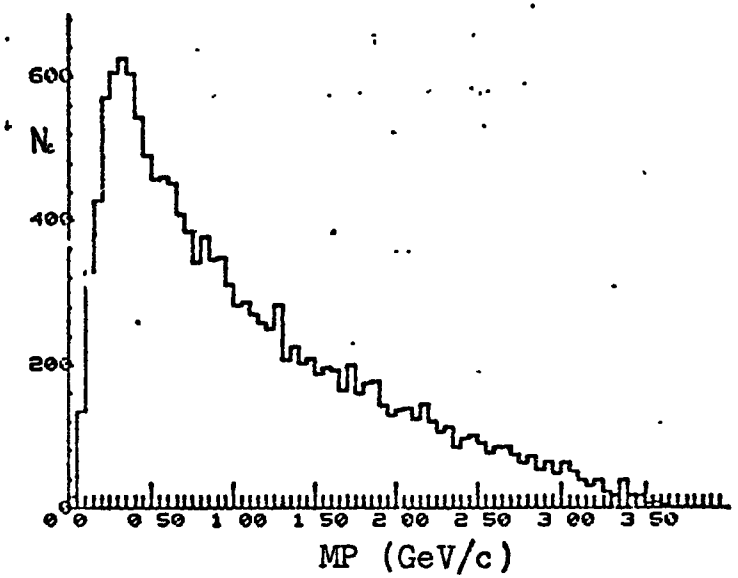

FIG. 3.8(b) THE MISSING MASS SQUARED (MM^2), MISSING ENERGY (ME), MISSING MOMENTUM (MP), AND χ^2 PROBABILITY (P) DISTRIBUTIONS FOR UNSEEN SPECTATOR PROTON EVENTS OF THE CHANNEL $\pi^+ D \rightarrow Ps\ P\ \pi^+\ \pi^-\ \pi^0$

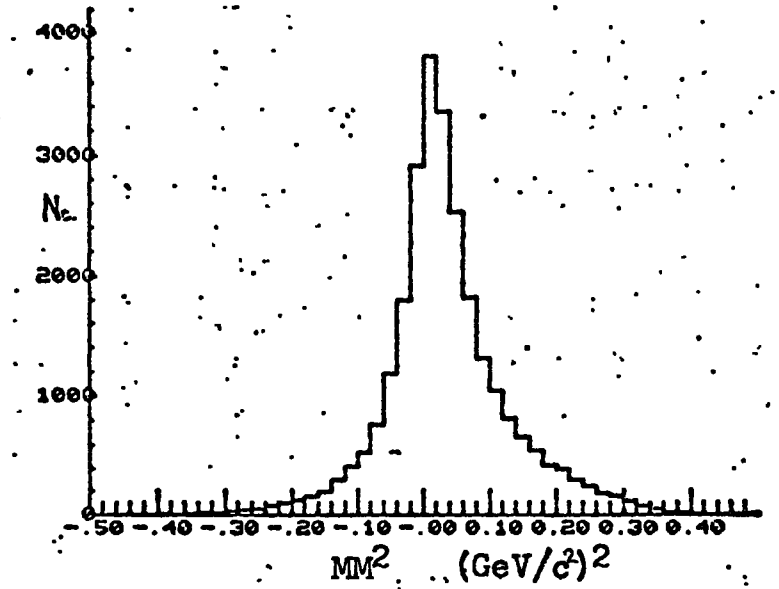

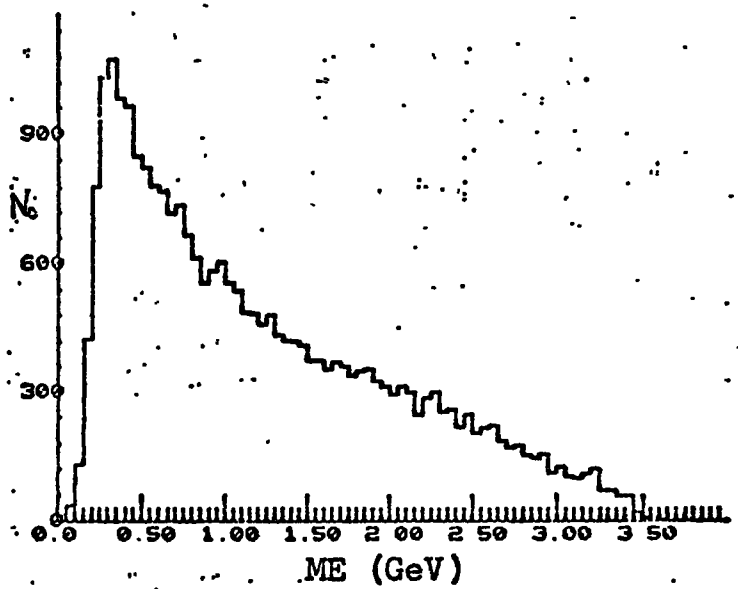

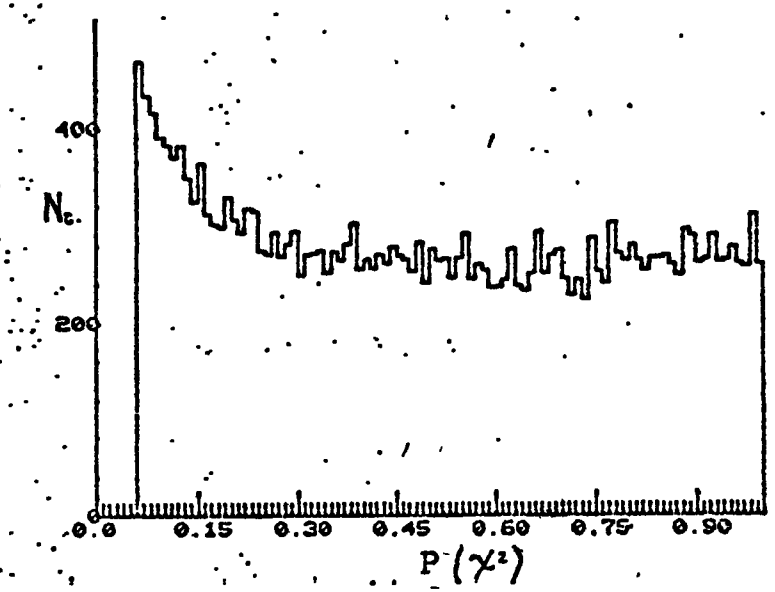

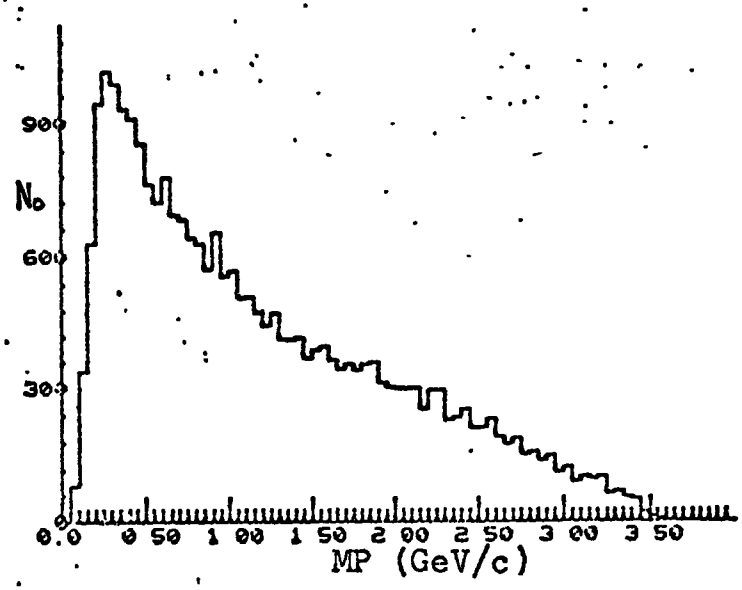

function alone is sufficient to describe the experimentally observed shape of this resonance.

The shape of the resolution function is that resulting from the superposition of gaussians corresponding to the distribution of errors on the effective mass. Depending on the form of this distribution the final shape of the resolution function can vary considerably, ranging from gaussian to approximately Breit Wigner in mass squared. Hence to determine the parameterisation best suited to the resolution function, it is firstly necessary to determine the form of the distribution of the errors on the effective mass.

The error on the effective mass was determined by expressing the effective mass of the system of particles in terms of the fitted momentum, azimuthal and dip angles of the final state particles. The error on the effective mass is then given by:-

$$\Delta M = \frac{1}{2M} \left[\sum_{i=1,n} \left(\frac{\partial M^2}{\partial P_i} \right)^2 dP_i^2 + \left(\frac{\partial M^2}{\partial \lambda_i} \right)^2 d\lambda_i^2 + \left(\frac{\partial M^2}{\partial \phi_i} \right)^2 d\phi_i^2 \right]^{\frac{1}{2}}$$

where the numbers 1 to n represent the final state particles contributing to the effective mass M, P the momentum, λ_i the dip angle and ϕ_i the azimuthal angles of the associated tracks. The values of P, λ and ϕ, and their associated errors are calculated in KINEMATICS. The final form and derivation of the above expression for the particular cases of two particle and three particle mass combinations are shown in Appendix two. The results for the mean error on the effective mass, plotted as a function of the effective mass for the $\pi^+\pi^-$ mass system, for seen and unseen spectator

proton events in the 4c channel

$$\pi^+ D \rightarrow P_s\, P\, \pi^+\pi^-$$

are shown in FIG. 3.9. Similarly the results for the $\pi^+\pi^-\pi^o$ mass system as calculated for the 1c channel

$$\pi^+ D \rightarrow P_s\, P\, \pi^+\pi^-\pi^o$$

are shown in FIG. 3.10. In all cases the error is seen to increase as a function of the effective mass, and as expected, the resolution is worse for the 1c fits and unseen spectator proton events.

(b) THE RESOLUTION IN THE 4 - MOMENTUM TRANSFER SQUARED

Plots of the 4 - momentum transfer squared, t , and the density matrix elements as a function of t contain information concerning the nature of the exchange mechanisms in an interaction. In particular Regge theory predicts structure at certain values of t , and hence it is essential to know the experimental resolution in this variable.

The derivation for the expression for the error on the 4 - momentum transfer squared between the target deuteron and the interaction proton is shown in Appendix two. Essentially it is expressed in terms of the fitted values for P, λ and ϕ for the spectator and fast protons, and the error in t calculated from the expression

$$\Delta t = \left[\sum_{i=1,2} \left(\frac{\partial t}{\partial P_i}\right)^2 dP_i^2 + \left(\frac{\partial t}{\partial \lambda_i}\right)^2 d\lambda_i^2 + \left(\frac{\partial t}{\partial \phi_i}\right)^2 d\phi_i^2 \right]^{\frac{1}{2}}$$

the variables used being the same as those used in the expression for ΔM shown above. The results for the above mentioned 4c and 1c channels for both seen and unseen spectator protons are shown in FIG. 3.11 and 3.12. For the 4c

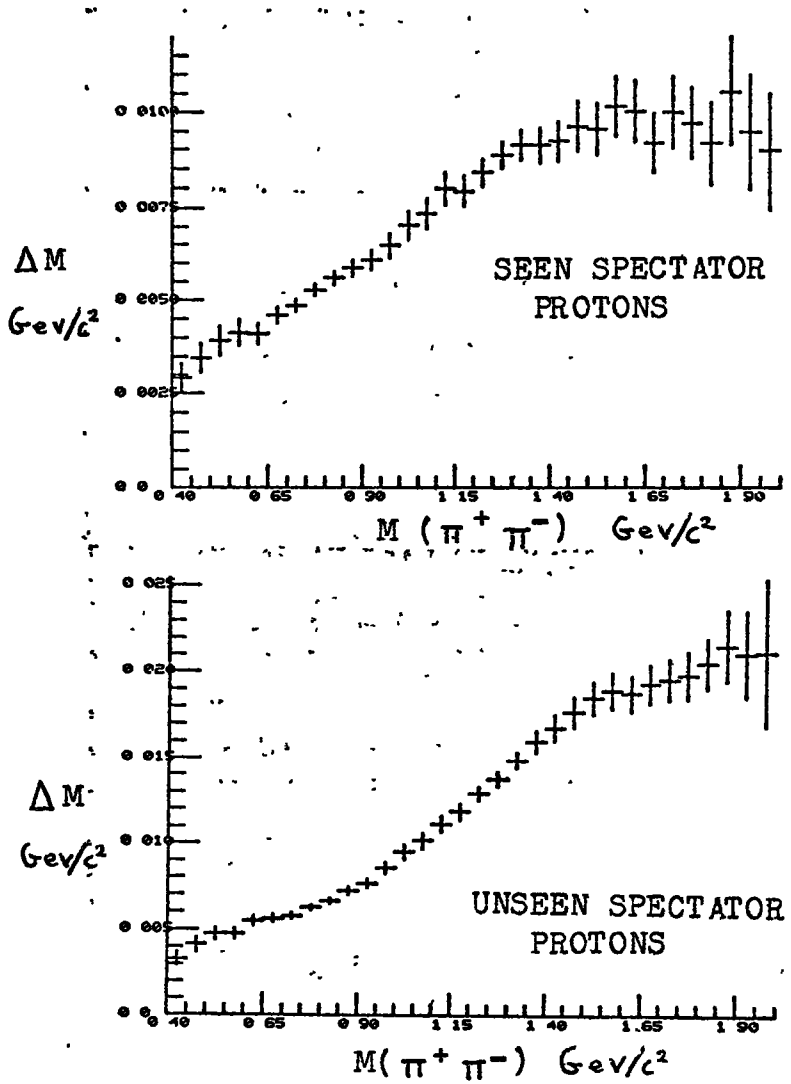

FIG. 3.9 ΔM v M FOR THE ($\pi^+ \pi^-$) MASS COMBINATION OF THE CHANNEL $\pi^+ D \rightarrow Ps\ P\ \pi^+ \pi^-$

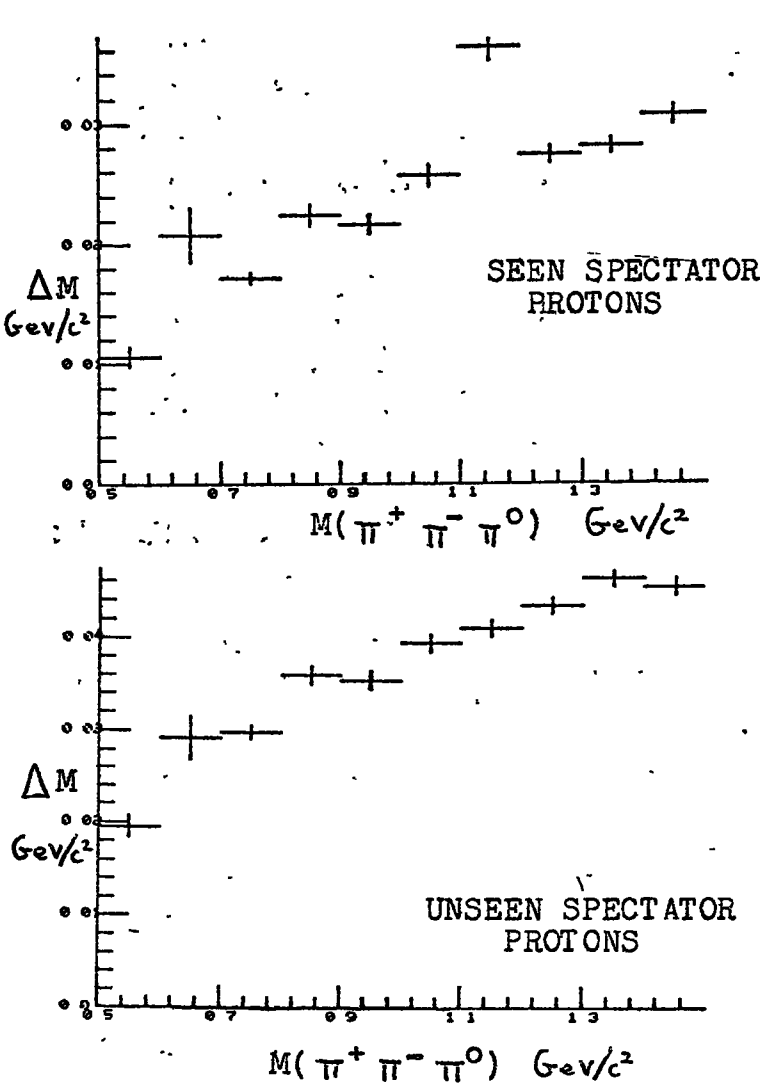

FIG. 3.10 ΔM v M FOR THE ($\pi^+ \pi^- \pi^0$) MASS COMBINATION OF THE CHANNEL $\pi^+ D \rightarrow Ps\ P\ \pi^+ \pi^-\ \pi^0$

FIG. 3.11 Δt v t IN THE ρ^0- REGION FOR THE CHANNEL

$\pi^+ D \rightarrow Ps\ P\ \pi^+ \pi^-$

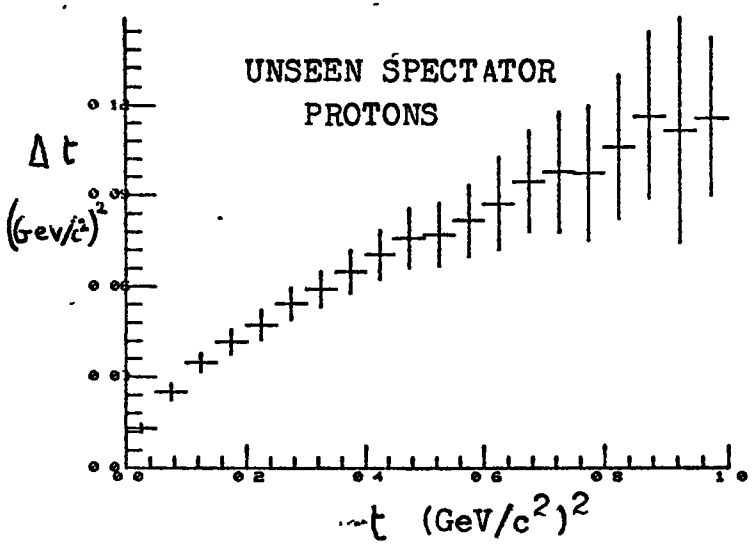

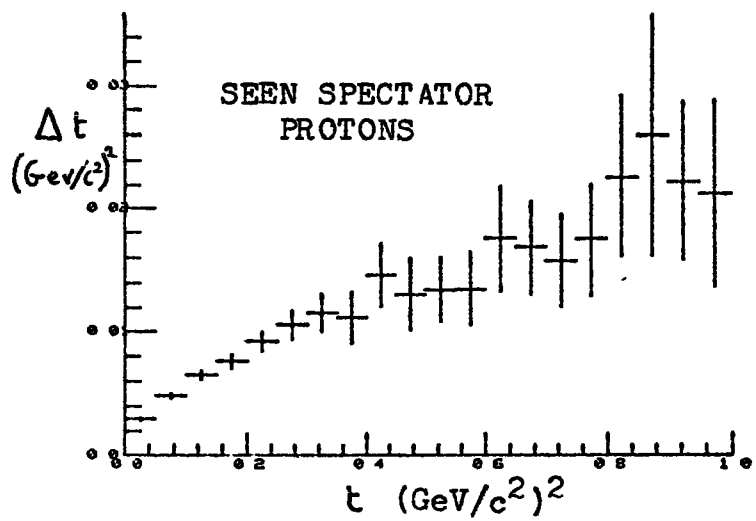

FIG. 3.12 Δt v t IN THE ω^0 REGION FOR THE CHANNEL

$\pi^+ D \rightarrow Ps\ P\ \pi^+ \pi^- \pi^0$

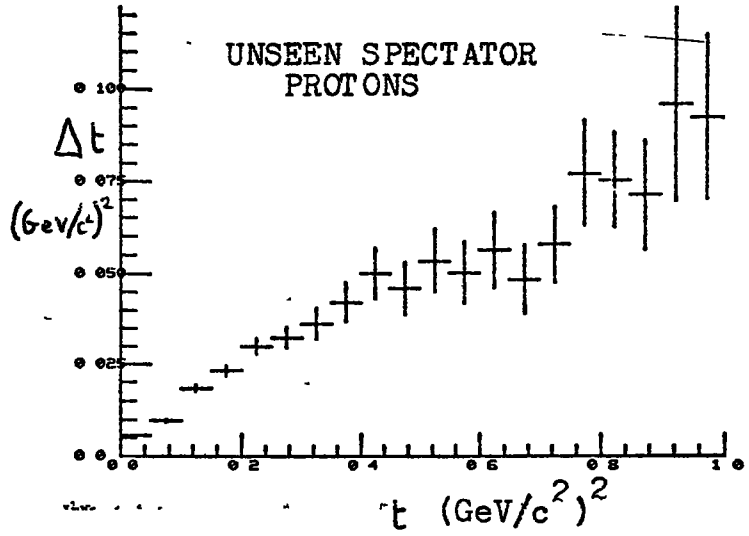

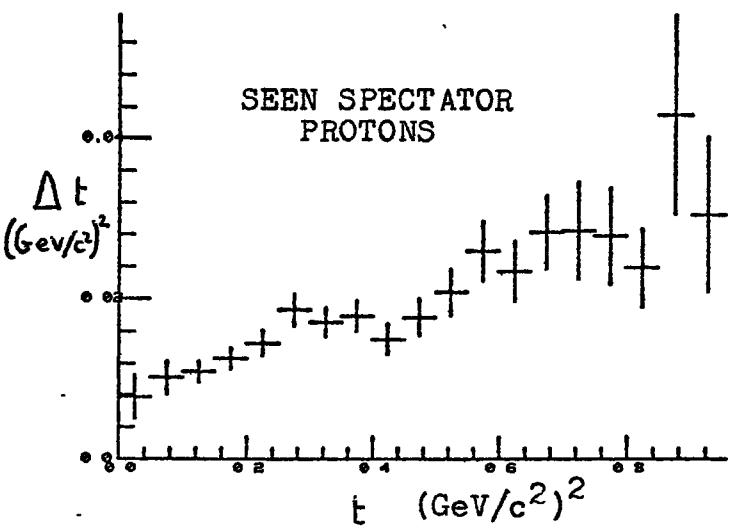

channel the mean error in t is plotted as a function of t in the ρ^o-meson region 0.71 → 0.81 (GeV/c^2), whereas for the 1c channel the same plot is shown for the ω^o meson region 0.76 → 0.81 (GeV/c^2). The magnitude of these errors essentially sets a limit to the minimum size of the t-intervals used in the determination of the variation of the differential cross section or spin density matrix elements as a function of t. In this analysis however, as described in chapter 6, the minimum size for the t intervals was decided by demanding sufficient statistics in each region to minimize the generation of apparent structure by statistical fluctuations, and in all cases the t-intervals were found to be well in excess of the above limit set by the t resolution.

The results for both the mass and t resolutions are only an indication of the magnitude of the errors, since they represent the mean values in any given mass or t-interval. In addition it must be remembered that the values of P, λ and ϕ used in the above expression are the fitted values, and hence correlations may exist between the variables, whereas the above expressions assume no correlations.

CHAPTER FOUR

THE DETERMINATION OF THE TOTAL AND DIFFERENTIAL CROSS SECTIONS FOR THE PRODUCTION OF ω^0-MESONS

INTRODUCTION

The ω^0-meson, first discovered in 1961, has been observed in numerous reactions, and consequently has become a well defined and accurately parameterised resonance. The world averages for its central mass, width, quantum numbers and decay modes, as summarised by the Review of Particle Properties of April, 1974, (Ref. 4.1), are shown in table 4.1. Although well defined in these respects, considerable controversy exists over the interpretation of its production mechanism.

For ω^0-mesons produced in the forward direction in the π-N centre of mass system, conservation of isospin and G - parity restrict the possible low lying exchange particles to the ρ and the B-mesons. In the earlier theoretical interpretations (ref. 4.2), the production process was assumed to result entirely from the exchange of the ρ -meson, the more massive exchanges being considered negligible. Hence the ρ - Regge Pole exchange model, (see Appendix 3), was expected to be in good agreement with the experimental data. In practice however, the agreement was found to be very poor. Both the predicted behaviour of the spin density matrix elements and the expected minimum in the differential cross section at $t \sim 0{\cdot}6$ $(GeV/c^2)^2$ were found to be in complete disagreement with the experimental data.

The failure of this approach indicates the following

TABLE 4.1

PROPERTIES OF THE ω^0 - MESON		
$I^G\ J^P\ C_N$	DECAY MODES	%
$0^-\ 1^-\ -$	$\pi^+\ \pi^-\ \pi^0$	90 ± 0.6
MASS (MeV/c^2)	$\pi^+\ \pi^-$	1.3 ± 0.3
782.7 ± 0.6	$\pi^0\gamma$	8.7 ± 0.5
FULL WIDTH (MeV/c^2)	$e^+\ e^-$	0.0076 ± 0.0017
10.0 ± 0.4		

possibilities:-

either (a) the Regge Pole model is incorrect,

or (b) the contributions from the more massive exchanges such as the ρ' and B-mesons are larger than expected,

and/or (c) the predicted features of the data are obscured by the effects of background.

Since the predictions for the Regge Pole model for many other reactions are in good agreement with experiment, the least favourable alternative is that this reaction should indicate the direct failure of the model, and indeed, before such a conclusion can be made the alternative explanations mentioned in points (b) and (c) have first to be investigated in detail. Hence the aim of this analysis, and of many earlier analyses, (Ref. 4.3), is to determine the spin density matrix elements and differential cross section for the ω^0-mesons, and examine them to determine the contributions from the more massive exchanges. In addition it is intended in this analysis to make a detailed investigation of the background and thereby determine the validity of point (c), and examine how the background effects may influence the conclusions concerning either points (a) or (b).

4.1 THE SELECTION OF THE EVENTS

The events analysed are those resulting from the strong decay mode of the ω^0-meson into the π^+ π^- and π^0 - mesons, as seen in the 1c channel

$$\pi^+ D \rightarrow P_S P \quad \pi^+ \pi^- \pi^0$$

The selection of this channel has already been discussed in chapter 3, the tripion mass spectra corresponding to the

accepted and rejected events being illustrated in FIG. 3.7. As pointed out in the previous chapter the accepted sample contains two distinct groups of events, namely those with seen and unseen spectator protons. In many cases in previous analyses, the lack of statistics has required that these two subsets be analysed as one, the assumption being made that neither group is in any way biased, and that their production mechanisms are identical. Although for the majority of the events the above assumption is valid, it must be remembered that at low t - transfersfrom the primary to the tripion mass system, the Pauli exclusion effects become important, and as pointed out in chapter 2, the exchange mechanisms resulting in spin non-flip of the target nucleon will dominate the unseen spectator proton events in this region. Consequently at low t - transfers compatibility between the seen and unseen spectator proton events should not be expected. For this reason, and the additional fact that the fitting of the unseen spectator proton events is less accurate, it was considered advisable to analyse these two samples separately. The corresponding tripion mass spectra for the seen and unseen spectator proton events are shown in FIG .4.1, the total number of events in each sample corresponding to

26,668 unseen spectator proton events

and 14,673 seen spectator proton events

In both of these plots the ω^0-resonance can be clearly seen, the above mentioned difference in accuracy between the two samples being well illustrated by the vastly different widths of the resonance peaks.

Where possible, the most desirable method for analysing

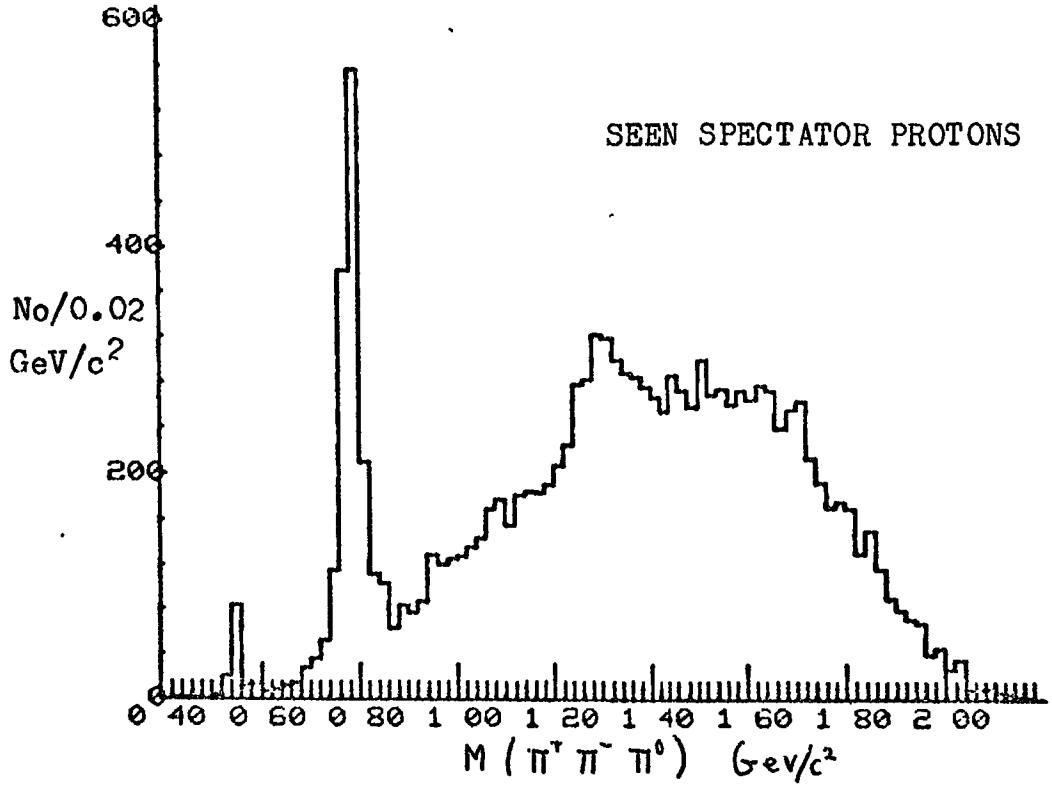

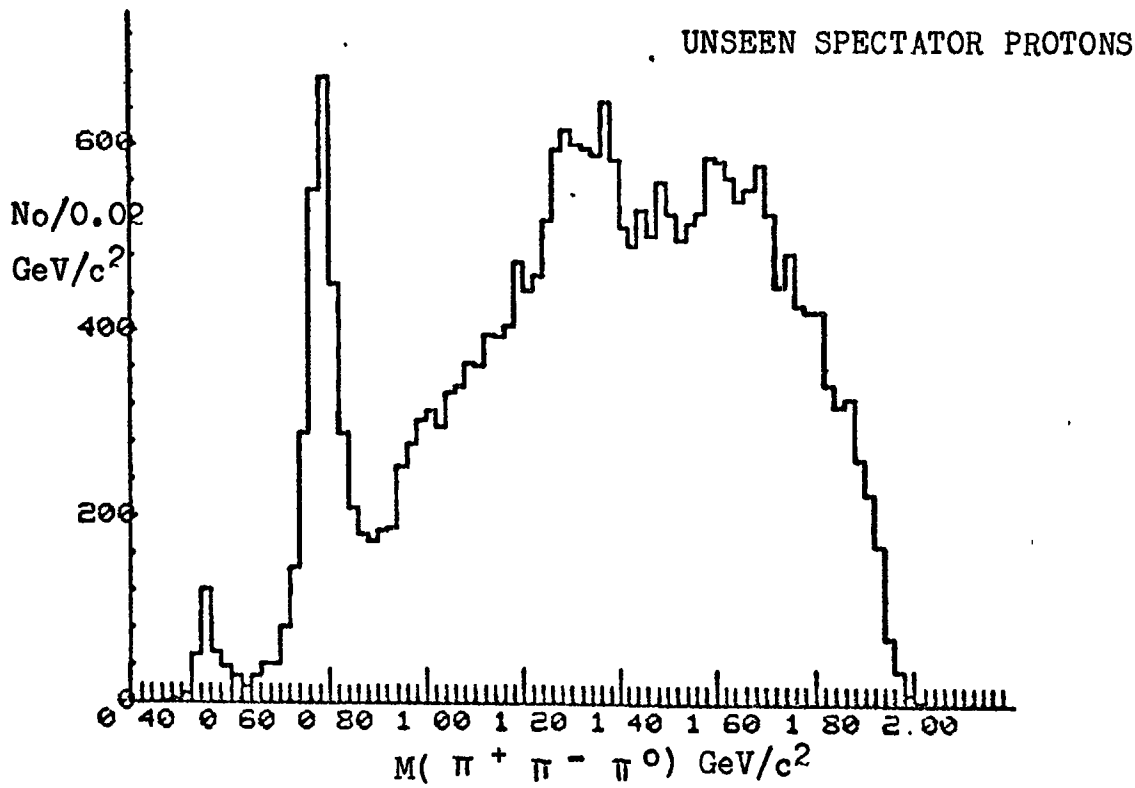

FIG. 4.1 THE ($\pi^+ \pi^- \pi^0$) MASS SPECTRA FOR THE SEEN AND UNSEEN SPECTATOR PROTON EVENTS OF THE CHANNEL

$\pi^+ D \rightarrow Ps\ P\ \pi^+ \pi^- \pi^0$

the production mechanisms is to divide the sample of events into distinct groups, each corresponding to a different type of exchange. The most obvious and easily made division is between events involving baryon exchange and meson exchange. The corresponding Feynman diagrams for these two processes are shown in FIG. 4.2, and from these it is evident that baryon exchange will result in backward going ω^{o}-mesons in the $\pi - N$ centre of mass system. Prior to this experiment there has been little or no evidence for the production of ω^{o}-mesons via such a process. However, as illustrated in FIG. 4.3, an ω^{o}-signal is clearly visible for both the seen and unseen spectator proton events with tripion mass combinations produced in the backward direction in the $\pi - N$ centre of mass system. The corresponding mass spectra for the forwardly produced ω^{o}-mesons are shown in FIG. 4.4. For these events, as mentioned in the previous section, the possible low lying exchanges are restricted to the ρ, ρ' and the B-mesons, and since in this case no obvious division exists between the events associated with each individual exchange, the forwardly produced ω^{o}-mesons are analysed as one group.

The policy of the colaboration was that Durham University should analyse the forward production of ω^{o}-mesons and the Rutherford Laboratory the backward production, (Ref. 4.4). Hence apart from the calculation of the total ω^{o}-meson production cross section the majority of this analysis is concerned entirely with the forward production of ω^{o}-mesons.

4.2 THE TOTAL ω^{o}-MESON PRODUCTION CROSS SECTION

To calculate a meaningful cross section it is essential

FIG. 4·2

FEYNMAN DIAGRAMS ILLUSTRATING FORWARD AND BACKWARD ω^0 PRODUCTION.

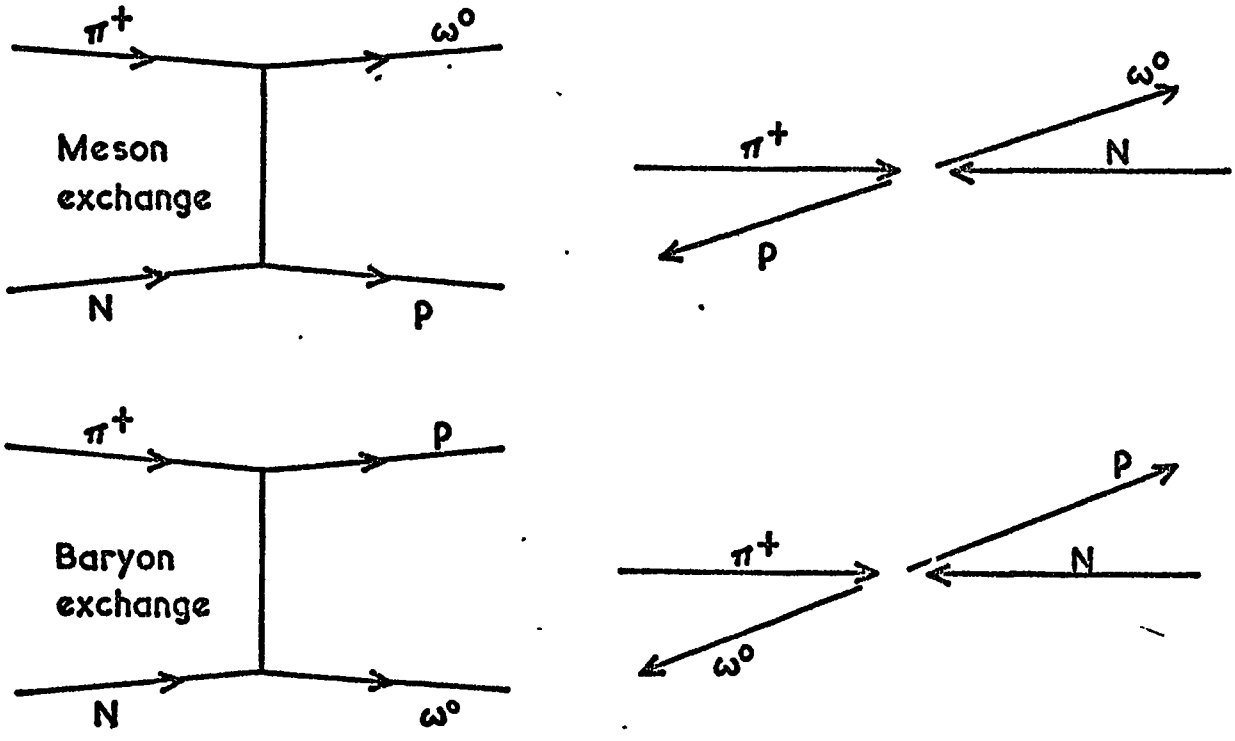

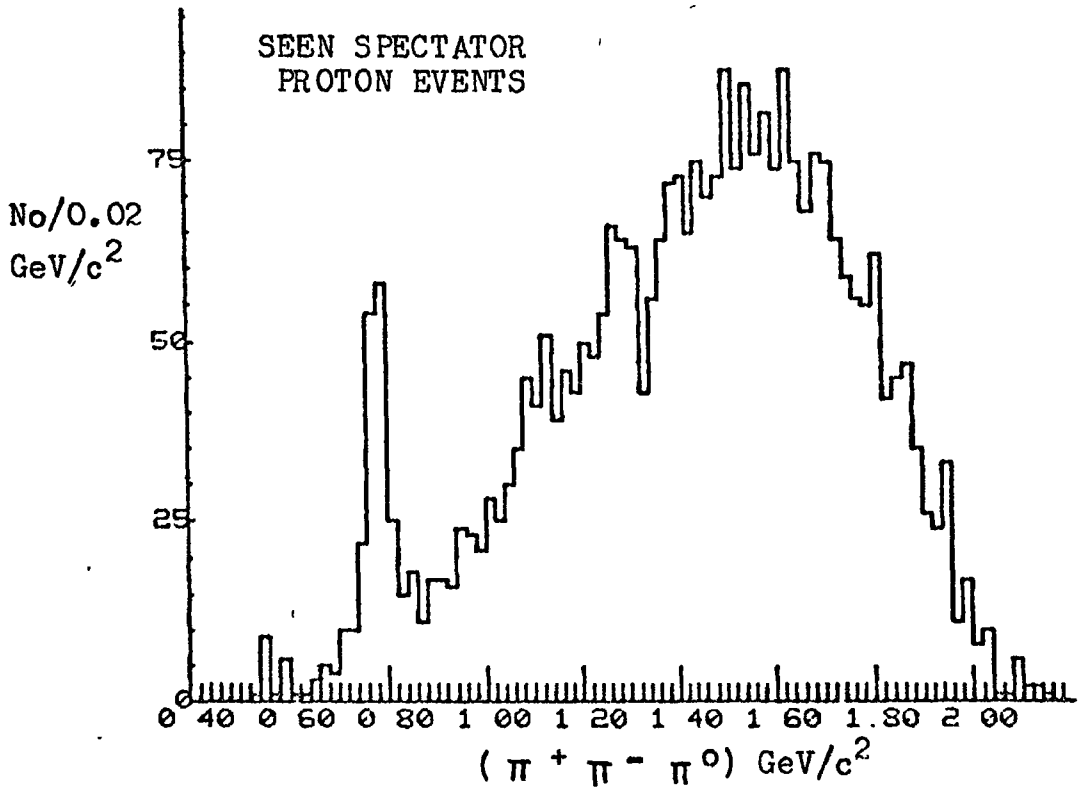

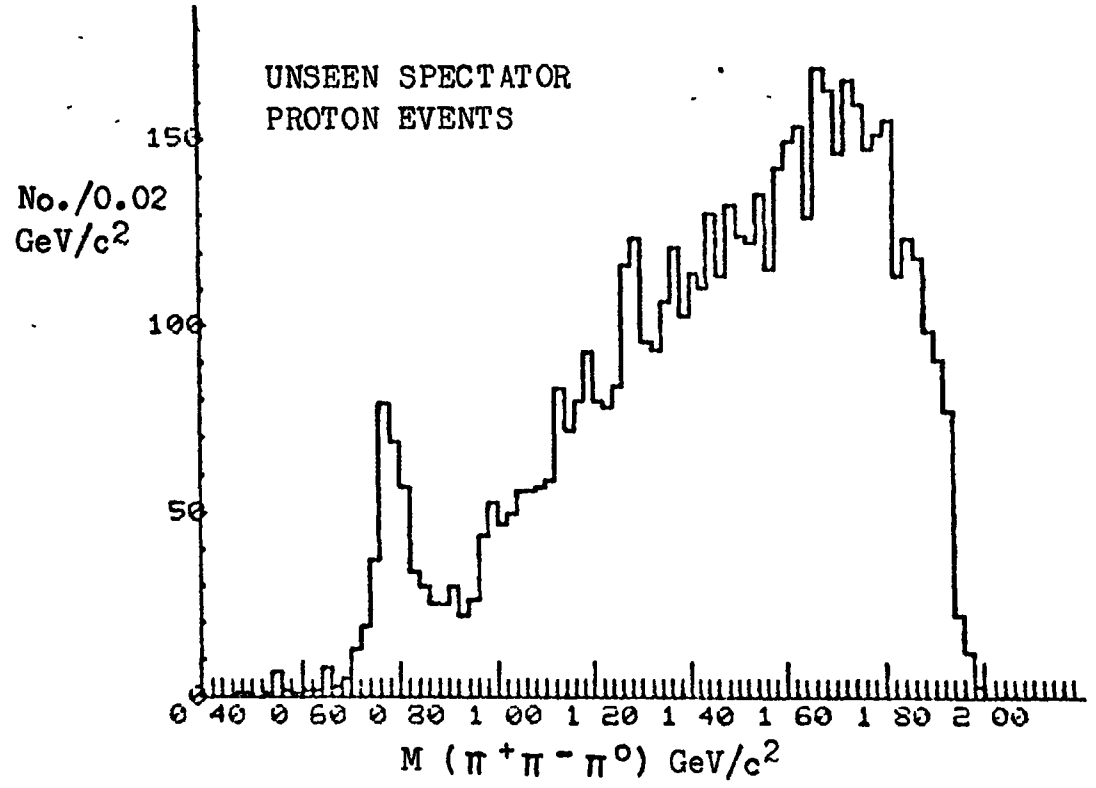

FIG. 4.3 THE $\pi^+\pi^-\pi^0$ MASS SPECTRA FOR TRIPION MASS COMBINATIONS PRODUCED IN THE BACKWARD DIRECTION IN THE π-N CENTRE OF MASS SYSTEM.

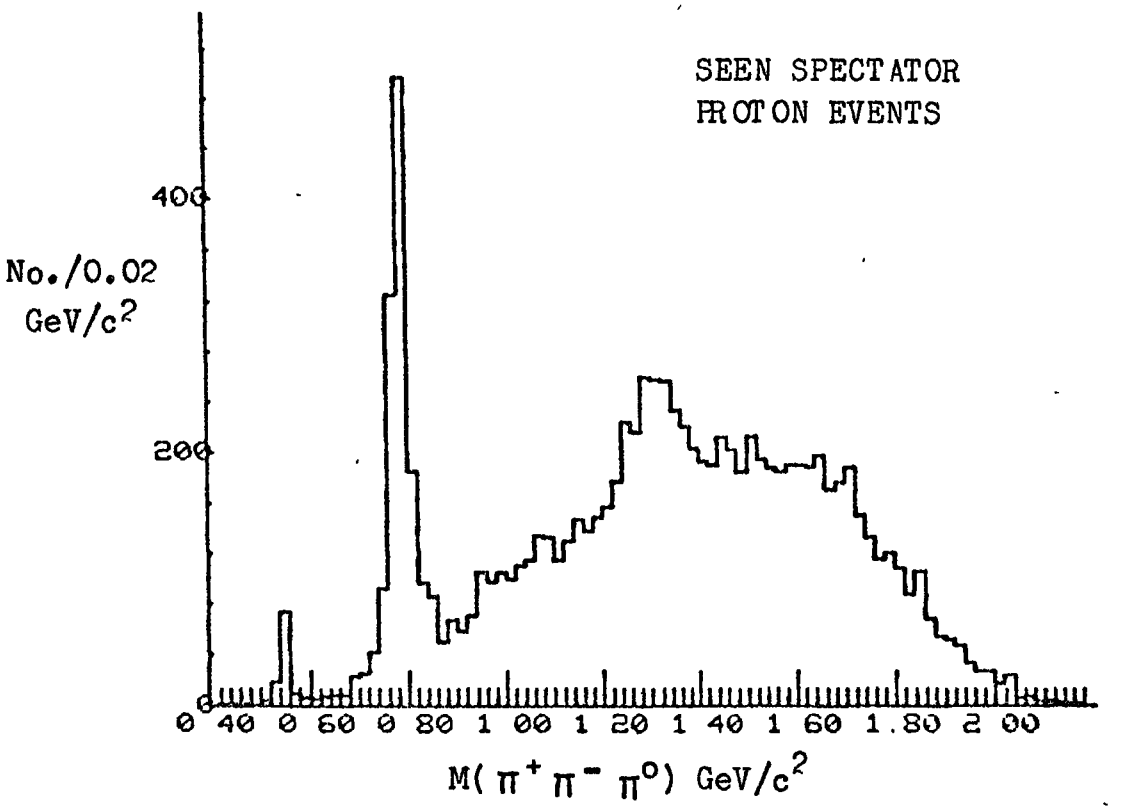

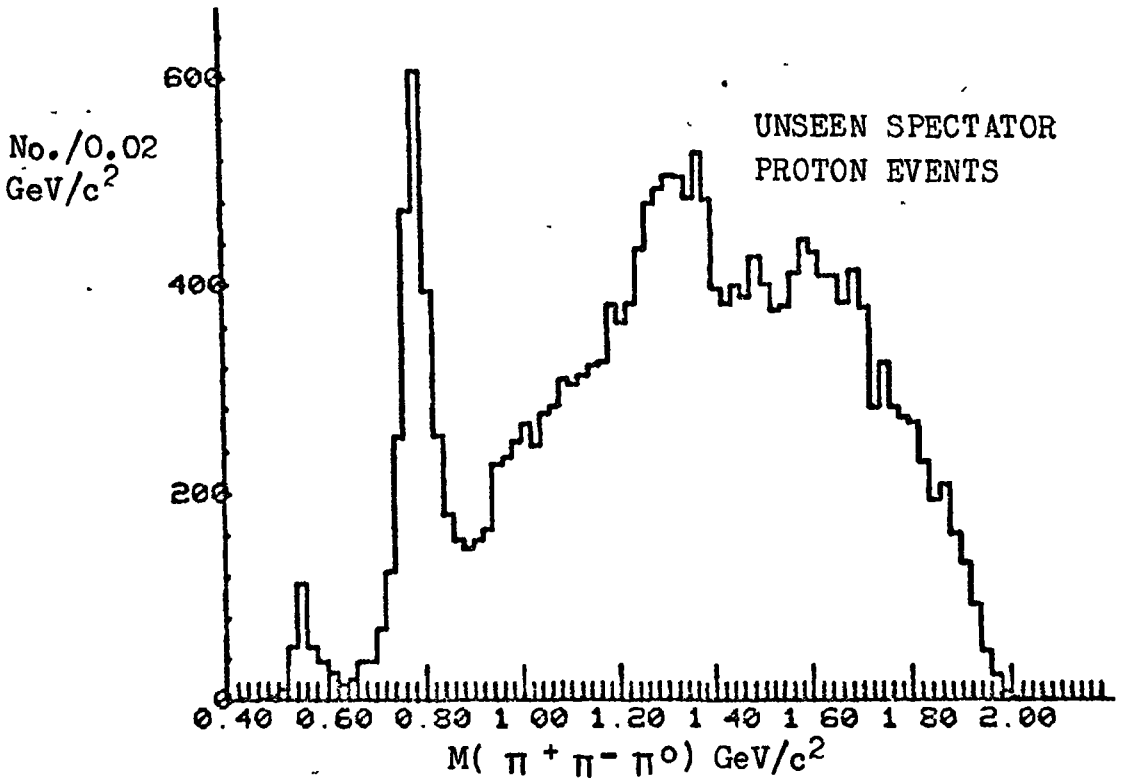

FIG. 4.4 THE $\pi^+ \pi^- \pi^0$ MASS SPECTRA FOR TRIPION MASS COMBINATIONS PRODUCED IN THE FORWARD DIRECTION IN THE π-N CENTRE OF MASS SYSTEM.

to determine the best fit to both the signal and the background. In the case of ω^0-meson production, the shape of the signal is well defined, the review of particle properties showing it to be represented by a Breit-Wigner of central mass 782.7 ± 0.6 MeV, with a full width Γ of 10.0 ± 0.4 MeV. However, from the tripion mass spectra shown in FIG. 4.1 it is evident that the width of the ω^0 peak is considerably larger than 10 MeV, and in addition is different for seen and unseen spectator proton events. These increased values result from the limited experimental resolution, which as illustrated in chapter 3 is different for seen and unseen spectator proton events. Hence when fitting the signal, the precise form of the error distribution, or resolution function, has to be convoluted into the fit.

(a) THE RESOLUTION FUNCTION

It is expected that the distribution of errors on the square of the tripion mass is gaussian in identical events, and that the errors on events with higher or lower tripion masses, or on events in other parts of the chamber will be distributed as other gaussians. Therefore the expected error distribution, the resolution function, will be the superposition of many gaussians.

In order to determine the final shape of this superposition it is firstly necessary to determine the frequency with which each gaussian occurs. In this analysis this was achieved by calculating the error on the tripion mass, as described in section 3.8. The resulting frequency distributions calculated for the seen and unseen spectator proton events in the tripion

mass squared region 0.4 $\rightarrow$ 0.8 $(GeV/c^2)^2$ are shown in FIG.4.5. Hence by reconstructing the superposition of gaussians in accordance with the above frequency distributions, the shapes of the resolution functions were determined. The results shown in FIG. 4.6 indicate that the resolution function for the seen spectator proton events is as predicted narrower than for the unseen spectator proton events, thereby confirming that the different widths for the ω^o-signals observed in FIG. 4.1 are due to the different mass resolutions.

The best fitting gaussian shapes are shown on the resolution functions, and the results indicate that these fits are poor. This is because the resolution functions are narrow in the central regions and broad in the tails. These characteristics suggest Breit Wigner shapes, and as can be seen in FIG. 4.6, the Breit Wigner fits are considerably better. The details of the fits are shown in table 4.2.

As a result of this analysis it was decided that in the fitting of the tripion mass spectra, the resolution functions were to be parameterised as Breit Wigner shapes in mass squared. Although the widths of the resolution functions have already been determined from the above fits it was considered advisable for the following reasons to allow the width of the resolution function to be a free parameter in the final fitting of the tripion mass spectra.

Firstly, as pointed out in section 3.8, the results for the error on the tripion mass may not be exact, since the calculations assume the fitted variables to be uncorrelated. Hence although the general shape of the frequency distributions and resolution functions will be correct, the values for the

FIG. 4.5 THE FREQUENCY DISTRIBUTION OF ERRORS IN THE ω^0-REGION

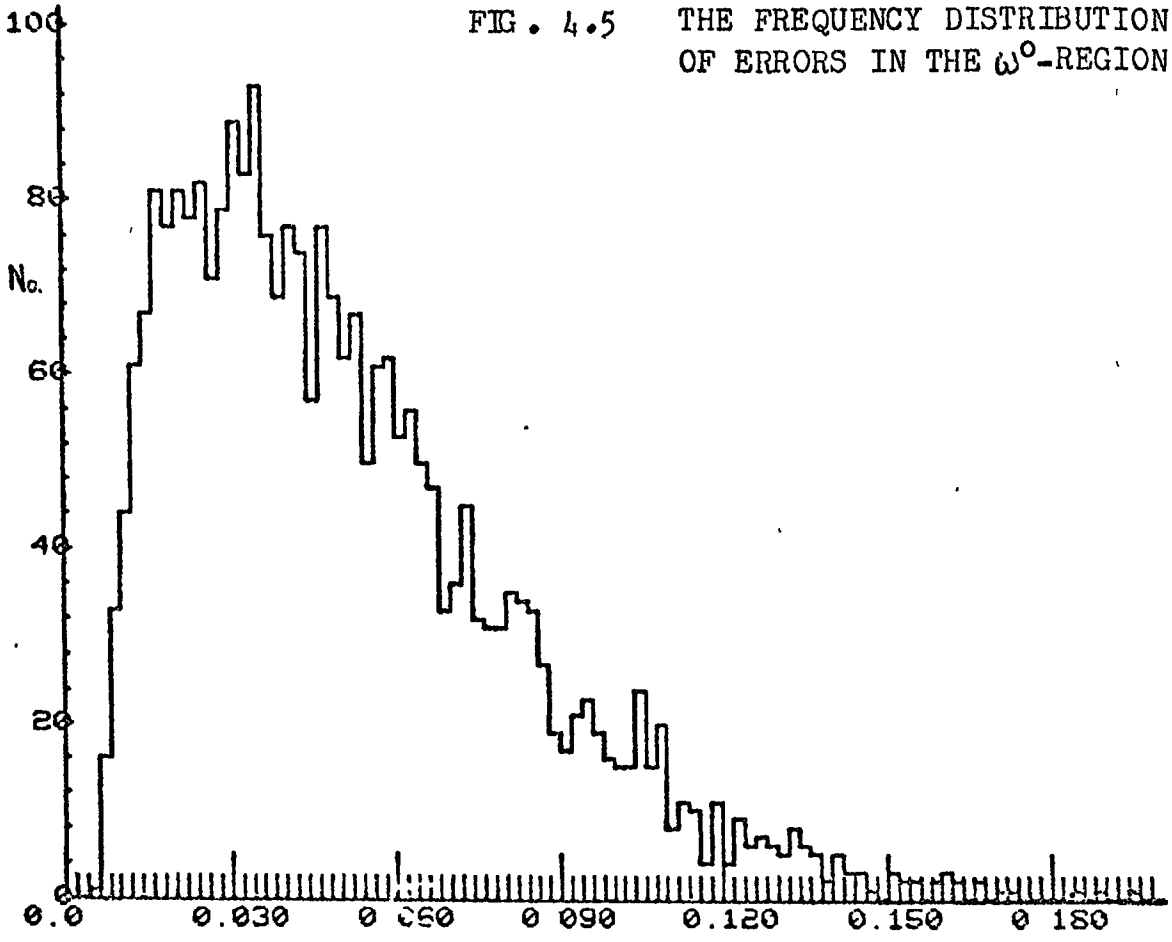

ΔM^2 $(GeV/c^2)^2$ UNSEEN SPECTATOR PROTON EVENTS

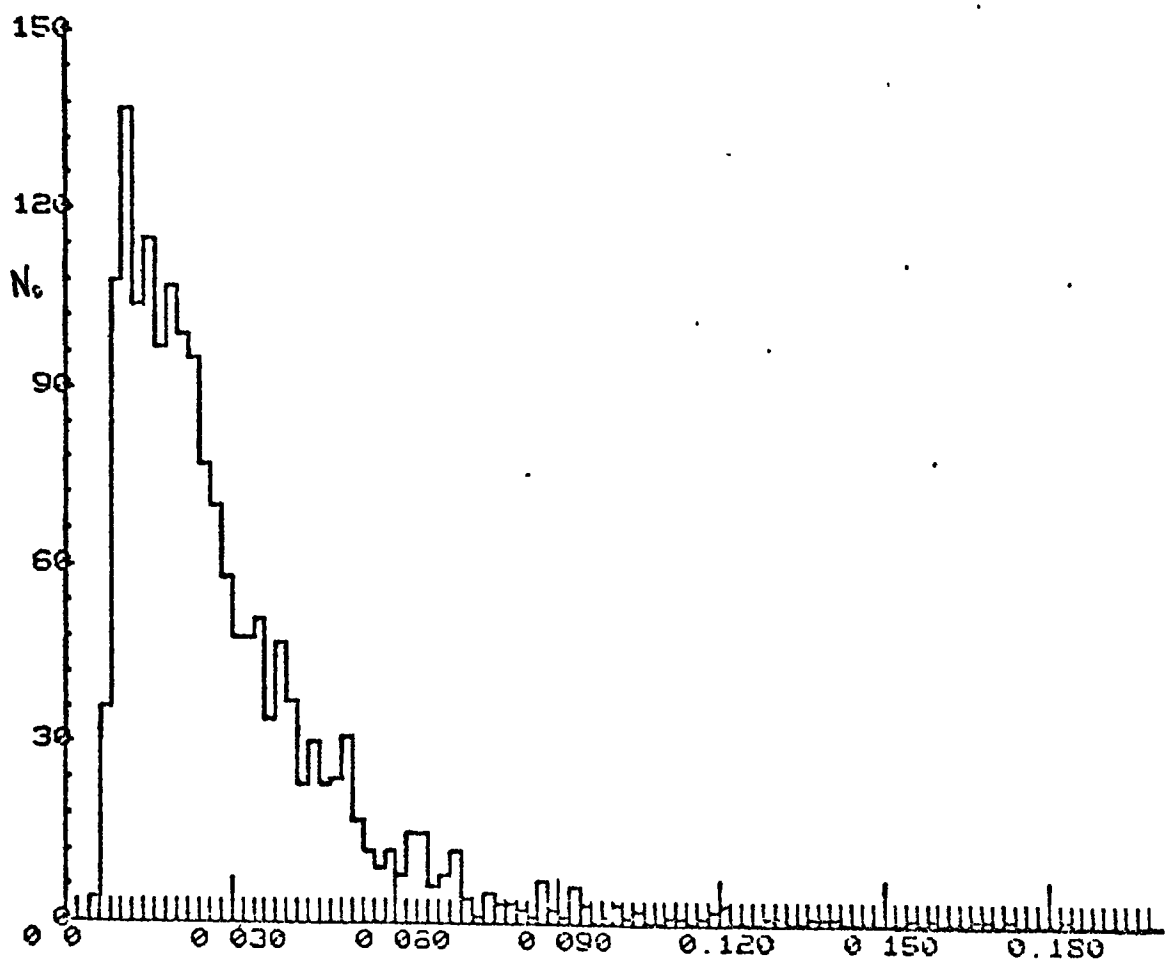

ΔM^2 $(GeV/c^2)^2$ SEEN SPECTATOR PROTON EVENTS.

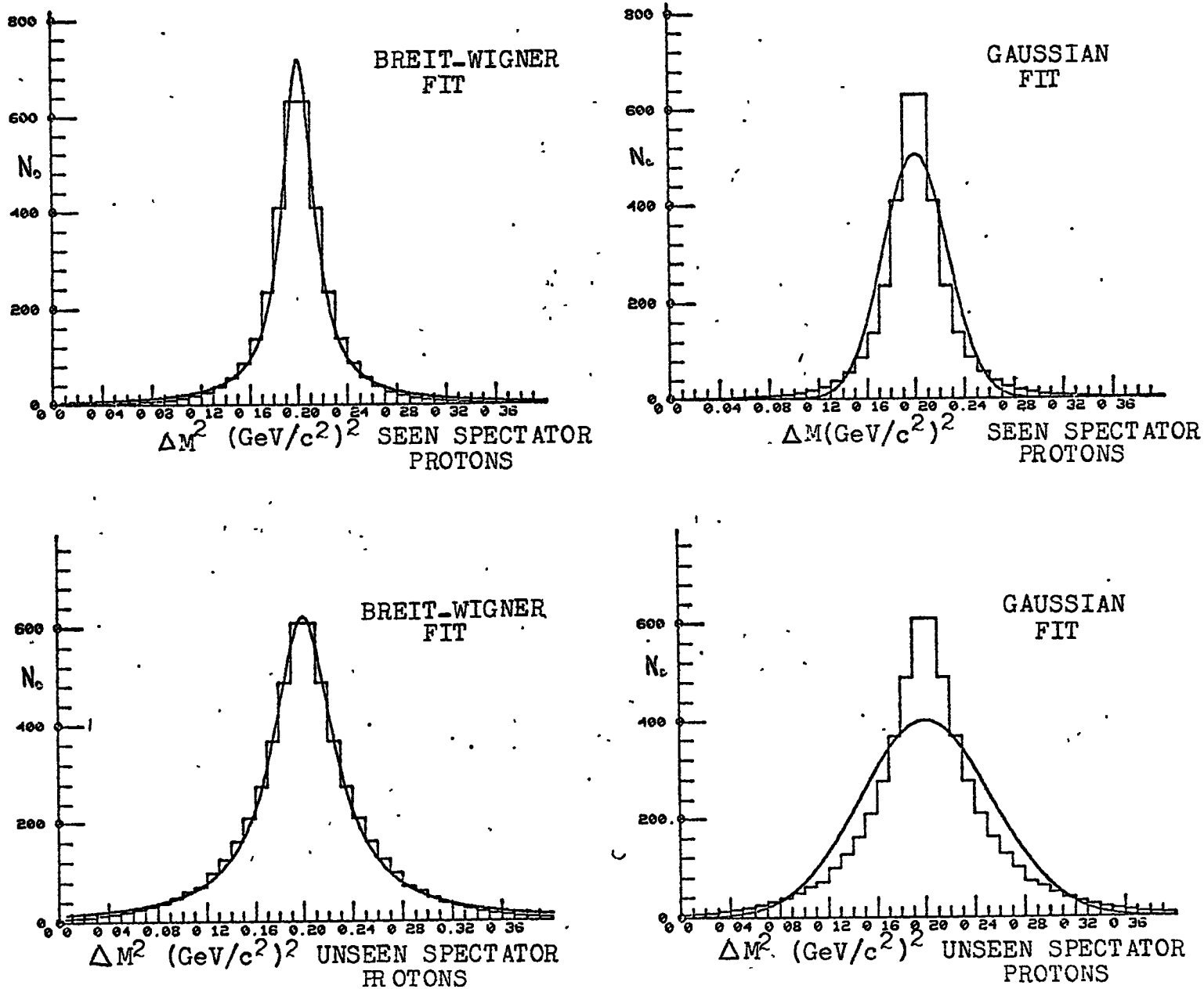

FIG. 4.6

THE RESOLUTION FUNCTIONS FOR THE ω^o-REGION

TABLE 4.2

THE FITS TO THE RESOLUTION FUNCTIONS OVER 40 BINS USING 2 PARAMETERS		
GAUSSIAN FITS	Γ res	χ^2
UNSEEN SPECTATOR EVENTS	53.0	691.0
SEEN SPECTATOR EVENTS	26.0	417.0
BREIT WIGNER FITS		
UNSEEN SPECTATOR EVENTS	61.0	52.3
SEEN SPECTATOR EVENTS	31.0	98.6

final widths may not be exact.

Secondly, assuming the effects of the correlations to be negligible, a comparison of the widths of the resolution functions resulting from the fits to the tripion mass spectra with those shown in table 4.2, provides a useful check on the validity of the fits.

One final point concerning the resolution function is that in the above discussion the variation of the resolution throughout the ω^o-region of the tripion mass spectrum has been considered negligible, and only the average value over the fitted region has been considered. The validity of this approximation is well illustrated in FIG. 3.10 in which it is evident that the error on the tripion mass is a slowly varying function throughout the ω^o-region. As additional confirmation a linear variation in the resolution was included in the earlier fits, and as predicted the results indicated that this additional parameterisation was unnecessary.

(b) THE PARAMETERISATION OF THE BACKGROUND

From the tripion mass spectra shown in FIG. 4.1, it is evident that the parameterisation of the background is likely to consist of a smoothly varying low order polynomial. To confirm this assumption, the background was initially over - parameterised and represented by a polynomial in mass squared of the form

$$N = a\,(M^2)^b + c\,(M^2)^d + e$$

thereby allowing the fit to assume a large variety of possible shapes for the background. The results of such a fit are

shown in FIG. 4.7, and from this it is evident that the chosen background is essentially linear in mass squared. Hence the redundant parameters were removed and the background parameterisation replaced by the linear form,

$$N = a\,(M^2) + b$$

(c) THE PARAMETERISATION OF THE SIGNAL

As mentioned in the introduction to this chapter the central mass and width of the ω^o - resonance are known to a high degree of accuracy. Consequently these quantities were made pseudo parameters of the fit and confined to the range defined by the particle table values shown in table 4.1. The form of the Breit Wigner used is as shown below:-

$$N(M) = M^{\frac{1}{2}} \times \left[\frac{\Gamma}{(M^2-M_o^2)^2 + (M_o\Gamma)^2}\right]$$

where $\Gamma = 2M^{\frac{1}{2}}\ \Gamma_o \left(\frac{Q}{Q_o}\right)^3$, $Q = \frac{1}{3}\,(M-9m_\pi{}^2)^{\frac{1}{2}}$ and

$$Q_o = \tfrac{1}{3}\,(M_o - 9m_\pi{}^2)^{\frac{1}{2}}$$

The expression is in terms of mass squared (M), with M_o refering to the central mass squared and Γ_o to the full width in terms of mass. The motivation for choosing a P - wave Breit Wigner is that the ω^o - meson has a spin of 1 and hence the resonance shape should be slightly asymmetric. The narrow width of the resonance however, renders the effects of such a refinement to be minimal and infact the use of a symmetric Breit Wigner shape yields almost identical results. The value of Q in the above expression, which by definition is the momentum of one of the decay products in the rest system of the resonance, was evaluated for the particular case where the momenta of the 3 pions in the ω^o rest system are equal. Although an

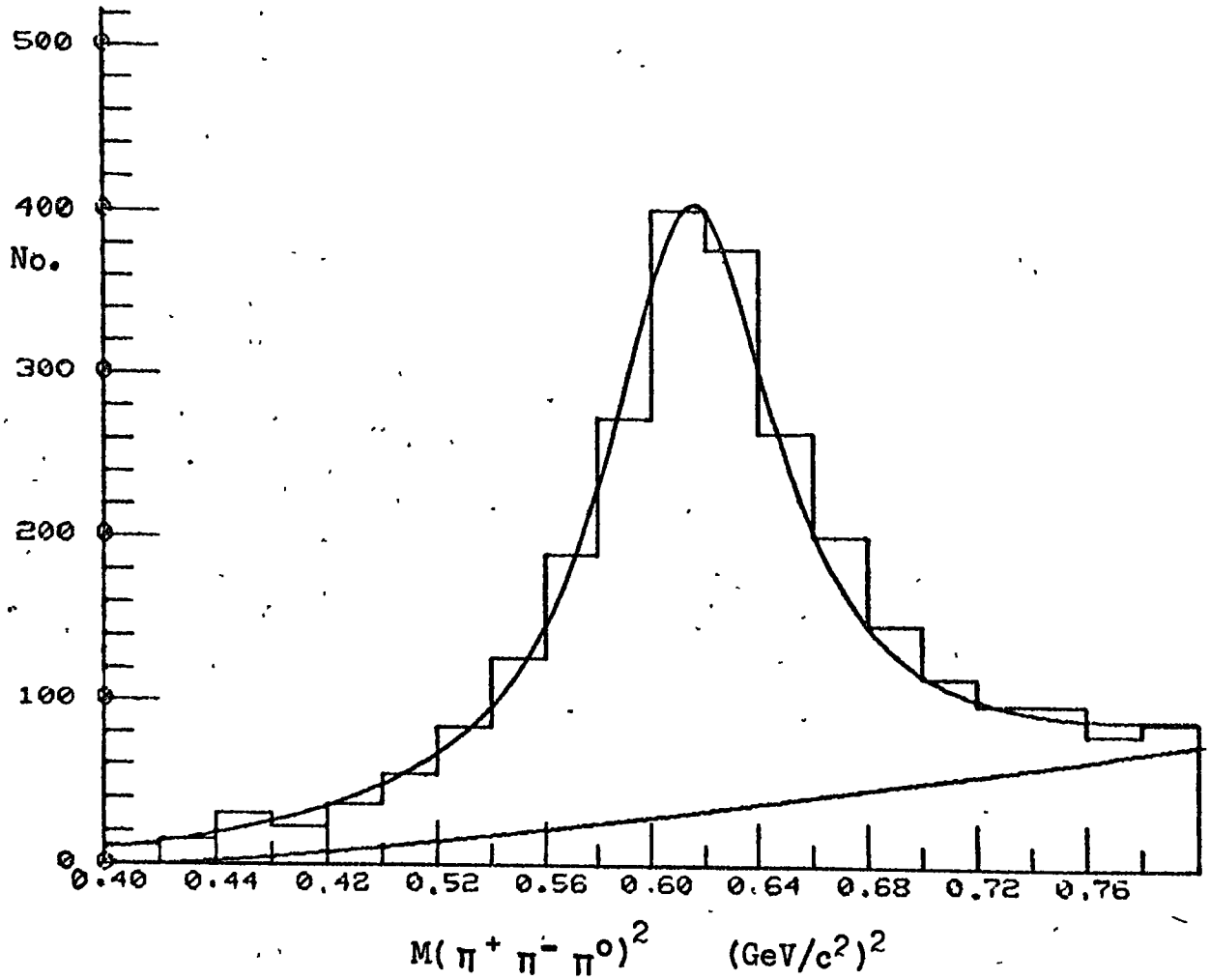

FIG. 4.7 THE FIT TO THE ω°-REGION USING A POLYNOMIAL BACKGROUND.

approximation, this was considered the most accurate estimate, since it corresponds to the centre of the Dalitz plot and hence to the most probable configuration, (see chapter 5).

(d) THE CONVOLUTION OF THE BREIT WIGNER AND RESOLUTION FUNCTION

With zero measurement and fitting errors, the ω^0 signal could be displayed in discrete intervals of mass and parameterised by the ω^0-Breit Wigner function alone. The introduction of errors however, effectively re-distributes the events in each discrete mass interval, in accordance with the shape of the resolution function. Consequently some of the events initially assigned to a given mass interval will be re-distributed into the neighbouring regions, and the final shape resulting from this will be the experimentally observed distribution. This in essence is how the Breit Wigner and resolution functions were convoluted together, and the results of such a fit are described below.

(e) THE RESULTS OF THE FITS TO THE ω^0-REGION OF THE TRIPION MASS SPECTRUM

The results of the fits to the tripion mass spectra corresponding to the production of ω^0- mesons in the fowward and backward direction in the π - N centre of mass system are shown in FIG. 4.8 and table 4.3, the events associated with seen and unseen spectator protons being fitted separately. In all cases, the fits were made as a function of mass squared, over the tripion mass squared region 0.4 $\rightarrow$ 0.8 $(GeV/c^2)^2$, the signal being represented by a P-wave Breit Wigner, the resolution function as an s - wave Breit Wigner, and the background as a straight line, in accordance with sections (a)

FIG. 4.8 THE FINAL FITS TO THE ω^0-REGION OF THE TRIPION MASS SPECTRUM

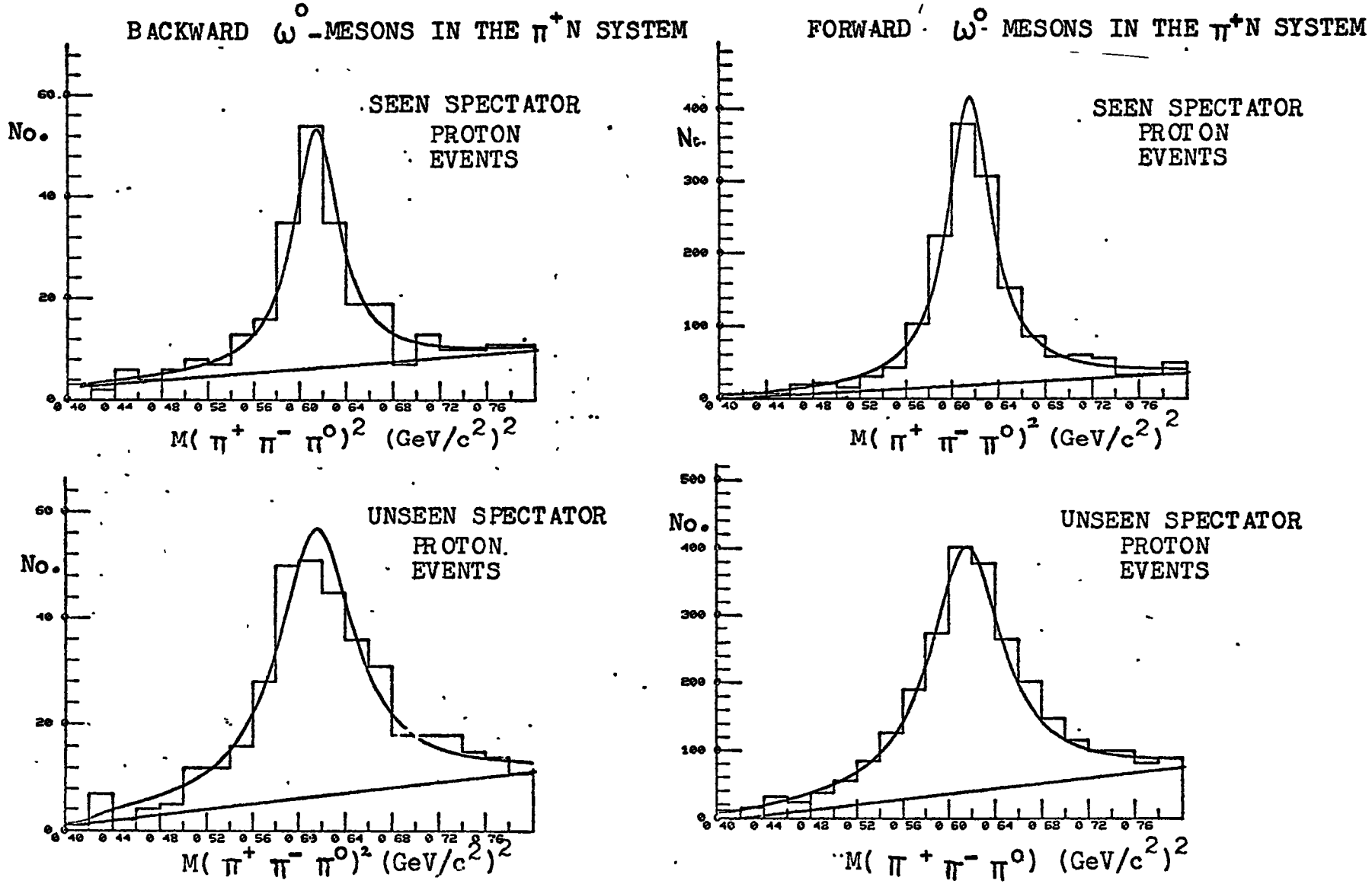

TABLE 4.3

THE RESULTS OF THE FITS TO THE ω^o - REGION OF THE TRIPION MASS SPECTRUM	FORWARD PRODUCTION		BACKWARD PRODUCTION	
	UNSEEN SPECTATOR PROTON EVENTS	SEEN SPECTATOR PROTON EVENTS	UNSEEN SPECATOR PROTON EVENTS	SEEN SPECTATOR PROTON EVENTS
THE NUMBER OF ω^o - MESONS	1994	1346	271	167
THE NUMBER OF BACKGROUND EVENTS	733	342	125	122
Γ OF RESOLUTION FUNCTION $(MeV/c)^2$	58.0	29.6	62.3	33.5
Γ OF RESOLUTION FUNCTION DETERMINED FROM KINEMATICS OUTPUT IN $(MeV/c^2)^2$	61.0	31.0	61.0	31.0
χ^2 OF THE FIT OVER 20 BINS	33.1	32.1	15.0	7.1

to (c) above. From the results shown in table 4.3 it is evident that the fitted widths for the resolution functions are in excellent agreement with those determined from the errors calculated in the KINEMATICS programme. The results for the various cross sections are summarised in table 4.4, the conversion of the number of events into cross sections being achieved by use of the microbarn equivalent calculated in section 3.2.

(f) CORRECTIONS

Corrections are made to the total cross section for the unseen decay modes described in table 4.1, and for the events rejected by the selection criteria. Additional corrections are made for events lost as a result of the Pauli exclusion effects, described in section 2.4, and for events lost in scanning.

As discussed in section 3.1, the scanning losses correspond to events in which both the spectator and recoiling protons are invisible in the bubble chamber. Such events are recorded as 2-prongs and hence omitted from the channel. FAKE calculations estimate this loss to correspond to some 2% of the total, assuming that protons are visible at momenta greater than 100 MeV/c. These losses are mainly restricted to the t-transfer region, measured from the primary to the tripion mass system, of less than 0.1 $(GeV/c^2)^2$, and hence to the region dominated by the Pauli exclusion effects. Therefore the inclusion of both the scanning and Pauli corrections will provide an absolute upper limit to the losses, since in many cases an event will be lost for not just one, but both

TABLE 4.4

CROSS SECTIONS FOR ω^o - PRODUCTION	μb	PAULI CORRECTIONS	
		TOTAL SPIN FLIP μb	TOTAL SPIN NON FLIP μb
THE TOTAL FORWARD PRODUCTION CROSS SECTION WHICH INCLUDES:-	269 ± 27	272 ± 27	280 ± 28
(a) EVENTS WITH SPECTATOR MOMENTA > 300 MeV/c	14 ± 2	14 ± 2	14 ± 2
(b) EVENTS REJECTED BY SELECTION CRITERIA.	17 ± 2	17 ± 2	17 ± 2
(c) SCANNING LOSSES	5 ± 1	5 ± 1	5 ± 1
(d) UNSEEN DECAY MODES	27 ± 3	27 ± 3	27 ± 3
THE TOTAL BACKWARD PRODUCTION CROSS SECTION	34 ± 4	34 ± 4	34 ± 4
THE TOTAL CROSS SECTION	303 ± 30	306 ± 31	314 ± 31

of the above reasons. The estimated losses due to the Pauli exclusion effect correspond to 1% and 4% for the occurence of total spin flip and total spin non-flip of the recoiling proton respectively.

(g) THE COMPARISON OF THE PRODUCTION CROSS SECTION WITH THE RESULTS FROM PREVIOUS EXPERIMENTS

A survey of the results for the ω^o - production cross sections calculated in previous experiments is shown in table 4.5. The table includes a description of the fits made to the various signals and the corrections incorporated into the final results. The plot of these production cross sections as a function of the primary momentum in the laboratory system is illustrated in FIG. 4.9. The line drawn represents the result, $\sigma \propto P^{-n}$ where n is in the region of 2.5 , and P is the primary momentum, and as can be seen the experimental data is in good agreement with this relationship. The deviations that do exist may well result from the different corrections applied to the results and in particular to the variety of parameterisations used for the signal and background. The latter problem is well illustrated by the large range of answers resulting from the fits to the forwardly produced ω^o-meson events from this experiment, with unseen spectator protons.

Using the variety of parameterisations shown in table 4.6, on the data of this experiment the expected amounts of ω^o-signal vary by as much as 800 events, equivalent to some 40% of the total estimated ω^o-signal. Consequently great caution must be exercised in the type of parameterisation

TABLE 4.5

A SURVEY OF THE TOTAL ω^o - PRODUCTION CROSS SECTIONS DETERMINED IN PREVIOUS ANALYSES

		PARAMETERISATIONS			CORRECTIONS			
BEAM MOMENTUM GeV/c	CROSS SECTION b	SIGNAL	BACK-GROUND	RESOLUTION FUNCTION	UNSEEN DECAY MODES	PAULI	SCANNING LOSSES	REF.
1.7	1800± 200	B(M)	P	√				4.5
2.7	800± 80	G(M^2)	P		√		√	4.6
3.65	350± 40	G(M)	Q				√	4.7
4.0	306± 31	B(M^2)	L	√	√	√	√	4.8
4.19	345± 50	B(M)	L		√	√	√	4.9
4.50	220± 40	G(M)	Q				√	4.10
5.10	195± 40							4.11
5.40	149± 35				√			4.12
5.50	145± 30	G(M)	Q				√	4.13
6.0	117± 14	B(M)	P	√	√	√		4.14
6.95	93± 17	B(M)	P	√	√	√		4.15
11.7	10± 2							4.16
13.0	12± 4				√			4.17
KEY	G, GAUSSIAN; B, BREIT WIGNER; M, MASS; M^2, MASS SQUARED; P, POLYNOMIAL, Q, QUADRATIC; L, LINEAR.							

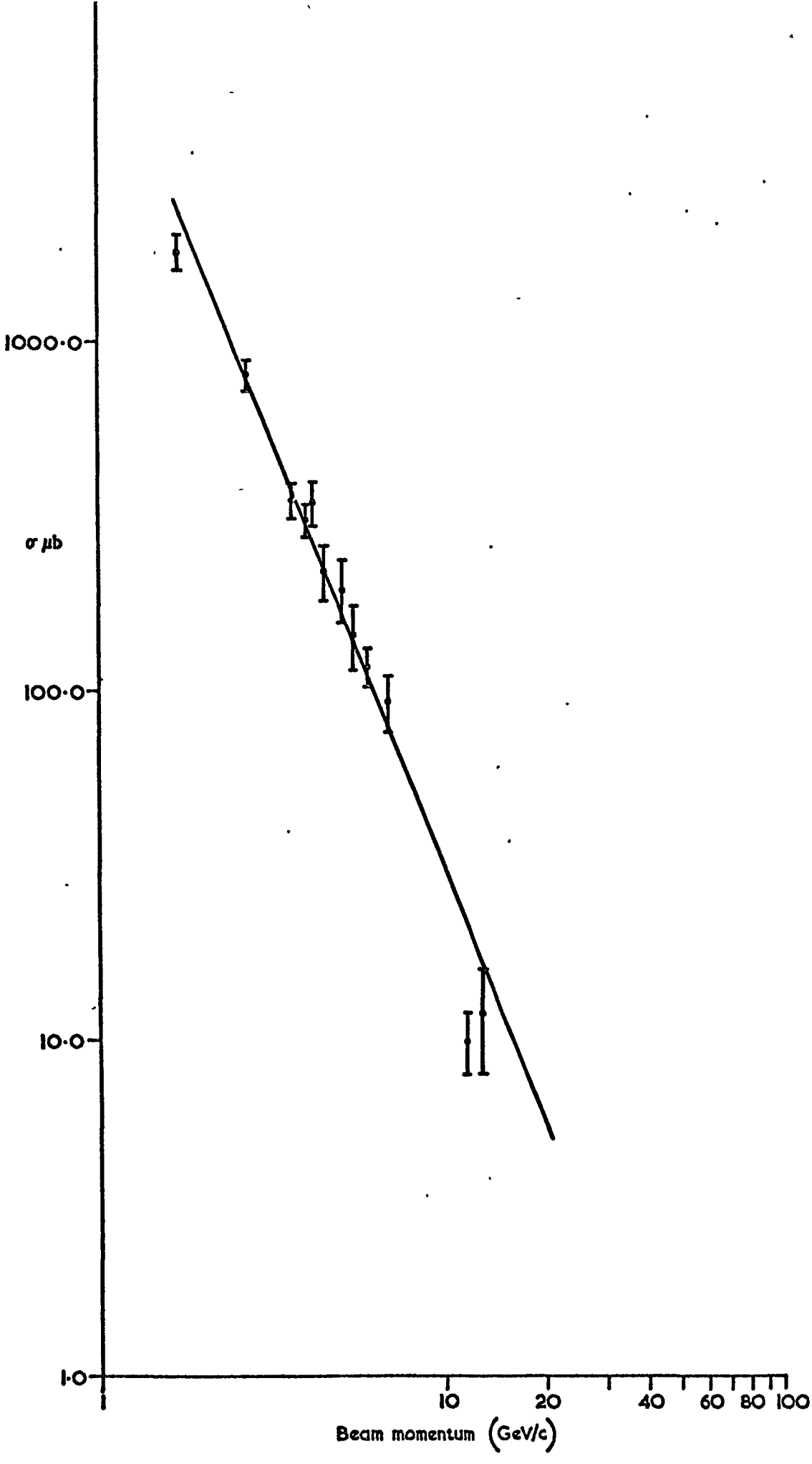

FIG. 4·9

THE VARIATION OF THE PRODUCTION CROSS SECTION WITH THE INCIDENT MOMENTUM.

TABLE 4.6

FIT TO THE SIGNAL	FIT TO BACKGROUND	SIGNAL	BACK - GROUND	No. BINS	χ^2
GAUSSIAN (M)	P	1527	1223	25	30.2
GAUSSIAN (M^2)	P	1551	1176	20	22.7
BREIT WIGNER (M)	P	2247	503	25	17.6
BREIT WIGNER (M^2)	P	2325	402	20	12.0
CONVOLUTION OF BREIT WIGNER AND RESOLUTION FUNCTION	L	1994	733	20	33.1

THE KEY IS THE SAME AS IN TABLE 4.5

chosen. In this analysis, the choice of parameterisation was decided by accepting the fit believed to contain the most physical significance, the choice of perhaps a spuriously better fitting parameterisation, simply on the grounds of it having a smaller χ^2, being considered unacceptable. On this basis, the results from the parameterisation described in the previous section, comprising the convolution of the Breit Wigner and resolution function in mass squared were taken in preference to those resulting from the other fits described in table 4.6. In addition the results of this fit are also found to be in better agreement with the signal to background ratio calculated independently from the ω^0 Dalitz plot analysis described in chapter 5.

4.3 THE DETERMINATION OF THE DIFFERENTIAL CROSS SECTION $\left(\frac{d\sigma}{dt}\right)$

In the determination of the differential cross section for the forward production of ω^0-mesons in the π -N centre of mass system, the events produced in association with spectator protons with momenta in excess of 300 MeV/c have been excluded. The number of these events is expected to be small from the Hulthen distribution, and it is considered that these events may have been involved in a final state interaction which would distort the t distribution.

As in most conventional analyses, the differential cross section $\left(\frac{d\sigma}{dt}\right)$ was firstly determined for a narrow mass region centred on the ω^0-mass. The results for $\left(\frac{d\sigma}{dt}\right)$ as a function of the 4-momentum transfer squared t, measured from the primary to the tripion mass system for both the seen and unseen spectator proton events are shown in FIG. 4.10, all

FIG. 4.10 THE DIFFERENTIAL CROSS SECTION ($d\sigma/dt$) FOR THE ω^0-REGION 0.76→0.81 (GeV/c^2) OF THE TRIPION MASS SPECTRUM

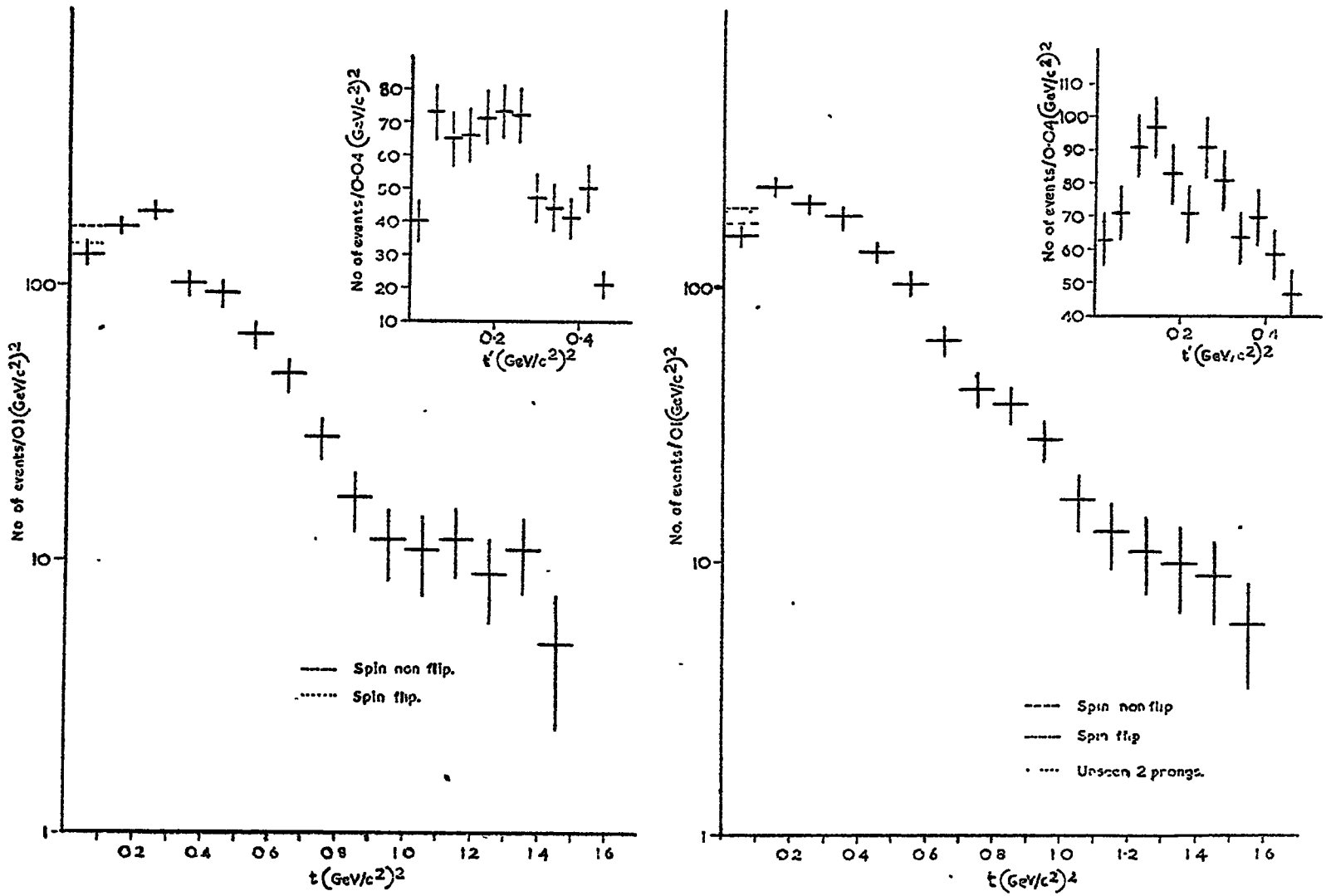

events being restricted to the tripion mass range $0.76 \rightarrow 0.81$ (GeV/c^2). For values of t in excess of 0.1 $(GeV/c^2)^2$, the distributions show no significant structure and are both well fitted by exponential functions e^{-at} where $a = 2.9 \pm 0.8$ and 2.5 ± 0.6 for the seen and unseen spectator proton events respectively. Inset in these diagrams are the variations of $\left(\frac{d\sigma}{dt'}\right)$ for small values of t', where $t' = t - t_{MIN}$ These indicate that the observed dips at low t are still present as $t' \rightarrow 0.0$ in both the seen and unseen spectator proton events, thereby confirming that this effect does not result from the kinematical cut off at $t = t_{MIN}$.

In addition the dip structure has been examined to determine whether it results from technical features of the data. The maximum corrections for the scanning losses and Pauli exclusion effects are drawn on the plots, and as can be seen, although much reduced, there is still some indication of a dip at low t.

In the above plots no corrections have been made for the effects of background, and it has yet to be shown that the expected minimum at $t \sim 0.6$ $(GeV/c^2)^2$ resulting from the ρ Regge Pole exchange is not obscured by the background events. In addition the effects of the background on the observed dip at low t have also to be determined. To minimize the effect of background only a narrow region of mass in the central ω^0 - region has been used. Consequently many events in the tails of the ω^0 - distribution have been rejected. These restrictions can be obviated by extracting the amount of ω^0 - signal and background in each t'-interval. This is achieved in precisely the same way as in the previous

section for the determination of the total ω^0 - production cross section. The tripion mass spectrum of the events in a given t'- interval is fitted with a Breit Wigner convoluted with a resolution function and a linear background. In this way, events in a given t'- interval are divided into ω^0-signal and background. The differential cross sections $\left(\frac{d\sigma}{dt'}\right)$ for the seen and unseen spectator proton events corresponding to the ω^0-signal and background for the fitted mass squared region $0.4 \rightarrow 0.8$ $(GeV/c^2)^2$ are shown in FIG. 4.11.

Although the use of a linear parameterisation for the background under the ω^0-signal was found to be valid in the determination of the total ω^0-meson production cross section, such a parameterisation may not be correct for all t'-intervals. Hence as a check, fits to each t'-region were also made using the polynomial background parameterisation described earlier, and in all cases the results were found to be in excellent agreement with those shown in FIG. 4.11. In addition, to improve the available statistics for the fits, the samples containing the seen and unseen spectator proton events were combined. Although the widths of the resolution functions are different for these two classes of events the use of a Breit Wigner resolution function is still valid, since the sum of two Breit Wigners also approximates to a Breit Wigner. The results are summarised in table 4.7, and as can be seen the results for the seen and unseen spectator proton events fitted both separately and together, are in good agreement.

From the results shown in FIG. 4.11 it can be concluded that there is no evidence for a minimum in the differential cross section at $t' \sim 0.6$ $(GeV/c^2)^2$. The distributions for

TABLE 4.7

THE RESULTS OF THE FITS TO $\left(d\sigma/dt'\right)$								
$(GeV/c^2)^2$	UNSEEN SPECTATOR PROTONS		SEEN SPECTATOR PROTONS		TOTAL		FITS TO SEEN AND UNSEEN COMBINED	
T' INTERVAL	SIGNAL	BACK-GROUND	SIGNAL	BACK-GROUND	SIGNAL	BACK-GROUND	SIGNAL	BACK-GROUND
0.0 → 0.1	223	237	158	96	381	333	362	352
0.1 → 0.2	313	183	200	56	513	239	516	236
0.2 → 0.3	324	58	225	23	549	81	549	81
0.3 → 0.4	320	41	138	39	458	80	455	83
0.4 → 0.5	186	58	101	28	287	86	294	79
0.5 → 0.6	130	43	81	21	211	64	216	59
0.6 → 0.8	164	44	114	11	278	55	279	54
0.8 → 1.0	82	45	45	14	127	59	133	53

both the seen and unseen spectator proton events exhibit a smooth t'- dependence for $t' > 0.3$, with exponents of 2.8 ± 0.8 and 3.8 ± 0.6 respectively. The main feature of the results is the contrast in behaviour between the differential cross sections at low t'-values for the ω^o - signal and background, which is manifest as a strong dip for the ω^o - signal and an absence of a dip for the background. This feature is present for both the seen and unseen spectator proton events. The errors quoted are statistical errors only and do not include the precision with which the fitting programme seperates the signal and background. The tripion mass spectra for the seen and unseen spectator proton events are shown in FIG. 4.12, in t'- intervals of 0.1 $(GeV/c^2)^2$ from 0.0 to 1.0 $(GeV/c^2)^2$, and a comparison of the background under the ω^o for the first two t'- intervals confirms the absence of any dip in the background as $t' \rightarrow 0.0$. As illustrated in FIG. 4.11 however, the differential cross section for the background under the ω^o - signal for the unseen spectator proton events indicates not only the absence of a dip in this region, but also suggests an upward trend. It might be argued therefore that the dip in the t' distribution as $t' \rightarrow 0.0$ for the ω^o - signal is simply a downward fluctuation produced directly by the upward fluctuation of the background.

To put this into perspective the t'- distributions are also shown in FIG. 4.13 for the higher mass regions neighbouring that of the ω^o, (below the ω^o mass there is very little background). The distributions are shown separately for events corresponding to the first and second exposures. Such

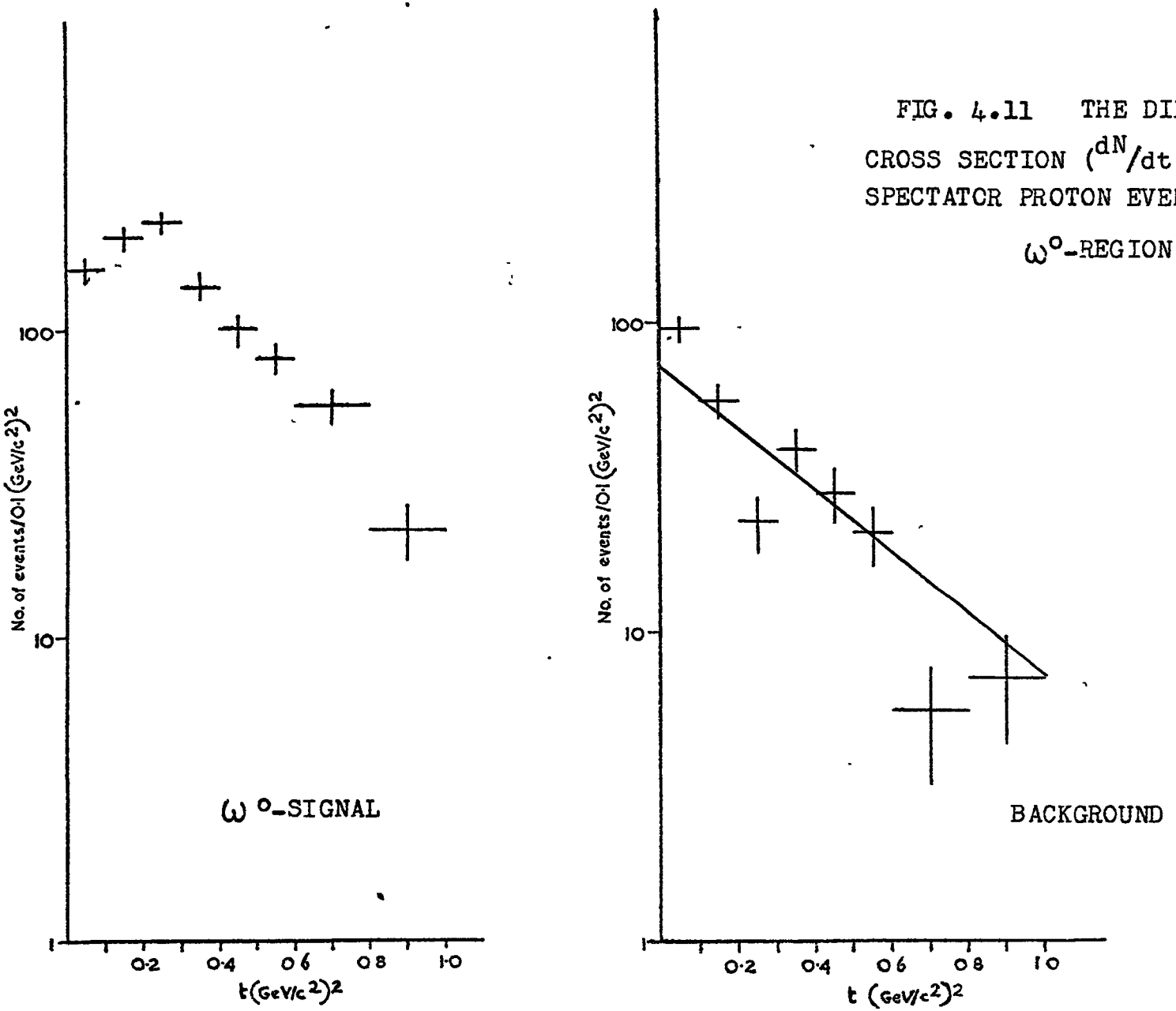

FIG. 4.11 THE DIFFERENTIAL CROSS SECTION ($^{dN}/_{dt}$) FOR THE SEEN SPECTATOR PROTON EVENTS IN THE FITTED ω^{o}-REGION

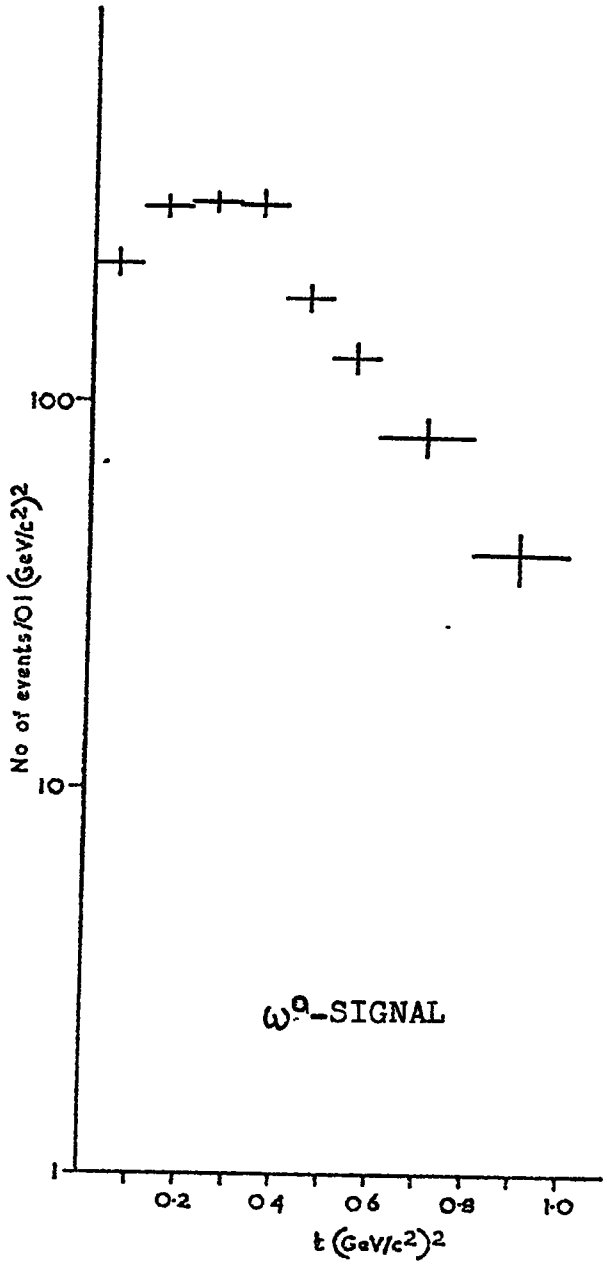

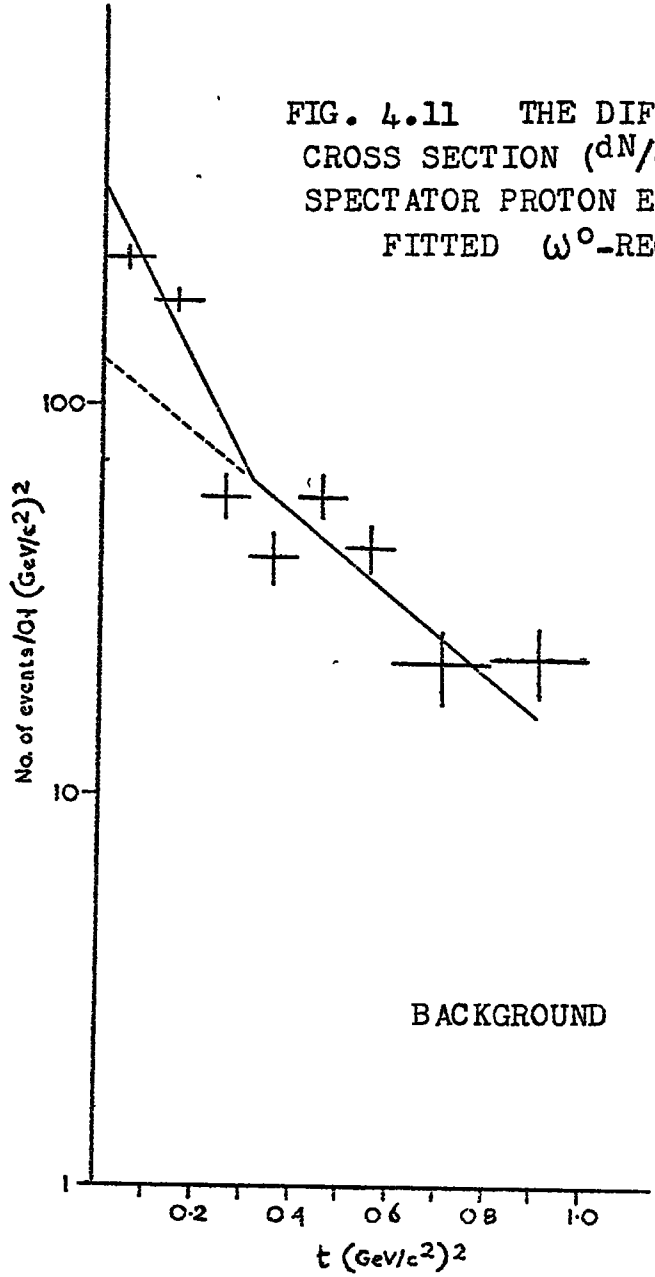

FIG. 4.11 THE DIFFERENTIAL CROSS SECTION ($^{dN}/_{dt}$) FOR UNSEEN SPECTATOR PROTON EVENTS IN THE FITTED ω^{o}-REGION

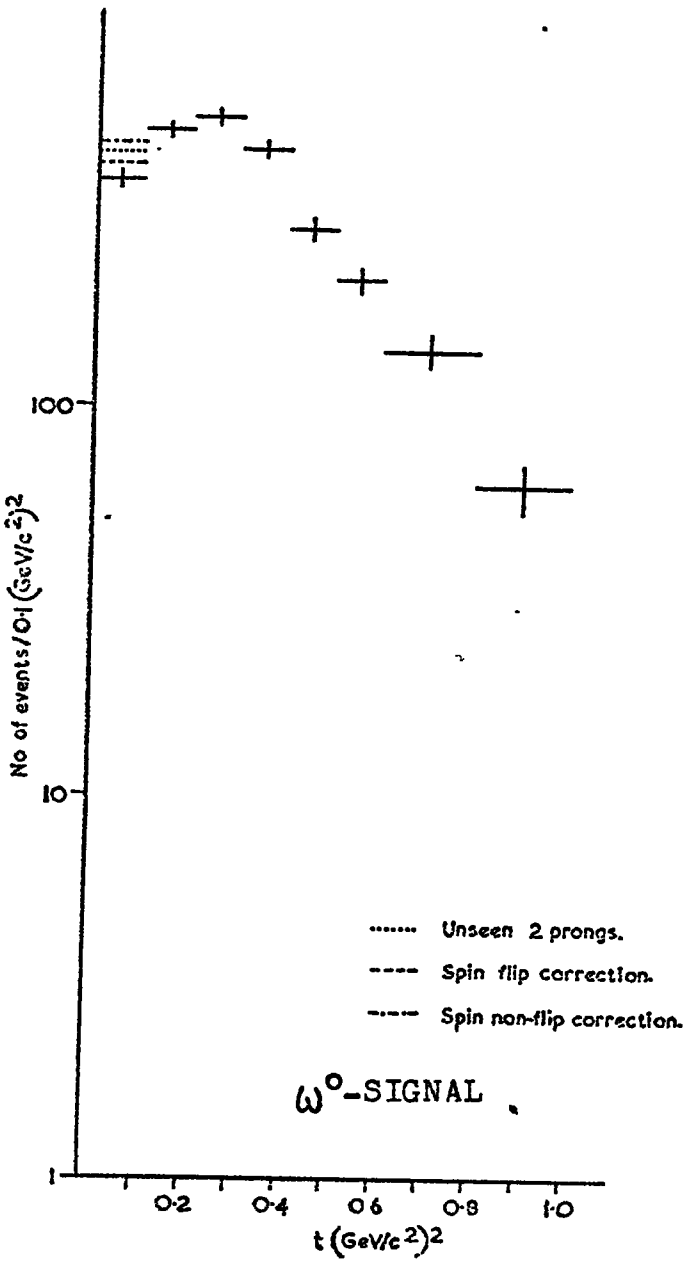

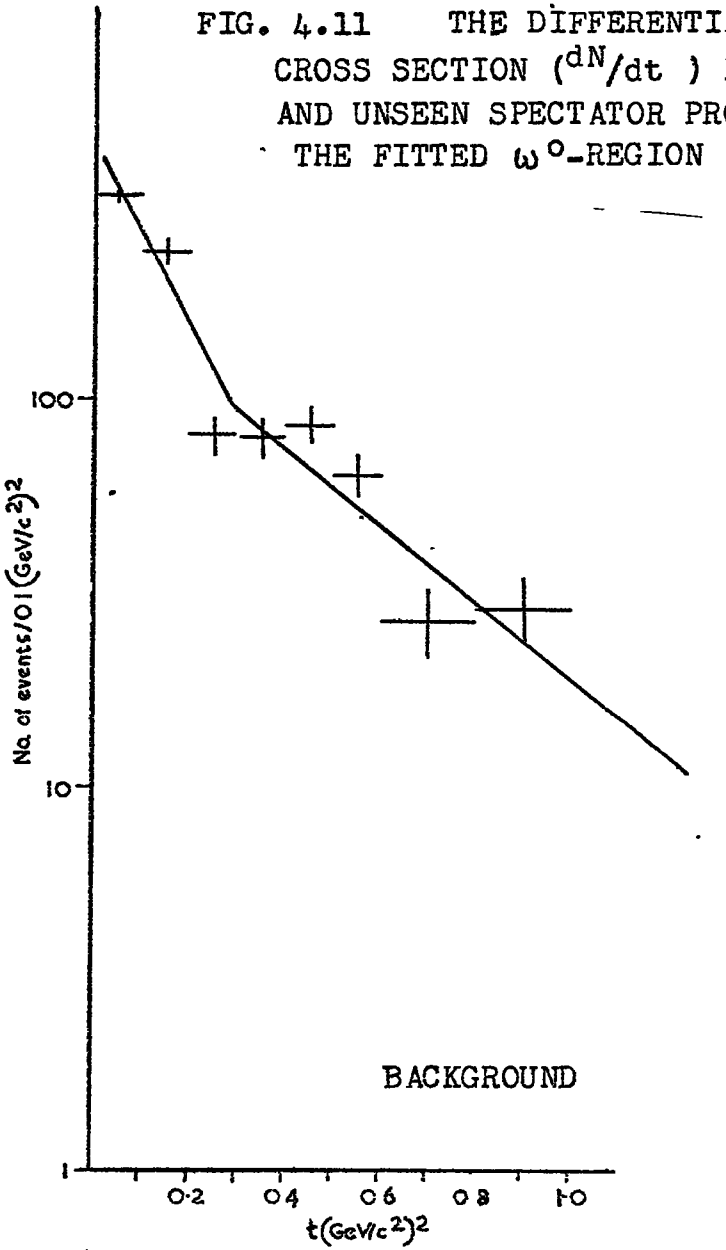

FIG. 4.11 THE DIFFERENTIAL CROSS SECTION ($^{dN}/_{dt}$) FOR BOTH THE SEEN AND UNSEEN SPECTATOR PROTON EVENTS IN THE FITTED ω^{o}-REGION

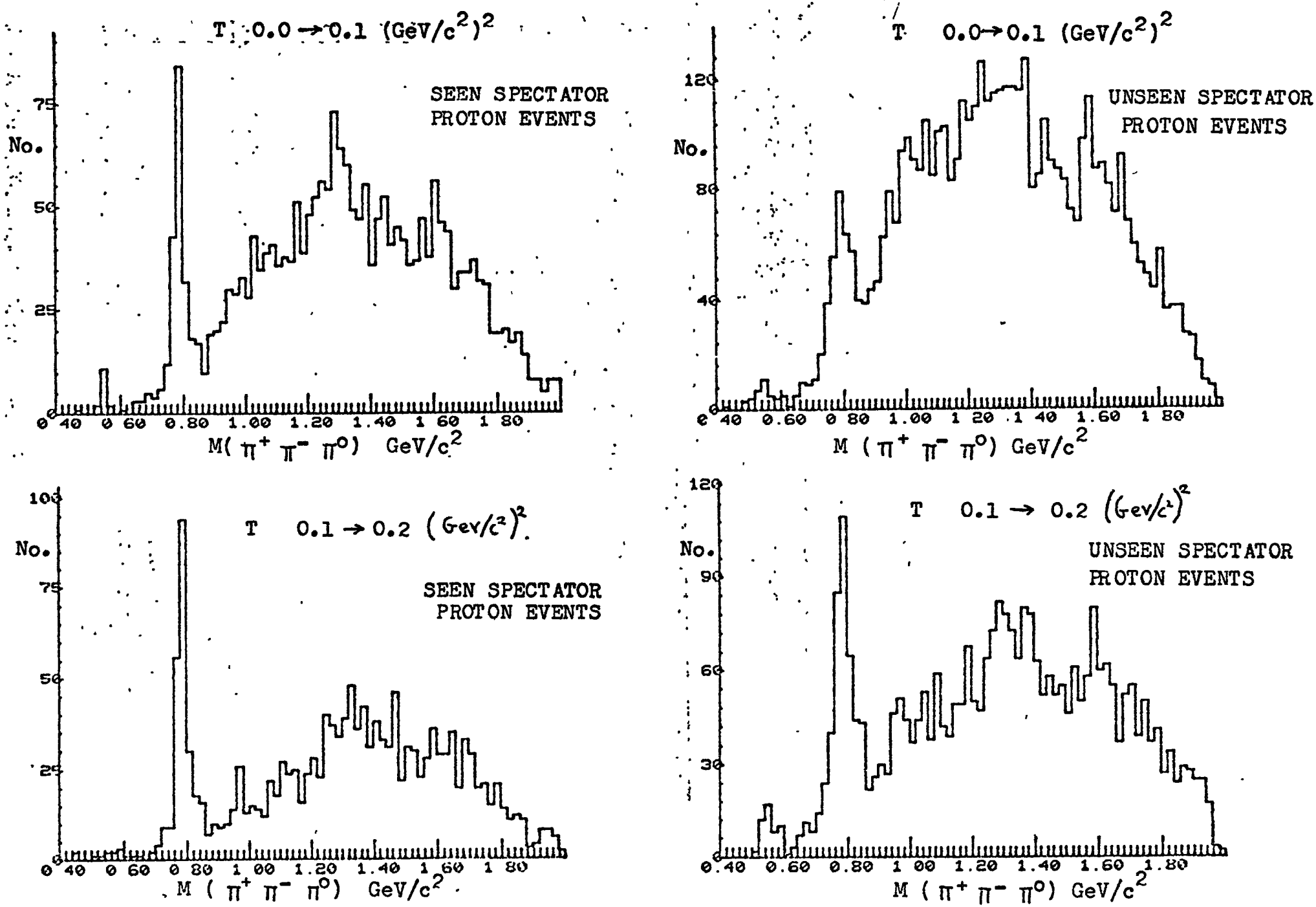

FIG. 4 12 THE TRIPION MASS SPECTRA FOR EVENTS IN THE T INTERVALS INDICATED

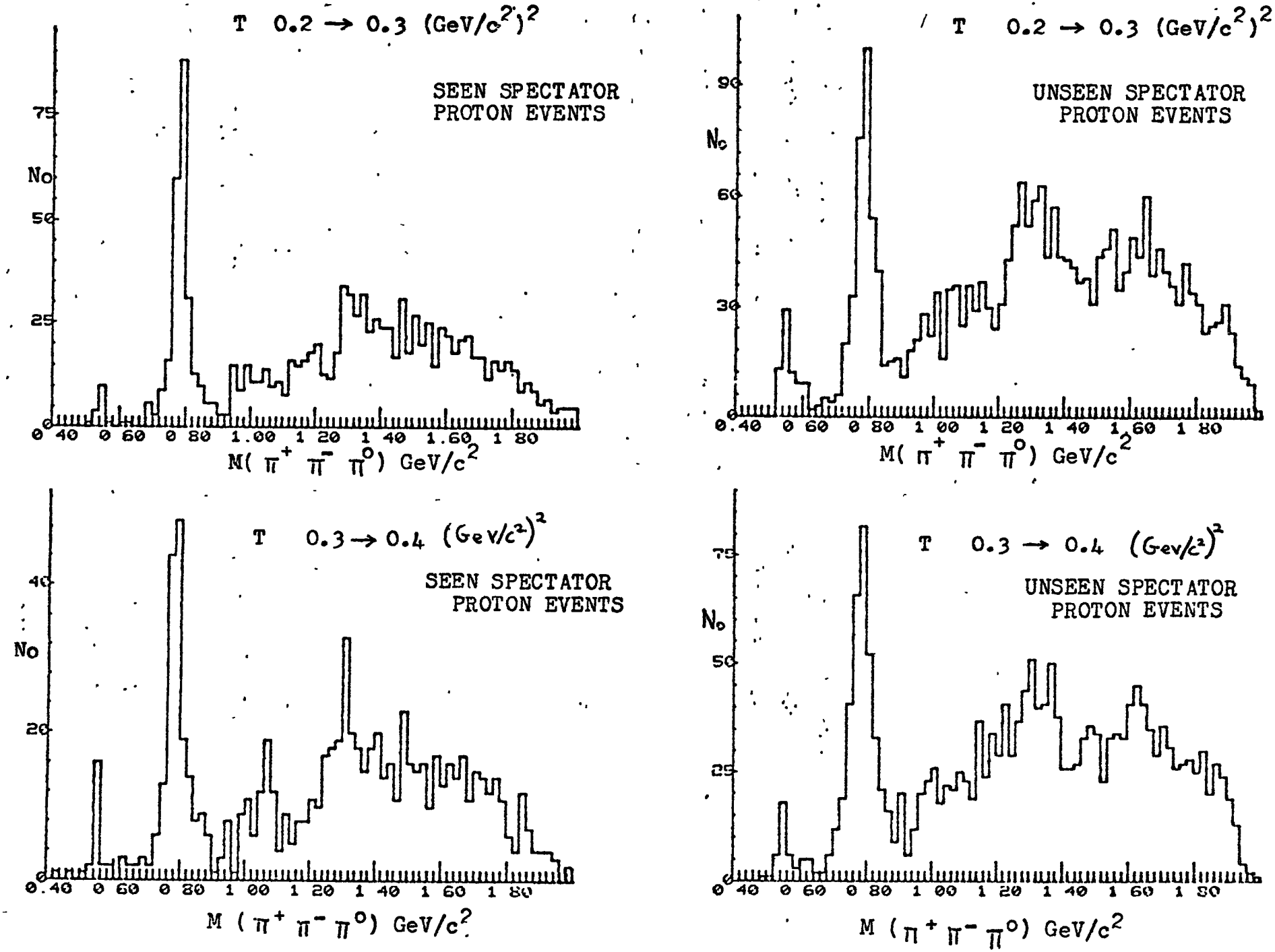

FIG. 4 12 THE TRIPION MASS SPECTRA FOR EVENTS IN THE T INTERVALS INDICATED

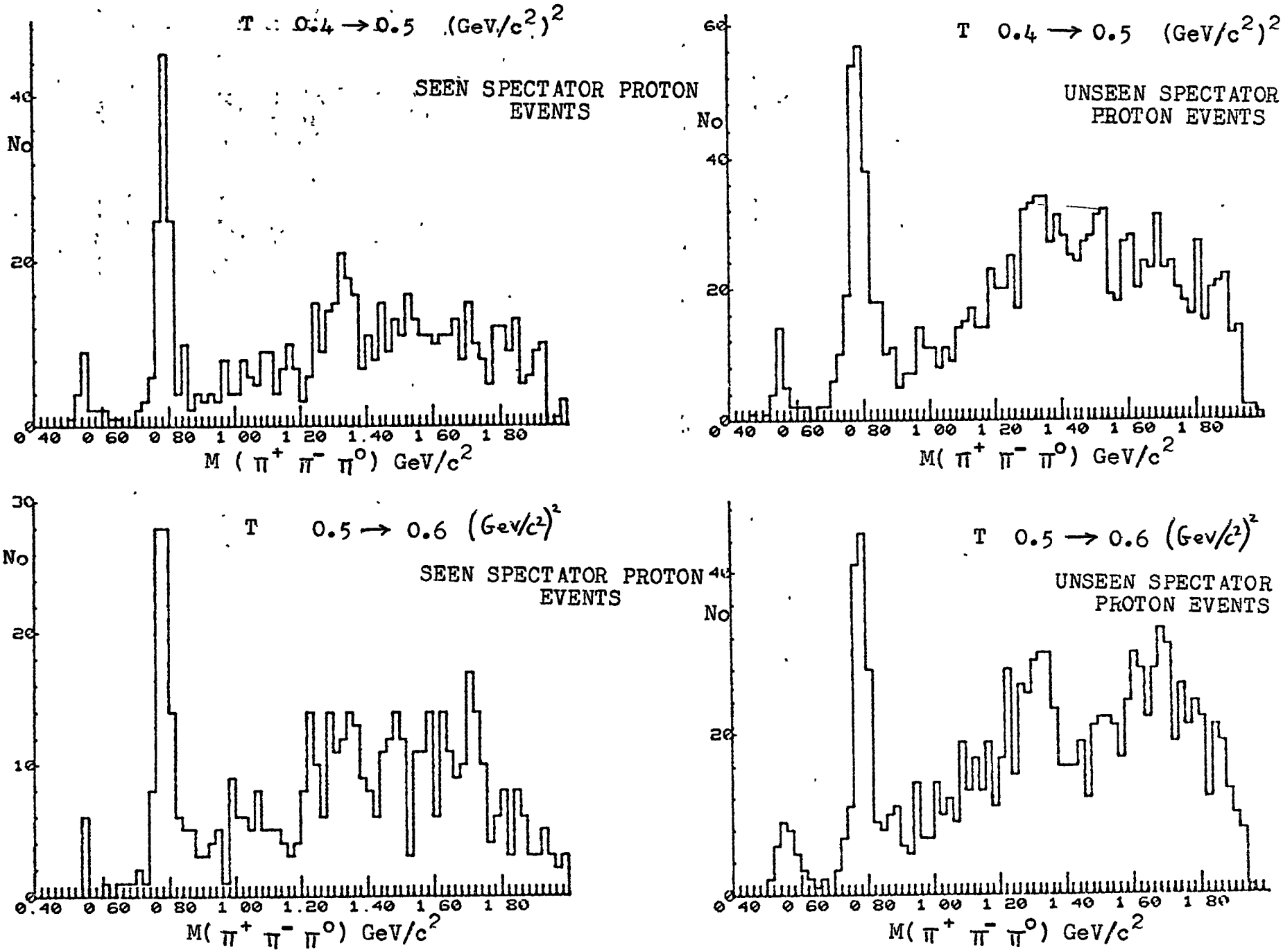

FIG. 4 12 THE TRIPION MASS SPECTRA FOR EVENTS IN THE T INTERVALS INDICATED

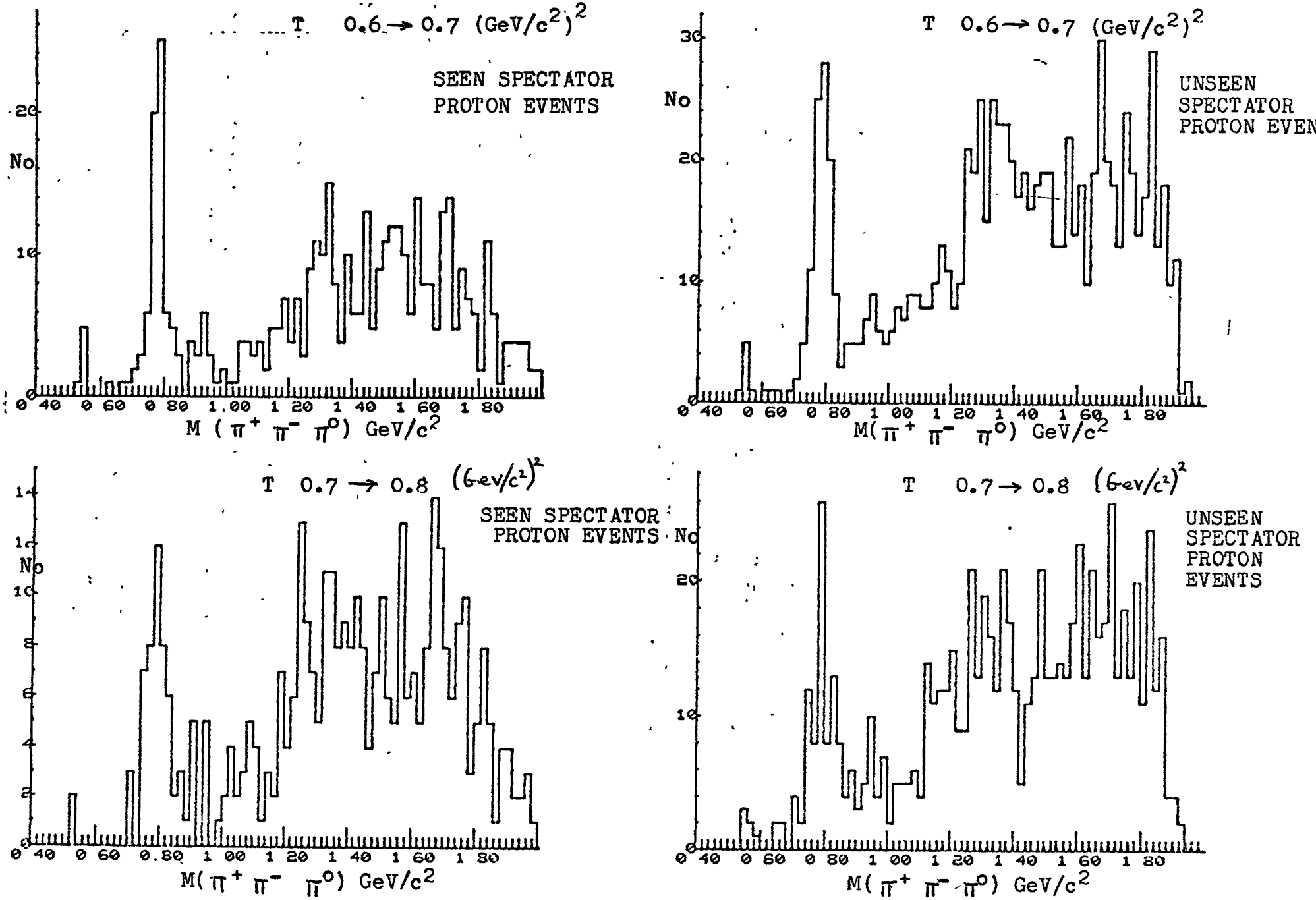

FIG. 4.12 THE TRIPION MASS SPECTRA FOR EVENTS IN THE T INTERVALS INDICATED

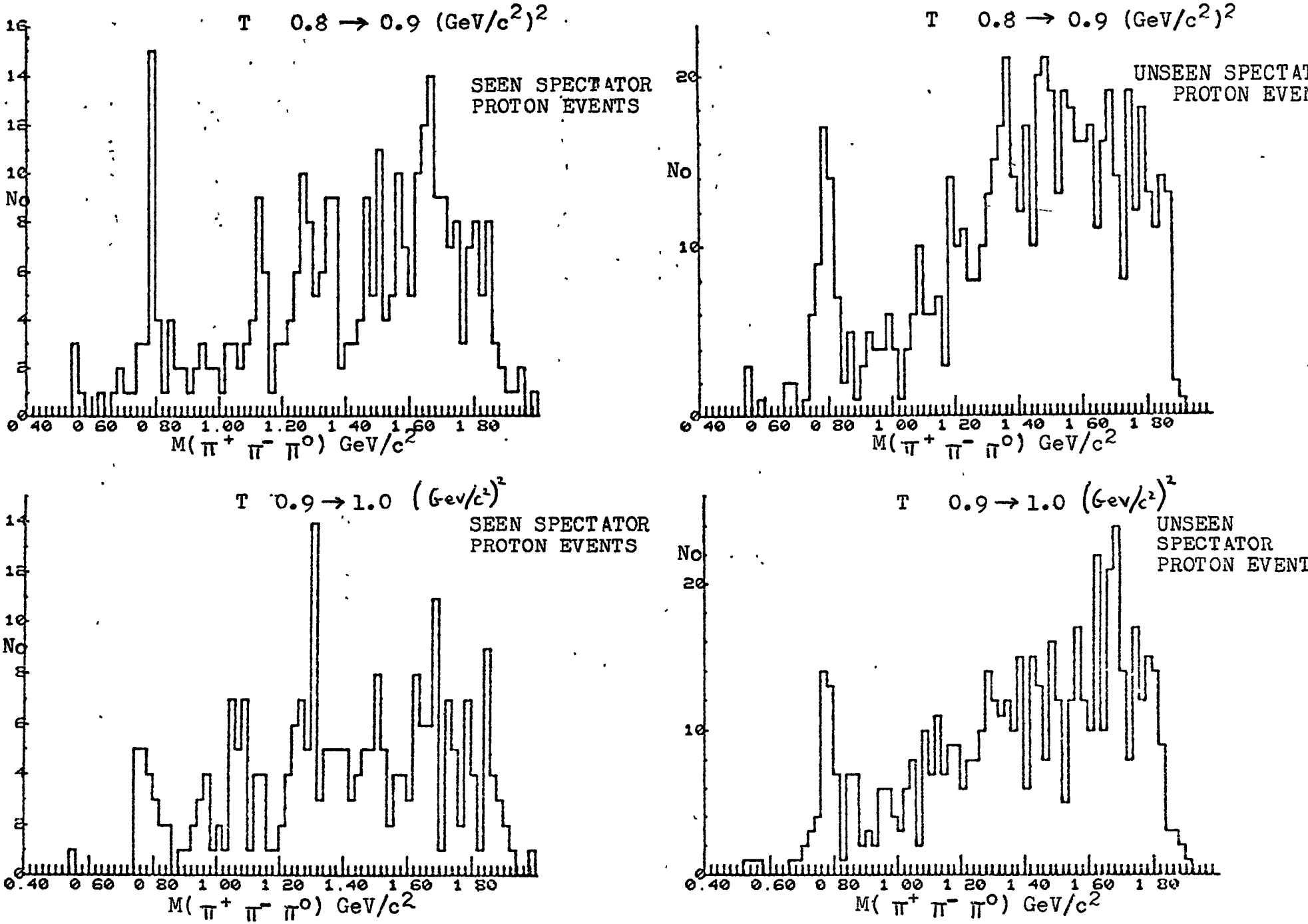

FIG. 4.12 THE TRIPION MASS SPECTRA FOR EVENTS IN THE T INTERVALS INDICATED

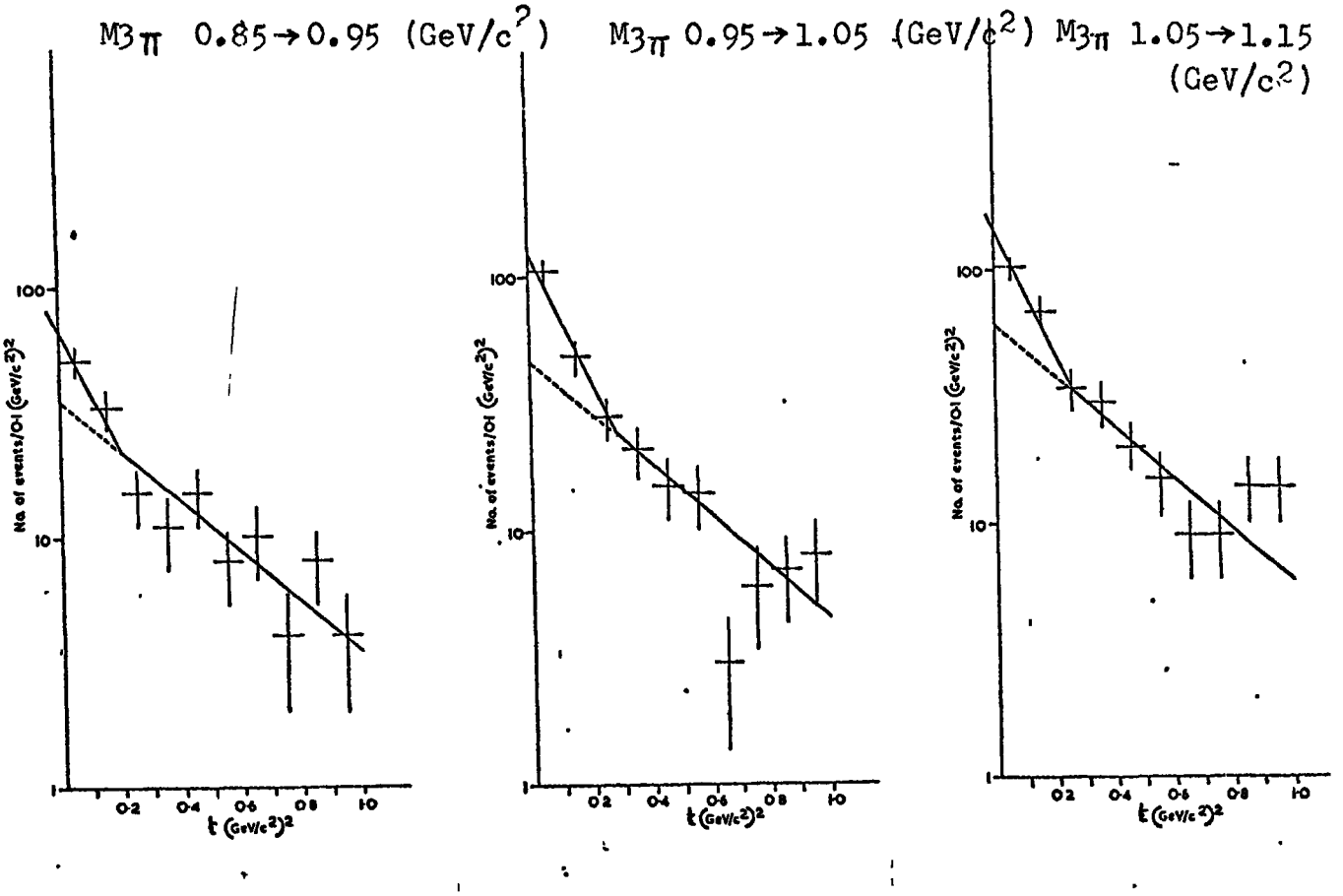

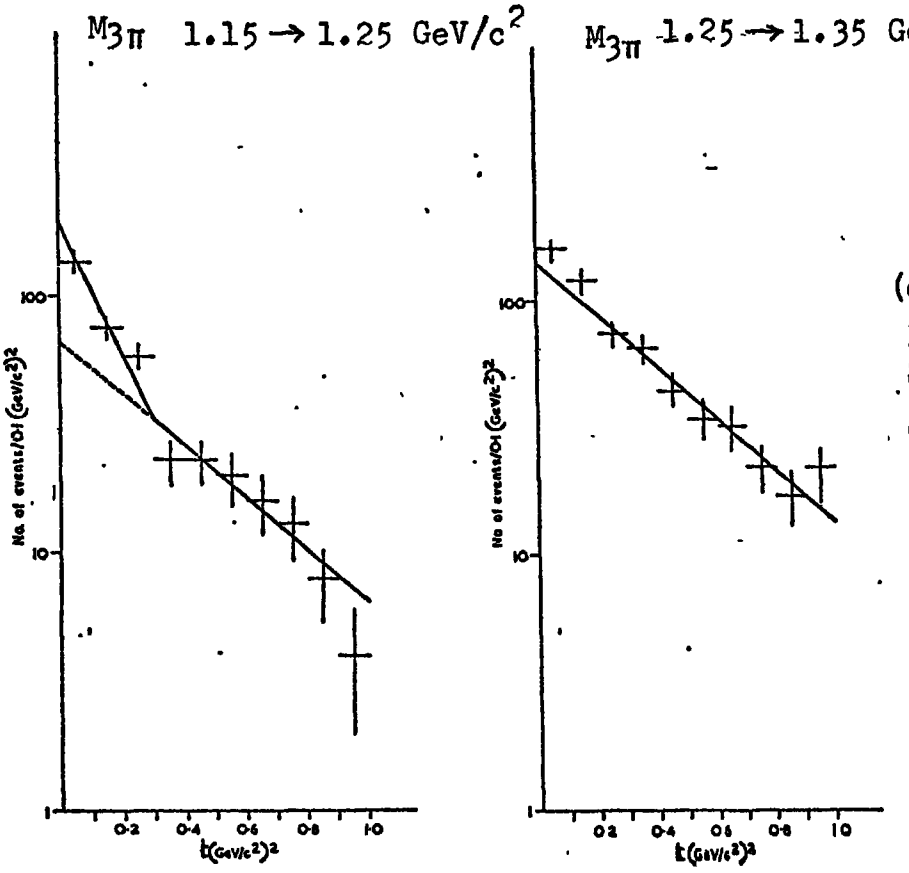

FIG. 4.13

(dN/dt) DISTRIBUTIONS FOR 1st EXPOSURE SEEN SPECTATOR PROTON EVENTS CONFINED TO THE TRIPION MASS-INTERVALS INDICATED

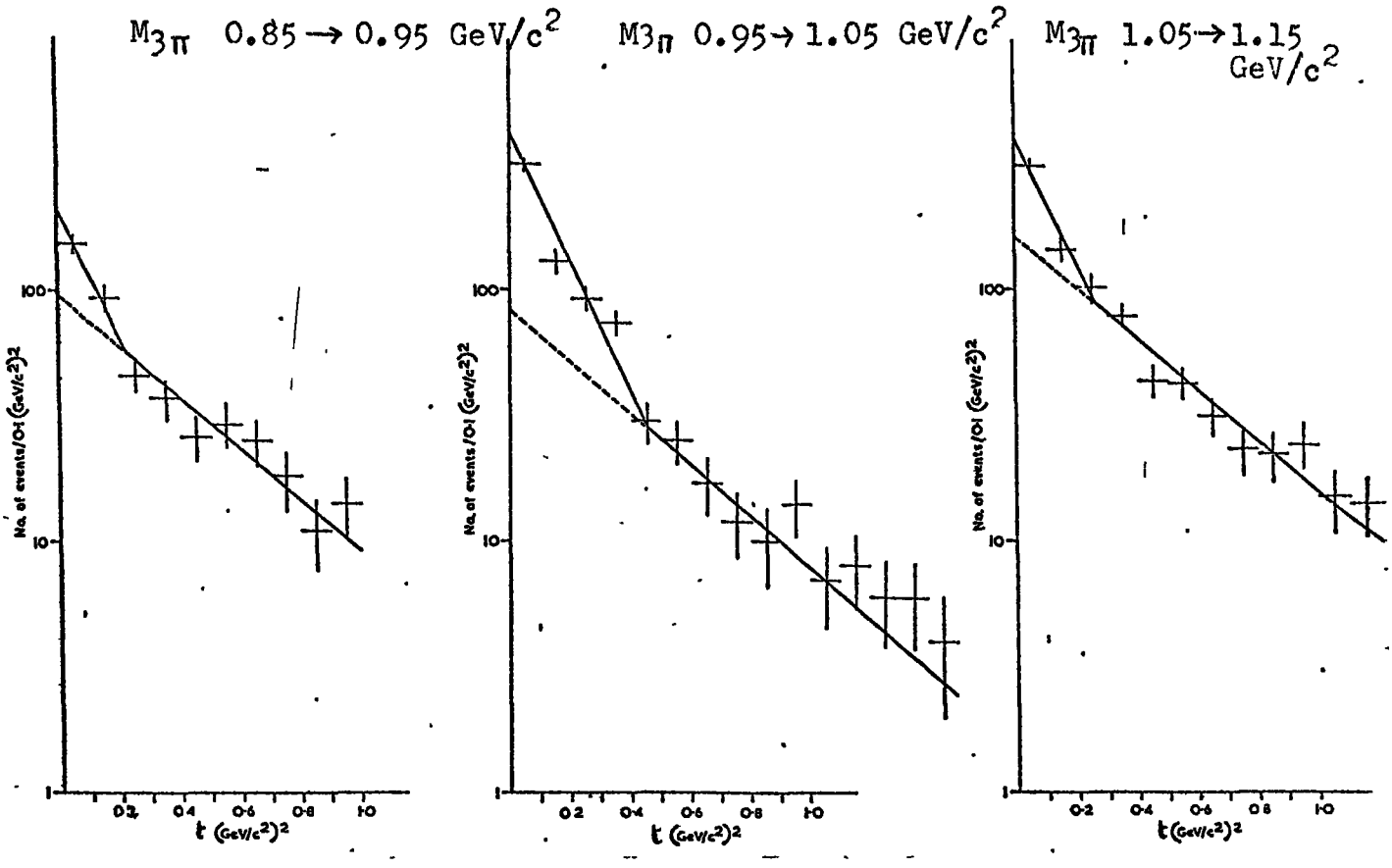

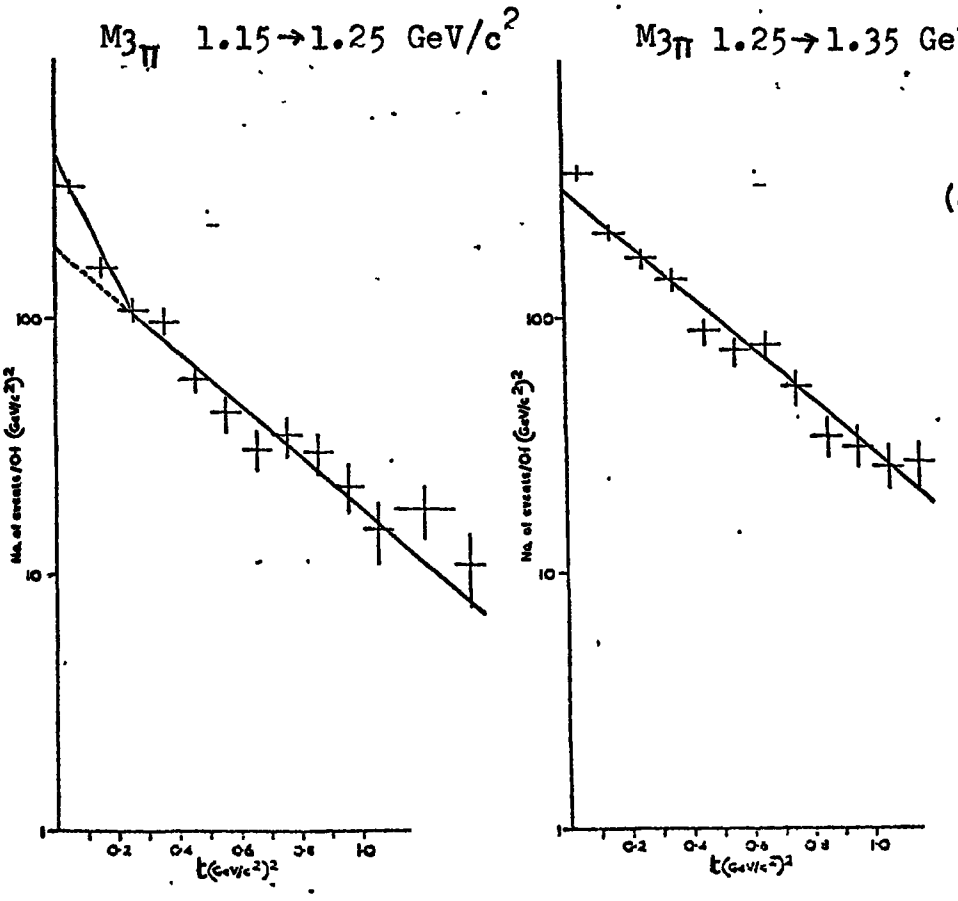

FIG. 4.13

(dN/dt) DISTRIBUTIONS FOR 1st EXPOSURE UNSEEN SPECTATOR PROTON EVENTS CONFINED TO THE TRIPION MASS INTERVALS INDICATED

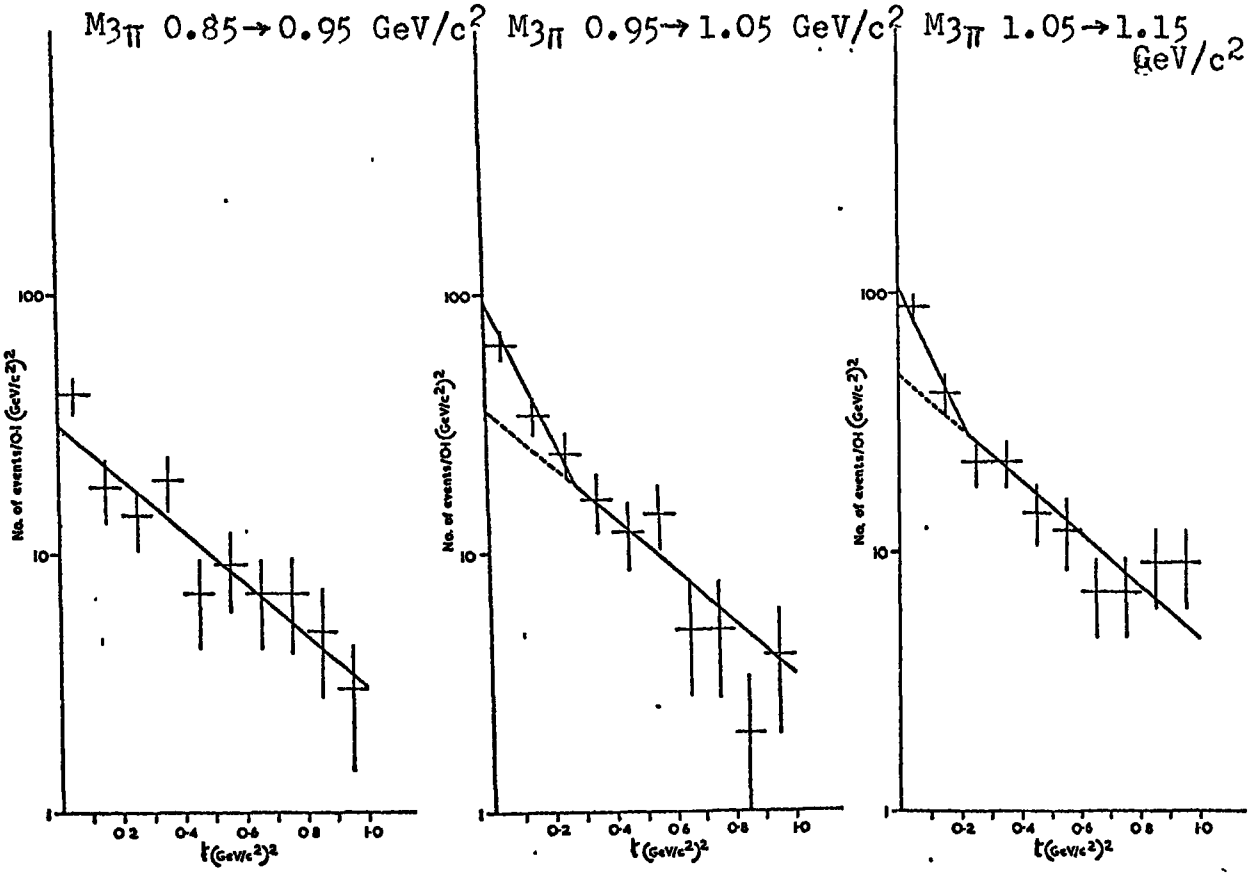

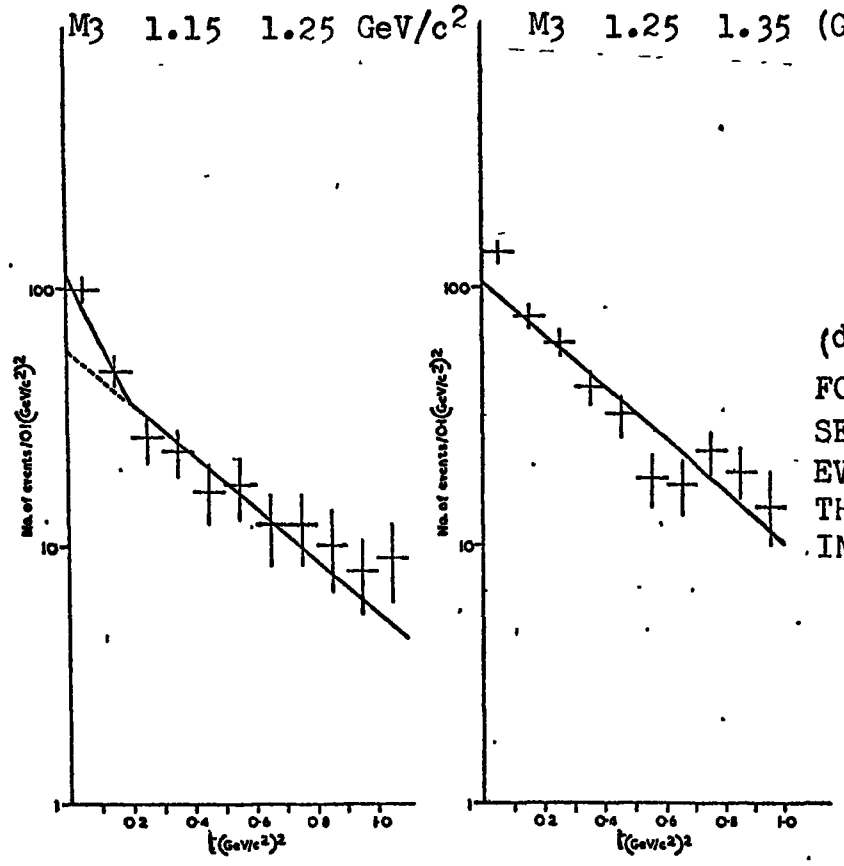

FIG. 4.13
(dN/dt) DISTRIBUTIONS FOR 2nd EXPOSURE SEEN SPECTATOR PROTON EVENTS CONFINED TO THE TRIPION MASS INTERVALS INDICATED

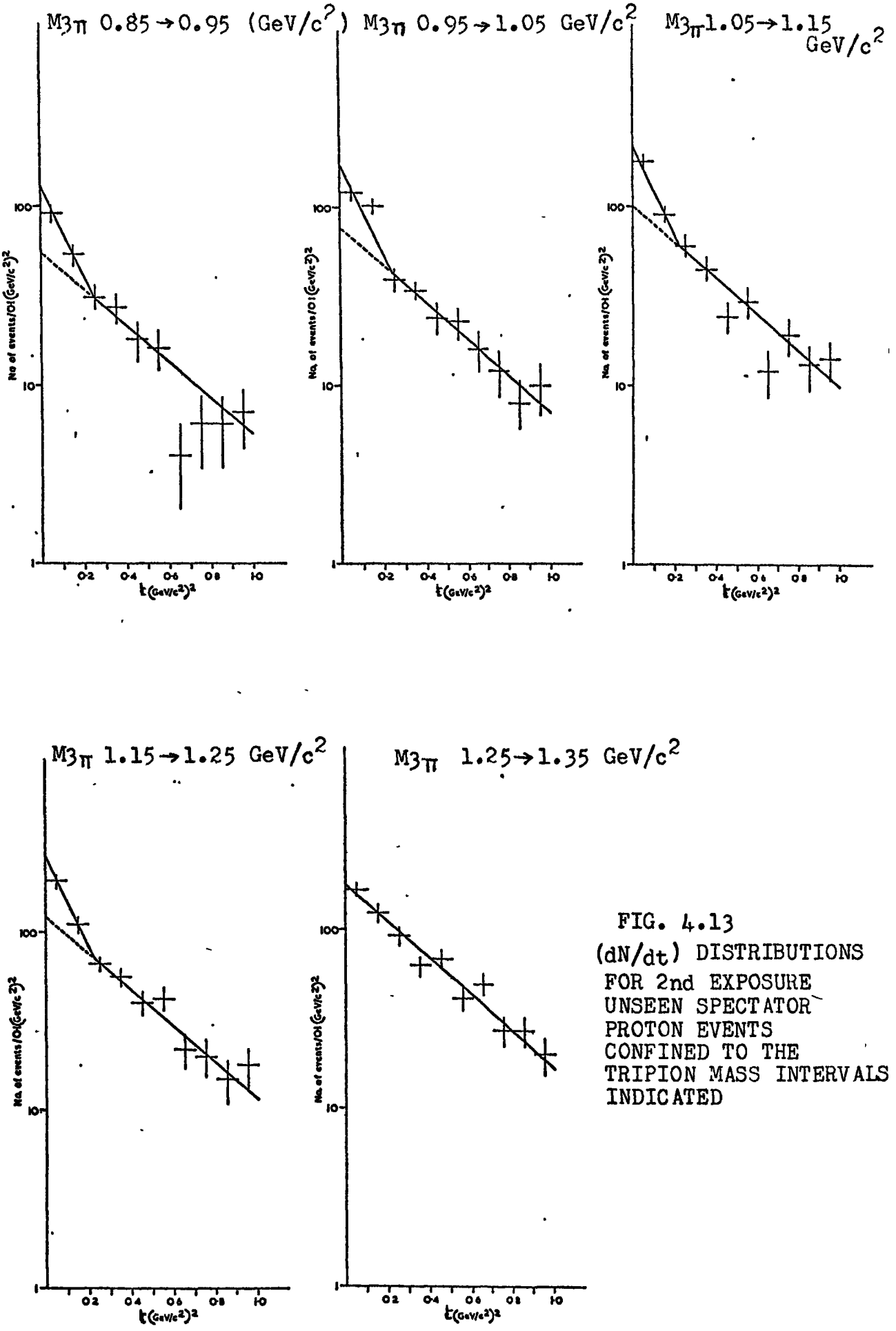

FIG. 4.13
(dN/dt) DISTRIBUTIONS FOR 2nd EXPOSURE UNSEEN SPECTATOR PROTON EVENTS CONFINED TO THE TRIPION MASS INTERVALS INDICATED

a division of the data was considered necessary because of the observed differences in the tripion mass spectra for $t' < 0.05$ $(GeV/c^2)^2$ for the unseen spectator proton events. The differences are well illustrated in FIG.4.14 in which it is evident that that the strong 1.0 (GeV/c^2) peak observed in the 1st exposure is not apparent in the 2nd exposure. From FIG. 4.13 it can be seen that the distributions in the higher mass regions can in the same way as the background under the ω^o - signal be described by the sum of two exponential distributions, the shallower distribution having a slope of ~ 2.4 and the steeper one a slope of ~ 6.0. Lines of these slopes are drawn on all the plots and the results indicate that the upward turn in the differential cross section for the background under the ω^o - region is real, and hence that the observed dip in FIG. 4.11 as $t' \rightarrow 0.0$ is associated entirely with the ω^o - signal.

(a) A SUMMARY OF THE RESULTS

After making corrections for the Pauli exclusion effect, scanning losses, and the effects of the background it can be concluded that the differential cross section $(d\sigma/dt')$ for the forward production of ω^o - mesons in the $\pi - N$ centre of mass system dips as $t' \rightarrow 0.0$, peaks at $t' \sim 0.25$ $(GeV/c^2)^2$ and exhibits a smooth exponential fall off for $t' > 0.3 (GeV/c^2)^2$ with an exponent of 3.5 ± 0.5, there being no evidence for any structure at $t' \sim 0.6$ $(GeV/c^2)^2$. In addition it is evident that the behaviour of the background is not the same as for the ω^o - signal. It appears to be constructed from events associated with two different production processes,

FIG. 4.14 THE TRIPION MASS SPECTRA FOR THE 1st AND 2nd EXPOSURE EVENTS FOR $t < 0.1$ $(GeV/c^2)^2$

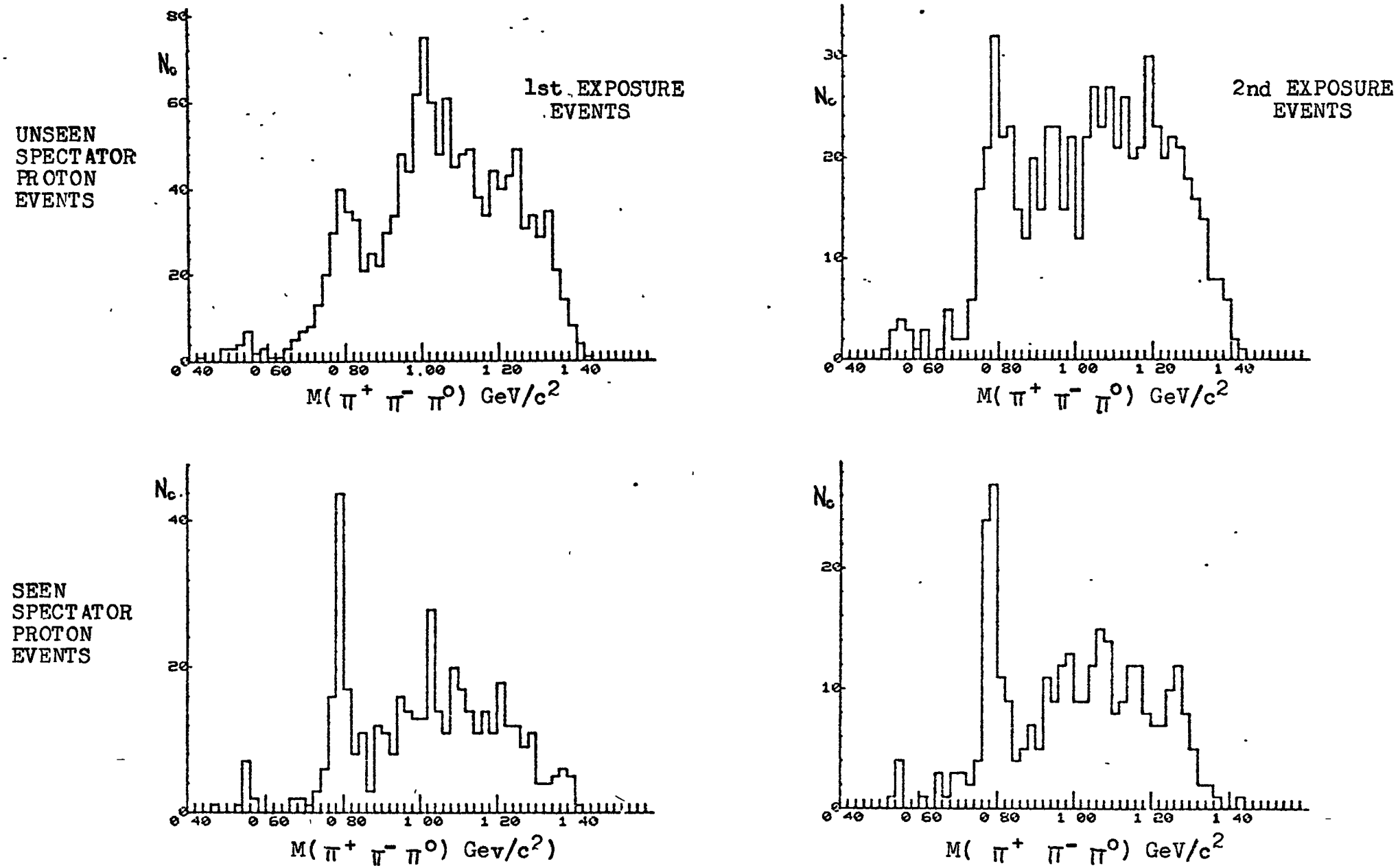

one characterised by a slope of ~ 2.4 and the other by a slope of ~ 4.0, their net effect tending to obscure the presence of a dip at low t' values for the ω^0 - signal.

CHAPTER FIVE

AN INVESTIGATION OF THE NATURE OF THE BACKGROUND ASSOCIATED WITH THE ω^o - REGION OF THE TRIPION MASS SPECTRUM

INTRODUCTION

The results of the previous chapter suggested the presence of at least two different contributions to the background in the ω^o - region of the tripion mass spectrum. In this chapter the nature of this background is analysed in detail. In particular the contributions to the ω^o - region and the H and A1 regions of the spectrum are discussed.

5.1 THE SOURCES OF THE BACKGROUND

Of particular importance is the nature of the background whose t distribution has an exponent of ~ 4, since it is this which tends to obscure the presence of a dip at low t in the ω^o - differential cross section. An estimate of the number of events characterised by this exponent can be found by summing the excess of events above the shallow line drawn in FIG. 4.13. It will only correspond to an estimate since the true behaviour of either of these backgrounds is unknown at low t. Indeed, either may dip or rise here rather than conform to the behaviour indicated by the straight lines. The results of summing these events as a function of the tripion mass spectrum for the 1st and 2nd exposure seen and unseen spectator proton events are shown in FIG. 5.1, along with the total estimated number of events. The results

FIG. 5.1 THE TRIPION MASS SPECTRUM FOR THE BACKGROUND EVENTS DOMINATING THE 1.0 GeV/c^2 REGION

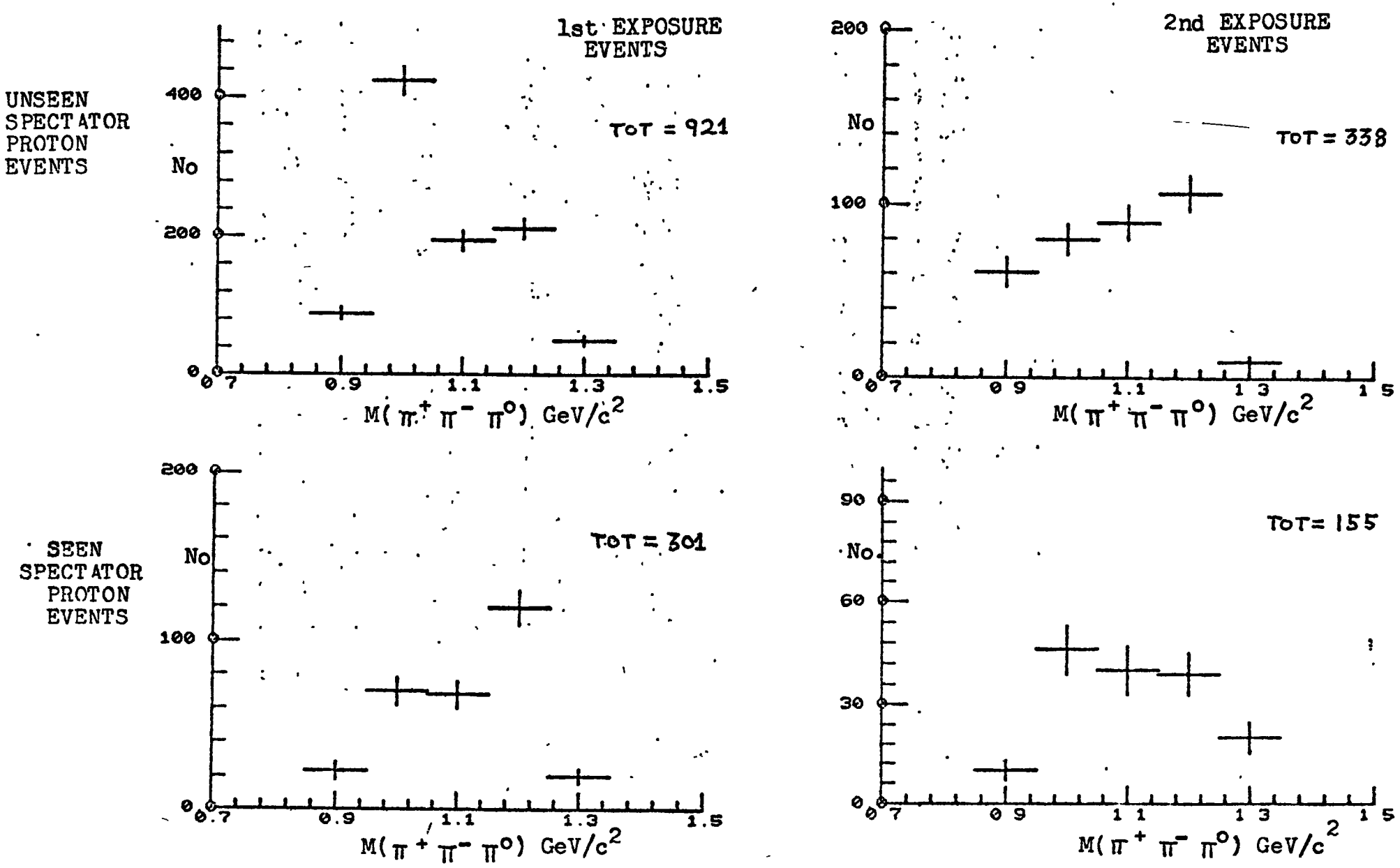

indicate that these events are associated with a broad enhancement in the 1.0 GeV/c^2 region of the tripion mass spectrum, and in particular to the low t region of the 1st exposure events with unseen spectator protons. The presence of this feature is clearly seen in the tripion mass spectra shown in FIG. 4.14

The different results in the low t' - region for the two exposures indicates a technical fault in one or other of the samples. It is not clear whether the technical fault has resulted in the removal of the 1.0 GeV/c^2 enhancement from the 2nd exposure events, or resulted in its inclusion in the 1st exposure events.

If the assumption were to be made that the results for the seen and unseen spectator proton events should be consistent, the 1st exposure events would be assumed to be dominated by the technical fault, since the 1.0 GeV/c^2 enhancement is mainly associated with the unseen spectator proton events in this sample. However, as illustrated in section 2.4, the effects of the Pauli exclusion principle make the latter assumption uncertain. Indeed, for a production process resulting in spin non-flip of the recoiling proton, the events are expected to populate the unseen spectator proton events preferentially. Consequently the comparison of the seen and unseen spectator proton events cannot be used to identify the presence of a technical fault.

5.2 A DISCUSSION OF THE ORIGINS OF THE ENHANCEMENT IN THE 1.0 GeV/c^2 REGION OF THE TRIPION MASS SPECTRUM

The above problem can be resolved by examining the nature

of the 1.0 GeV/c^2 enhancement and determining whether it is a genuine feature of the tripion mass spectrum.

The dipion mass combinations for the unseen spectator proton events confined to the tripion mass interval 0.95 → 1.05 GeV/c^2 and to the t - region < 0.1 (GeV/c^2)^2 are shown in FIG. 5.2, and the results clearly illustrate that the 1.0 GeV/c^2 enhancement is associated with a strong ρ^0- signal. There is little or no evidence for any ρ^- production, and only a slight indication of ρ^+ production. This observation implies that the 1.0 GeV/c^2 enhancement is unlikely to be a resonance since a resonance decaying via ρ^0 π^0 will also contribute equally to the ρ^+ π^- and ρ^- π^+ modes. It could be argued however that a technical fault in the data might tend to obscure the presence of the ρ^+ and ρ^- signals, eg. by inaccurate fitting of the π^0 secondaries. Consequently the possibility of the 1.0 GeV/c^2 enhancement corresponding to a resonance cannot be disregarded.

From the Review of Particle properties 1974 (Ref. 4.1), the listed resonances associated with ρ^0 - decays in and around the 1.0 GeV/c^2 region of the tripion mass spectrum are as shown below:-

η' (958), H (990), Φ (1019)

the existence of the H - meson being in some doubt. In the following sections, however, it will be seen that none of these is able to account for the 1.0 GeV/c^2 enhancement.

(a) <u>The η' (958)</u>

Some 27% of the η' decays proceed via the mode ρ^0 γ and since the kinematical fitting programmes are unable to

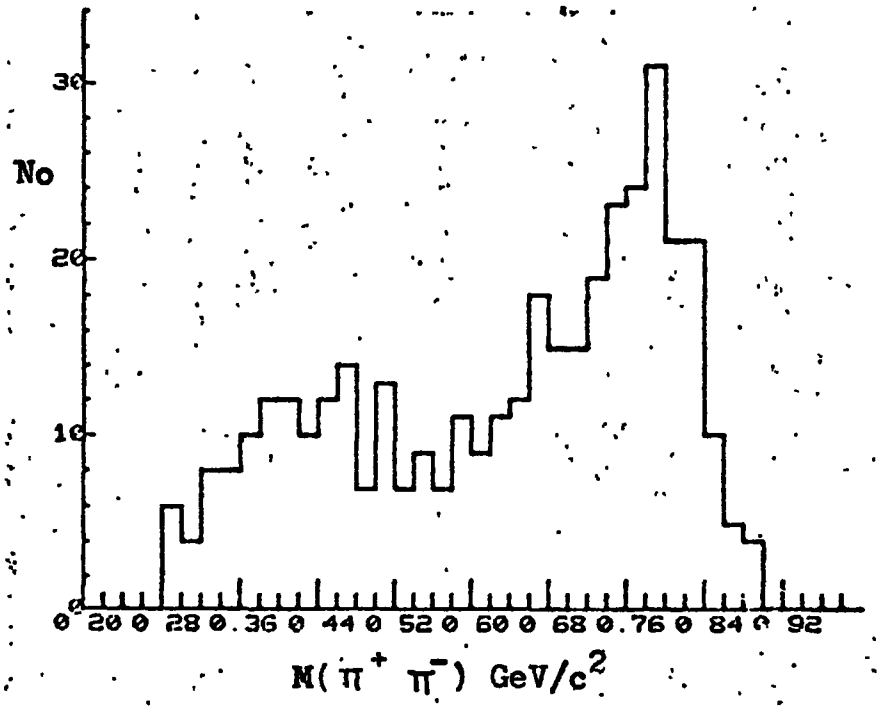

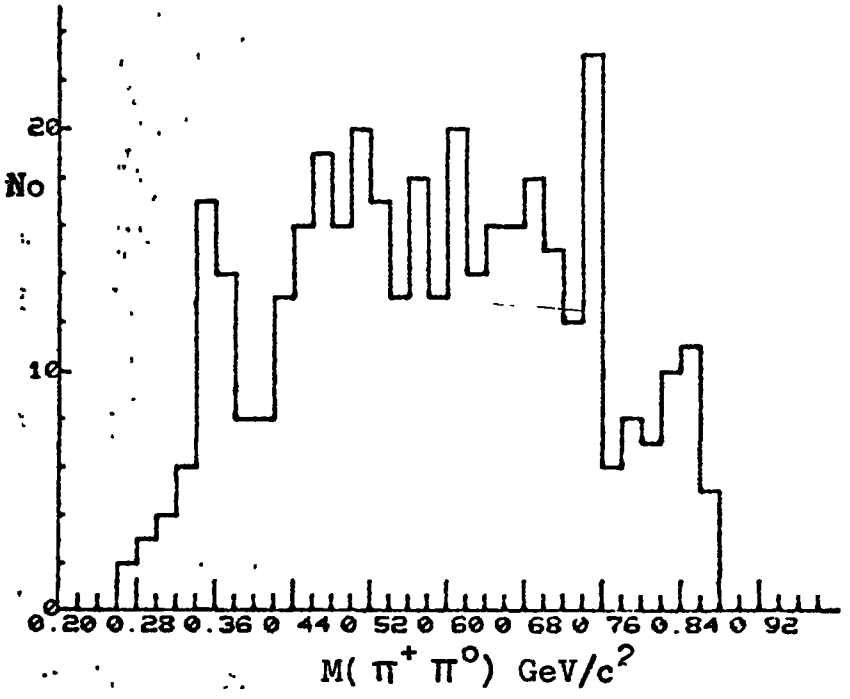

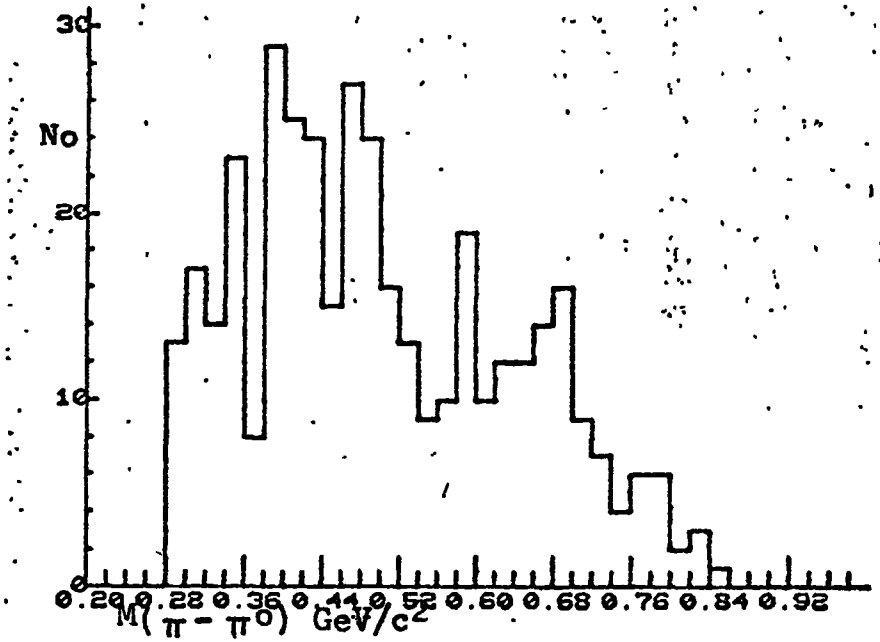

FIG. 5.2 THE DIPION MASS SPECTRA FOR EVENTS IN THE TRIPION MASS INTERVAL 0.95 → 1.05 GeV/c^2 FOR T < 0.1 (GeV/c^2)^2

distinguish between a γ and a π^0, the substitution of a π^0 for a γ will result in ρ^0 π^0 mass combinations in the 1.0 GeV/c^2 region. However the expected η' cross section at this incident energy is $\sim 17\,\mu$ b (Ref. 5.1). Hence since only some 27% proceed via the ρ^0 γ mode, the predicted contributions from this process is ~70 events. This, however, obviously represents an upper limit to the $\pi\pi\gamma$ contamination of the channel

$$\pi^+ D \rightarrow P_S P \pi^+ \pi^- \pi^0$$

since not all events will produce assceptable fits and, in particular, ones associated with low momentum γ's will be more likely to provide a fit to the 4c channel,

$$\pi^+ D \rightarrow P_S P \pi^+ \pi^-$$

particularly if the spectator proton is unseen.
Consequently the contributions from this process are considered insufficient to explain the 1.0 GeV/c^2 enhancement.

(b) <u>THE Φ (1019)</u>

This candidate is considered unlikely to result in the observed 1.0 GeV/c^2 enhancement, for the following reasons.

Firstly its full resonance width is only some 4 MeV/c^2 and hence the enhancement associated with this should have an experimental width < to that of the ω^0 - signal. Experimentally, however, the reverse is observed.

Secondly its production cross section at this incident energy is far too small, and equivalent to only some 20 events in this mode.

Finally, having the same quantum numbers as the ω^0 - meson

its production process is unlikely to be associated with a t slope of ~ 4.0 and moreover its differential cross section, if the same as that of the ω^0, will tend to dip at low t, rather than produce the large contribution observed.

(c) THE H (990)

As mentioned in the introduction to this section, the evidence for the existence of the H - meson is now no longer considered very strong and it is omitted from the main lists in Particle Tables.

One of the strongest pieces of evidence in favour of the H - meson resulted from the analysis of the 3.65 GeV/c $\pi^+ D$ experiment of Benson et al. (Ref. 5.2). Subsequently, however, the data have been re-analysed (Ref. 5.3), and the previous results were attributed to a technical fault in the data. The question now arises whether the 1.0 GeV/c^2 enhancement seen in our experiment results from a similar fault.

To investigate this possibility further it is necessary firstly to examine the previous evidence presented for the H enhancement and determine the similarity of the results with those from this experiment.

The estimated H^0 production cross sections reported in the earlier analyses were later found to be overestimated since no allowance has been made for the effects resulting from the use of p - cuts, which as pointed out by Fung et al (Ref.5.4), result in the distortion of phase space and the subsequent generation of a spurious enhancement in the 1.0 GeV/c^2 region of the tripion mass spectrum. This effect, however, could not account for all of the observations, since in many cases

the enhancement was also apparent without making any p - cuts at all, which indeed is also the case in the present experiment. Moreover, the results could not be explained in terms of the $\pi\pi\gamma$ decay mode of the η' . Indeed as illustrated in Ref. 5.5, when the events in this region were fitted to the $\pi\pi\gamma$ hypotheses, the results could not generate the expected η' peak. Consequently prior to 1970 there were four positive claims for the existence of the H enhancement, namely:-

CHANNEL		INCIDENT MOMENTUM	CROSS SECTION b	NUMBER OF EVENTS	REF.
π^+P	Δ^{++} H^0	4 GeV/c	70 ± 25	~ 90	5.6
π^+D	P_SP H^0	3.65 GeV/c	75 ± 15	~ 62	5.2
π^+D	P_SP H^0	3.29 GeV/c	50	~ 70	5.7
π^+P	$P\pi^+H^0$	3.7 GeV/c		~ 140	5.8

As can be seen, all the results are based on very low statistics.

The main difference between the above results and the results of the present 4 GeV/c experiment are that the above also claim to see the charged decay modes p^+ π^- and ρ^- π^+. However, since the statistics for the H^0 - signals are very small, the evidence for the individual decay modes is obviously not very strong. Indeed, in none of the above cases were the results based on the observation of clear p signals, and instead the analyses resorted to observing the numbers of events in the various p - bands. However, it could be argued that the observation of equal numbers of events in each p - band is to be expected, and does not automatically imply an equal probab-

ility for each of the three $p\pi$ decay modes. Indeed, assuming all the decays to occur via the $p^0\ \pi^0$ mode, the restriction of the tripion effective mass to the 1.0 GeV/c^2 region automatically implies that the other $\pi-\pi$ combinations will be in their respective p - bands. This is simply the converse of the observations made by Fung et al who demonstrated that p - cuts result in a 1.0 GeV/c^2 enhancement in the tripion mass spectrum. Hence it is to be concluded that the 1.0 GeV/c^2 enhancement seen in this analysis would be in agreement with the previous observations of the so called H^0 resonance.

The validity of these previous observations were however placed in considerable doubt when the results of Benson et al (Ref. 5.2), were found to arise from a technical fault in the data, (Ref. 5.3). This fault was revealed by the remeasurement of their original data comprising some 1000 or so events in the tripion mass range $\leq$ 1200 MeV/c^2, which were then refitted to the following three hypotheses,

$$\pi^+D \rightarrow P_SP\ \pi^+\ \pi^-\ \pi^0 \quad \ldots\ldots\ldots (1)$$

$$\pi^+D \rightarrow P_SP\ \pi^+\ \pi^-\ \gamma \quad \ldots\ldots\ldots (2)$$

$$\pi^+D \rightarrow P_SP\ \pi^+\ \pi^- \quad \ldots\ldots\ldots (3)$$

From the initial sample of 1083 events corresponding to reaction (1), the re-processing yielded the results illustrated in table 5.1, and the previously observed H^0 enhancement disappeared. However, if indeed the "H^0" events were originally associated with a p^0 signal it could be concluded that the disappearance of the 1.0 GeV/c^2 enhancement was directly related to the re-assignment of 45 of the events to the 4c channel

TABLE 5.1

THE RESULT OF RE-PROCESSING THE H^0 EVENTS OF REF. 5.3

$\pi^+ D \rightarrow$	HYPOTHESES ASSIGNED TO THE EVENT			
	$P_S P \pi^+ \pi^- \pi^0$	$P_S P \pi^+ \pi^- \gamma$	$P_S P \pi^+ \pi^-$	OTHERS
INITIAL SAMPLE	1083			
AFTER RE-PROCESSING	961	7 .	45	70

$$\pi^+ D \rightarrow P_S P \pi^+ \pi^-$$

since this channel is known to be dominated by ρ^0 production. Moreover it is also significant that in all the previous observations of the H^0 enhancement the associated 4c channels are all dominated by ρ^0 production. Therefore if as in the above experiment some of these 4c events were wrongly assigned to the 1c π^0 channel, the introduction of the π^0 may well have resulted in the observed 1.0 GeV/c^2 enhancements in the tripion mass spectrum.

Consequently a possible explanation of the observed 1.0 GeV/c^2 enhancements seen in both this and previous experiments is a breakthrough of events from the 4c channel. Moreover since the extent of such a breakthrough is unlikely to be the same in all experiments this would also explain why the H^0 enhancement is not always observed. The evidence that 4c breakthrough occurs in this experiment is presented in the following section.

5.3 THE EVIDENCE FOR THE CONTAMINATION OF THE 1c CHANNEL $\pi^+ D \rightarrow P_S P \pi^+ \pi^- \pi^0$ BY EVENTS FROM THE 4c CHANNEL $\pi^+ D \rightarrow P_S P \pi^+ \pi^-$

One method of investigating the nature of the 4c events which have been wrongly assigned to the 1c π^0 channel is to examine the 4c/1c ambiguous events. These events as illustrated in chapter 3 are known to be true 4c events of the channel

$$\pi^+ D \rightarrow P_S P \pi^+ \pi^-$$

which have also provided a fit to the 1c channel

$$\pi^+ D \rightarrow P_S P \pi^+ \pi^- \pi^0$$

Hence by wrongly choosing the 1c fit the effects of misinter-

preted 4c events can be simulated. It should be noted however that although similar in nature, these events will not be exactly the same as the 4c breakthrough events, since the former do at least provide a fit to the 4c channel, and as such will be rejected from the 1c data sample.

(a) THE TRIPION MASS DISTRIBUTION FOR THE 4c/1c AMBIGUOUS EVENTS

The tripion mass spectrum associated with the 4c/1c ambiguous events corresponding to t' values measured from the primary to the tripion mass system of less than 0.05 $(GeV/c^2)^2$ is shown in FIG. 5.3. From this it is evident that such events will indeed result in a 1.0 GeV/c^2 enhancement.

(b) THE DIFFERENTIAL CROSS SECTION FOR THE 4c/1c AMBIGUOUS EVENTS

The fitted t' slope to the differential cross section for these events is 4.4 ± 0.5 which is in agreement with the value of ~ 4.0 found for the 1.0 GeV/c^2 enhancement in the 1c channel.

(c) THE ANGULAR DISTRIBUTION FOR THE 4c/1c AMBIGUOUS EVENTS

The angular distribution for the normal to the decay plane of the three pions in the Gottfried Jackson frame of reference corresponding to the tripion mass region $0.9 \rightarrow 1.1$ (GeV/c^2) and the t - interval < 0.1 $(GeV/c^2)^2$ is shown in FIG. 5.4a. From this it can be concluded that should the 1.0 GeV/c^2 region of the 1c channel also be associated with 4c events, the corresponding plot should also indicate a strong $\sin^2\theta$ dependence, and as illustrated in FIG. 5.4b, this is indeed found to be

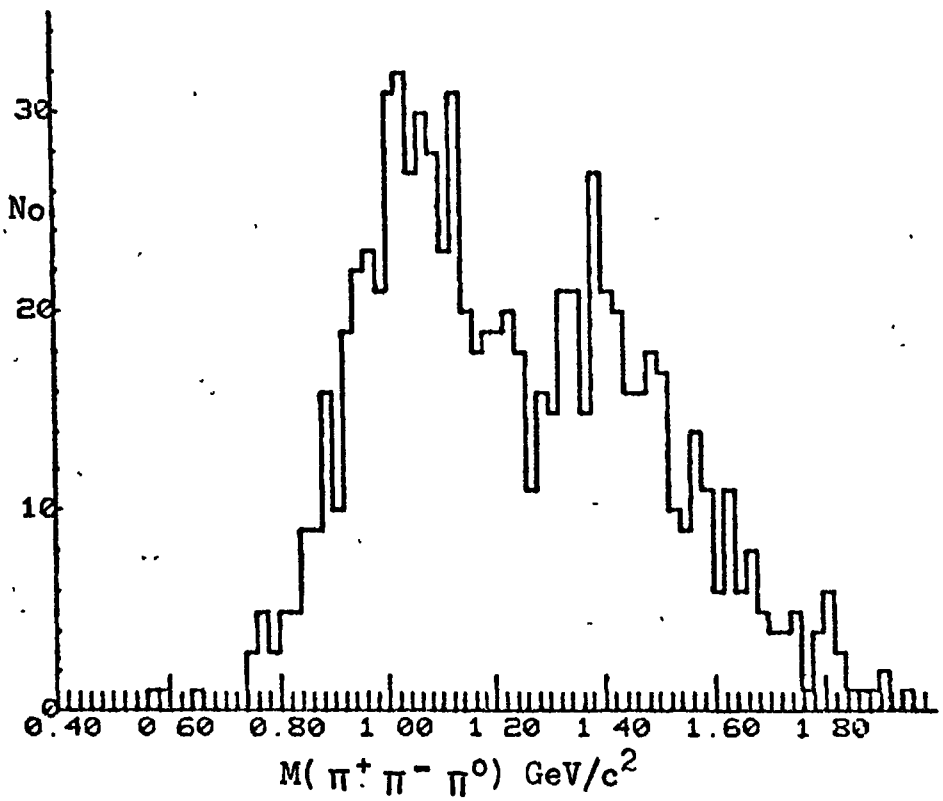

FIG. 5.3 THE TRIPION MASS SPECTRUM
FOR THE 4c/1c AMBIGUOUS EVENTS.

FIG. 5.4 THE ANGULAR DISTRIBUTION IN THE G - J FRAME OF REFERENCE OF THE NORMAL TO THE DECAY PLANE FOR THE 4c/1c AMBIGUOUS EVENTS, AND THE 1c EVENTS IN THE 1.0 GeV/c^2 REGION OF THE TRIPION MASS SPECTRUM

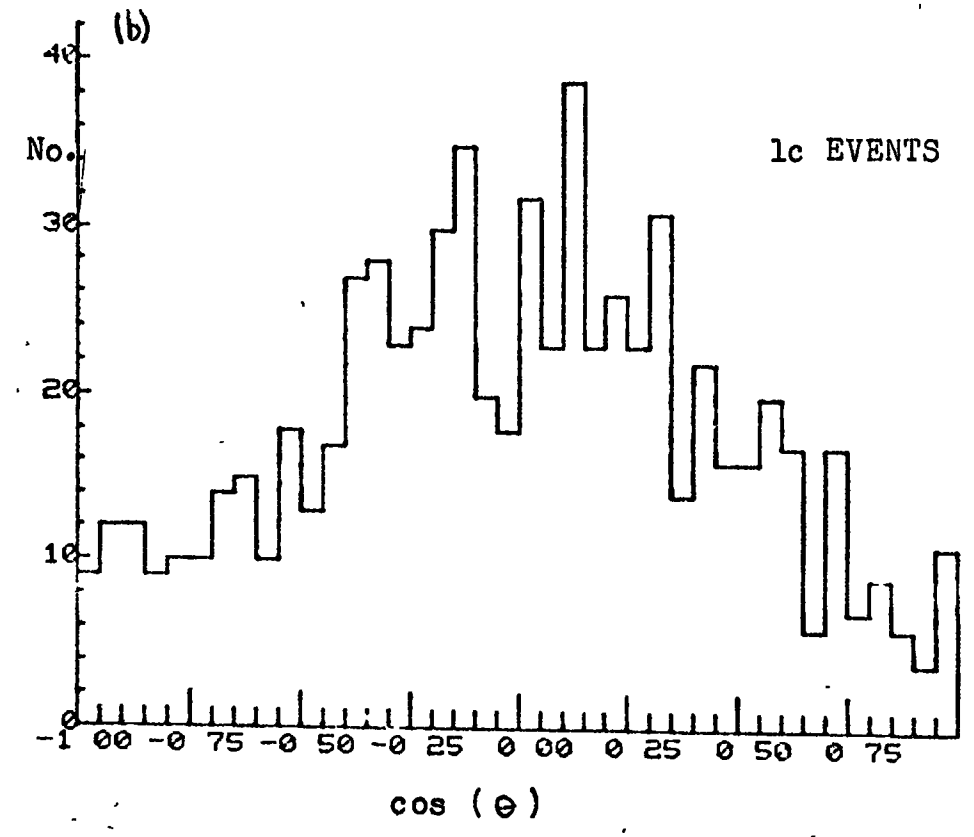

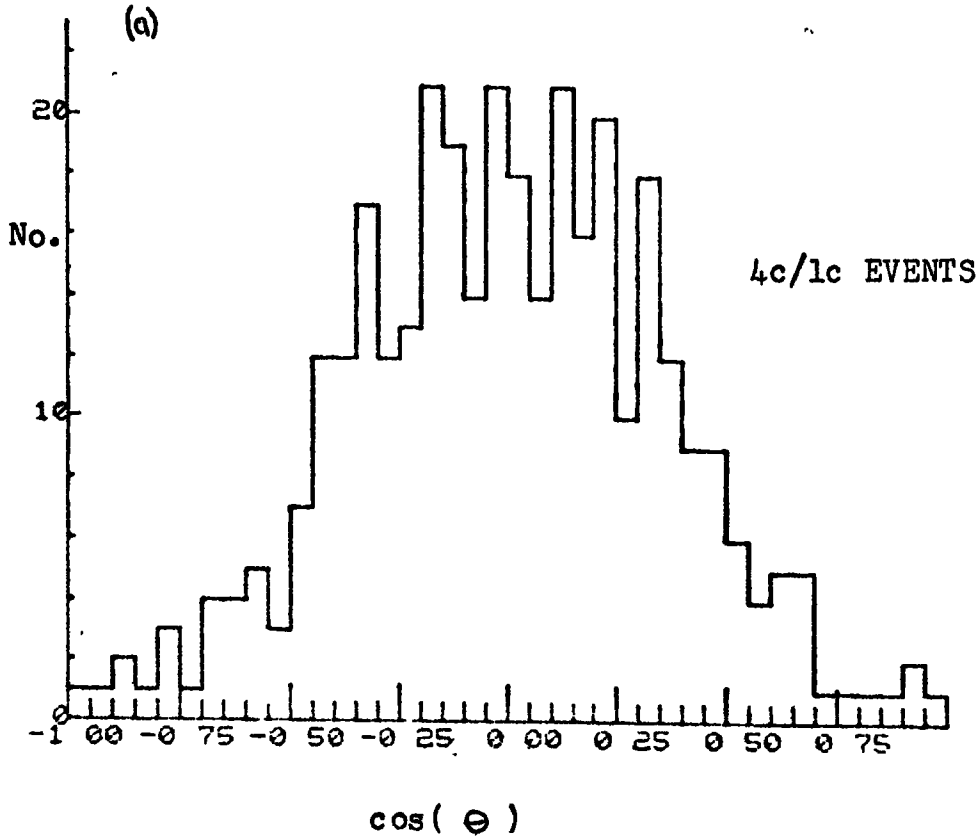

the case. Moreover, it is also significant that the angular distribution for the normal to the decay plane for the H^o - resonance reported by Benson et al, (Ref. 5.2), is also characterised by a $\sin^2\Theta$ dependence.

(d) THE DISTRIBUTION OF THE EVENTS IN THE DALITZ PLOT

The distribution of the 4c/1c ambiguous events in the $\pi^+ \pi^- \pi^o$ Dalitz plot is shown in table 5.2. The results shown correspond to events in the tripion mass region 0.9 → 1.1 GeV/c^2, and from the results it is evident that should 4c breakthrough occur, it will mainly populate sectors (1) and (6), the boundaries of the sectors being defined in FIG. 5.5. The equivalent distribution corresponding to the 1st exposure unseen spectator proton events is shown in table 5.3, the events being confined to the tripion mass range 0.9 → 1.1 (GeV/c^2) and the t' - interval < 0.05 (GeV/c^2)^2. From this it is evident that these events also have a tendency to populate sectors (1) and (6) preferentially.

(e) THE AMOUNT OF 4c BREAKTHROUGH

By assuming that the 1.0 GeV/c^2 enhancement observed in the tripion mass spectrum results from the breakthrough of 4c events from the channel

$$\pi^+ D \rightarrow P_S P \pi^+ \pi^-$$

the number of events illustrated in FIG. 5.1 can be used to estimate the extent of the breakthrough in the two exposures. Hence using the estimated p^o cross section of ~ 900 μb in the 4c channel, the breakthrough is equivalent to some 18% in

TABLE 5.2

THE DISTRIBUTION OF 4c/1C AMBIGUOUS EVENTS IN THE DALITZ PLOT FOR $0.9 < M_{3\pi} < 1.1$ (GeV/c^2) AND $t' < 0.05$ (GeV/c^2)^2

DALITZ SECTORS	1	2	3	4	5	6
NUMBER OF EVENTS	63	11	5	5	8	39

TABLE 5.3

THE DISTRIBUTION OF 1c EVENTS IN THE DALITZ PLOT FOR $0.9 < M_{3\pi} < 1.1$ (GeV/c^2) AND $t' < 0.05$ (GeV/c^2)^2

DALITZ SECTORS	1	2	3	4	5	6
NUMBER OF EVENTS	67	23	36	19	17	40

FIG. 5·5

THE BOUNDARIES OF THE DALITZ PLOT SECTORS.

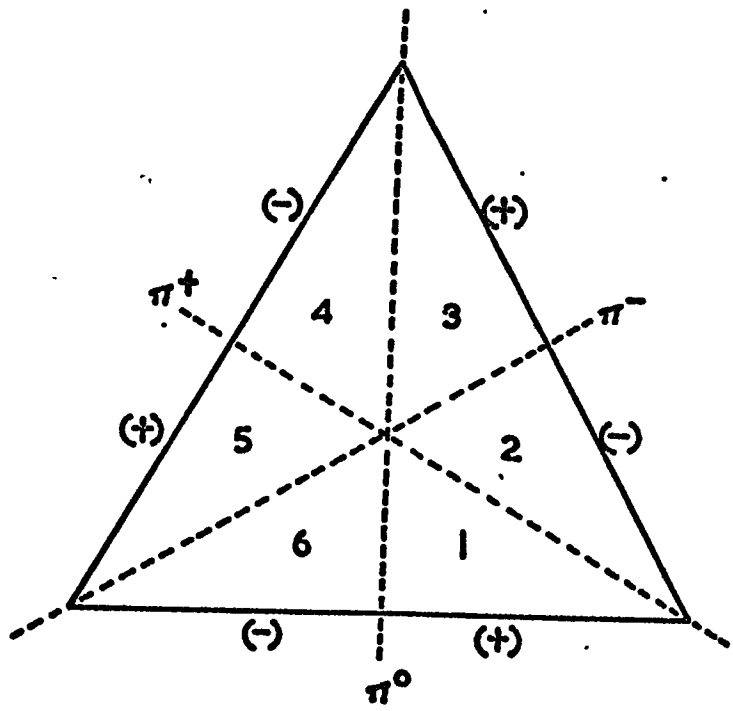

the 1st exposure AND ~ 8% in the 2nd exposure. The main difference between the two exposures has been the introduction of improved convergence criteria in the fitting routines of the KINEMATICS programme for the 2nd exposure. The alterations were introduced by D.J. Crennell of the Rutherford Laboratory and more recently he has modified the convergence criteria still further. A brief description of the improvements is described in Ref. 5.9.

Assuming the results of Benson et al to result from a similar problem it is interesting to note that his estimated H^0 cross section corresponds to some 8% of the p^0 cross section in the corresponding 4c channel, indicating a potential 4c breakthrough at a similar level to that found in this experiment.

5.4 THE RESULT OF APPLYING THE KINEMATICAL FITTING PROCEDURE TO GENERATED 4c EVENTS

By generating FAKE events of the type

$$\pi^+ D \rightarrow P_S P \pi^+ \pi^-$$

it is possible to examine how many will be wrongly assigned to other channels by the kinematical fitting procedure.

A version of the programme FAKE was specially modified to handle deuterium interactions, including the generation of the spectator protons with momenta in accordance with the Hulthen distribution. The events were generated for an incident beam momentum of 4 GeV/c and the resulting secondaries assigned error estimates consistent with those associated with this experiment.

By this procedure 5000 p^0 events

$$\pi^+ D \rightarrow P_S P p^0 \rightarrow P_S P \pi^+ \pi^-$$

and 5000 f^0 events

$$\pi^+ D \rightarrow P_S\ P\ f^0 \rightarrow P_S\ P\ \pi^+\ \pi^-$$

were generated, typical t' - distributions and angular distributions being included in both cases. These events were then processed by the kinematical fitting programme, KINEMATICS, with convergence criteria identical to those used in the first exposure, the equivalent of the ionisation tests described in chapter 3 also being applied. The hypotheses subsequently assigned to these events are illustrated in table 5.4. From this it is evident that of the 5000 ρ^0 events generated ~ 14% will be lost and re-assigned to other channels, 3% of them to the 1c π^0 channel

$$\pi^+ D \rightarrow P_S\ P\ \pi^+\ \pi^-\ \pi^0$$

Moreover it is also apparent that the seen and unseen spectator protons tend to be re-assigned to different hypotheses, i.e. whereas the seen spectator events are mainly lost to the 1c neutron channel

$$\pi^+ D \rightarrow P_S\ n\ \pi^+\ \pi^+\ \pi^-$$

the unseen spectator proton events are mainly lost to the 1c π^0 channel. This would explain why the 1.0 GeV/c^2 enhancement in the 1c π^0 channel is mainly associated with the unseen spectator proton events.

For the f^0 events however, the predicted loss is even larger, since some 25% of the events are re-assigned to other channels, 9% of them to the 1c π^0 channel. In addition, as found for the generated ρ^0 events, whereas those associated with seen spectator protons tend to be lost to the 1c neutron

TABLE 5.4

THE HYPOTHESES ASSIGNED TO THE FAKE EVENTS OF THE TYPE $\pi^+ D \rightarrow P_S P \rho^0$

$\pi^+ D \rightarrow$	HYPOTHESES							
	$P_S P \pi^+ \pi^-$		$P_S P \pi^+ \pi^- \pi^0$		$P_S N \pi^+ \pi^+ \pi^-$		NOFITS	
SPECTATOR PROTONS	SEEN	UNSEEN	SEEN	UNSEEN	SEEN	UNSEEN	SEEN	UNSEEN
INITIAL SAMPLE	1579	3421						
RESULTS OF KINEMATICAL FITTING	1159	3136	28	139	328	86	64	60

THE HYPOTHESES ASSIGNED TO THE FAKE EVENTS OF THE TYPE $\pi^+ D \rightarrow P_S P f^0$

$\pi^+ D \rightarrow$	HYPOTHESES							
	$P_S P \pi^+ \pi^-$		$P_S P \pi^+ \pi^- \pi^0$		$P_S N \pi^+ \pi^+ \pi^-$		NOFITS	
SPECTATOR PROTONS	SEEN	UNSEEN	SEEN	UNSEEN	SEEN	UNSEEN	SEEN	UNSEEN
INITIAL SAMPLE	1616	3384						
RESULTS OF KINEMATICAL FITTING	894	2859	104	371	556	65	62	89

channel, those associated with unseen spectator protons are lost to the 1c π^o channel.

The tripion mass spectrum corresponding to the 4c/1c π^o ambiguous events illustrated in FIG. 5.3 suggests that any breakthrough of f^o events into the 1c π^o channel should appear in the 1.4 GeV/c^2 region, and from the calculated f^o cross section in the 4c channel, the predicted number of such events is ~ 300 for the 1st exposure. Experimentally however, there is no evidence for such a breakthrough. It could be argued however that since the general level of the background in this region is very high the presence of any f^o breakthrough may well be obscurred.

5.5 THE REMOVAL OF THE 4c CONTAMINATION IN THE 1c π^o CHANNEL

To simplify the analysis of the 1c channel, various methods were investigated for the removal of the 4c contamination. Unfortunately however, no suitable method was found, and the characteristics of all the following parameters for the 1.0 GeV/c^2 enhancement were found to be consistent with those for the majority of the 1c events,

(a) the pulls on the tracks
(b) the χ^2 probability
(c) the missing energy
(d) the missing momentum
(e) the missing mass squared
(f) the beam momentum
(g) the position of the events within the chamber
(h) the lengths of the measured tracks
(i) the angular distribution for the fitted π^o
(j) the momentum of the fitted π^o

This result however is to be expected since the events in question are those which have failed to provide an acceptable fit to the 4c hypothesis and as such will have values for the above parameters in better agreement with the $1c\,\pi^0$ values rather than the 4c values.

Consequently it follows that the only effective method for the removal of these events is the same procedure as used by Benson et al, i.e. the re-fitting of the events in this particular region of the tripion mass spectrum, using a version of KINEMATICS with improved convergence criteria.

5.6 OTHER CONTRIBUTIONS TO THE BACKGROUND

Apart from any contributions to the background resulting from technical faults there will also be contributions from phase space and reflections of real physical processes. The known contributions to the channel

$$\pi^+ D \rightarrow P_S P \pi^+ \pi^- \pi^0$$

are shown in table 5.5, along with their estimated cross sections taken from Ref. (5.1).

It was noted however that both the $\rho^0 \Delta^+$ and $\rho^0 P \pi^0$ channels will contribute towards the observed ρ^0 signals, and hence the possibility of these channels generating the 1.0 GeV/c^2 enhancement in the tripion mass spectrum was investigated. By FAKING these channels however it was found that such events will only create a broad enhancement ranging from 0.8 → 1.9 GeV/c^2 in the tripion mass spectrum and hence cannot be attributed to the observed 1 GeV/c^2 peak. This conclusion is also in agreement with the observation that should the ρ^0 Δ^+ events contribute towards the 1.0 GeV/c^2 enhancement so also should

TABLE 5.5

CHANNEL	ESTIMATED CROSS SECTIONS	CONTRIBUTIONS TO THE REGION $0.4 < M^2_{3\pi} < 0.8 (GeV/c^2)^2$	
$\pi^+ N \rightarrow$	μb	$t < 0.1$	$t < 0.1$
A_2^0 P	120	0	0
$f^0 \Delta^+$	22	0	0
$\rho \Delta$	300	46	16
$\rho (P\pi)$	300 +	12	20
$\pi (P \pi \pi)$	100 +	8	20
A_1^0 P	?		
DECK PROCESSES	?		

Where electric charge is not indicated it is to be understood that all possible charge configurations have been examined.

\+ These reactions have been faked as quasi two body processes in which the $(P \pi)$ or $(P\pi\pi)$ is considered as a broad enhancement with $\Gamma \sim$ 300 MeV/c centred at a mass value of 1650 MeV/c

the $\rho^+ \Delta^0$ events, and hence there should be as many ρ^+ s as ρ^0 s associated with this region. Experimentally however, the ρ^0 signal is seen to dominate.

Also mentioned in table 5.5 are the signals resulting from the A_1 resonance and the Deck process, (Ref. 5.10). The expected cross sections for these processes however are not easily estimated, but since both are predicted to contribute towards the 1.1 GeV/c^2 region of the tripion mass spectrum, the experimental evidence suggests that their contributions towards the 1c π^0 channel are not very significant.

From the above discussion of 4c contamination of the 1c π^0 and 1c neutron channels it is evident that great caution must be exercised in the interpretation of enhancements in and around the 1.0 GeV/c^2 region of tripion mass spectra, the region which is also associated with the controversial H^0, A_1 and $A_{1.5}$ resonances. Although in this experiment the mis-interpreted 4c events mainly populate the 1.0 GeV/c^2 region, there is no reason to assume that experiments at other primary energies using different kinematical fitting programmes will produce an enhancement either in the same region or to the same extent. Hence to a certain degree the possibility of 4c contamination will explain why the observations of the H^0, A_1 and $A_{1.5}$ resonances are inconsistent when going from one experiment to another. Moreover it is significant that in the results presented by French at the Vienna conference, (Ref. 5.11), the observed A_1 signal in a compilation of

$$\pi^- \; P \rightarrow P \rho^0 \; \pi^- \; \ldots\ldots\ldots (1)$$

data is less obvious than that associated with the combined samples of

$$\pi^+ N \rightarrow N \rho^0 \pi^+ \quad \ldots\ldots\ldots\ldots (2)$$

and $\pi^+ P \rightarrow P \rho^0 \pi^+$

data. In the event of 4c contamination however, this is to be expected since whereas reaction (2) may be subjected to 4c contamination reaction (1) should be free from such effects.

5.7 CONCLUSIONS

The results of the previous chapter suggested the presence of at least two different contributions to the background in the ω^0 - region of the tripion mass spectrum.

In this chapter, the examination of the background associated with the larger $d\sigma/dt$ exponent of ~ 4 has revealed that due to inadequate convergence criteria in the kinematical fitting programme there has been a breakthrough of events from the 4c channel

$$\pi^+ D \rightarrow P_S P \pi^+ \pi^-$$

As a result of this breakthrough a strong ρ^0 dominated 1.0 GeV/c^2 enhancement in the tripion mass spectrum was generated and the nature of this enhancement is considered consistent with previous observations of the so called H^0 resonance. The extent of this breakthrough was found to be different in the two exposures for this experiment, corresponding to $\sim$ 18% and 8% for the 1st and 2nd exposures respectively, the difference being attributed to the different convergence criteria used in the kinematical fitting programme.

The results also indicate that when analysing the A_1 region particularly in the channel

$$\pi^+ D \rightarrow P_S N \pi^+ \pi^+ \pi^-$$

not only should the effects of the Deck process and ρ - cuts be considered, but also the possibility of 4c breakthrough should be investigated.

In section 5.6 the predicted contributions from phase space and the reflections of real physical processes were considered, and as illustrated in table 5.5, the main contributions to the ω^o - region arise from the $\rho\Delta$ process.

5.8 THE EFFECTS OF THE BACKGROUND ON THE ω^o - ANALYSIS

(a) THE DIFFERENTIAL CROSS SECTION

As illustrated in chapter 4, although the effects of background on the form of the differential cross section have been eliminated in this analysis, it can be concluded that in analyses where this has not been done, the occurence of 4c breakthrough will tend to obscure the presence of a dip at low t. In addition, since the t - exponents for the background are found to be different from that of the ω^o - signal, previous measurements of the t - slope which have not included allowances for the background, will be incorrect.

(b) THE DENSITY MATRIX ELEMENTS

The determination of the density matrix elements for the ω^o production is discussed in the following chapter, and as in the evaluation of the differential cross section, where possible the background effects are eliminated.

From the results discussed in the previous sections it is evident that 4c breakthrough will result in a $\sin^2$ distribution for the normal to the decay plane in the Gottfried Jackson

frame of reference. Hence the value of ρ_{00} for 4c breakthrough events will tend to zero. Consequently the contamination of the low t interval of the ω^0 - region by 4c events will tend to reduce the average value of ρ_{00} in this region.

How the contributions to the background listed in table 5.5 affect the spin density matrix elements is not well known, but since the numbers of these events are observed to be very small in the central ω^0 - region they are considered unlikely to have a marked effect. Indeed it is considered that the effects of 4c breakthrough are likely to be more important, since the angular distribution for these events is so strongly $\sin^2$.

(c) THE DISTRIBUTION OF THE EVENTS IN THE DALITZ PLOT

Since the ω^0 meson has I J^{PG} values of 0^{1--} its distribution in the Dalitz plot is known to be symmetric about its maximum at the centre of the Dalitz triangle. Added to this distribution however, will be the phase space and events associated with other processes such as 4c breakthrough or the $p\Delta$ channel, and although the phase space will be uniformly distributed throughout the Dalitz plot, the latter processes will tend to congregate in specific regions, the 4c breakthrough mainly occuring in sectors (1) and (6) described earlier. From the numbers of such events involved however, the overall Dalitz plot distribution should be little affected, and the possible distortions introduced will only be of importance when making detailed asymmetry analyses.

The validity of the above assumption is well illustrated in FIG. 5.6 which illustrates the distribution in the ω^0

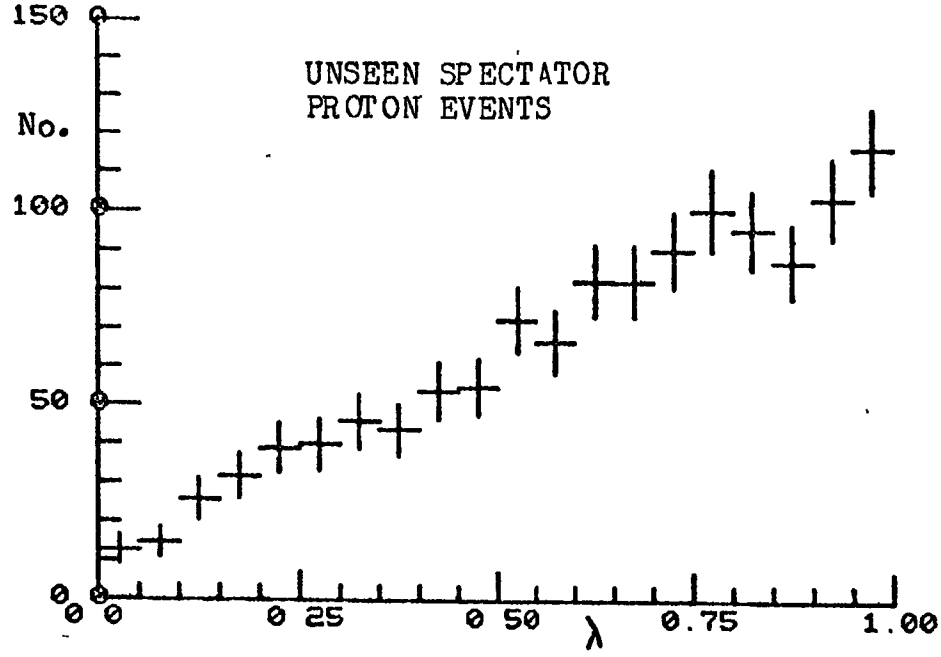

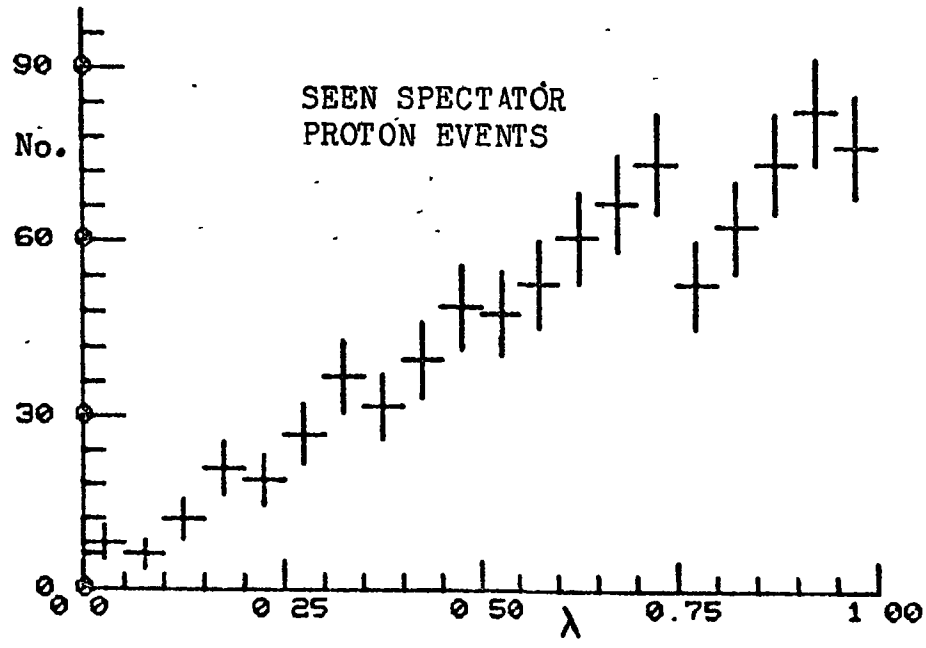

FIG. 5.6 THE DISTRIBUTION OF EVENTS IN THE ω^{o} DALITZ PLOT AS A FUNCTION OF THE ω^{o} DECAY MATRIX ELEMENT λ

Dalitz plot corresponding to the seen and unseen spectator proton events in the ω^0 - region 0.76 $\rightarrow$ 0.81 (GeV/c^2) of the tripion mass spectrum as a function of the ω^0 decay matrix element squared λ . This parameter is evaluated from the expression,

$$\lambda = \left| \vec{P}_{\pi^+} \times \vec{P}_{\pi^-} \right|^2 \Big/ \left(\frac{3}{4} \left(M_{3\pi}^2 / 9 - M_{\pi}^2 \right)^2 \right)$$

where $\vec{P}_{\pi^+}$ and $\vec{P}_{\pi^-}$ are the momenta of the π^+ and π^- mesons in the ω^0 - rest frame, and λ is so defined that the centre of the Dalitz plot corresponds to λ = 1.0 and the boundary to λ = 0.0. The advantage of describing the Dalitz plot distribution in terms of this variable is that the distribution of non-resonant background within the Dalitz plot is isotropic in λ , whereas the ω^0 - signal is distributed linearly from 0.0 at the boundary of the Dalitz plot , (λ = 0.0), to a maximum at the centre, (λ = 1.0). By placing the level of the background at 4 $\pm$ 2 and 10 $\pm$ 3 for the seen and unseen spectator proton events respectively, the corresponding signal to background ratios are 10.0 ± 5.0 and 7.0 ± 2.0 , which as discussed in section 4.2g are in agreement with the signal to background ratios resulting from the convoluted Breit Wigner and resolution function fits made to the ω^0 - signal.

CHAPTER SIX

THE ANALYSIS AND INTERPRETATION OF THE ω^o MESON PRODUCTION MECHANISM

INTRODUCTION

In this chapter, the investigation of the exchange mechanisms for ω^o - mesons, produced in the forward direction in the π-N centre of mass system is continued by analysing the mixture of superpositions of spin states associated with the ω^o - mesons, as determined from their decay angular distributions.

To begin with, the concept of spin density matrix elements is introduced and the association is made between the nature of the spin states and the exchange mechanisms. This is followed by the presentation of the experimental results for the spin density matrix elements and a discussion of their accuracy and the effects of the associated background. Finally a comparison is made with other experiments, and the results are discussed in terms of the various models for forward ω^o - meson production.

6.1 THE DEFINITION OF SPIN DENSITY MATRIX ELEMENTS

Spin density matrix elements are used to investigate the production mechanism of a given system of particles by analysing the mixture of superpositions of spin states associated with that system of particles, and in general the variation in the types of exchanges is investigated as a function of the produc-

tion angle or 4 - momentum transfer squared to the produced system of particles.

For the particular case of an assembly of ω^o - mesons in their individual rest systems, the use of an unpolarised beam and target implies that the assembly will be a mixture of superpositions of spin states, the latter depending upon the spin and parity of the exchanged particle. In the case of an assembly of states, the average value of a physical quantity Q will be given by:-

$$Q = \sum_i Wi \cdot \langle Qi \rangle \quad \ldots\ldots\ldots\ldots (1)$$

where Wi represents the weight of each state and $\langle Qi \rangle$ the corresponding expectation value, i.e.

$$\langle Qi \rangle = \langle \chi^*_i |Q| \chi_i \rangle$$

The states χ_i however, can be expressed in terms of the eigenfunctions of the z- components of angular momentum m,

e.g. $$|\chi_i\rangle = \sum_m a^i_m \cdot |\chi_m\rangle$$

where a^i_m is the amplitude of each eigenstate of m.
For a particular state of spin J, there are (2J + 1) such eigenstates, with magnetic quantum numbers m ranging from +J to -J. The values of m are defined with respect to a specific axis of quantisation, which in this analysis is the direction of the exchanged particle transformed into the rest system of the ω^o - meson in the frame of reference corresponding to either the direct or crossed channel interactions. This is discussed in more detail in section 6.3. Hence by expressing equation (1) in terms of the eigenstates of m, the average value of the physical quantity Q can be written as

$$\langle Q \rangle = \sum_{m,m'} Q\ m\ m'\ \rho\ m\ m'$$

where $Q\ m\ m' = \langle \psi^*_m \ |Q| \ \psi_m \rangle$

is the expectation value of Q between the various m states, and $\rho\ m\ m' = \sum_i Wi\ a^i_m\ a^i_{m'}$ are the corresponding density matrix elements.

From the above expression, it is evident that for a given value of J there are $(2J + 1)^2$ spin density matrix elements, e.g. J = 1, the matrix is of the form:-

$$\begin{pmatrix} \rho_{11} & \rho_{10} & \rho_{1-1} \\ \rho_{01} & \rho_{00} & \rho_{0-1} \\ \rho_{-11} & \rho_{-10} & \rho_{-1-1} \end{pmatrix}$$

each individual element containing information concerning the weights of the various superpositions of spin states, and the amplitudes and relative phases of the associated eigenstates of m. The properties of the spin density matrix can be summarised as follows:-

(a) it is hermitian

(b) the sum of the diagonal elements is 1

(c) the diagonal elements are positive

and (d) if the spin quantisation axis is chosen to be in the production plane and the beam is unpolarised then parity conservation implies that $\rho\ m\ m' = (-1)^{m-m'}\ \rho\ -m\ -m'$

6.2 PREDICTIONS FOR THE SPIN DENSITY MATRIX ELEMENTS

An indication of the connection between the final state eigenfunctions of m as described by the spin density matrix

elements, and the type of exchange is given in the following examples in which by considering the simple case of 1 - particle exchange, definite values are predicted for some of the spin density matrix elements.

Since the forward production of ω^o - mesons in the π - N centre of mass system can only result from the exchange of known particles with spin parity (J^P), of 1^+ or 1^-, the production process as seen from the rest frame of the ω^o - meson can be drawn schematically as shown in FIGs. 6.1a and 6.1b, L being the orbital angular momentum between the incident and exchanged particle, and z the above mentioned spin quantisation axis.

(a) THE EXCHANGE OF A ρ OR ρ' - MESON ($J^P = 1^-$)

This type of exchange is illustrated in FIG. 6.1a. For angular momentum conservation L = 0, 1 or 2 with $L_Z = 0$. However, for parity conservation $(-1)(-1)(-1)^L = -1$ and hence L must be odd and equal to 1. In addition, by conserving the Z - component of the angular momentum, m = 0 or $\pm$ 1. Hence to produce the final states of the ω^o - meson, $|Jw, m\rangle$, the exchange particle states, $|Jex, m\rangle$ corresponding to $|1, 0\rangle$, $|1, 1\rangle$ and $|1, -1\rangle$ are combined with the angular momentum state $|L, m\rangle = |1,0\rangle$. The combining of these states is described by the Clebsh Gordon coefficients, and in this particular case, the final state $|Jw, m\rangle = |1, 0\rangle$ is forbidden, since the coefficient for the combination of $|L = 1, 0\rangle$ and $|Jex = 1, 0\rangle$ is zero. Hence in the final mixture of states, the eigenstates $|m = 0\rangle$ do not occur, implying that $\rho_{om} = \rho_{mo} = 0$ and in particular that $\rho_{oo} = 0$ and $\rho_{11} = \rho_{1-1} = \frac{1}{2}$.

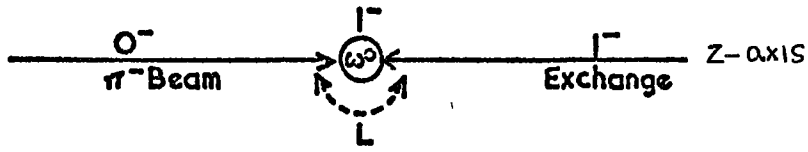

FIG. 6-1a

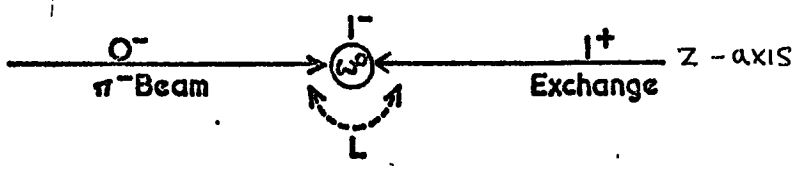

FIG. 6-1b

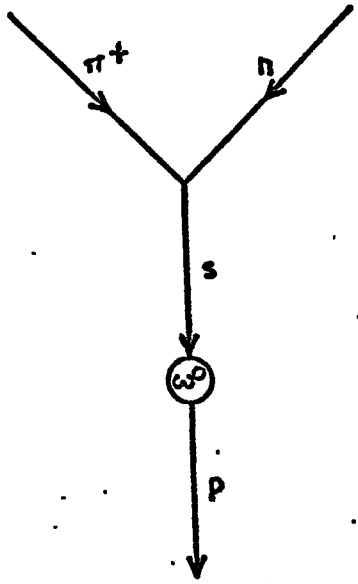

FIG. 6-2a

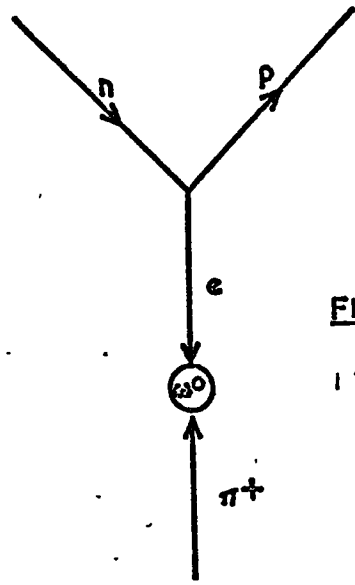

FIG. 6-2b

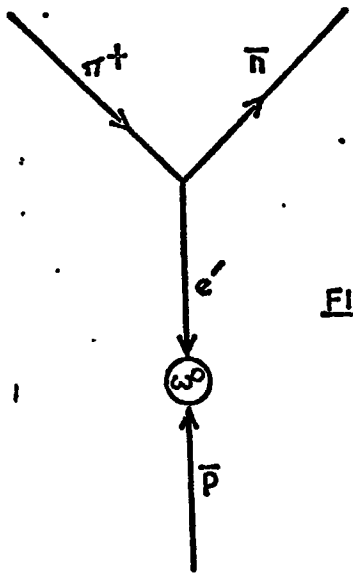

FIG. 6-2c

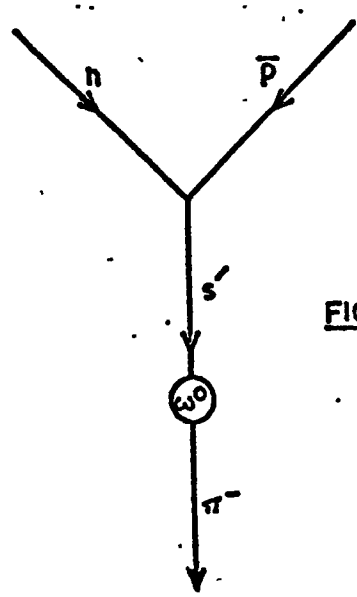

FIG. 6-2d

(b) THE EXCHANGE OF A B-MESON ($J^P = 1^+$)

This process is illustrated in FIG. 6.1b. By following the same technique as above, it can be shown that the allowed values of L are 0 or 2, and that all 3 spin orientations $m = 0, \pm 1$ are allowed in the final states. Hence in general all the $\rho_{mm'}$ will be different from zero.

To summarise therefore, the value of ρ_{00} in this simple model of one particle exchange is an excellent indicator of the presence of either type of exchange, since

$$\rho_{00} = 0 \text{ for } \rho \text{ or } \rho' \text{ exchange}$$

$$\text{and } \rho_{00} \neq 0 \text{ for B exchange.}$$

It should be noted however that these predictions have not included any absorptive effects and hence will only be valid at low values of t.

6.3 THE FRAMES OF REFERENCE

As mentioned above, the magnetic quantum numbers m are defined with respect to a specific axis of quantisation. The most commonly used frames of reference are the so called Gottfried - Jackson and Helicity frames, which enable the production mechanisms to be analysed in both the direct and the crossed channels respectively. By crossing symmetry, the crossed channel for the reaction

$$\pi^+ N \rightarrow P \omega^0$$

is

$$\bar{P} N \rightarrow \pi^- \omega^0$$

Both of these processes, illustrated in the ω^0 - rest frame in FIG. 6.2, can be described either in terms of the decay of an intermediate state S or by the interaction of the incident

and exchanged particle e, the intermediate state in the crossed channel corresponding to the exchanged particle in the direct channel and vice - versa.

To analyse the exchange mechanism in either of these channels, the axis of quantisation, Z, for the angular momentum components m, is defined as the direction of the exchanged particle transformed into the rest system of the ω^o - meson. Hence from the direction of the exchange particles illustrated in FIGs. 6.2b and 6.2c, the quantisation axes for the Gottfried-Jackson and Helicity frames are defined as follows:-

(a) THE GOTTFRIED - JACKSON FRAME

This reference frame is used to analyse the exchange mechanism for the direct channel process. Hence the quantisation axis, Z is defined as the direction of the beam transformed into the rest system of the ω^o - meson. However, as pointed out in section 6.1, if the quantisation axis is chosen to be in the production plane, and the beam is unpolarised, conservation of parity simplifies the density matrix such that

$$\rho_{mm'} = (-1)^{m-m'} \rho_{-m-m'}$$

Hence to maintain this condition, the y - axis is defined to be the normal to the production plane, and the x - axis is chosen to give a right-handed system.

(b) THE HELICITY FRAME

This reference frame is used to analyse the exchange mechanism in the crossed channel process, and hence in this particular analysis the quantisation axis is defined as the direction of the proton transformed into the rest system of

the ω^0 - meson. The x and y axes are then defined in the same manner as described in the Gottfried Jackson frame above.

6.4 THE DETERMINATION OF THE SPIN DENSITY MATRIX ELEMENTS

As shown in section 6.1, the average value of some physical quantity Q can be used to determine the spin density matrix elements i.e.

$$\langle Q \rangle = \sum_{m,m} Q_{m\,m'} \cdot \rho_{m\,m'}$$

In general as in this particular analysis, the physical quantity used is the decay angular distribution of the system of particles under investigation. Hence $Q_{m\,m'}$ can be replaced by the decay matrix elements $A_{m\,m'}(\Theta, \phi)$ and the decay angular distribution $W(\Theta, \phi)$ is given by:

$$W(\Theta, \phi) = \sum_{m,\,m'} \rho_{m\,m'} \cdot A_{m\,m'}(\Theta, \phi)$$

The angles Θ and ϕ, for a 3 body decay, correspond to the polar and azimuthal angles of the normal to the decay plane, as measured from the rest system of the resonance in the above mentioned reference frames. However, for the decay of a spin J particle into pions described in the above manner it can be shown, (Ref. 6.1), that

$$A_{m\,m'}(\Theta, \phi) = \frac{3}{4\pi} D_{m\,\lambda}^{J*}(\Theta, \phi) \cdot D_{m'\,\lambda}^{J}(\Theta, \phi)$$

where λ is the total helicity of the decay products. The terms $D_{m\,\lambda}^{J}$ essentially represent the rotation required to transform the measurements of the angular momentum states made with respect to the direction λ, back to the direction of the exchanged particle, and quantisation axis. Therefore by

expressing $A_{m\,m'}(\theta\ \phi)$ in terms of the known values of $D^{J}_{m\lambda}(\theta, \phi)$ the expression for the decay angular distribution $W(\theta, \phi)$ reduces to

$$W(\theta, \phi) = \frac{3}{4\pi}\left[\frac{1}{2}(1 - \rho_{00}) + \frac{1}{2}(3\rho_{00} - 1)\cos^2\theta - \rho_{1,-1}\sin^2\theta\cos 2\phi - 2\,\mathrm{Re}\,\rho_{10}\sin 2\theta\cos\phi\right].$$

Several methods exist for the extraction of the individual matrix elements $\rho_{m\,m'}$ from the above expression, and in this particular analysis, the technique used is the method of moments described below:-

(a) THE METHOD OF MOMENTS

The normalisation constant $\frac{3}{4\pi}$ in the above expression is chosen such that

$$\int_0^{2\pi} d\phi \int_{-1}^{+1} d\cos\theta \,.\, W(\cos\theta, \phi) = 1$$

Hence the average value $\bar{f}$ of a function $f(\cos\theta, \phi)$ is given by

$$\bar{f} = \int_0^{2\pi} d\phi \int_{-1}^{+1} d\cos\theta \; f(\cos\theta, \phi)\,.\,W(\cos\theta, \phi)$$

Therefore by substituting in the above expression with the value of $W(\theta, \phi)$ it can be shown that

$$\overline{\cos^2\theta} = \frac{1}{5}(1 + 2\rho_{00})$$

$$\overline{\sin^2\theta\cos 2\phi} = -\frac{4}{5}\rho_{1-1}$$

and $$\overline{\sin 2\theta\cos\phi} = -\frac{4\sqrt{2}}{5}\,\mathrm{Re}\,\rho_{10}$$

i.e. the values of the density matrix elements can be extracted by taking the average value of the corresponding coefficients in the expression for $W(\Theta, \phi)$, and the experimental statistical error on $\bar{f}$ is given by

$$\Delta \bar{f} = \left[n^{-1} \quad (\bar{f^2} - \bar{f}^2) \right]^{1/2}$$

where n is the number of events. The remaining density matrix elements i.e. ρ 11, ρ 1-1 etc. can be determined from the properties of the density matrix described in section 6.1.

In addition, we define the combinations

$$N(1, 1) = \rho\ 11 + \rho\ 1\text{-}1 \quad \text{Natural}$$

and $$U(1, 1) = \rho\ 11 - \rho\ 1\text{-}1 \quad \text{Unnatural}$$

which at low t measure the contributions from natural parity, e.g. ρ - mesons, and unnatural parity, e.g. B-mesons, to the helicity state 1.

(b) STATISTICAL FLUCTUATIONS

The use of limited statistics will always introduce fluctuations in the results. Hence before a meaningful analysis can be made it is firstly necessary to determine the magnitude of the fluctuations and estimate at what level they may tend to simulate structure.

This was achieved by observing the fluctuations created in the spin density matrix elements for various random samples of events. The results shown in FIG.6.3 correspond to spin density matrix elements calculated in the Gottfried Jackson frame of reference for the sample of unseen spectator proton events centred on the ω^0 - region and plotted as a function

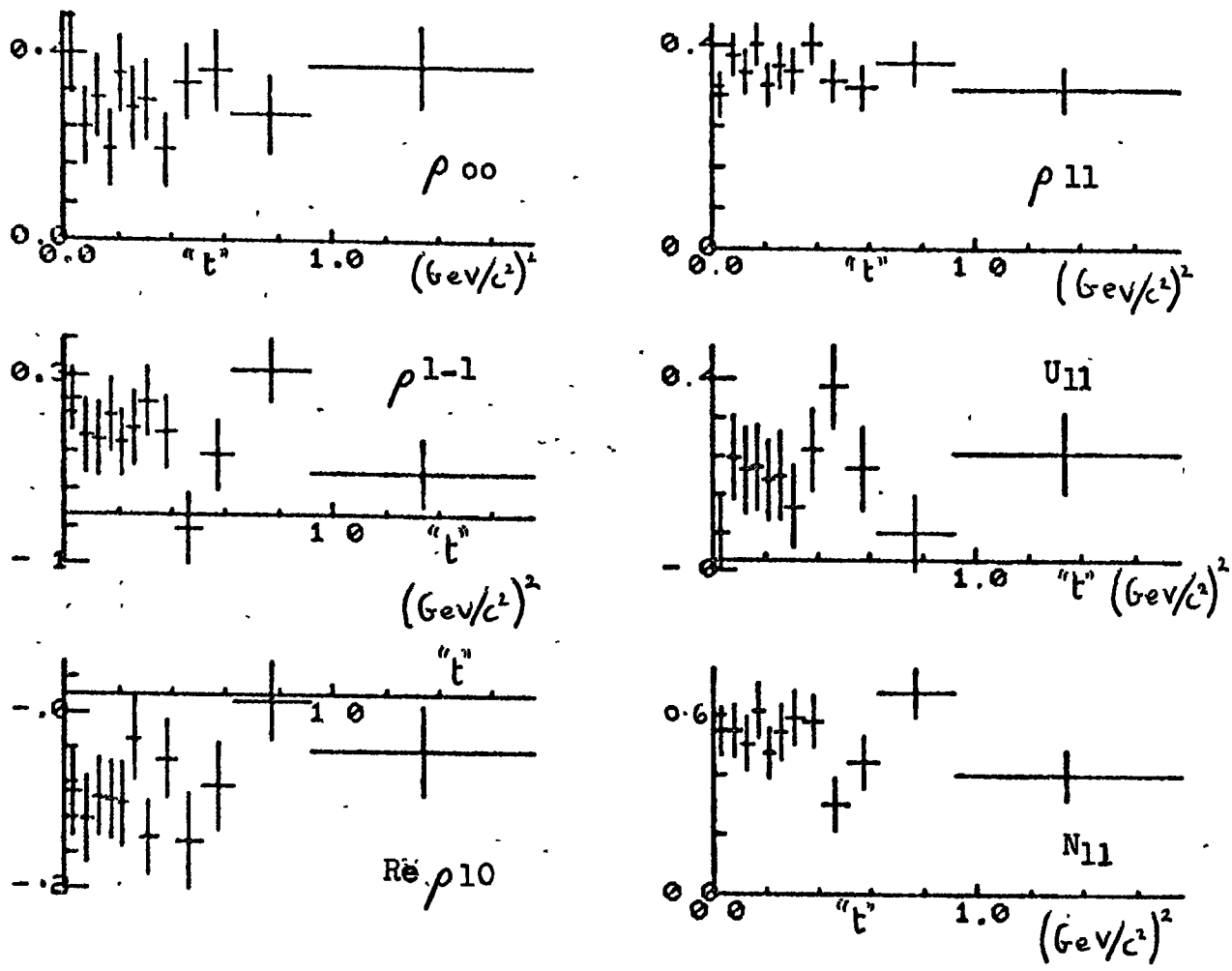

FIG. 6.3 THE SPIN DENSITY MATRIX ELEMENTS FOR RANDOM SAMPLES OF EVENTS.

of the t - transfer from the primary to the tripion mass system. To simulate the t - intervals the events have been ordered in t, the first N events defining the first t - interval and so on. The corresponding values for ρ i j however, have been calculated by randomly assigning the events to each "t" region, and hence apart from the statistical fluctuations, the results should be isotropic. In all cases the fluctuations are found to be consistent with the error estimates, but it is evident that for the cases where N is $\lesssim 70$ that apparent trends in the fluctuations may be misleading and simulate the appearance of structure at certain values of t. As a consequence of these results it was decided that the minimum value of N sufficient to reduce the statistical fluctuations and yet still provide sufficient t - regions to give the t - variation, is in the region of 150 for this experiment.

(c) THE SENSITIVITY OF THE RESULTS

The necessity for large statistics becomes even more apparent when the sensitivity of the results is considered. As illustrated below, the shapes of the angular distributions are extremely sensitive to the values of ρ i j.

As an example, consider the evaluation of ρ_{oo} . This is determined directly from the shape of the angular distribution in cos Θ , i.e.

$$W(\cos\Theta) = \frac{3}{4}\left[(1 - \rho_{oo}) + (3\rho_{oo} - 1)\cos^2\theta\right]$$

a $\sin^2\Theta$ distribution corresponding to $\rho_{oo} = 0.0$, a $\cos^2\theta$ distribution to $\rho_{oo} = 1.0$, and an isotropic distribution to $\rho_{oo} = 1/3$. Hence over the small range in ρ_{oo}

from 0.0 to 1.0 the corresponding changes in the angular distribution are very large. This is well illustrated in FIG. 6.4, which shows the ratio of the number of events in region A of the angular distribution compared to region B, plotted as a function of ρ_{00}, (the regions A and B being defined in the same figure). From this it is evident that the value of ρ_{00} is very sensitive to the angular distribution, particularly for $\rho_{00} < 1/3$ since this small part of the range covers the variation from $\sin^2\Theta$ to flat in $\cos\Theta$.

Similarly the value of $\rho\ 1\ -\ 1$ is highly dependent on the shape of the ϕ distribution i.e.

$$W(\ \phi\ ) = \frac{1}{2\pi}\ \left[(1 + 2\rho\ 1\ -\ 1) - 4\rho 1\ -\ 1 \cos^2\phi\right]$$

6.5 THE RESULTS FOR THE SPIN DENSITY MATRIX ELEMENTS CORRESPONDING TO THE FORWARDLY PRODUCED ω^0 MESONS IN THE π - N CENTRE OF MASS SYSTEM.

(a) THE SELECTION OF THE EVENTS

The main difficulty associated with the analysis of the spin density matrix elements of any resonance is that the signal under investigation cannot be cleanly seperated from the associated background. Consequently the analysis is generally restricted to specific regions such as a narrow mass interval centred on the resonance peak, in which the signal to background ratio is more favourable. It must be remembered however, that such restrictions are made at the expense of the available statistics, and hence a compromise has to be made.

The selection criteria chosen for this analysis are as follows:-

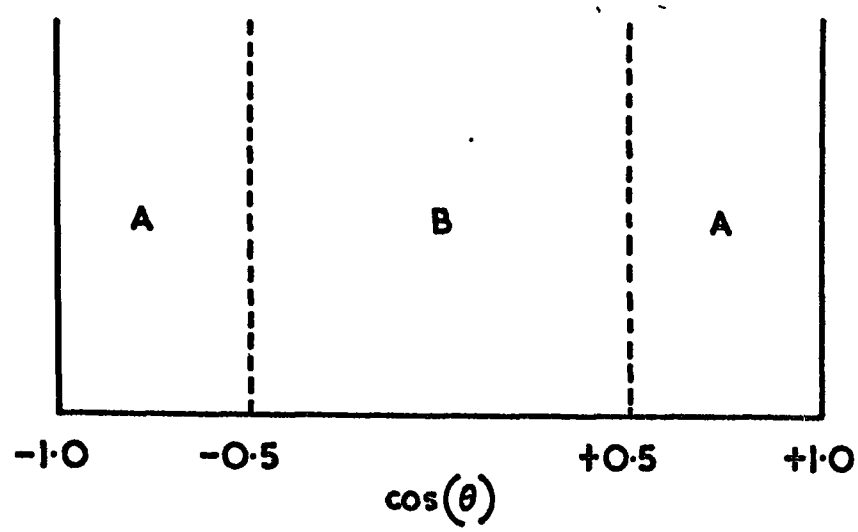

THE REGIONS A AND B OF THE ANGULAR DISTRIBUTION IN cos(θ).

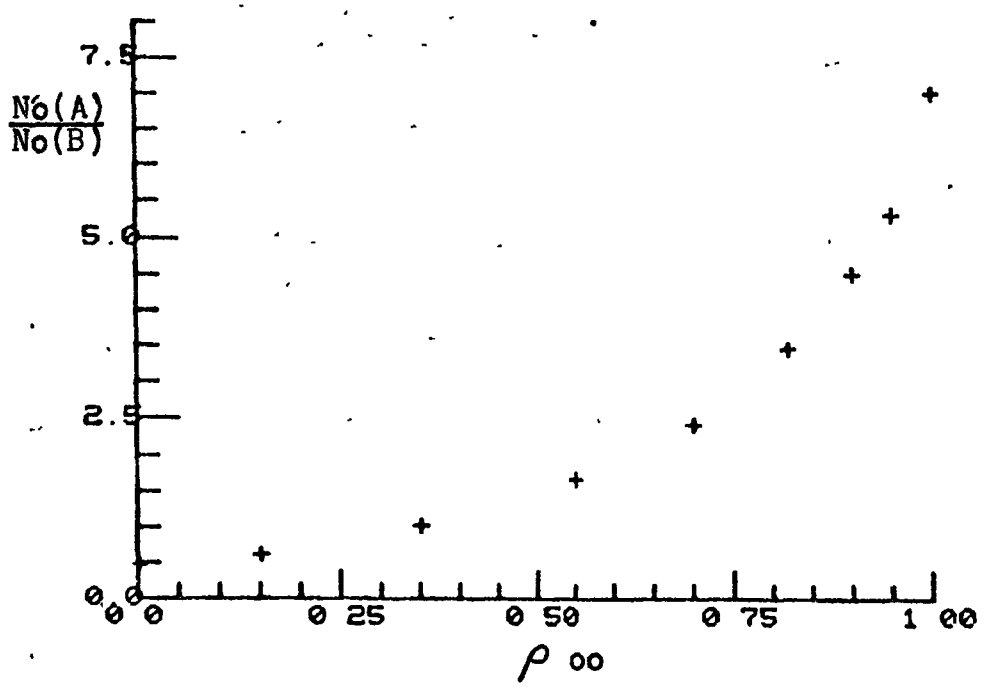

FIG.6.4 THE VALUE OF ρ_{00} AS A FUNCTION OF THE RATIO OF THE NUMBERS OF EVENTS IN REGIONS A AND B OF THE ANGULAR DISTRIBUTION IN cos (Θ), DEFINED ABOVE.

(1) Only events with tripion mass combinations produced in the forward direction in the π - N centre of mass system are selected.

and (2) The events are restricted to the tripion mass region (0.76 → 0.81) GeV/c^2

As in the previous chapter, events associated with seen and unseen spectator protons are analysed seperately. These selections result in signal to background ratios of ~10:1 and ~7 :1 respectively.

(b) THE EXPERIMENTAL RESULTS

The experimental results for the events selected in the manner specified above are shown in FIG. 6.5 for both the Helicity and Gottfried Jackson frames of reference for the seen and unseen spectator proton events. The results are plotted as a function of the 4 - momentum transfer squared measured from the primary to the tripion mass system. Tables of the results are also presented in table 6.1. The number of events per t - interval are 152 and 158 for the seen and unseen spectator proton events respectively, and the errors shown correspond to the statistical errors described in section 6.4a.

As discussed in section 6.3a, the density matrix elements in the Gottfried Jackson frame of reference are used to analyse the exchange mechanisms for the direct channel process. Consequently in order to examine the contributions from the ρ and B meson exchanges, the remainder of this analysis is concerned entirely with the results associated with this frame of reference. To achieve this objective however, it

FIG. 6.5 THE SPIN DENSITY MATRIX ELEMENTS IN THE G-J FRAME OF REFERENCE FOR EVENTS IN THE TRIPION MASS REGION 0.76 → 0.81 (GeV/c²).

SEEN SPECTATOR PROTON EVENTS

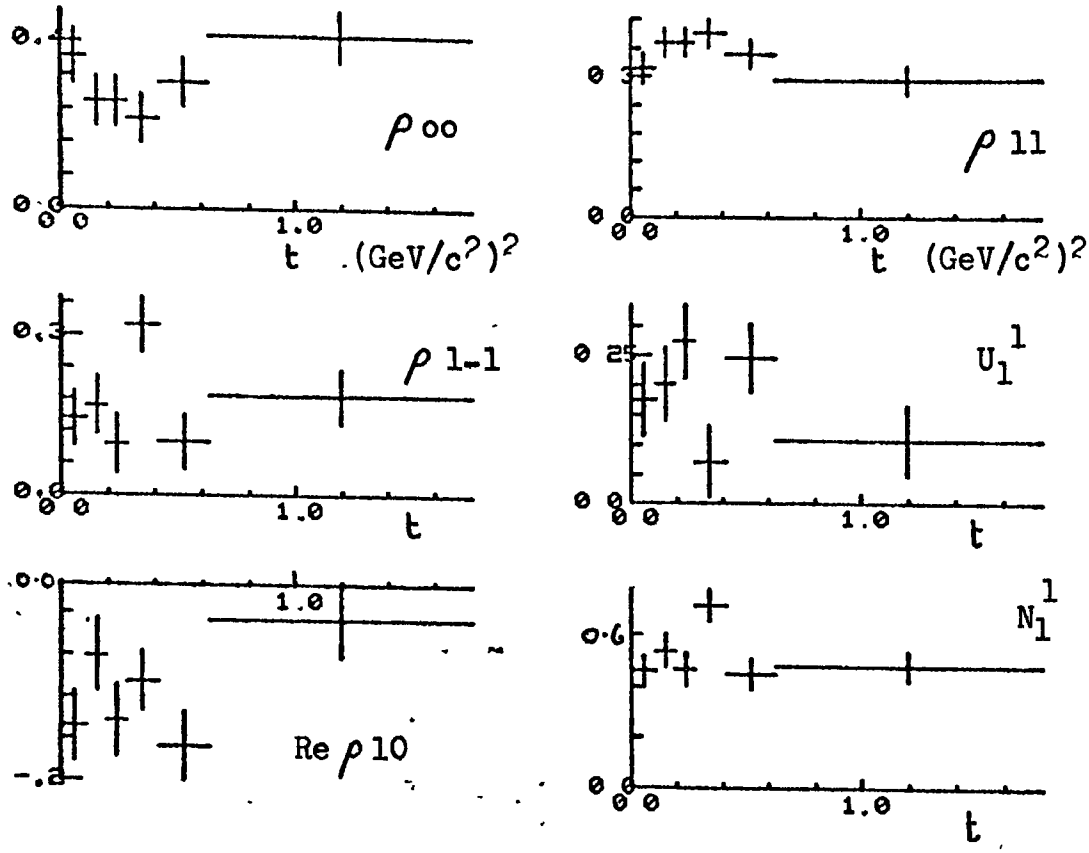

UNSEEN SPECTATOR PROTON EVENTS

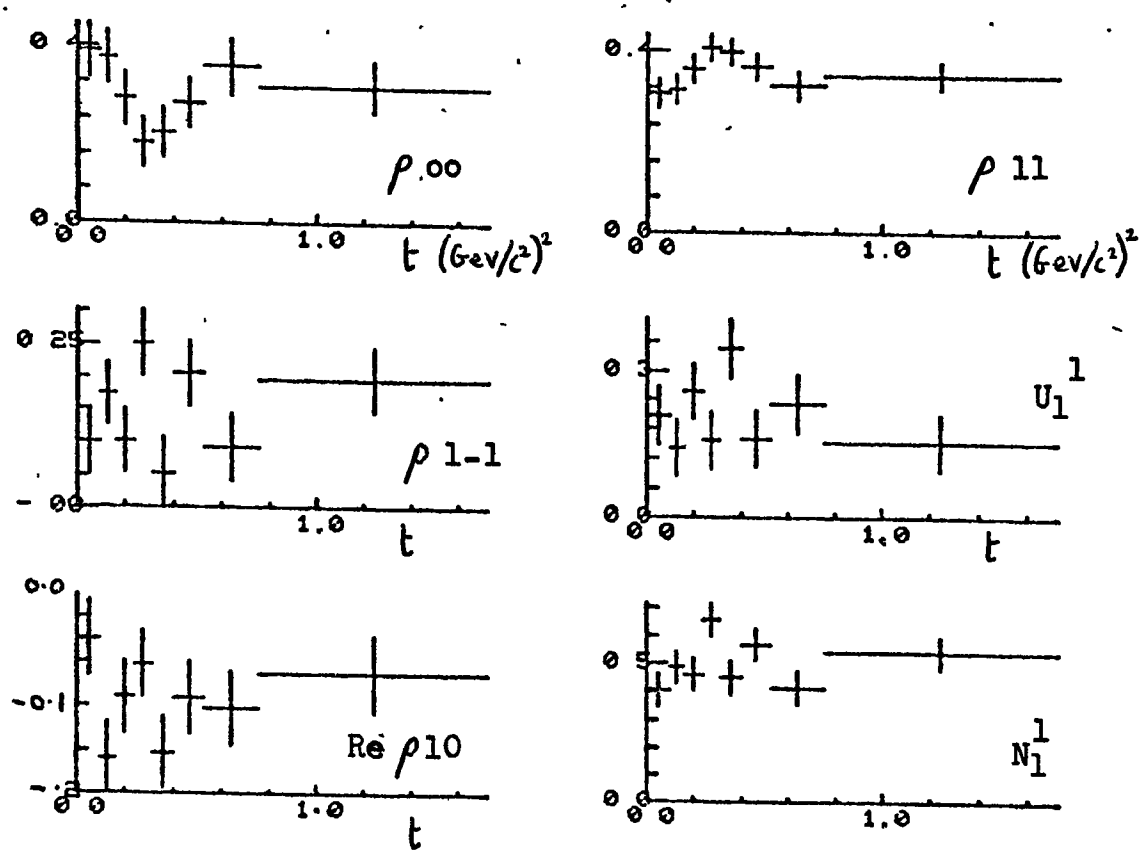

FIG.6.5 THE SPIN DENSITY MATRIX ELEMENTS IN THE HELICITY FRAME OF REFERENCE FOR EVENTS IN THE TRIPION MASS REGION 0.76 → 0.81 (GeV/c^2)

SEEN SPECTATOR PROTON EVENTS

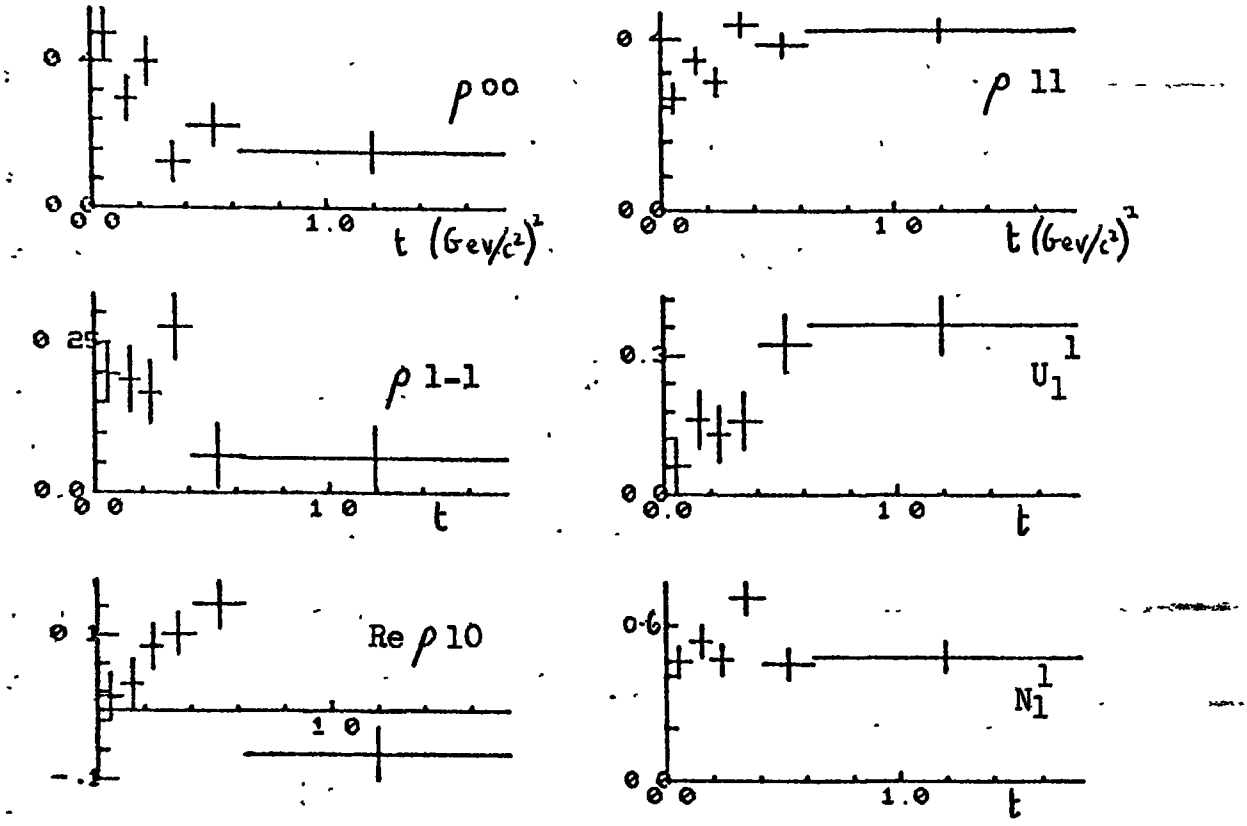

UNSEEN SPECTATOR PROTON EVENTS

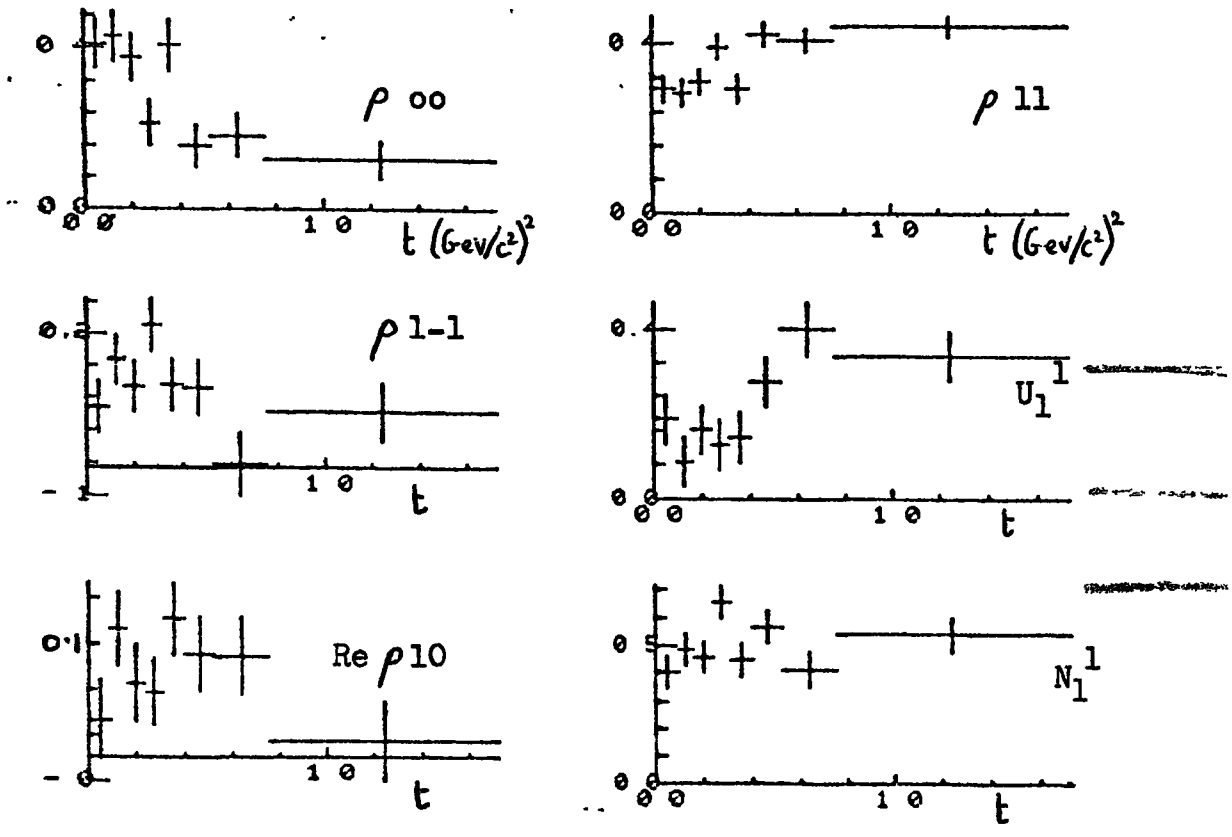

TABLE 6.1

THE SPIN DENSITY MATRIX ELEMENTS FOR THE ω^0 MESON

		THE GOTTFRIED-JACKSON REFERENCE FRAME											
	t - INTERVAL $(Gev/c^2)^2$	ρ 00	ERROR	ρ1-1	ERROR	Re ρ10	ERROR	ρ 11	ERROR	U_1'	ERROR	N_1'	ERROR
SEEN SPECTATOR PROTON EVENTS (152) EVENTS PER T-INTERVAL	0.0 → 0.11	0.36	0.06	0.14	0.05	-0.13	0.03	0.32	0.03	0.17	0.06	0.46	0.06
	0.11→ 0.19	0.26	0.06	0.17	0.05	-0.07	0.03	0.37	0.03	0.20	0.06	0.54	0.06
	0.19→ 0.28	0.26	0.06	0.10	0.05	-0.13	0.03	0.37	0.03	0.27	0.06	0.47	0.06
	0.28→ 0.41	0.22	0.06	0.32	0.05	-0.09	0.03	0.39	0.03	0.07	0.06	0.71	0.06
	0.41→ 0.63	0.30	0.06	0.10	0.05	-0.15	0.03	0.35	0.03	0.25	0.06	0.45	0.06
	0.63→ 1.76	0.41	0.06	0.19	0.05	-0.03	0.03	0.29	0.03	0.11	0.06	0.48	0.06
	AVERAGE OVER ALL t	0.30	0.02	0.17	0.02	-0.01	0.01	0.35	0.01	0.18	0.02	0.52	0.02
UNSEEN SPECTATOR PROTON EVENTS (158) EVENTS PER T-INTERVAL	0.0 → 0.09	0.39	0.06	0.10	0.05	-0.04	0.03	0.31	0.03	0.21	0.06	0.40	0.06
	0.09→ 0.16	0.38	0.06	0.17	0.05	-0.15	0.03	0.31	0.03	0.14	0.06	0.49	0.06
	0.16→ 0.24	0.28	0.06	0.10	0.05	-0.09	0.03	0.36	0.03	0.26	0.06	0.46	0.06
	0.24→ 0.31	0.18	0.06	0.25	0.05	-0.06	0.03	0.41	0.03	0.16	0.06	0.66	0.06
	0.31→ 0.40	0.21	0.06	0.05	0.05	-0.14	0.03	0.40	0.03	0.34	0.06	0.45	0.06
	0.40→ 0.53	0.27	0.06	0.20	0.05	-0.09	0.03	0.36	0.03	0.16	0.06	0.57	0.06
	0.53→ 0.75	0.35	0.06	0.0[illegible]	0.05	-0.10	0.03	0.32	0.03	0.23	0.06	0.41	0.06
	0.75→ 1.73	0.31	0.06	0.19	0.05	-0.07	0.03	0.35	0.03	0.15	0.06	0.54	0.06
	AVERAGE OVER ALL t	0.30	0.02	0.15	0.02	-0.09	0.01	0.35	0.01	0.21	0.02	0.50	0.02

TABLE 6.1 (Cont'd)

		THE HELICITY REFERENCE FRAME											
	t - INTERVAL $(Gev/c^2)^2$	$\rho 00$	ERROR	$\rho 1-1$	ERROR	$Re\rho 10$	ERROR	$\rho 11$	ERROR	U_1^1	ERROR	N_1^1	ERROR
SEEN SPECTATOR PROTON EVENTS (152) EVENTS PER T-INTERVAL	0.0 → 0.11	0.48	0.06	0.20	0.05	0.02	0.03	0.26	0.03	0.06	0.06	0.46	0.06
	0.11→ 0.19	0.30	0.06	0.19	0.05	0.04	0.03	0.35	0.03	0.16	0.06	0.54	0.06
	0.19→ 0.28	0.40	0.06	0.17	0.05	0.09	0.03	0.30	0.03	0.13	0.06	0.47	0.06
	0.28→ 0.41	0.13	0.06	0.28	0.05	0.11	0.03	0.44	0.03	0.16	0.06	0.71	0.06
	0.41→ 0.63	0.23	0.06	0.06	0.05	0.15	0.03	0.39	0.03	0.32	0.06	0.45	0.06
	0.63→ 1.76	0.15	0.06	0.06	0.05	-0.06	0.03	0.42	0.03	0.37	0.06	0.48	0.06
	AVERAGE OVER ALL t	0.28	0.02	0.16	0.02	0.06	0.01	0.36	0.01	0.20	0.02	0.52	0.02
UNSEEN SPECTATOR PROTON EVENTS (158) EVENTS PER T-INTERVAL	0.0 → 0.09	0.41	0.06	0.11	0.05	0.03	0.03	0.29	0.03	0.18	0.06	0.40	0.06
	0.09→ 0.16	0.43	0.06	0.20	0.05	0.11	0.03	0.29	0.03	0.09	0.06	0.49	0.06
	0.16→ 0.24	0.38	0.06	0.15	0.05	0.06	0.03	0.31	0.03	0.16	0.06	0.46	0.06
	0.24→ 0.31	0.22	0.06	0.27	0.05	0.06	0.03	0.39	0.03	0.13	0.06	0.66	0.06
	0.31→ 0.40	0.41	0.06	0.15	0.05	0.12	0.03	0.30	0.03	0.14	0.06	0.45	0.06
	0.40→ 0.53	0.16	0.06	0.15	0.05	0.09	0.03	0.42	0.03	0.27	0.06	0.57	0.06
	0.53→ 0.75	0.19	0.06	0.01	0.05	0.09	0.03	0.41	0.03	0.40	0.06	0.41	0.06
	0.75→ 1.73	0.13	0.06	0.10	0.05	0.01	0.03	0.44	0.03	0.34	0.06	0.54	0.06
	AVERAGE OVER ALL t	0.29	0.02	0.14	0.02	0.07	0.01	0.36	0.01	0.21	0.02	0.50	0.02

is firstly necessary to make allowances for the effects of background.

(c) BACKGROUND SUBTRACTION

Of particular importance is the behaviour of ρ_{oo} , U_1^1, and N_1^1 at low values of t, since these provide a direct measure of the contributions from natural and unnatural parity exchange.

For both the seen and unseen spectator proton events there is an indication that ρ_{oo} may increase at low values of t. This region however, as discussed in the previous chapter is thought to be contaminated by a breakthrough of events from the channel

$$\pi^+ D \longrightarrow P_S P \pi^+ \pi^-$$

and hence allowances must be made for this and also for the presence of the other background events described in chapter 5.

An indication of the behaviour of the background can be found by looking at the results for the tripion mass regions on either side of the central ω^o - peak, these regions being dominated by background of a similar type to that under the ω^o - region. The results for the tripion mass interval $0.81 \rightarrow 0.9$ (GeV/c^2) are shown in FIG. 6.6, (the lower mass interval containing insufficient statistics). The results indicate that ρ_{oo} may tend to 0.0 at low t - values for the background. If this effect is real, and moreover is the result of the above mentioned breakthrough of events from the 4c channel, the value of ρ_{oo} in the tripion mass interval $0.9 \rightarrow 1.1$ (GeV/c^2) for the unseen spectator proton events should indicate similar features, since it is this region

FIG. 6.6 THE SPIN DENSITY MATRIX ELEMENTS IN THE G-J FRAME OF REFERENCE FOR EVENTS IN THE TRIPION MASS REGION 0.81 → 0.9 (GeV/c^2)

SEEN SPECTATOR PROTON EVENTS

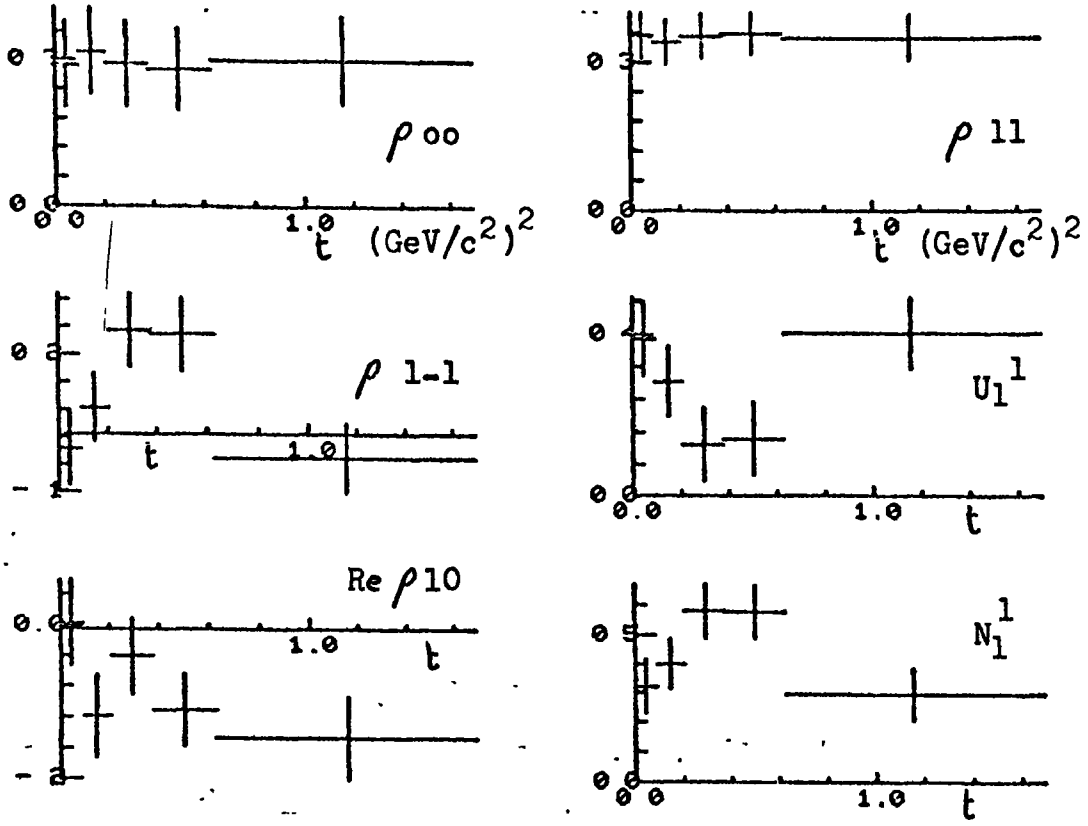

UNSEEN SPECTATOR PROTON EVENTS

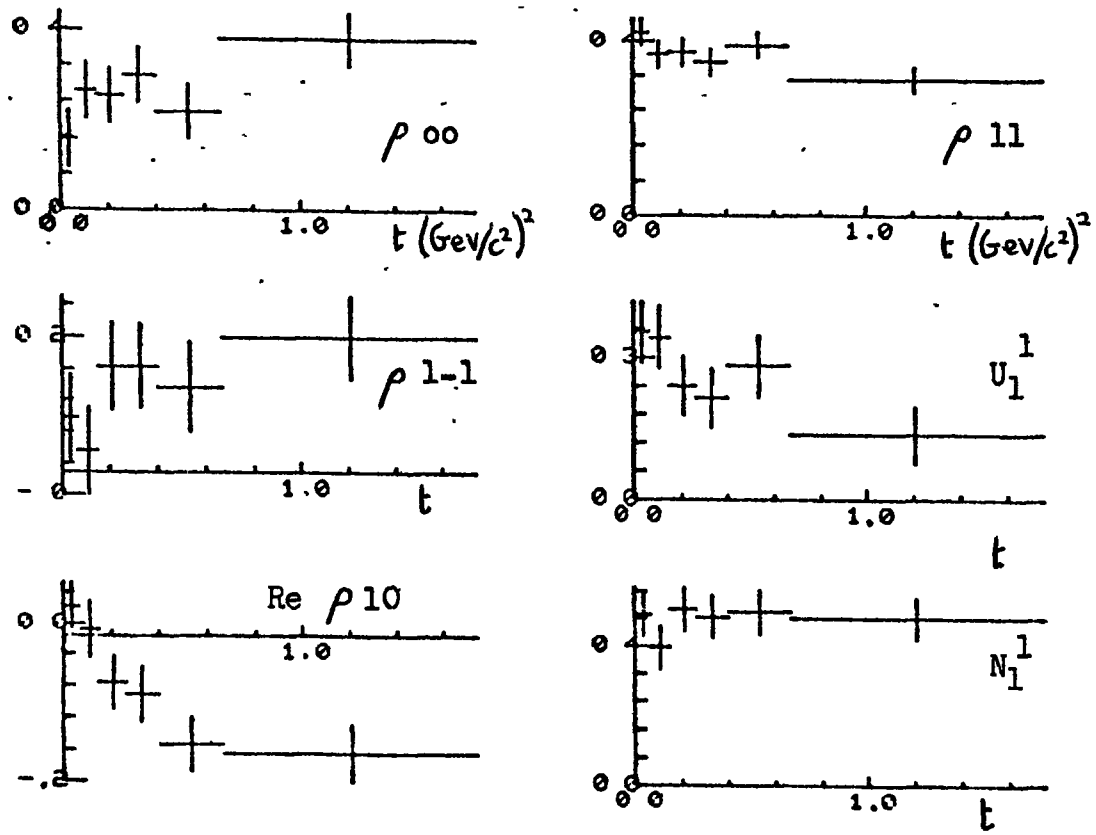

which is believed to be dominated by the 4c breakthrough. From the results shown in FIG. 6.7 it is evident that this same effect is very much apparent. Moreover, the results for the tripion mass region 0.76 → 0.81 (GeV/c^2) restricted to the Dalitz Plot sectors described in the previous chapter showed a similar tendency for ρ_{oo} to drop at low t in the sectors believed to be dominated by the 4c breakthrough. The statistical accuracy however, was insufficient for the results to be conclusive.

(d) THE DETERMINATION OF ρ_{oo} INDEPENDENT OF THE BACKGROUND

As discussed in section 6.4c, the value of ρ_{oo} is determined directly from the angular distribution in cos θ , and as illustrated in FIG. 6.4, the ratio of events in region A of this distribution compared to region B is directly related to the values of ρ_{oo} . Hence by fitting the tripion mass spectra for these regions the amounts of ω^o - signal can be extracted, and hence the background free values of ρ_{oo} determined. The fits made were as described in section 4.2, the available statistics only allowing this to be achieved for the unseen spectator proton events in t - intervals of 0.1 $(GeV/c^2)^2$ from 0.0 to 1.0 $(GeV/c^2)^2$. The fitted tripion mass region was 0.4 → 0.8 $(GeV/c^2)^2$ in mass squared.

The advantages of this type of calculation are that it uses all the ω^o - signal and not just the central peak, and in addition determines the value of ρ_{oo} free from background effects. The disadvantages however, are that large statistics are required, and it is difficult to assess the

FIG. 6.7 THE SPIN DENSITY MATRIX ELEMENTS IN THE G-J FRAME OF REFERENCE FOR EVENTS IN THE TRIPION MASS REGION 0.9 → 1.1 GeV/c^2

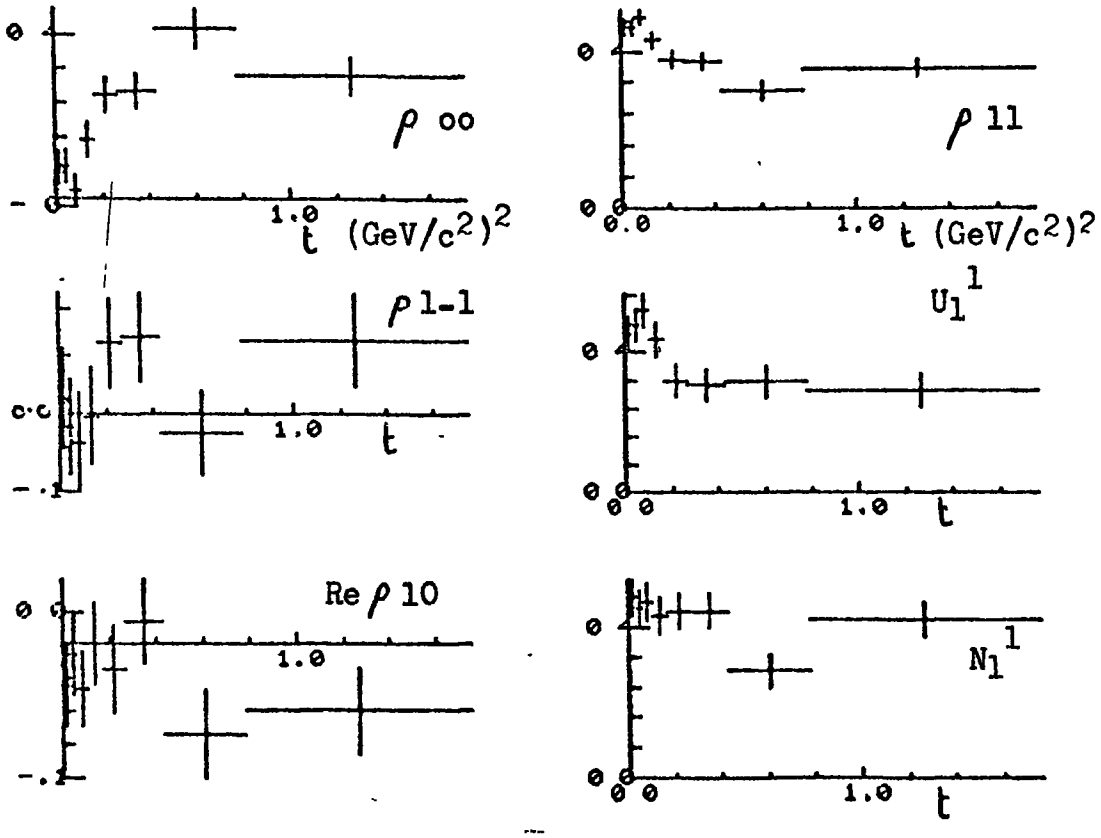

UNSEEN SPECTATOR PROTON EVENTS

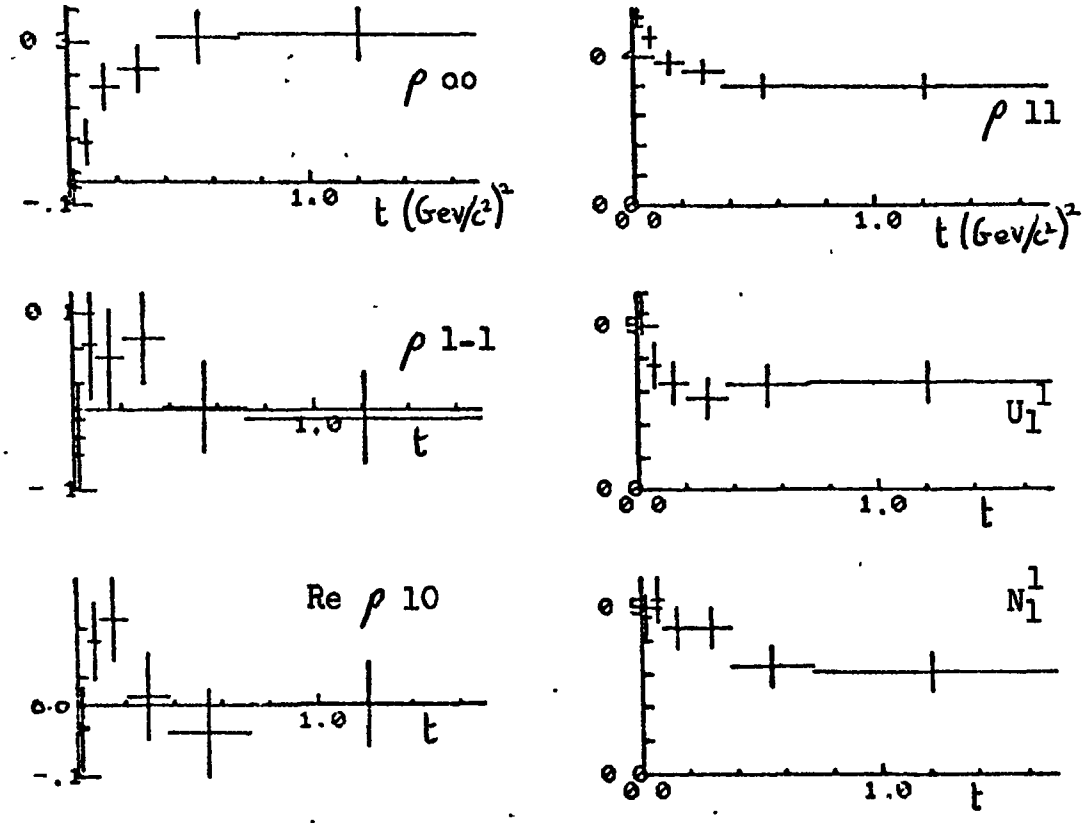

SEEN SPECTATOR PROTON EVENTS

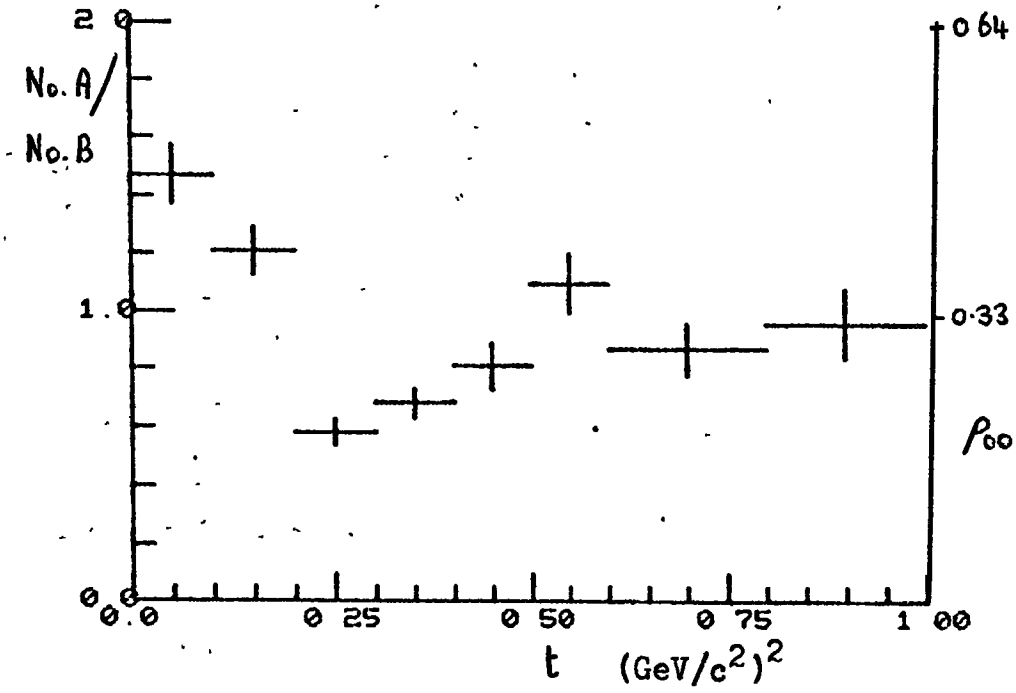

FIG. 6.8 THE VALUE OF ρ_{00} INDEPENDENT OF BACKGROUND EFFECTS AS A FUNCTION OF t

accuracy of the fitting technique.

The results shown in FIG. 6.8 are in good agreement with the above calculations, and indicate that the non-zero value for ρ_{oo} for the ω^o - signal at low t - values is genuine, and in addition supports the possibility of a slight increase in its value at low t. Moreover, the results also indicate the presence of a minimum in ρ_{oo} at t $\sim$ 0.3 $(GeV/c^2)^2$, a feature which is also apparent in FIG. 6.5 in the results for the central ω^o - region (0.76 $\rightarrow$ 0.81) GeV/c^2 of the tripion mass spectrum, thereby confirming that this effect is associated with the ω^o - signal.

(e) A SUMMARY OF THE RESULTS

A summary of the results for the spin density matrix elements for the forward production of ω^o - mesons in the π - N centre of mass system in the Gottfried Jackson frame of reference is given below:-

(1) The results for the seen and unseen spectator proton events are consistent at all values of t

(2) The value of ρ_{oo} at low t is non zero and in the region of 0.4

(3) A minimum occurs in ρ_{oo} at t $\sim$0.3 $(GeV/c^2)^2$

(4) ρ_{1-1} is positive throughout the entire t - range, and in certain regions may be consistent with zero. Consequently N_1^1 is always $\gg U_1^1$

(5) The value of Re ρ_{10} is negative at all values of t.

(6) None of the spin density matrix elements indicate any structure at t $\sim$ 0.6 $(GeV/c^2)^2$, corresponding to the NWSZ for ρ - trajectory exchange.

(f) A COMPARISON OF THE RESULTS WITH PREVIOUS EXPERIMENTS

A survey of the values for ρ_{00} , ρ 1 - 1 and Re ρ 10 averaged over all t from previous experiments in the range of incident energies from 1.7 to 13.0 GeV is shown in table 6.2. Also indicated are the position of any observed minima in ρ_{00}

The results indicate the following features:-

(1) $\overline{\rho_{00}}$ tends to decrease with increasing energy,

(2) $\overline{\rho_{1-1}}$ tends to increase with increasing energy,

(3) $\overline{\text{Re } \rho \; 10}$ is approximately energy independent.

It is also evident that the vast majority of the experiments are in favour of a broad minimum in ρ_{00} at $t \sim 0.3$ $(\text{GeV}/c^2)^2$. Although the position, width and depth of this minimum tends to vary from one incident energy to another, it must be remembered that in many cases the accuracy is somewhat limited and hence statistical fluctuations may tend to obscure its exact position. In certain cases it may be argued that the dip itself results from such statistical fluctuations. In this experiment however, using high statistics and removing background effects, the minimum was found to be a genuine feature associated with the ω^0 - signal. Adding further weight to the existence of this feature is the marked similarity with the results at 4.19 GeV/c. In none of the experiments is there any evidence for structure at $t \sim 0.6$ $(\text{GeV}/c^2)^2$, corresponding to the NWSZ for ρ - exchange.

6.6 THE INTERPRETATION OF THE RESULTS

(a) THE TOTAL PRODUCTION CROSS SECTION

The summary of the total production cross section as calculated in this and previous experiments is given in

TABLE 6.2

BEAM MOMENTUM (GeV/c)	AVERAGE OF ρ oo	AVERAGE OF ρ 1 - 1	AVERAGE OF Re ρ 10	DIPS IN ρ oo +	DIPS IN $d\sigma/dt$ *	REF
1.7	0.53 ± 0.04	0.02 ± 0.04	-0.08 ± 0.02	0.3	L	4.5
3.65	0.35 ± 0.04	0.09 ± 0.04	-0.10 ± 0.03	0.3	L	4.7
3.65	0.4 ± 0.04	0.15 ± 0.04	-0.08 ± 0.025		L	6.9
4.0	0.3 ± 0.02	0.15 ± 0.02	-0.10 ± 0.01	0.3	D	4.8 (Present Work)
4.19	0.3 ± 0.04	0.12 ± 0.04	-0.18 ± 0.03	0.25	L	4.9
4.50	0.29 ± 0.04	0.13 ± 0.04	-0.07 ± 0.03		L	4.10
5.10	0.31 ± 0.04	0.03 ± 0.04	-0.05 ± 0.03			4.11
5.40	0.28 ± 0.06	0.12 ± 0.06	-0.04 ± 0.04	0.4	L	4.12
5.50	0.30 ± 0.04	0.18 ± 0.04	-0.07 ± 0.03	0.35	D	4.13
6.0	0.35 ± 0.02	0.18 ± 0.02	-0.11 ± 0.02	0.25	D	4.14
6.95	0.37 ± 0.04	0.13 ± 0.03	-0.11 ± 0.02		D	4.15
11.7	0.27 ± 0.07	0.05 ± 0.06	-0.36 ± 0.04			4.16
13.0	0.13 ± 0.08	0.24 ± 0.11	0.0 ± 0.05		L	4.17

* The dips in $d\sigma/dt$ all occur at low t, L refering to the distribution levelling off, and D to it dipping.

+ Dips occur in ρ oo at the t - values indicated in $(GeV/c^2)^2$

table 4.5, and as illustrated in FIG. 4.9, the cross section variation with the incident energy is well described by the relation

$$\sigma \propto p^{-n}$$

where p is the primary momentum. The exact value of n however is somewhat uncertain, since as illustrated in chapter 4, the positioning of the data points contributing to FIG. 4.9 is highly dependent upon the type of parameterisation used to fit the ω^o - signal. Moreover, not all the results have been corrected for unseen decay modes and scanning losses. Despite this however, a conservative estimate would place n at 2.5 ± 0.5.

As discussed in Appendix 3, the energy dependence of the peripheral model with or without absorption, for vector meson exchange, is incorrect, since it diverges at higher energies. This is well illustrated for ω^o - production, since although the model is in good agreement at incident energies of $\sim$ 2.7 (GeV/c), (Ref. 6.2) it predicts a cross section about 6 times too large in the 4 GeV/c region. This divergence with energy is overcome in the Regge pole model by replacing the spin of the exchange particle with the value of the trajectory parameter at $t = 0$

$$\text{i.e.} \quad \sigma \propto S^{2\alpha(t=0)-2}$$

which at high energies, where $S \propto p$ is in agreement with Morrison's relationship $\sigma \propto p^{-n}$, (Ref. 6.3), for

$$-n = 2\alpha(t=0) - 2$$

Therefore the value of n gives a direct indication of the dominating exchange trajectory, ρ trajectory exchange

predicting a value of n in the region of -1.5. The larger value observed experimentally is therefore incompatible with the exchange of the ρ - trajectory alone, and is consistent with a significant contribution from the exchange of the B trajectory.

Should the Regge pole predictions be correct the ρ trajectory exchange should start to dominate at higher energies and hence the slope of the line drawn in FIG. 4.9 would be expected to gradually become more shallow. Further data points at higher energies would therefore be desirable. Moreover, the inclusion of more well defined points calculated from reliable parameterisations of the ω^0 - signal and including consistent correction factors will enable a fit to be made to the energy dependence of the production cross section, and hence the contributions from the above trajectories determined as a function of the incident energy.

(b) THE DIFFERENTIAL CROSS SECTION ($d\sigma/dt$)

One of the main successes of the Regge Pole Model is that it not only predicts the correct energy dependence for the high energy charge exchange reaction,

$$\pi^- P \rightarrow \pi^0 n$$

but it also successfully predicts the observed minima at $t \sim 0.0$ and 0.6 $(GeV/c^2)^2$ in the differential cross section. Since this process is dominated by the exchange of the ρ trajectory, similar features were also predicted for ω^0 production, (Ref. 4.2). As illustrated in table 6.2 however, although the majority of the experiments are in favour of a

dip at low t, none indicate any structure at t $\sim$ 0.6 $(GeV/c^2)^2$. Moreover, as demonstrated in this analysis, although background events may tend to obscure the presence of a dip at low t, their removal does not reveal any structure in the 0.6 $(GeV/c^2)^2$ region.

Several mechanisms have been suggested for the non appearance of this structure, namely, conventional absorption theory, (Ref. 6.4), or strong cut models, (Ref. 6.5). The effects of the former however were found to be insufficient, and the latter predicted values of Re ρ 10 $>$ 0 in disagreement with the experimental results. The most favoured solution is the incorporation of a large contribution from B - meson exchange. Not only is this in agreement with the above mentioned energy dependence of the production cross section, but it is also in agreement with the behaviour of the spin density matrix elements described in the following section. Moreover, the dominance of the ω - π decay mode for the B - meson suggests that the B - meson trajectory may well be important for ω production via π - N collisions. However, in neither this nor any of the above mentioned experiments is there any evidence for structure in the differential cross section in the region of the NWSZ for the B- trajectory (t $\sim$ 0.2 GeV/c^2 ^{2}), and indeed in many cases the differential cross section is observed to peak in this region.

The predictions of two ρ and B Regge exchange models are drawn on the differential cross section determined from the analysis of this experiment. The results, taken from fits made to the 4.19 GeV/c data (Ref. 6.6 and 6.7), are illustrated in FIG. 6.9. Note that the model described in the first

FIG. 6.9 REGGE MODEL FITS TO THE DIFFERENTIAL CROSS SECTION

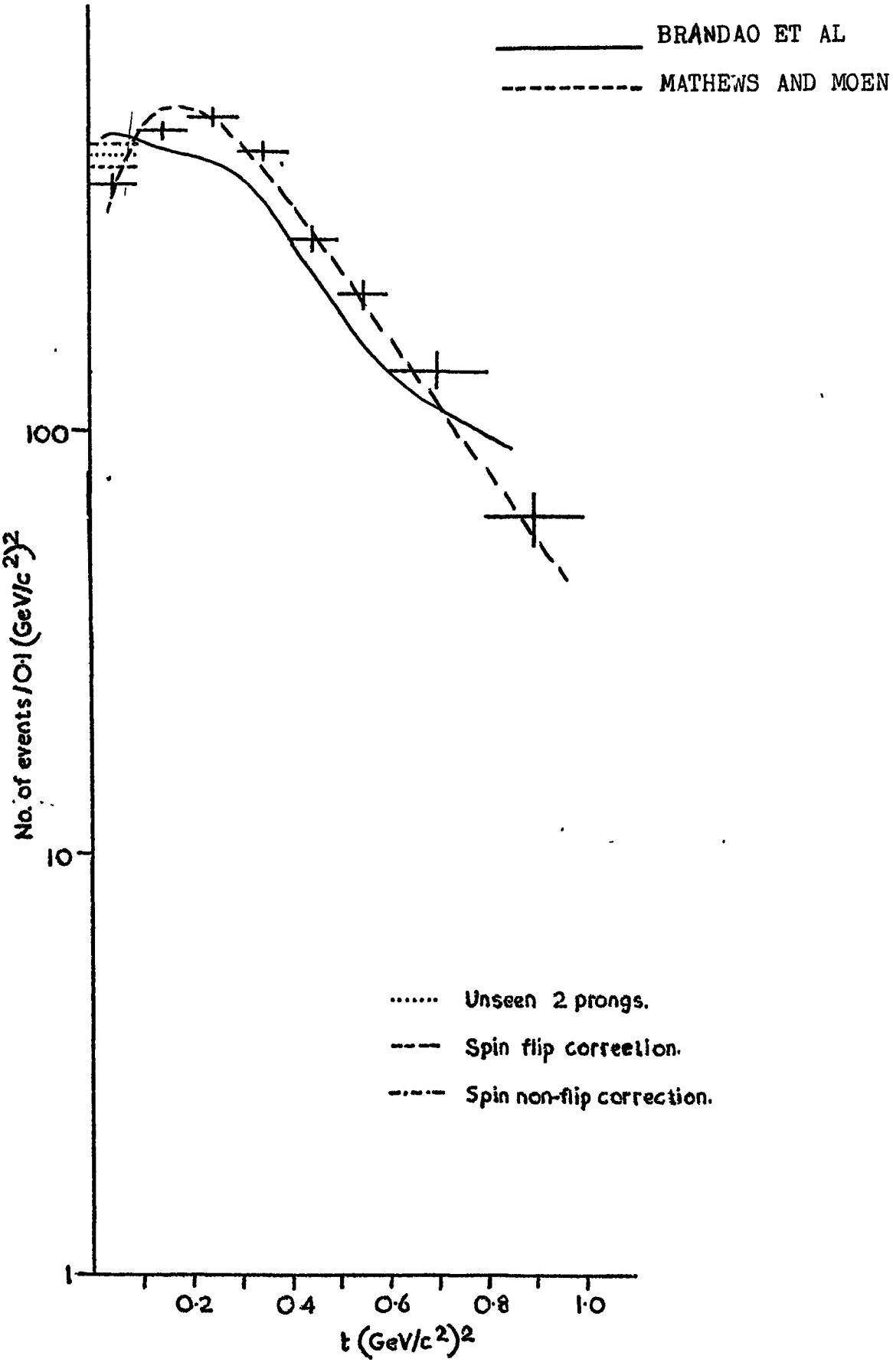

reference also includes absorptive effects, and the latter reference also illustrates the results of incorporating ρ' exchange into the model. Both of the fits are in reasonable agreement with the data, the smoother varying non absorptive model reproducing the results somewhat better.

(c) THE SPIN DENSITY MATRIX ELEMENTS

The results of the survey of the spin density matrix elements given in the previous section can be interpreted as follows:-

As discussed in section 6.2a and 6.2b, the value of ρ_{00} at low t is a direct measure of the amount of unnatural parity exchange, (B exchange), contributing to the production process. Hence the value of $\rho_{00} \sim 0.4$ indicates that some 40% of the events proceed via B - exchange, which is in good agreement with the observed values for U_1^1 and N_1^1, which indicate that the contributions from natural parity exchange are slightly larger than from the unnatural parity exchange. Moreover, as suggested by Hogaasen and Lubatti, (Ref. 6.8), the observed minimum in ρ_{00} at $t \sim 0.3$ $(GeV/c^2)^2$ is consistent with the vanishing of the unnatural parity exchange at the NWSZ for the B - meson.

Hence, as deduced from the behaviour of the production and differential cross sections, the spin density matrix elements also indicate a significant contribution from the exchange of the B - trajectory.

The erratic behaviour in the shape and position of the minimum in ρ_{00} at $t \sim 0.3$ $(GeV/c^2)^2$ in going from one incident

energy to another has led to some speculation as to whether the effect is genuine. The results of this analysis however, strongly suggest that it is, and hence it is a feature which should be reproduced by meaningful Regge model fits.

The observed decrease in the average value of ρ_{00} and the increase in the average value of ρ_{1-1} with increasing energy are both in agreement with the predicted domination of ρ exchange at higher energies. The observed negative values of $\mathrm{Re}\,\rho_{10}$ however, are in complete disagreement with the strong cut models.

Predictions for the density matrix elements corresponding to the ρ and B Regge exchange models described in the previous section are shown in FIG. 6.10. In this case the results for the absorptive model are in better agreement, and reproduce the observed minimum in ρ_{00} .

(d) REGGE MODELS AND ω^0 - PRODUCTION

In general the gross features of the reaction

$$\pi^+ N \rightarrow \omega^0 P$$

are well described by Regge pole models incorporating both ρ and B exchange trajectories. The detailed features however, namely the observed minimum in ρ_{00} at $t \sim 0.3$ $(\mathrm{GeV}/c^2)^2$ and the dip in $d\sigma/dt$ at low t are less well fitted.

The results of this analysis indicate that great care should be taken in trying to fit results in which proper account has not been taken of the background, particularly at low t, and also of fitting what may be spurious fluctuations in spin density matrix elements, using insufficient statistics.

FIG. 6.10 REGGE MODEL FITS TO THE ω^0 SPIN DENSITY MATRIX ELEMENTS

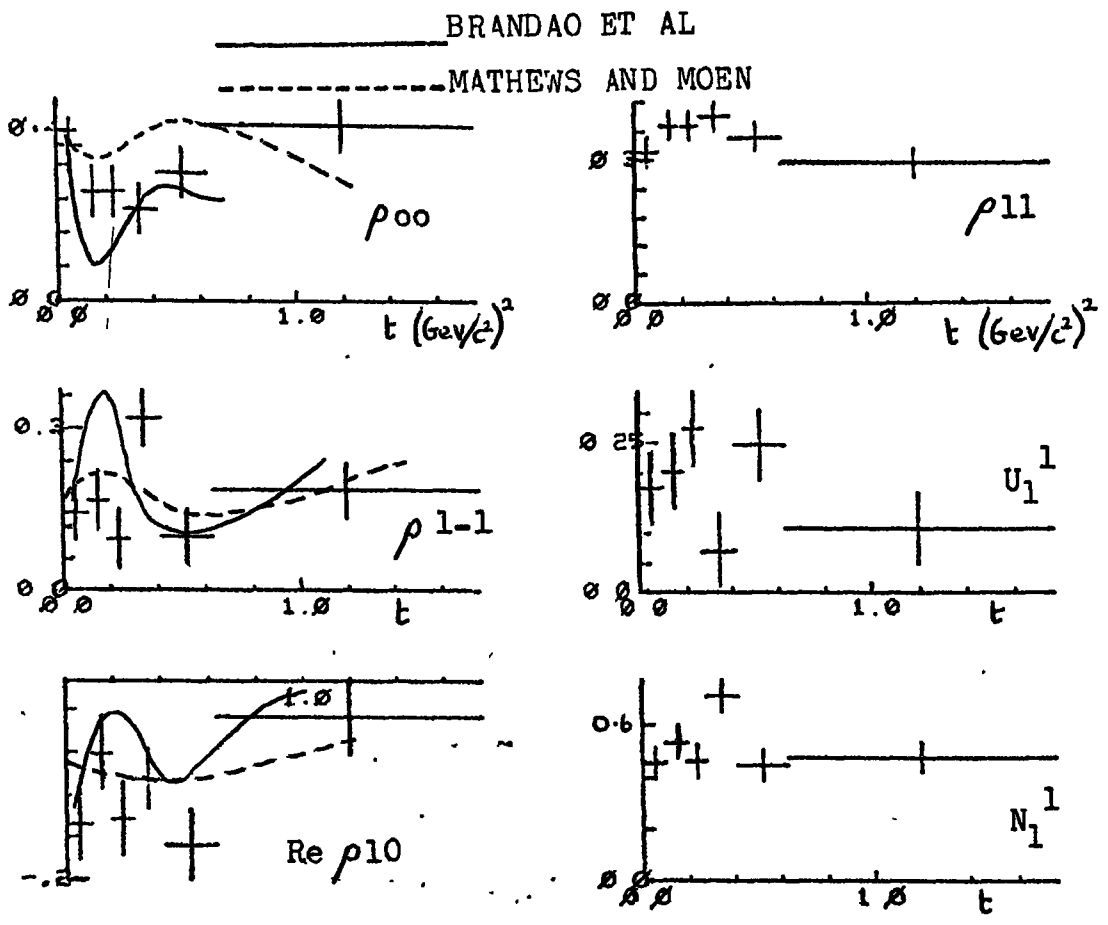

SEEN SPECTATOR PROTON EVENTS

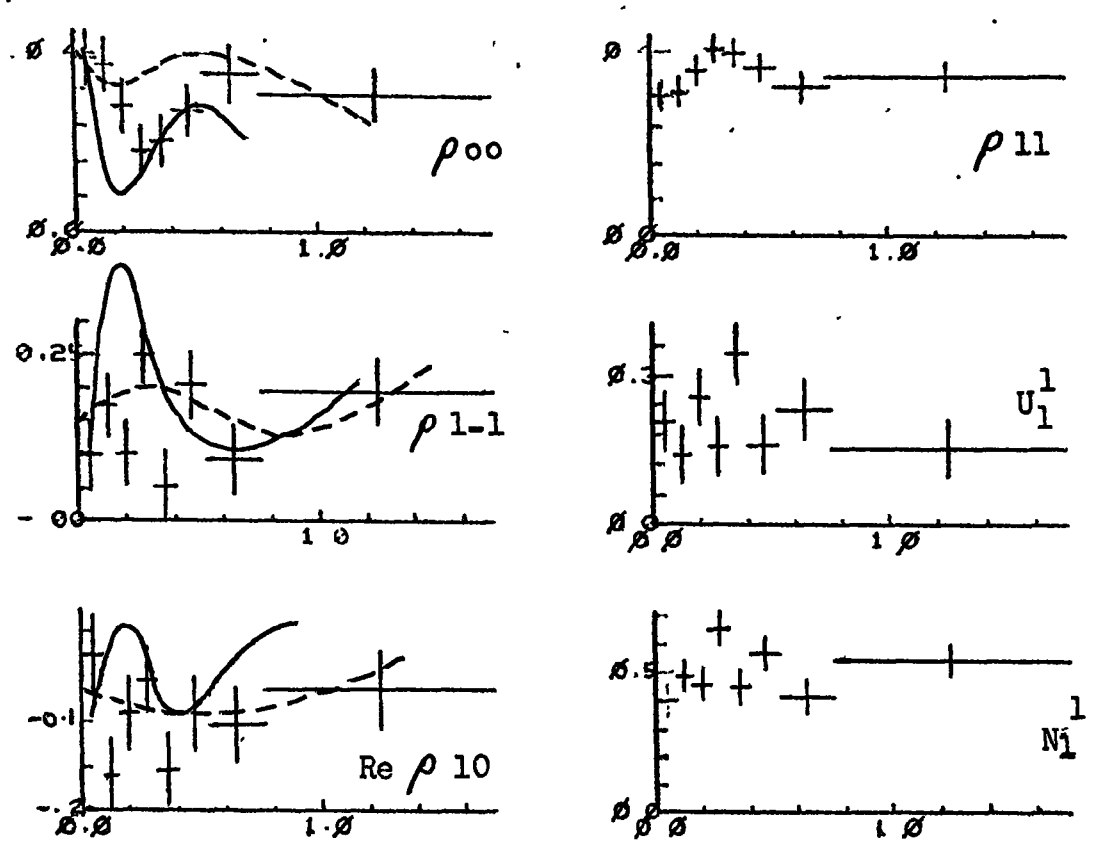

UNSEEN SPECTATOR PROTON EVENTS

The models are however very close to correctly predicting the behaviour of both $d\sigma/dt$ and the spin density matrix elements, and a better knowledge of the correct parameterisation of the B trajectory may solve the problem.

CHAPTER SEVEN

THE ANALYSIS OF THE PRODUCTION OF THE η - MESON

INTRODUCTION

This analysis is concerned with the "charged" decay mode

$$\eta \rightarrow \pi^+ \pi^- \pi^o$$

which occurs via an electromagnetic decay with non-conservation of G - parity, the decay products being analysed in the lc - channel

$$\pi^+ D \rightarrow P_S P \pi^+ \pi^- \pi^o$$

The central mass width, quantum numbers and decay modes for the η - mesons, as summarised by the Review of Particle Properties of April, 1974, (Ref. 4.1) are shown in table 7.1.

The selection of the above channel has already been described in chapter 3, and the occurrence of the η - meson is clearly seen in the tripion mass spectra for both the seen and unseen spectator proton events, as illustrated in FIGs. 4.3 and 4.4. As expected the majority of the η events are associated with tripion mass combinations produced in the forward direction in the π - N centre of mass system, but as indicated in FIG. 4.3, there is also some evidence for backward production.

The limited statistics do not enable such a rigorous analysis to be carried out as was made for the ω^o - production. Fortunately however, since in this experiment the η - resonance is produced in association with considerably less reflected resonance background than the ω^o signal, and moreover is

TABLE 7.1

PROPERTIES OF THE η - MESON

	DECAY MODES	%
$I^G\ J^P\ C_N$		
$0^+\ 0^-\ +$	$\gamma\ \gamma$	38.0 ± 1.0
	$\pi^0\ \gamma\ \gamma$	3.1 ± 1.1
	$\pi^0\ \pi^0\ \pi^0$	30.0 ± 1.1
	$\pi^+\ \pi^-\ \pi^0$	23.9 ± 0.6
CENTRAL MASS	$\pi^+\ \pi^-\ \gamma$	5.0 ± 0.1
548 ± 0.6 MeV/c^2	$\pi^0\ e^+\ e^-$	
	$\pi^+\ \pi^-$	
	$\pi^+\ \pi^-\ e^+\ e^-$	< 0.1
	$\pi^+\ \pi^-\ \pi^0\ \gamma$	
FULL WIDTH	$\pi^+\ \pi^-\ \gamma\ \gamma$	
2.63 ± 0.58 KeV/c^2	$\mu^+\ \mu^-$	
	$\mu^+\ \mu^-\ \pi^0$	

further removed from the possible spurious results produced around the 1.0 GeV/c^2 region of the tripion mass spectrum, the analysis is much simplified.

In the following sections the total η - production cross section is calculated, including an estimate of the backward production . In addition, the results are presented for the differential cross section for η mesons produced in the forward direction in the π -N centre of mass system.

7.1 THE TOTAL PRODUCTION CROSS SECTION

(a) THE PARAMETERISATION OF THE SIGNAL

As illustrated in table 7.1, the η - meson has an extremely narrow resonance width, sufficiently narrow infact for it to be classified among the stable particles. Consequently the observed widths and shapes of the resonance peaks seen in FIGs. 4.3 and 4.4, result entirely from the limited mass resolution. Hence unlike the parameterisation of the ω^o - signal described in section 4.2, the resolution function alone should be sufficient to fit the η - signal.

As discussed in section 4.2a, the resolution function is essentially the superposition of gaussians in mass squared, corresponding to the frequency distribution determined from the errors on the tripion mass. The frequency distribution of gaussians for the seen and unseen spectator proton events corresponding to the η - region 0.2 $\rightarrow$ 0.4 (GeV/c^2)^2 of the tripion mass squared spectra are shown in FIG. 7.1. The corresponding resolution functions, constructed in accordance with the above frequency distributions, are illustrated in FIG. 7.2. Drawn on these plots are the best fitting Gaussian and Breit Wigner shapes, the details of the fits being shown

FIG. 7.1 THE FREQUENCY DISTRIBUTION OF ERRORS IN THE η - REGION

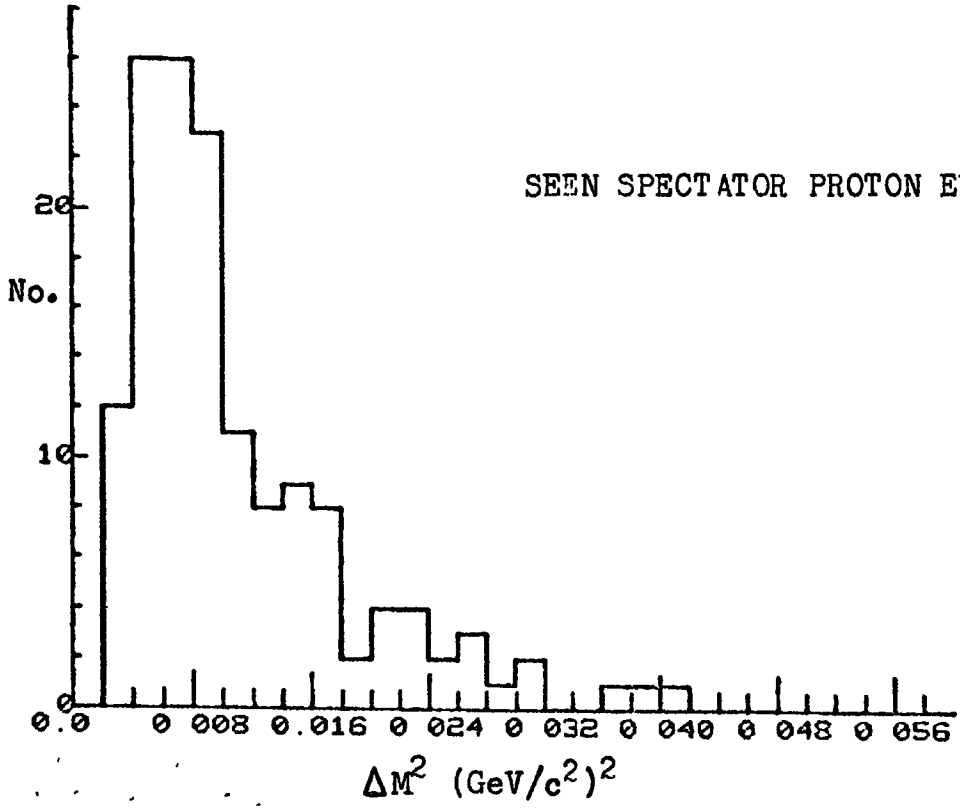

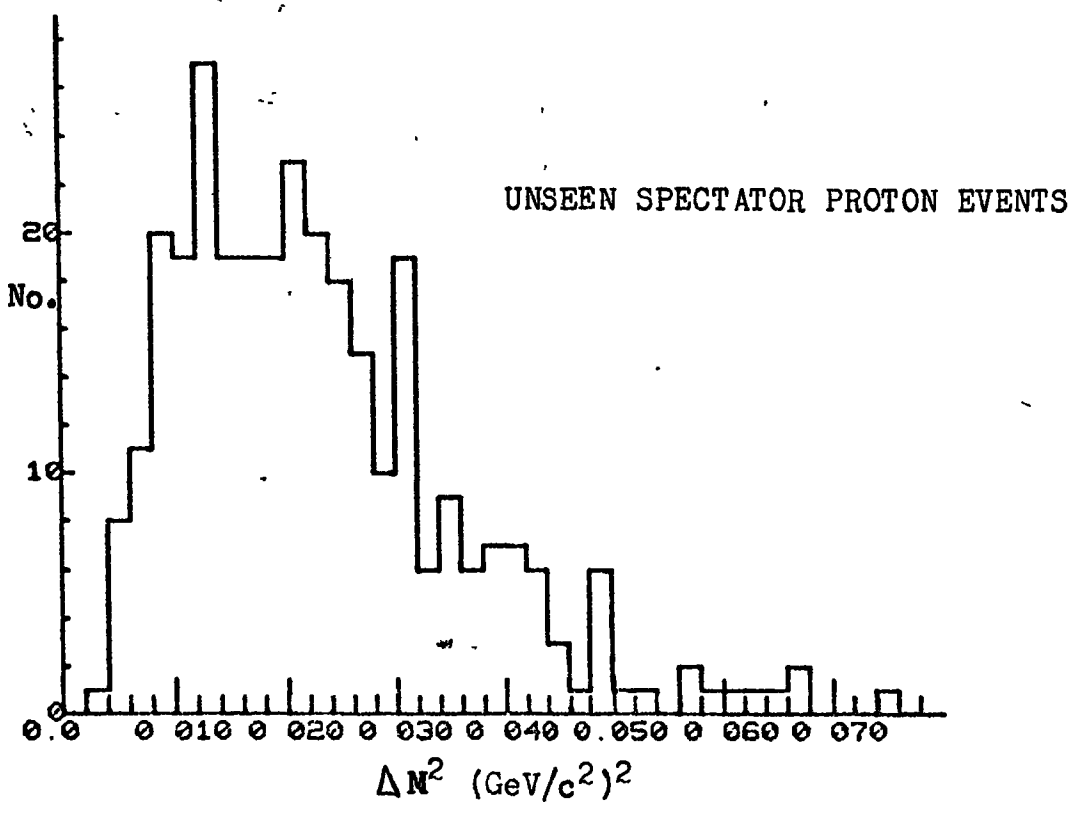

FIG. 7.2 THE RESOLUTION FUNCTION FOR THE η $\frac{1}{2}$ REGION

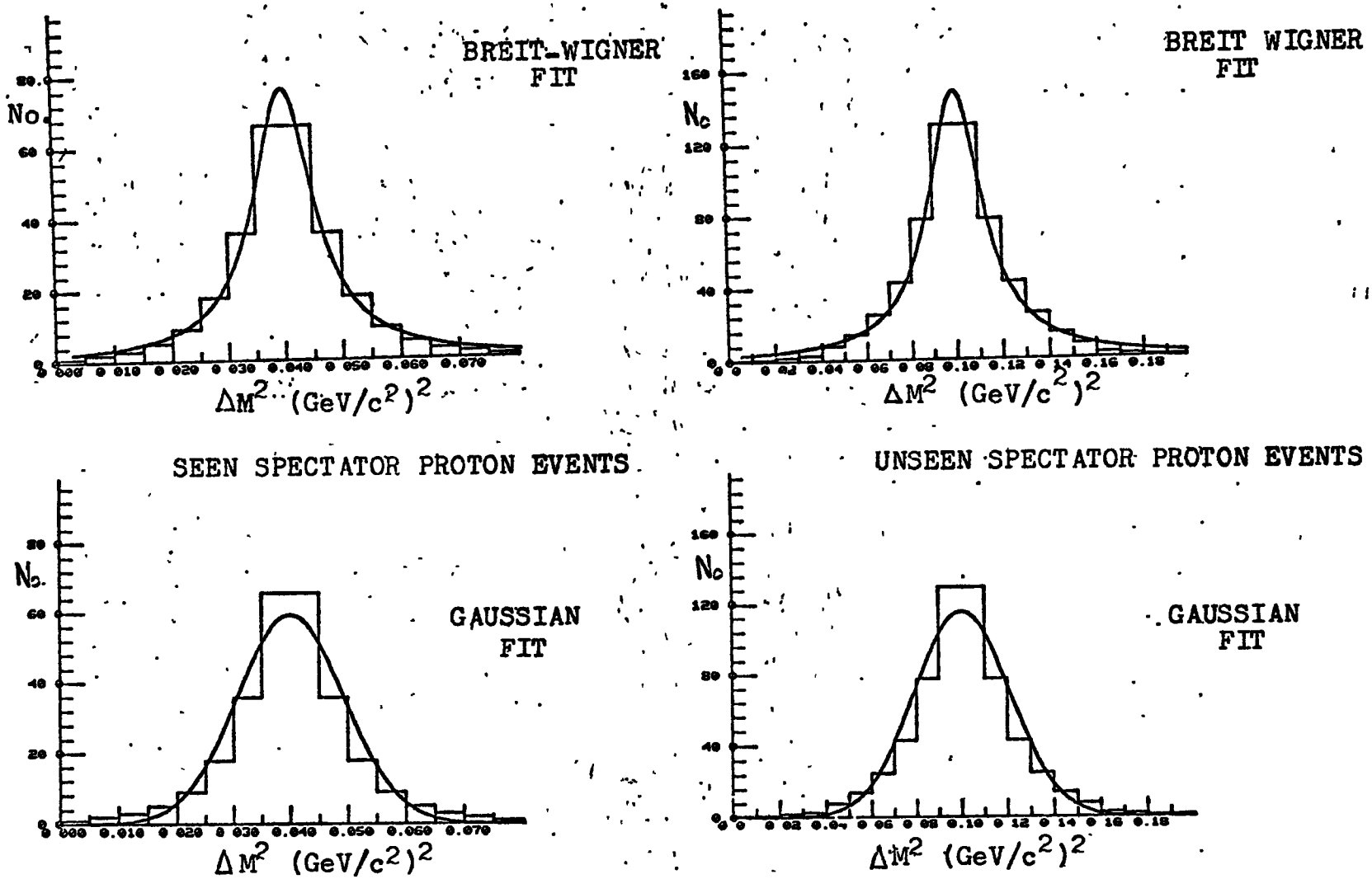

in table 7.2. As in the case of the ω^o - resolution functions, the Breit Wigner fits are marginally better. The limited statistics however, renders the results of the fits to be less reliable than their ω^o - equivalents and since in addition the difference between the two fits is somewhat less, it was decided to try both the Breit Wigner and Gaussian fits to the η - signals.

The slight difference in the shapes of the resolution functions in the η and ω^o regions can be understood by comparing the frequency distributions of the gaussian for these regions. From the comparison of FIGs. 7.1 and 4.5 it is evident that the contributions to the tails of the resolution functions from the broader gaussians is somewhat less for the η - region. Hence the shape of the resolution function will tend more towards the ultimately gaussian shape when the frequency distribution is very sharp. As an example of the more extreme case, the frequency distribution for the 4c channel

$$\pi^+ D \rightarrow P_S P \pi^+ \pi^-$$

is even sharper than for the η - region, and consequently the associated resolution function is best represented by a gaussian. Hence as the errors increase, the resolution function varies from Gaussian to Breit Wigner in shape, the resolution function for the η - region being somewhere between the two, and perhaps slightly nearer to the Breit Wigner representation.

(b) THE PARAMETERISATION OF THE BACKGROUND

As in the fits made to the ω^o - region, the background

TABLE 7.2

FITS TO THE RESOLUTION FUNCTIONS				
TYPE OF PARAMETERISATION	UNSEEN SPECTATOR PROTON EVENTS		SEEN SPECTATOR PROTON EVENTS	
	Γ	χ^2	Γ	χ^2
GAUSSIAN	21	26.9	9	10.4
BREIT WIGNER	29	21.6	13	3.8

was initially overparameterised by the polynomial in mass squared of the form,

$$N(M^2) = a(M^2)^b + C(M^2)^d + e$$

The results of this parameterisation are illustrated in FIG. 7.3, and as in the ω^o - region, the background is found to be essentially linear in mass squared.

(c) THE RESULTS OF THE FITS

The results of the fits to the η region $0.2 \rightarrow 0.4$ $(GeV/c^2)^2$ of the tripion mass squared spectra for both the seen and unseen spectator proton events are shown in FIG.7.3. From the details of the fits illustrated in table 7.3 it is evident that the widths of the resolution functions are once again in excellent agreement with those calculated from the error quantities in KINEMATICS.

As in the fits made to the ω^o - region, the predicted amounts of signal and background are observed to vary depending on the parameterisation chosen. In this case however, the variation is only $\sim 10\%$ as opposed to the 40% for the ω^o fits. This difference can be understood from the above discussion of the resolution function. The calculated forward production cross section shown in table 7.4 corresponds to the average result for the two fits. The backward production cross section was estimated from the tripion mass spectra shown in FIG. 4.3. As for the ω^o production cross section, corrections were made for scanning losses, unseen decay modes and the effects of the Pauli exclusion principle.

A comparison of the results with those calculated in previous experiments is shown in table 7.5, and from FIG. 7.4

TABLE 7.3

THE RESULTS OF THE FITS TO THE

η - SIGNAL

SAMPLE	FIT	Γ FIT	Γ KINE	χ^2	SIGNAL	BACK-GROUND	NO. BINS
UNSEEN SPECTATOR PROTON EVENTS	BREIT-WIGNER	31	29	9.6	217	93	10
	GAUSSIAN	19	21	6.3	196	114	10
SEEN SPECTATOR PROTON EVENTS	BREIT-WIGNER	12	13	4.6	108	23	12
	GAUSSIAN	8	9	8.4	84	47	12

TABLE 7.4

THE TOTAL η PRODUCTION CROSS SECTION

		PAULI CORRECTIONS	
	μb	SPIN-FLIP μb	SPIN NON FLIP μb
THE TOTAL FORWARD PRODUCTION CROSS SECTION WHICH INCLUDES:-	94 ± 9	95 ± 9	98 ± 10
(a) THE NUMBER EXTRACTED FROM THE TRIPION MASS SPECTRA	20 ± 2	20 ± 2	21 ± 2
(b) THE EVENTS REJECTED BY THE SELECTION CRITERIA	1 ± 0.2	1 ± 0.2	1 ± 0.2
(c) SCANNING LOSSES	0.3 ± 0.1	0.3 ± 0.1	0.3 ± 0.1
(d) THE NUMBER WITH P_s MOMENTA > 300 MeV/c	0.9 ± 0.2	0.9 ± 0.2	0.9 ± 0.1
(e) UNSEEN DECAY MODES	72 ± 7	73 ± 7	76 ± 8
THE TOTAL BACKWARD PRODUCTION CROSS SECTION WHICH INCLUDES:-	7.5 ± 0.8	7.5 ± 0.8	7.5 ± 0.8
(a) THE NUMBER ESTIMATED FROM THE TRIPION MASS SPECTRA	1.6 ± 0.2	1.6 ± 0.2	1.6 ± 0.2
(b) TOTAL LOSSES	0.2 ± 0.1	0.2 ± 0.1	0.2 ± 0.1
(c) UNSEEN DECAY MODES	5.7 ± 0.6	5.7 ± 0.6	5.7 ± 0.6
THE TOTAL CROSS SECTION	102 ± 10	103 ± 10	106 ± 11

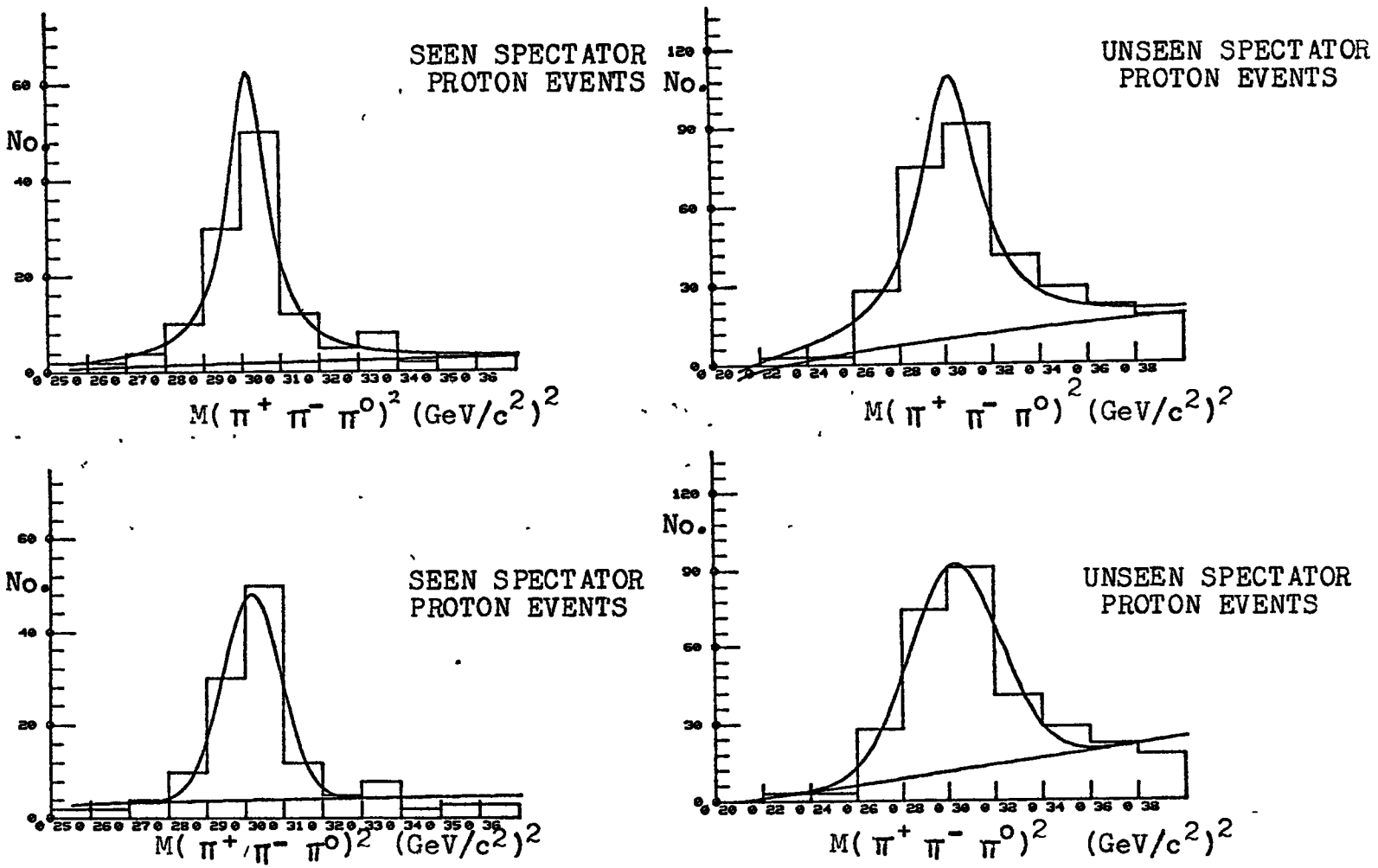

FIG. 7.3 THE FITS TO THE ω REGION OF THE TRIPION MASS SPECTRUM.

TABLE 7.5

A SURVEY OF THE TOTAL η PRODUCTION CROSS SECTIONS CALCULATED IN PREVIOUS EXPERIMENTS

BEAM MOMENTUM (GeV/c)	CROSS SECTION μb	COPRECTIONS			No. OF EVENTS	REF.
		PAULI EXCLU-SION LOSSES	UNSEEN MODES	SCAN LOSSES		
0.8 ± 0.1	1000 ± 250		✓			7.1
1.14	800 ± 200		✓		~ 70	7.2
1.7	628 ± 170		✓		~ 20	7.3
2.7	210 ± 40	✓	✓	✓	~ 50	7.4
4.0	95 ± 9	✓	✓	✓	~ 300	7.5 (THIS ANALYSIS)
4.19	78 ± 21		✓			7.6
5.4	117 ± 42		✓		~ 20	7.7

FIG. 7-4 THE VARIATION OF THE η-PRODUCTION CROSS-SECTION WITH INCIDENT MOMENTUM.

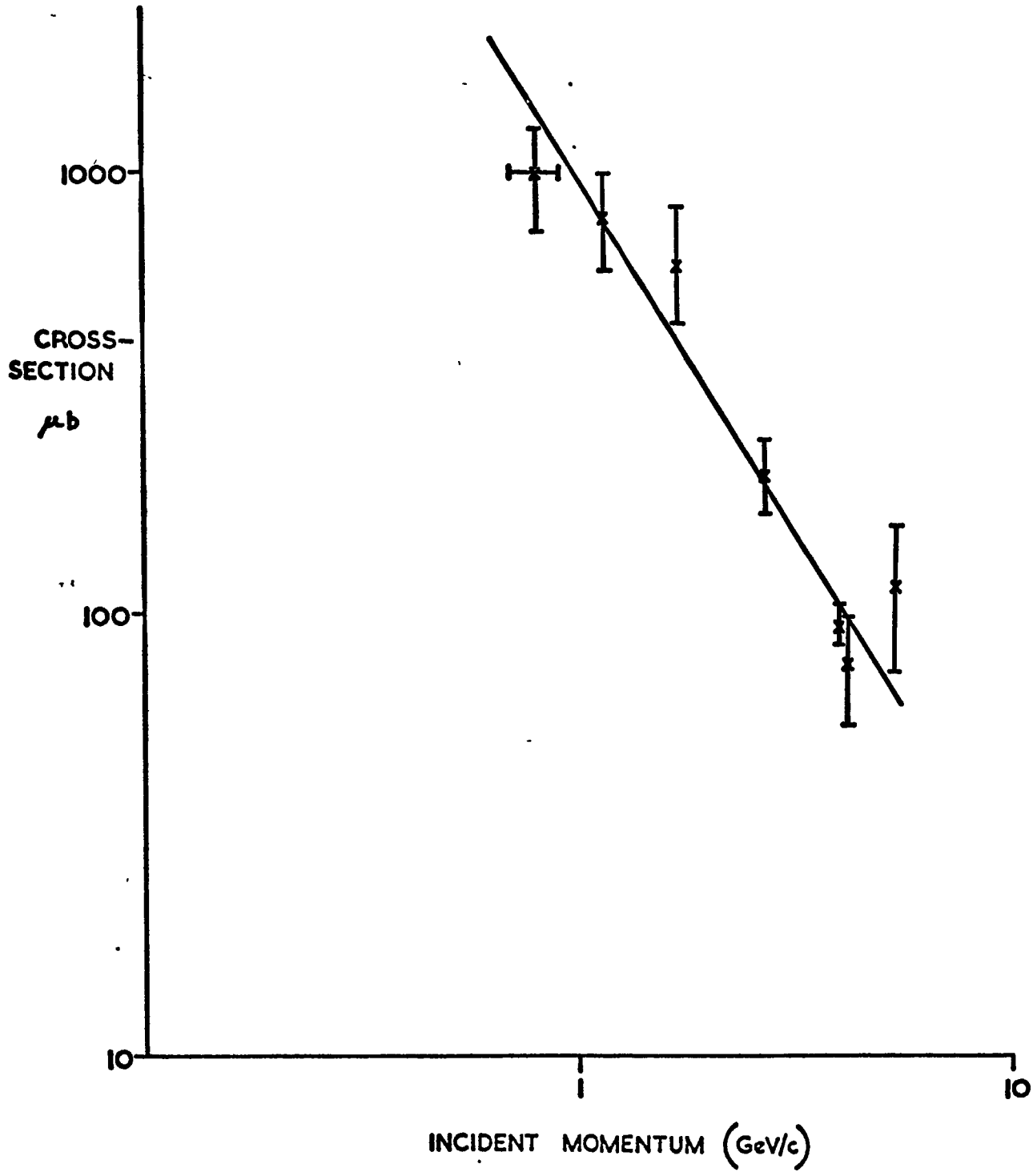

it is evident that the results are in good agreement with the relation $\sigma \propto P^{-n}$ where σ is the total production cross section and P the primary momentum in the laboratory system. The slope of the fitted line is -1.6 ± 0.5.

7.2 THE DIFFERENTIAL CROSS SECTION

The results for the differential cross section for the region $0.5 \rightarrow 0.6$ (GeV/c^2) of the tripion mass spectra for the seen and unseen spectator proton events plotted as a function of the Δ - momentum transfer squared measured from the primary to the tripion mass system are shown in FIG. 7.5. The limited statistics do not enable the effects of background to be considered. Since however, within the statistical errors the results for the seen and unseen spectator proton events are consistent, these two samples were combined and as seen in FIG. 7.5 this sample provides a better description of the differential cross section. Drawn on this plot are the corrections for the Pauli exclusion effect and scanning losses.

Even allowing for these corrections, the differential cross section is observed to dip as $t \rightarrow 0.0$, peak at $t \sim 0.25$ $(GeV/c^2)^2$ and exhibit a smooth exponential fall off for $t > 0.3$ $(GeV/c^2)^2$, with a fitted exponent of 3.5 ± 1.0. It must be emphasised however that the results are based on very limited statistics, and no allowance has been made for the effects of background. The effects of the kinematical cut off at $t = t$ minimum are considered negligible for the above results.

FIG. 7.5 THE DIFFERENTIAL CROSS SECTION (dN/dt) FOR THE FORWARDLY PRODUCED η - MESONS IN THE π -N CENTRE OF MASS SYSTEM.

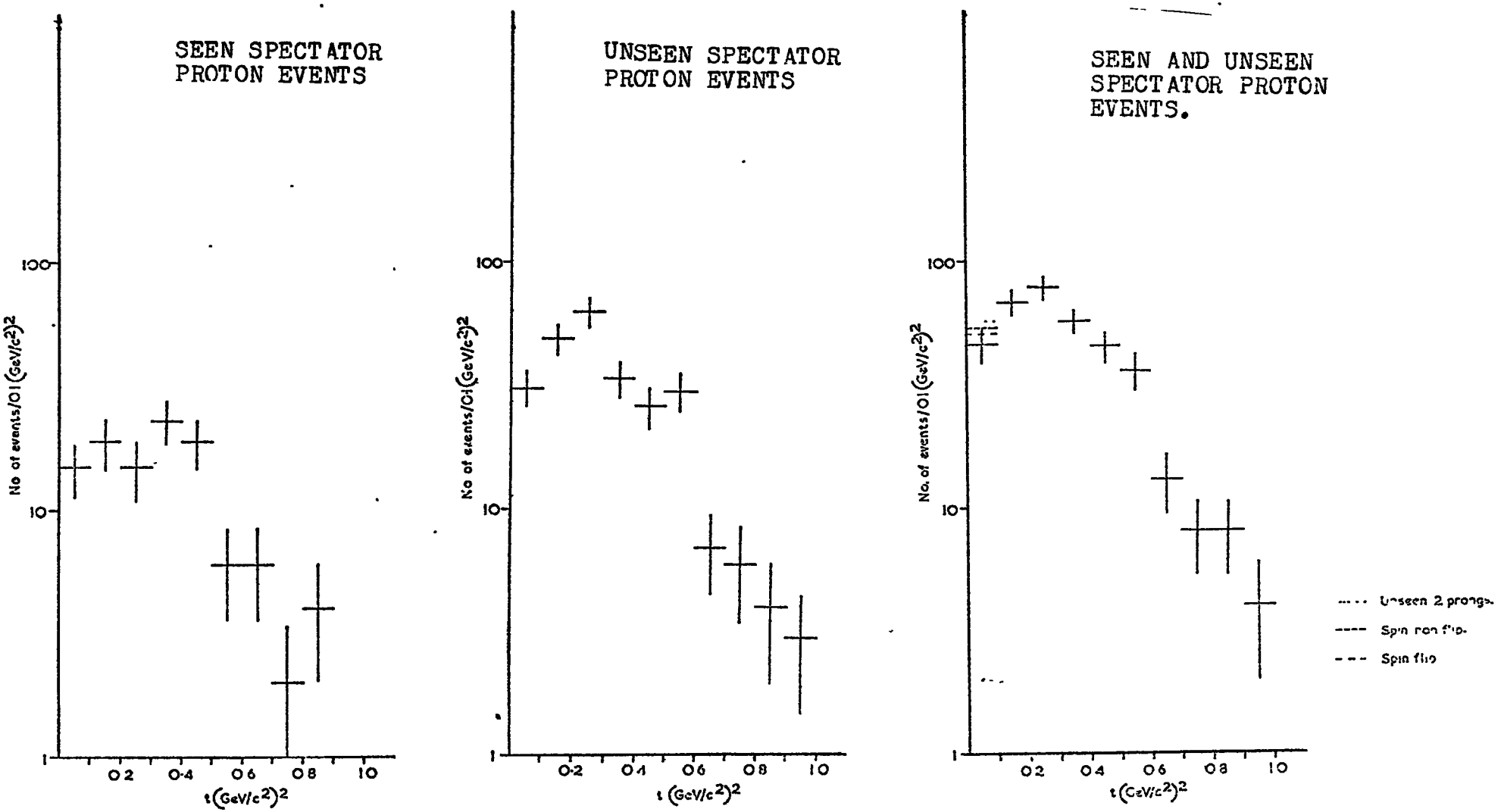

7.3 A SUMMARY AND DISCUSSION OF THE RESULTS

(a) THE TOTAL FORWARD PRODUCTION CROSS SECTION

The results for the total forward production cross sections as calculated in this and previous experiments are summarised in tables 7.4 and 7.5, and as illustrated in FIG. 7.4, the results are in good agreement with the relationship

$$\sigma \propto \rho^{-n}$$

where n is the order of 1.6 ± 0.5.

Regge Pole models predict the value of n to be given by

$$-n = 2\alpha(t = 0) - 2$$

where $\alpha(t = 0)$ is the value of the trajectory parameter at $t = 0$. Hence since η - production involves the exchange of the A_2 - meson only, a trajectory slope of unity predicts a value of n of 1.5, in good agreement with the experimentally observed value.

(b) THE TOTAL BACKWARD PRODUCTION CROSS SECTION

Apart from the results of this experiment, there is little or no evidence for backward η production in any previous experiments, mainly because of their limited statistics. This analysis yields a backward production cross section of $7.5 \pm 0.8\ \mu b$, corresponding to some 24 observed events. The lack of statistics however does not enable any further analysis to be made on these events.

(c) THE DIFFERENTIAL CROSS SECTION FOR FORWARDLY PRODUCED η - MESONS

As illustrated in FIG. 7.5, the differential cross section is observed to dip at low t, and exhibit a smooth

exponential fall off for $t > 0.3$ $(GeV/c^2)^2$, with an exponent of 3.5 ± 1.0. This is in general agreement with the Regge Pole model prediction (Ref. 7.8), but none are available for a direct comparison at this energy. It should be emphasised however that background effects have not been considered.

CHAPTER 8

GENERAL CONCLUSIONS

This thesis presents the results of an analysis of the η and ω^0 regions of the tripion mass spectrum associated with the channel

$$\pi^+ D \rightarrow p_s p \pi^+ \pi^- \pi^0$$

at an incident pion momentum of 4 GeV/c.

(A) THE ω^0-MESON

The total ω^0 production cross section was determined to be $306 \pm 31\,\mu$b, made up of the cross section for the forward production of ω^0 mesons in the π-N centre of mass system corresponding to $272 \pm 27\,\mu$b and the backward cross section to $34 \pm 4\,\mu$b. These values as described in section 4.2 were determined by parameterising the ω^0-signal with the convolution of a P-wave Breit Wigner and a resolution function in mass squared. Such a parameterisation was taken in preference to a Breit Wigner or Gaussian since it was considered to be physically better based. It was noted however, that the estimated cross section could vary by as much as 40% depending upon the type of parameterisation chosen. Consequently a direct comparison with the results from previous experiments is not easily made, since as illustrated in table 4.5, different parameterisations are used in the various analyses, and also different correction factors are applied. It is to be expected therefore that these inconsistencies will contribute to some extent towards the fluctuations in the results plotted in Fig. 4.9, which illustrates the variation of the production cross section as a function of the incident primary momentum.

In spite of these fluctuations however, the results are in good agreement with the relationship

$$\sigma \propto p^{-n}$$

where p is the primary momentum and $n \sim 2.5 \pm 0.5$. However, since the predicted value of n for ρ trajectory exchange is 1.5, the experimental results suggest that ρ-meson exchange alone is insufficient to explain the results and implies the presence of a significant contribution from B-meson exchange.

The differential cross section $(d\sigma/dt)$ for the forward production of ω^0 mesons in the π-N centre of mass system was determined independently of the background effects by extracting the amounts of signal and background in each individual t-interval. As illustrated in Fig. 4.11, after correcting for Pauli exclusion effects and scanning losses the differential cross section was found to dip at low t, and exhibit a smooth exponential fall off with an exponent of 3.5 ± 0.5 for $t > 0.3$ $(GeV/c^2)^2$. No evidence was found for any structure at $t \sim 0.6$ (GeV/c^2), the region corresponding to the NWSZ of the ρ-trajectory. The results, when compared with the predictions of two ρ and B Regge exchange models, were found to be in good agreement, indicating yet again that a significant contribution from B-meson exchange is required to explain the results.

The differential cross section for the background events was found to be constructed from two distinct classes of events, one characterised by an exponent of ~ 4.0 and the other by an exponent of ~ 2.4, the occurrence of the former component tending to obscure the presence of the dip in the

low t-region of the ω^0 differential cross section.

The events characterised by the exponent of ~ 4.0 were found to be associated with a 1.0 GeV/c^2 enhancement in the tripion mass spectrum. Upon examination however, the enhancement was found to result from a technical fault mainly associated with the 1st exposure unseen spectator proton events. Due to inadequate convergence criteria in the kinematical fitting programme (KINEMATICS), events from the 4c channel

$$\pi^+ D \rightarrow p_s p \pi^+ \pi^-$$

were misinterpreted as 1c π^0 events of the channel

$$\pi^+ D \rightarrow p_s p \pi^+ \pi^- \pi^0$$

As a result some 18% of the ρ^0 events associated with the 4c channel of the 1st exposure were lost to the 1c π^0 channel, and in particular to the low t, 1.0 GeV/c^2 region of the tripion mass spectrum. For the second exposure the improvement of the kinematical convergence criteria reduced the breakthrough to $\sim 8\%$. In addition it was noted that the characteristics of the 1.0 GeV/c^2 enhancement were consistent with previous observations of the so called H^0 resonance, and moreover that the occurrence of a similar technical fault in other experiments may effect the interpretation of the controversial A_1 region.

The effects of the background events on the results for the spin density matrix elements for the ω^0 region were considered negligible. This was verified in the results for ρ oo determined independently of the background effects. The results for the spin density matrix elements illustrated in table 6.1, and Fig. 6.5 can be

summarised as follows:-

(a) The value of ρoo at low t is $\sim$0.4 indicating that some 40% of the events proceed via B-meson exchange.

(b) A minimum was observed in ρoo at t $\sim$0.3 $(\text{GeV}/c^2)^2$ consistent with the positioning of the NWSZ for a B trajectory with a slope $\sim$0.5.

(c) ρ 1-1 is positive throughout the entire t-range and in certain regions may be consistent with zero. Consequently N_1^1 is always $\geq V_1^1$

(d) The value of Re ρ10 is negative at all values of t.

(e) None of the spin density matrix elements indicate any structure at t $\sim$0.6 $(\text{GeV}/c^2)^2$ corresponding to the NWSZ for ρ-trajectory exchange.

(f) A comparison with the predictions of two ρ and B Regge exchange models illustrated in Fig. 6.10 indicates reasonable agreement with the experimental results, the model incorporating absorptive effects providing better agreement in that it could also reproduce the observed minimum in ρoo at t $\sim$0.3 $(\text{GeV}/c^2)^2$.

A comparison of the results with those from previous experiments indicates that the vast majority of the experiments are in favour of a broad minimum in ρoo at t $\sim$0.3 $(\text{GeV}/c^2)^2$. The variation in the width position and depth of this minimum in going from one incident energy to another being attributed to the limited statistical accuracy of many of the previous experiments.

Averaging the results over all values of t indicates the following trends:-

(1) $\overline{\rho 00}$ tends to decrease with increasing energy

(2) $\overline{\rho 1\text{-}1}$ tends to increase with increasing energy

(3) $\overline{\mathrm{Re}\,\rho 10}$ is approximately energy independent

The interpretation of these trends in the predicted domination of the leading trajectory, namely the ρ trajectory at higher energies.

To conclude therefore, the results for the total cross section, differential cross section and spin density matrix elements determined for the ω^{o} resonance are generally in agreement with the predictions of Regge Pole models which incorporate not only ρ-trajectory exchange but also a significant contribution from the exchange of the B-trajectory.

(B) <u>THE η-MESON</u>

The total η production cross section was determined to be $103 \pm 10\mu$b, the cross section for the forward production in the $95 \pm 9\mu$b and the backward cross section to 7.6 ± 0.8 μb. In both cases corrections were made for Pauli exclusion effects, scanning losses and unseen decay modes. The optimum parameterisation for the η signal was considered to lie somewhere between the Breit Wigner and Gaussian representations as a function of mass squared. Consequently the above cross sections were determined from the average value of the results produced by the above two parameterisations. A comparison of the results with those from previous experiments indicates that the variation in the cross section as a function of the primary momentum is well described by the relationship

$$\sigma \propto p^{-n}$$

where p is the primary momentum and $n = 1.6 \pm 0.5$. Since η production involves the exchange of the A_2 meson only, a Regge trajectory slope of unity predicts a value of n of 1.5, in agreement with the experimentally observed value.

The limited statistics only allowed the differential cross section for the forwardly produced η meson in the π-N centre of mass system to be determined for a narrow mass interval taken about the central η^0 mass. After correcting for Pauli exclusion and scanning losses the differential cross section was found to dip at low t and exhibit a smooth exponential fall off for $t > 0.3$ $(GeV/c^2)^2$ with an exponent of 3.5 ± 1.0. Although in general agreement with the Regge model predictions, non was available for a direct comparison at this incident momentum. In addition it should be noted that due to the small statistics available the effects of background were not considered.

APPENDIX ONE

THE PAULI EXCLUSION EFFECT

As discussed in chapter 2, deuterium interactions involving two final state protons will be subject to Pauli exclusion effects. Expressing such an interaction in the general form

$$\pi^+ D \rightarrow PP\ X^o$$

the matrix element representing the process can be written as

$$M = \langle \vec{q}_{Xo},\ \vec{k}_{pp} \mid T \mid \vec{q}_{\pi^+},\ D \rangle$$

where D represents the deuteron at rest, $\vec{q}_i$ the momentum of the particle indicated, and $\vec{k}_{pp}$ the relative momentum of the 2 final state protons.

By applying the impulse approximation however, this can be re-expressed as

$$M = M_F(\vec{t}) \langle \vec{k}_{pp} \mid T(\vec{t}) \mid D \rangle$$

where $M_F(\vec{t})$ is the matrix element describing the equivalent interactions with free neutron targets i.e.

$$\pi^+ N \rightarrow P\ X^o$$

These reactions, as described in chapter 2, can proceed either via spin flip or spin non-flip of the target nucleon, and hence $M_F(\vec{t})$ can be represented by two seperate incoherent amplitudes i.e. for spin non flip $M_F(\vec{t}) = a$

and for spin flip $M_F(\vec{t}) = b$

Depending on which of these two processes occurs the final state protons will form one of two incoherent states, namely,

either (1) The TRIPLET STATE which must have an antisymmetric space wave function.

or (2) The SINGLET STATE which must have a symmetric space wave function.

As described in chapter 2, the spin non flip process can only populate the triplet spin state, whereas the spin flip process is divided between the two, $^1/_3$ contributing towards the singlet state and $^2/_3$ to the triplet state

hence $M_F(\vec{t})^2 = (|a|^2 + \frac{2}{3}|b|^2)$ for the triplet state

and $M_F(\vec{t})^2 = \frac{1}{3}|b|^2$ for the singlet state

Considering firstly the triplet state:-

THE TRIPLET STATE

This state is described by an overall antisymmetric wave function which can be written as

$$\langle \vec{k}_{pp}| = \frac{1}{\sqrt{2}} \cdot \left[e^{i\,\vec{k}.\vec{r}} - e^{-i\,\vec{k}.\vec{r}} \right]$$

The operation of $T(\vec{t})$ on this state can be considered as effectively subtracting $\vec{t}$ from the final di-proton state to give the relative momenta the nucleon has in the deuteron, (ignoring the binding energy, as implied in the use of the impulse approximation).

Since $\vec{t}$ is subtracted from one proton it has the effect of subtracting $\frac{1}{2}\vec{t}$ from the relative momentum $\vec{k}$

hence $\langle \vec{k}| \; T(t) = \langle \vec{k} - \frac{1}{2}\vec{t}|$

where $$\langle \vec{k} - \tfrac{1}{2}\vec{t}| = \frac{1}{\sqrt{2}} \left[e^{i\,(\vec{k} - \frac{1}{2}t).\vec{r}} - e^{-i\,(K+\frac{1}{2}t).\vec{r}} \right] \quad \ldots\ldots (1)$$

and since $\vec{P}_1 + \vec{P}_2 = \vec{t}$ and $\vec{k} = \frac{1}{2}(\vec{P}_1 - \vec{P}_2)$

equation (1) can be re-written in terms of the momentum of one of the protons,

$$\langle \vec{k} - \tfrac{1}{2}\vec{t} | = \langle k | T(\vec{t}) = \frac{1}{\sqrt{2}} \left(e^{i(\vec{P} - \vec{t}).\vec{r}} - e^{-i\vec{P}.\vec{r}}\right)$$

$$\langle \vec{k} | T(t) | D \rangle = \int \frac{1}{\sqrt{2}} \left(e^{i(\vec{P} - \vec{t}).\vec{r}} - e^{i\vec{P}.\vec{r}}\right) \chi_D(\vec{r})\, d^3\vec{r}$$

where $\chi_D(\vec{r})$ is the deuteron wave function

But $U_D(\vec{X}) = \int e^{-i\vec{X}.\vec{r}}\, \chi_D(\vec{r})\, d^3\vec{r}$

where $U_D(X)$ is the deuteron wave function in momentum space

$$\therefore \langle \vec{k} | T(\vec{t}) | D \rangle = \frac{1}{\sqrt{2}} \left(U_D(\vec{t} - \vec{P}) - U_D(\vec{P})\right)$$

Hence

$$\left(\frac{d\sigma}{dt}\right)_{TRIPLET} = \left(|a|^2 + \frac{2}{3}|b|^2\right) \int \frac{1}{2} \left|U_D(\vec{t} - \vec{P}) - U_D(\vec{P})\right|^2 d^3\vec{P}$$

Ignoring conservation of energy and momentum the first two terms of the expanded integral when integrated to infinity reduce to unity, and hence the expression reduces to

$$\left(\frac{d\sigma}{dt}\right)_{TRIPLET} = \left(|a|^2 + \frac{2}{3}|b|^2\right) \left[1 - I\right]$$

where $I = \int U_D(\vec{t} - \vec{P})\, U_D(\vec{P})\, d^3\vec{P}$

THE SINGLET STATE

For this state an overall symmetric wave function is required, and hence

$$\langle \vec{k}| = \frac{1}{\sqrt{2}} \left(e^{i\vec{k}.\vec{r}} + e^{-i\vec{k}.\vec{r}}\right)$$

and by following the same procedure as above

$$\langle \vec{k} | T(\vec{t}) | D \rangle = \frac{1}{\sqrt{2}} \left(U_D(\vec{t} - \vec{P}) + U_D(\vec{P})\right)$$

and hence $\left(\frac{d\sigma}{dt}\right)_{SINGLET} = \frac{1}{3}|b|^2 \left[1 + I\right]$

where $I = \int U_D(\vec{t} - \vec{P}) \cdot U_L(\vec{P}) \cdot d^3\vec{P}$ as above.

THE TOTAL DIFFERENTIAL CROSS SECTION

Combining the above two contributions to give the total differential cross sections we have

$$\left(\frac{d\sigma}{dt}\right)_{TOT} = \left(|a|^2 + \frac{2}{3}|b|^2\right)\left[1 - I\right] + \frac{1}{3}|b|^2\left[1 + I\right]$$

The integral I is evaluated by the following procedure.

$$I = \int U_D(\vec{t} - \vec{P})\, U_D(\vec{P})\, d^3\vec{P} = \iint_{\vec{r}_1\vec{r}_2} d^3\vec{P}\, \chi_L(\vec{r}_1) e^{i(\vec{t}-\vec{P})\vec{r}_1} \chi_D(\vec{r}_2)\, e^{i\vec{P}\cdot\vec{r}_2}$$

by performing a Fourier transform on each U.

$$\text{Hence } I = \int_{\vec{r}_1\vec{r}_2} \chi_D(\vec{r}_1)\, \chi_D(\vec{r}_2)\, e^{i\vec{t}\cdot\vec{r}_1} \int d^3_{\vec{p}}\; e^{i\vec{P}(\vec{r}_2 - \vec{r}_1)}$$

$$I = \int_{\vec{r}_1\vec{r}_2} \chi_D(\vec{r}_1)\, \chi_D(\vec{r}_2)\, e^{i\vec{t}\cdot\vec{r}_1}\, \delta(\vec{r}_2 - \vec{r}_1) = \int_{\vec{r}} \chi_D(\vec{r})^2 e^{i\vec{t}\cdot\vec{r}}$$

$$\therefore I = H(\vec{t})$$

where H(t) is the deuteron form factor

$$\text{Hence } \left(\frac{d\sigma}{dt}\right)_{TOT} = \left(|a|^2 + \frac{2}{3}|b|^2\right)\left(1 - H(\vec{t})\right) + \frac{1}{3}|b|^2\left(1 + H(\vec{t})\right) \quad \ldots\ldots(2)$$

and it is the use of this expression as illustrated in chapter 2 which is used to calculate the losses due to the Pauli exclusion effect.

However, from the derivation of this expression it is evident that not only is energy and momentum not conserved for the full

range of integration over P but all information concerning the final state proton momenta is lost by integrating over all possible proton momenta to infinity.

To retain this information, the expression is left in the form

$$\left(\frac{d\sigma}{dt}\right) = \left(|a|^2 + \frac{2}{3}|b|^2\right)\left\{\frac{1}{2}\left|U_D(\vec{t}-\vec{P}) - U_D(\vec{P})\right|^2 \delta(\vec{P}-\vec{P}_T-\vec{t})\right.$$
$$\left. d^3\vec{P} + \frac{1}{3}|b|^2\left\{\frac{1}{2}\left|U_D(\vec{t}-\vec{P}) + U_D(\vec{P})\right|^2 \delta(\vec{P}-\vec{P}_r-\vec{t})d^3\vec{P}\right.\right.$$

where $\vec{P}_r$ is the momentum of the resonance X^o described in the introduction. The function $\delta(\vec{P}-\vec{P}_r-\vec{t})$ is included to restrict the values of $\vec{P}$ to those allowed by momentum and energy conservation. The expression used for $U_D(\vec{P})$ is that of the Hulthen distribution

$$U_D(P) = \frac{1}{\alpha^2 + P^2} - \frac{1}{\beta^2 + P2}$$

with values of $\alpha^2 = 2.2 \times 938\ (\text{MeV})^2$ and $\beta = 5.5$

The Pauli exclusion effect correction factors resulting from this calculation are illustrated in FIG. 2.9, and by comparing the results with those shown in FIG. 2.8, calculated from equation (3), it is evident that for practical purposes the inclusion of energy and momentum conservation makes little difference. This result is to be expected since the expression for the Hulthen distribution effectively cuts off at $\sim$ 300 MeV and hence problems of momentum conservation will only be of importance at very low t - transfers, where there is little data in the present experiment.

The effect the Pauli principle has on the individual samples of seen and unseen spectator proton events can be found by making separate integrations of the above expressions

up to and beyond a specified visibility limit for the proton momenta. Using a visibility limit of 110 MeV/c, the predicted ratio of unseen spectator proton events to seen spectator proton events as a function of t was calculated. The results illustrated in FIG. 2.10, do not include the category of events where both protons are not visible since, as described in chapter 3, these events are lost from the data sample. Also included in the calculations were weighting factors allowing for the flux and centre of mass energy variations, which as discussed in chapter 2 are dependent upon the spectator proton momenta. The results clearly illustrate that at low t - values the ratio of unseen to seen spectator proton events is larger for spin non-flip processes than for spin flip processes. Moreover, since in both cases the ratio is observed to increase at low t it follows that compatibility between the seen and unseen spectator proton events should not be expected at low t - values. Hence as discussed in chapter 5, the presence of a disproportionate number of unseen spectator proton events at low t does not necessarily imply a technical fault in the data since both phase space restrictions and Pauli effects will increase the ratio in this region.

The different behaviour in the curves for spin flip and spin non-flip processes indicates that a comparison of the predicted ratio with the experimental results should enable a direct measurement to be made of the proportion of events proceeding via spin flip and spin non-flip of the recoiling proton in a given data sample. Such information would be very important for many production processes. For ω^{o} production for instance, although ρ and B meson exchanges

are believed to result in spin flip of the recoiling proton, a direct measurement of this would not only allow this to be verified, but would also enable an investigation to be made of the presence of any spin non flip processes which may result from other exchanges.

The experimental results for the ω^0 region 0.66 → 0.86 GeV/c^2 are shown in FIG. 2.10, and although the results are closer to the spin flip curve than the spin non flip curve, the agreement is insufficient to make any conclusions concerning the relative amounts of the spin flip and spin non flip processes.

It is to be noted however, that the effects of background have not been allowed for, and work is continuing at the University of Durham to improve the calculation by the inclusion of secondary scattering effects of the spectator proton.

APPENDIX TWO

THE ERROR ON THE EFFECTIVE MASSES AND 4 - MOMENTUM TRANSFERS

(a) THE ERROR ON TWO - PARTICLE MASS COMBINATIONS

The error was evaluated by expressing the effective mass in terms of the momentum (P), dip (λ) and Phi (ϕ) angles of the individual particles. The latter variables were chosen in preference to Px, Py and Pz since they were considered to be more independent. The expression was then differentiated in terms of P, λ and ϕ , the assumption being made that the variables are independent for the two particles, and from the results, the R.M.S. error was calculated. The details of the calculation are shown below:-

The effective mass of the system is given by

$$M^2 = E^2 - P^2 \quad \ldots\ldots\ldots (1)$$

where E and P represent the total energy and momentum of the system.

But $$E = E_1 + E_2 = (P_1^2 + M_1^2)^{\frac{1}{2}} + (P_2^2 + M_2^2)^{\frac{1}{2}}$$

where the subscripts 1 and 2 refer to the constituent particles

since $$P^2 = (Px_1 + Px_2)^2 + (Py_1 + Py_2)^2 + (Pz_1 + Pz_2)^2$$

equation (1) reduces to

$$M^2 = ((P_1^2 + M_1^2)^{\frac{1}{2}} + (P_2^2 + M_2^2)^{\frac{1}{2}})^2 - (Px_1+Px_2)^2 + (Py_1+Py_2) + (Pz_1+Pz_2)^2$$

and by re - expressing Px, Py and Pz in terms of P, λ and ϕ the relation becomes:-

$$M^2 = M_1^2+M_2^2 + 2(P_1^2+M_1^2)^{\frac{1}{2}}(P_2^2+M_2^2)^{\frac{1}{2}} - 2\,P_1P_2\cos\lambda_1\cos\lambda_2$$

$$\cos\phi_1\cos\phi_2 - 2\,P_1P_2\cos\lambda_1\cos\lambda_2\sin\phi_1\sin\phi_2 - 2P_1P_2\sin\lambda_1$$

$$\sin\lambda_2$$

Hence

$$\Delta M = \frac{1}{2M}\left[\sum_{i=1,2}\left(\frac{\partial M^2}{\partial P_i}\right)^2 dP_i^2 + \left(\frac{\partial M^2}{\partial\lambda_i}\right)^2 d\lambda_i^2 + \left(\frac{\partial M^2}{\partial\phi_i}\right)^2 d\phi_i^2\right]^{\frac{1}{2}}$$

where

$$\frac{\partial M^2}{\partial P_i} = 2\,P_1\,E_1^{-1}E_2 - 2\,P_2\cos\lambda_1\cos\lambda_2\,(\cos\phi_1\cos\phi_2 + \sin\phi_1$$

$$\sin\phi_2) - 2\,P_2\,\sin\lambda_1\sin\lambda_2$$

$$\frac{\partial M^2}{\partial\lambda_i} = 2\,P_1\,P_2\sin\lambda_1\cos\lambda_2\,(\cos\phi_1\cos\phi_2 + \sin\phi_1\sin\phi_2)$$

$$- 2\,P_1\,P_2\cos\lambda_1\sin\lambda_2$$

$$\frac{\partial M^2}{\partial\phi_i} = 2\,P_1\,P_2\cos\lambda_1\cos\lambda_2\,(\sin\phi_1\cos\phi_2 - \cos\phi_1\sin\phi_2)$$

The above indices can be interchanged to give the corresponding expressions for

$$\left(\frac{\partial M^2}{\partial P_2}\right) \quad \left(\frac{\partial M^2}{\partial\lambda_2}\right) \quad \text{and} \quad \left(\frac{\partial M^2}{\partial\phi_2}\right)$$

(b) <u>THE ERROR ON THREE PARTICLE MASS COMBINATIONS</u>

The expression is calculated in precisely the same way as above, except in this case,

$$\frac{\partial M^2}{\partial P_1} = \frac{2P_1}{E_1}\,(E_2+E_3) - 2\,P_2\cos\lambda_1\cos\lambda_2\,(\cos\phi_1\cos\phi_2 +$$

$$\sin\phi_1\sin\phi_2) - 2\,P_3\cos\lambda_1\cos\lambda_3\,(\cos\phi_1\cos\phi_3 + \sin\phi_1\sin\phi_3$$

$$- 2\sin\lambda_1\,(P_2\sin\lambda_2 + P_3\sin\lambda_3)$$

$$\frac{\partial M^2}{\partial \lambda_1} = 2P_1 P_2 \sin\lambda_1 \cos\lambda_2 (\cos\phi_1 \cos\phi_2 + \sin\phi_1 \sin\phi_2)$$

$$+ 2 P_1 P_3 \sin\lambda_1 \cos\lambda_3 (\cos\phi_1 \cos\phi_3 + \sin\phi_1 \sin\phi_3) -$$

$$2 P_1 \cos\lambda_1 (P_2 \sin\lambda_2 + P_3 \sin\lambda_3)$$

and

$$\frac{\partial M^2}{\partial \phi_1} = ? P_1 P_2 \cos\lambda_1 \cos\lambda_2 (\sin\phi_1 \cos\phi_2 - \cos\phi_1 \sin\phi_2) +$$

$$2 P_1 P_3 \cos\lambda_1 \cos\lambda_3 (\sin\phi_1 \cos\phi_3 - \cos\phi_1 \sin\phi_3)$$

Once again the indices can be interchanged to give the values of

$$\frac{\partial M^2}{\partial P_2} \qquad \frac{\partial M^2}{\partial \lambda_2} \text{ and } \frac{\partial M^2}{\partial \phi_2} \text{ etc.}$$

(c) THE ERROR ON THE 4 - MOMENTUM TRANSFER

This is calculated in a similar manner as above. For reactions of the type $\pi^+ D \rightarrow P_S P X^o$ the 4 - momentum transfer from the primary to the X^o system is given by:-

$$t = (qD - (q_{PS} + qP))^2 \quad \ldots\ldots\ldots(1)$$

where the q's are the 4 - momenta of the particles indicated in the subscripts. Hence by re-expressing this in terms of P, λ and ϕ for the spectator and interaction protons, relation (1) becomes:-

$$t = -(M_D^2 + M_1^2 + M_2^2) + 2 P_1 P_2 \cos\lambda_1 \cos\lambda_2 (\cos\phi_1 \cos\phi_2 + \sin\phi_1 \sin\phi_2) + 2 P_1 P_2 \sin\phi_1 \sin\phi_2 + 2 M_D ((P_1^2 + M_1^2)^{\frac{1}{2}} + (P_2^2 + M_2^2)^{\frac{1}{2}}) - 2(P_1^2 + M_1^2)^{\frac{1}{2}} (P_2^2 + M_2^2)^{\frac{1}{2}}$$

and hence

$$\Delta t = \left[\sum_{i=1,2} \left(\frac{\partial t}{\partial Pi} \right)^2 dPi^2 + \left(\frac{\partial t}{\partial \lambda_i} \right)^2 d\lambda_i^2 + \left(\frac{\partial t}{\partial \phi_i} \right)^2 d\phi_i^2 \right]^{\frac{1}{2}}$$

where

$$\frac{\partial t}{\partial P_1} = \frac{2 M_D P_1}{E_1} - \frac{2 P_1 E_2}{E_1} + 2 P_2 (\cos \lambda_1 \cos \lambda_2 \cos \phi_1 \cos \phi_2$$

$$+ \cos \lambda_1 \cos \lambda_2 \sin \phi_1 \sin \phi_2 + \sin \phi_1 \sin \phi_2)$$

$$\frac{\partial t}{\partial \lambda} = - 2 P_1 P_2 (\sin \lambda_1 \cos \lambda_2 \cos \phi_1 \cos \phi_2 + \sin \lambda_1 \cos \lambda_2$$

$$\sin \phi_1 \sin \phi_2) \quad \text{and}$$

$$\frac{\partial t}{\partial \phi_1} = - 2 P_1 P_2 (\cos \lambda_1 \cos \lambda_2 \sin \phi_1 \sin \phi_2 - \cos \lambda_1 \cos \lambda_2$$

$$\cos \phi_1 \sin \phi_2 - \cos \phi_1 \sin \phi_2)$$

APPENDIX THREE

THE REGGE POLE MODEL

INTRODUCTION

One of the compelling arguments for the Regge Pole hypothesis was the failure of the Absorption model to handle particles with non-zero spin.

The evolution of Regge Poles was started by Regge and his collaborators in the late 1950's and developed from concepts in potential theory. Essentially it was demonstrated that the partial wave amplitude was not only analytic as a function of energy, but was also analytic as a function of the angular momentum. The first claim of the model was the existence of trajectories $\alpha(E)$, such that whenever E equals the mass of a particle on a trajectory, Re α (E) equals the spin of that particle, $E \to$ E threshold corresponding to resonances, and $E <$ E threshold corresponding to bound states. In particular, the trajectories correlate bound states and resonances of the same internal quantum numbers, with spins that differ in units of two, the continuation of the trajectory into the s - channel physical region giving rise to the so called exchange trajectory. The basic difference between this model and the peripheral model is that the concept of exchange particles is replaced by exchange trajectories. In the relation for the energy dependence of the peripheral model,

$$\sigma \alpha s^{2J-2}$$

the spin J of the exchange particle is replaced by the trajectory parameter $\alpha(t)$ at $t = 0$, and since this is always less than 1, the exponent of the energy dependence is always zero or negative, thereby overcoming the divergence of the peripheral model for spins > 1. Some of the additional properties of the model are listed below:-

(a) SIGNATURE

This is introduced in order to take into account the different effects of exchange forces for even and odd ℓ. A Regge Pole of even (odd) signature only contributes to a partial wave of even (odd) ℓ, and hence an even (odd) signature trajectory can only contain particles of even (odd) ℓ.

(b) FACTORISATION

One characteristic property of the peripheral model is the occurence of the coupling constants for each vertex, and the fact that the overall scattering amplitude is proportional to the product of these two terms. This feature is termed factorisation, since the amplitude factorises into one contribution from each vertex. This property also applies to the Regge Pole model, but only to the particular case of one Regge Pole exchange. As soon as several trajectories are exchanged there are in general no clear cut predictions from this principle. The importance of factorisation lies in the fact that one and the same Regge Pole coupling may occur in different reactions, and since it is independent of how it couples to the other particles, it is possible to predict relations between the scattering amplitudes of different processes e.g.

$$\sigma_{TOT}^{(pp)} \cdot \sigma_{TOT}^{(\pi\pi)} = \sigma_{TOT}^{(\pi p)\ 2}$$

(c) GHOSTS

Poles which occur for $t < 0$ cannot be incorporated into the model since they imply an infinite differential cross-section at that t-value. Such poles are termed Ghosts, and are effectively removed by reducing the residue to zero by putting it proportional to $\alpha(t)$.

(d) DAUGHTER TRAJECTORIES

Unwanted singularities occur at $t = 0$ in the scattering amplitudes of reactions that do not have their masses pairwise equal, as in elastic scattering. The most popular method of overcoming this problem is to invoke further Regge trajectories known as "daughters", which have singular residues which precisely cancel the singularities produced by the original parent trajectory.

(e) CONSPIRACY AND EVASION

Constraints at a particular t - value can be produced by the intersection of a set of trajectories which "conspire" together to give the desired effect. Conspiracy can be "evaded" by imposing conditions not on the trajectories, but on the residues that appear in the amplitudes. Any combination of conspiracy and evasion is possible.

(f) SHRINKAGE

For the exchange of a single Regge Pole the t-dependence is given by

$$\frac{d\sigma}{dt} \alpha \left(\frac{s}{s_0}\right)^{2\alpha(t)-2}$$

where s is the centre of mass energy. This implies that as s increases the slope of the differential cross section becomes steeper, and hence the peak is observed to "shrink".

(g) REGGE DIPS

Minima occur in the differential cross sections at momentum transfers for which a contributing meson trajectory passes through a zero or negative integer,

$$\alpha(t) = -n,\ n = 0,1,2 \ldots\ldots$$

of for a baryon trajectory where

$$\alpha(t) = -\tfrac{1}{2},\ -\tfrac{3}{2} \ldots\ldots$$

The contribution of a single Regge Pole is real at its right signature point, and imaginary at its wrong signature point. At unphysical values of the angular momentum, for a given helicity configuration kinematical factors cause the amplitude to vanish at its wrong signature points, giving rise to the so called nonsense wrong signature zeros.

(h) REGGE CUTS

A Regge cut is a line of singularities in the angular momentum plane caused by the exchange of two or more poles. Such a region has to be avoided in the overall integral, in order to obtain the total cross section. Although their positions are well defined, their precise interpretation is open to speculation.

(I) THE COMPARISON OF THE MODEL WITH EXPERIMENT

The main success of the model has been in the fitting of vector meson exchange processes e.g. $\pi^- P \rightarrow \pi^0 N$ and in particular for the reproduction of the observed dips in the differential cross sections.

In general, the properties of the model listed above, combined with absorption effects render it sufficiently

flexible to fit a whole host of reactions, a fairly comprehensive list being tabulated in an article by P.D.B. Collins (Ref. A3.1). However, it is perhaps the flexibility of the model which draws most criticism, and many consider the introduction of cuts etc. to weaken its credibility considerably.

ACKNOWLEDGEMENTS

The Author wishes to thank Dr. J.V. Major, Dr. D. Evans and Dr. K.P. Neat for their guidance, assistance and helpful suggestions throughout all stages of this work. Many thanks are also due to other colleagues in the High Energy Nuclear Physics group, in particular Ian Bell and Alan Lotts, not only for their informative discussions but also for providing a very congenial atmosphere within the research group.

His thanks are also due to the technical staff of the Physics department and Computer Unit, and in particular to Mrs. D.C. Pickles for her help in drawing the figures.

Last but not least he would like to thank Mrs. J. Lincoln for her careful typing of this thesis.

This work has been financed by the Science Research Council.

LIST OF REFERENCES

REF.

CHAPTER 2

2.1 Gordon, Ph.D. thesis, the University of Illinois, 1970

2.2 Kellner, CERN/TC/NBC, 65-4, 1965

2.3 Thomas, CERN, 67-26, vol.1, page 215, 1967

2.4 Julius, Daresbury lecture note No.8, DNPL/R20

2.5 To be published (Emms et al.)

2.6 Wilkin, PRL, 17, page 561, 1966

2.7 Mather and Swan, Cambridge monograph, 1958

2.8 Butterworth et al, PRL, Vol.15, page 734, 1965

CHAPTER 3

3.1 Compilation of π^+ induced reaction cross sections, CERN/HERA/70-5

3.2 Geometry, R.H.E.L. programming library

3.3 Kinematics, R.H.E.L. programming library

3.4 Judge, R.H.E.L. programming library

CHAPTER 4

4.1 The Review of Particle Properties, PL, 50B, 1974

4.2 Ling - Lie Wang, PRL, Vol.16, page 756, 1966

4.3 See references 4.5 to 4.17

4.4 Emms et al, PL, Vol.51B, No.2, page 195, 1974

4.5 Bacon et al, PR, Vol.157, page 1263, 1967

4.6 Miller et al, PR, vol.178, page 2061, 1969

4.7 Holloway et al, PRD, Vol.8, page 2814, 1973

4.8 This analysis (To be published)

4.9 Abrams et al, PRL, Vol.23, page 673, 1969

4.10 Holloway et al, PRD, Vol.8, page 2814, 1973

REF

4.11 Armenise et al, NC, Vol.65A, page 637, 1970

4.12 Farber et al, NP, Vol. B29, page 237, 1971

4.13 Holloway et al, PRD, Vol. 8, page 2814, 1973

4.14 Anderson et al, PL, Vol.45B, page 165, 1973

4.15 Matthews et al, PRL, Vol.26, page 400, 1971

4.16 J. Huc, These De Doctorat d'etat-ecole polytechnique

4.17 Paler et al, NCL, Vol.4, page 745, 1972.

CHAPTER 5

5.1 A compilation of π^+ P, π^+N and π^+D interactions, Chew et al, LBL, 53, 1973

5.2 Benson et al, PRL, Vol.17, No.24, page 1234, 1966

5.3 Chaudhary and Marquit, PRD, Vol.2, No.9, 1970

5.4 Fung et al, PRL, Vol.21, No.47, 1968

5.5 Aachen - Berlin - Birmingham etc. collaboration, PR, 138B, 897, 1965

5.6 Aachen - Berlin - Birmingham etc. collaboration, PL, 11, 167, 1964

5.7 Cohn et al, NP, B1, 57, 1967

5.8 Goldhaber, Lund Conference Proceedings, 1969.

5.9 Crennell and Holl, RL - 74 - 123, journal preprint, HEP division PRP/H/131

5.10 Deck, PRL, 13, page 169, 1964

5.11 French, 14th international conference, Vienna 1968

CHAPTER 6

6.1 Jacob and Wick, anols of physics, page 404, 1959

6.2 Jackson et al, PR, Vol.139, B428, 1965

6.3 Morrison, CERN/TC/PHYSICS, 66-20

REF

6.4 Tran Than Van, NCL, Vol.3, page 678, 1970

6.5 Henyey et al, PRL, Vol.21, page 1788, 1968

6.6 Brandao et al, NCL, Vol.2, page 135, 1971

6.7 Matthews and Moen, NCL, Vol.1, page 255, 1971

6.8 Hogaasen and Lubatti, PL, Vol,26B, page 166, 1968

CHAPTER 7

7.1 Litchfield et al, PR, Vol.183, page 1152, 1969

7.2 Kramer et al, PR, Vol.136, B496, 1964

7.3 Bacon et al, PR, Vol.157, page 1263, 1967

7.4 Miller et al, PR, Vol.157, page 1263, 1967

7.5 This analysis (to be published)

7.6 Gordon et al, ILL, 1195, 1970

7.7 Farber et al, NP, B29, 237, 1971

7.8 Collins, Physics reports, Vol.1C, No.4, page 203, 1971

APPENDIX 1

A1.1 Butterworth et al, PRL, 15, page 734, 1965

A1.2 Stenger et al., PR, 134B, 1116, 1964

A1.3 Chew, PR, 80, page 196, 1950

A1.4 Fernbach et al, PR, 84, page 1084, 1951

A1.5 Rockmore, PR, 105, page 256, 1957

A1.6 Ferreira, PR, 115, page 1727, 1959

A1.7 Levy-Lebland and Groudin, NC 23, 1163, 1962

A1.8 Gourdin and Martin, NC 11, 670, 1959

A1.9 Gourdin and Martin, NC 14, 722, 1959

APPENDIX 3

A3.1 Collins, Physics reports, Vol. 1C, No.4, 1971